APPLICATIONS OF THE TRIMETHYL LOCK

IN FLUOROGENIC ENYZYME SUBSTRATES

by

Michael Nathan Levine

A dissertation submitted in partial fulfillment

of the requirements for the degree of

Doctor of Philosophy

(Biochemistry)

at the

UNIVERSITY OF WISCONSIN–MADISON

(2011)

APPLICATIONS OF THE TRIMETHYL LOCK

IN FLUOROGENIC ENYZYME SUBSTRATES

submitted to the Graduate School of the

University of Wisconsin-Madison

in partial fulfillment of the requirements for the

degree of Doctor of Philosophy

By

Michael Nathan Levine

Date of final oral examination: September 22, 2011

Month and year degree to be awarded: December 2011

The dissertation is approved by the following members of the Final Oral Committee:

Ronald T. Raines, Henry Lardy Professor of Biochemistry

Brian Fox, Marvin J. Johnson Professor in Fermentation Biochemistry

Douglas Weibel, Assistant Professor of Biochemistry

Deane Mosher, Professor of Biomolecular Chemistry

Helen Blackwell, Associate Professor of Chemistry

APPLICATIONS OF THE TRIMETHYL LOCK
IN FLUOROGENIC ENZYME SUBSTRATES

Michael Nathan Levine

Under the supervision of Professor Ronald T. Raines

at the University of Wisconsin–Madison

The trimethyl lock has been utilized to generate fluorogenic enzyme substrates that have been applied to high-throughput screening, biomolecular imaging, and cellular assays. The trimethyl lock provides a modular platform with which to mask fluorophores. The amide linkage is stable under physiologic conditions and insulates substrate reactivity from fluorescence development. Thus, chemically stable substrates may be generated, which rapidly become fluorescent subsequent to a user-defined triggering reaction.

CHAPTER 1 is a literature review of the applications of the trimethyl lock that span chemistry, pharmacology, and biology. The use of the trimethyl lock in prodrugs, biological switches, and solid-phase synthesis resins is discussed. Additionally, the many fluorescent substrates incorporating the trimethyl lock are reviewed.

In CHAPTER 2, a chemically stable chromogenic esterase substrate is described. This substrate improves upon the instability and pH-sensitivity of previous substrates. It is amenable to high-throughput screening.

CHAPTER 3 reports the development of a novel substrate for alkaline phosphatase, an enzyme important to enzymology, medicine, and biotechnology. Alkaline phosphatase is

commonly used as the reporter in enzyme-linked immunosorbent assays (ELISAs), yet it suffers from potent product inhibition. Substrates must possess high assay sensitivity, which fluorophores typically do; however, many common substrates are hindered by two-hit kinetics, poor stability, and pH-sensitivity. The substrate described herein overcomes all of the challenges in developing a successful alkaline phosphatase substrate.

A novel lipid endocytosis assay is described in CHAPTER 4. Constitutive endocytosis is assayed with a fluorescent lipid that may be observed by microscopy or flow cytometry. The rates of endocytosis are measured and may be compared between cancerous and normal matched cell lines. This provides insight into the hallmarks of cancer, and may lead to new treatment options.

Finally, CHAPTER 5 discusses the future directions of fluorescent assays that utilize the trimethyl lock. Improvements to current methods are suggested, and the potential of trimethyl lock entry into new topics in biology and pharmacology are explored. Fluorescent techniques to assay cellular processes are discussed in the context of cytotoxic ribonucleases and their cancer cell specificity.

Acknowledgements

This manuscript is dedicated to my grandfather, Sydney Cashner.

To my parents, David and Paula Levine, thank you for all of the opportunities you have provided me in life. You have always been supportive and knew when I needed encouragement, or gentle prodding to keep me on course. Thank you for allowing me to explore seemingly scattered interests as a child, and for not abandoning me at the Museum of Science in Boston when I wanted to stay a little too long. I want to thank my brother, Jason, who has visited me in Madison several times, and who always seems to call just when I need him to. Thank you to my grandparents, Barbara and Richard Levine and Ann Cashner for taking the time to hear about my projects in the lab, reading manuscripts, and for always being proud of me. Thank you to my family in Chicago, Barry and Cathy Levine, for adopting me during the holidays when I could not make it home to Boston.

Thank you to the Medical Scientist Training Program, and its directors, Deane Mosher, Anna Huttenlocher, Robert Blank, and Brad Schwartz. Many thanks to Paul Cook, our administrator for making the transition from the medical school to the graduate school, and back, as painless as possible. I want to mention my committee members, Helen Blackwell, Brian Fox, Deane Mosher, and Doug Weibel for their helpful guidance and suggestions.

Thank you to my friends David Manthei, Jabe Best, Jeremy Lavine, and Shawn Jackson for an incredibly eventful run in Madison. You guys have been supportive, influential (good and bad), and of course, really entertaining. Thank you for participating in our whiffle ball league, of which I am The Commissioner (now a published fact). Thank you to Rebecca Turcotte, for recruiting me both to the University of Wisconsin and to the Raines laboratory. You have shaped me as a person and a researcher. I think the 2004 Red Sox should be thanking us for the insanely superstitious actions we took that propelled them to a World Series Championship. Thank you to Leopold Stotch for 15 years of entertainment. I would also like to thank my MSTP classmates, Eric Landsness, Lisa Maurer, Krystal Onatolu, Nadia Sundlass, Stacy Valkenaar, David Vonk, and Sarah Wernimont, for providing a great learning environment during journal clubs, and boards review groups.

Thank you to all of the members of the Raines laboratory, whom I have had the privilege of working with. Special thanks to my bay-mate Eddie Myers, for hours of scientific discussions and amazing research insights. Thank you to Luke Lavis for laying the groundwork for many of my projects. Thank you to Cindy Chao, Chelcie Eller, and Rex Watkins for helping me to learn microscopy, and molecular biology techniques. I am very grateful to Trish Hoang for sharing her expertise with tissue culture, and bringing new excitement and ideas to the lab. I also owe gratitude to the undergraduate coworkers that I had the opportunity to mentor, Ryan Hayes, Vanessa Kung, and Matt Walker. Thank you to many past and present members—Kristen Andersen, Joe Binder, Thomas Baumann, Christine Bradford, Margie Borra, Ben Caes, Lauren Carroll, Sayani

Chattopadhyay, Ho-Hsuan Chou, Amit Choudhary, Mariëlle Delville, Kevin Desai, Kim Dickson, Greg Ellis, Kelly Gorres, Daniel Gottlieb, Greg Jakubczak, Katrina Jensen, Jeremy Johnson, Sean Johnston, Jeet Kalia, Frank Kotch, Joelle Lomax, John Lukesh, Langdon Martin, Nicky McElfresh, Nick McGrath, Mike Palte, Rob Presler, Tom Rutkoski, Matt Shoulders, Annie Tam, Caglar Tanrikulu, Brett VanVeller, and Jim Vasta—for helpful discussions and making the lab a great place to work.

Finally, I would like to thank my advisor, Ron Raines. Ron has encouraged us to pursue research in a collaborative manner. We are given great flexibility to explore the intricacies of our projects. I have learned much from Ron, especially regarding chemical biology, and communicating my research. I am grateful for the opportunity to have worked in his research group.

Table of Contents

CHAPTER 2

Trimethyl Lock: A Stable Chromogenic Substrate for Esterases 75

List of Figures

List of Schemes

List of Tables

List of Abbreviations

A	absorbance
Å	Ångström
Ac	acetyl
AcOH	acetic acid
ACS	American Chemical Society
ADEPT	antibody-directed enzyme prodrug therapy
ADP	adenosine 5′-diphosphate
AMC	aminomethyl coumarin
ATCC	American Type Culture Collection
ATP	adenosine 5′-triphosphate
AU	arbitrary units
BIF	Biophysics Instrumentation Facility
Bn	benzyl
bs	broad singlet
BSA	bovine serum albumin
°C	degrees Celsius
C_6-NBD-SM	N-[N-(7-nitro-2,1,3-benzoxadiazol-4-yl)-ε-aminohexanoyl]-sphingosylphosporylcholine
cm	centimeter
CMV	cytomegalovirus

CPP	cell-penetrating peptide
d	doublet
DAPI	4,6′-diamidino-2-phenylindole
DCM	dichloromethane
DIC	N,N′-diisopropylcarbodiimide
DIPEA	diisopropylethylamine
DMAP	dimethylaminopyridine
DMEM	Dulbecco's Modified Eagle Medium
DMF	dimethyl formamide
DMSO	dimethylsulfoxide
DNA	deoxyribonucleic acid
DNR	daunorubicin
DOPE	dioleylphosphatidylethanolamine
DPBS	Dulbecco's Phosphate Buffered Saline
DPPTE	1,2-dihexadecanoyl-*sn*-glycero-3-phosphothioethanol
[E]	enzyme concentration
EC	Enzyme Commission number
EDC	1-ethyl-3-(3-dimethylaminopropyl)carbodiimide
EDTA	ethylenediaminetetraacetic acid
EI	electron impact ionization
ELISA	enzyme-linked immunosorbent assay

EPR	enhanced permeation and retention
ESI	electrospray ionization
Et	ethyl
EtOAc	ethyl acetate
FBS	fetal bovine serum
FDA	United States Food and Drug Administration
FM 1-43	N-(3-triethylammoniumpropyl)-4-(4-dibutylamino)styryl)pyridinium dibromide
FRET	Förster resonance energy transfer
g	acceleration of gravity
g	gram
GDEPT	gene-directed enzyme prodrug therapy
gem	geminal
h	hours
HMPA	hexamethylphosphoramide
HPLC	high-performance liquid chromatography
HRMS	high resolution mass spectrometry
Hz	hertz
i.p.	intraperitoneally
IRES	internal ribosomal entry site
i.v.	intravenously
J	coupling constant

k_{cat}	first-order enzymatic rate constant
kDa	kilodaltons
K_i	inhibitor dissociation constant
K_M	Michaelis constant
M	molar
m	multiplet
m/z	mass to charge ratio
MALDI	matrix assisted laser desorption ionization
MalURh$_{110}$	maleimidourea rhodamine-110
Me	methyl
MeOH	methanol
mg	milligram
MHz	megahertz
min(s)	minute(s)
mL	milliliter
mM	millimolar
mmol	millimole
MOPS	3-(N-morpholino)propanesulfonic acid
MS	mass spectrometry
MSD	mass selective detector
MURh$_{110}$	morpholinourea rhodamine-110
MW	molecular weight

N	normal
N-Rh-PE	N-(lissamine rhodamine B sulfonyl)phosphatidylethanolamine
NADH	nicotinamide adenine dinucleotide, reduced
NES	nuclear export signal
ng	nanogram
NIGMS	National Institute of General Medical Sciences
NIH	National Institutes of Health
NLS	nulear localization signal
nm	nanometer
nM	nanomolar
NMR	nuclear magnetic resonance
NMRFAM	National Magnetic Resonance Facility At Madison
NSF	National Science Foundation
NTR	nitroreductase
o-	ortho
ONC	Onconase
p-	para
P450	Cytochrome P450
PBS	phosphate buffered saline
PCC	pyridinium chlorochromate
PEG	poly(ethylene glycol)
pH	negative log of proton concentration

pK_a	negative log of the acid dissociation constant
PLE	porcine liver esterase
PMB	*p*-methoxybenzyl
PNA	peptide nucleic acid
*p*NA	*p*-nitroaniline
*p*NP	*p*-nitrophenol
*p*NPA	*p*-nitrophenyl acetate
ppm	parts per million
pyr	pyridine
Rf	retention factor
RI	ribonuclease inhibitor
RNA	ribonucleic acid
RNase	ribonuclease
s	second
s	singlet
SD	standard deviation
t	time
t	triplet
TBAF	tetrabutylammonium fluoride
tert-	tertiary
TFA	trifluoroacetic acid
THF	tetrahydrofuran

TLC	thin layer chromatography
T_m	melting temperature
TMS	trimethylsilyl
TOF	time of flight
UV	ultraviolet
v/v	volume to volume ratio
v_0	initial velocity
w/v	weight to volume ratio
$\int F$	area under the curve of the fluorescence spectrum
δ	chemical shift
ε	extinction coefficient
λ	wavelength
λ_{ab}	absorbance wavelength
λ_{em}	emission wavelength
λ_{ex}	excitation wavelength
λ_{max}	wavelength of maximum intensity
μM	micromolar
μm	micron
Φ	quantum efficiency

CHAPTER 1

Trimethyl Lock as a Trigger for Molecular Release

in Chemistry, Biology, and Pharmacology

1.1 Introduction

Molecular scientists often need to control the reactivity of their molecules in a temporal and spatial manner. This need is being met by the "trimethyl lock", an *o*-hydroxydihydrocinnamic acid derivative (**1.1**) that undergoes rapid lactonization under physiological conditions to yield a dihydrocoumarin (**1.2**) and release an amine or alcohol (Figure 1.1). Its name arises from the three interlocking methyl groups that account for an extreme rate-enhancement. The lactonization of trimethyl lock **1.1** proceeds at a rate that is much faster than that of *o*-hydroxydihydrocinnamic acids **1.4–1.6**, which lack methyl groups (Figure 1.2) (Milstien and Cohen, 1970). Blocking the phenolic oxygen with a labile moiety (as in **1.3**) prevents lactonization, acting as an enzymatic, chemical, or photolytic trigger (Amsberry, *et al.*, 1991). Here, we discuss the application of the development of the trimethyl lock as a privileged means to release small-molecule drugs, fluorophores, and peptides.

1.1.1 History

The trimethyl lock was developed during an era fixated on ascertaining the mechanism by which ATP synthase catalyzed the synthesis of adenosine 5'-triphosphate (ATP) via oxidative phosphorylation. In the 1960's, Louis Cohen and his coworkers at the National Institutes of Health (USA) were in the midst of this quest. They developed a model to test whether ubihydroquinone, which was then suspected (and now known) to be a key cofactor in the electron-transport chain, could be esterified by protein

carboxylates to produce a high-energy intermediate upon oxidation (Figure 1.3) (Thanassi and Cohen, 1969). The high-energy intermediate would be able to activate inorganic phosphate to form a phosphoanhydride. Phosphoanhydrides are sufficiently activated to transfer a phosphoryl group to adenosine 5'-diphosphate (ADP), generating ATP and releasing free protein. Reduction of ubiquinone regenerates the starting materials. A requirement of the model was that a phenolic hydroxyl group must attack an unactivated carboxyl group. Initial model compounds did not undergo lactonization at an appreciable rate under physiological conditions, until the realization of trimethyl lock **1.1** (Milstien and Cohen, 1970). Although Cohen's putative high-energy intermediate was never found, his astute recognition of the utility of the trimethyl lock led to the numerous advances described herein.

Cohen believed that enzymes catalyzed chemical reactions, in part, by freezing the substrate into a unique conformation that minimized nonproductive conformers. Analogous to conformational restriction through enzyme–substrate binding, the interlocking of the methyl groups in the trimethyl lock led to rates of lactonization that match or even exceed the rates of enzyme-catalyzed reactions. This satisfying parallel helped to explain some of the rate enhancement in the reactions imparted by enzymes, and this device to effect catalysis was termed "stereopopulation control" (Borchardt and Cohen, 1972a; Borchardt and Cohen, 1972b; Milstien and Cohen, 1972)

1.1.2 Kinetics

The basis for the extreme rate of lactonization of the trimethyl lock has been studied over the last 40 years, and is still under debate. Winans and Wilcox believed that the relief of strain could explain the observed rapid kinetics (Winans and Wilcox, 1976). The relief-of-strain model proposed that steric hindrance of the abutting methyl groups in dihydrocinnamic acid **1.1** (Figure 1.1) was relieved upon cyclization to dihydrocoumarin **1.2**, a model that was supported by an unusual discovery—a "steric" isotope effect. Replacing all six hydrogens in the *gem*-dimethyl groups of compound **1.1** with deuterium increased the rate of lactonization by 10%, presumably because deuterium–carbon bonds, which are slightly shorter than hydrogen–carbon bonds, imposed less strain (Danforth, *et al.*, 1976). In support of the relief-of-strain hypothesis, crystal structures of quinone trimethyl locks **1.7–1.11** (Figure 1.4) showed that the methyl group distances did not change between the open and closed forms; however, the open forms **1.8–1.11** were severely strained with the carbonyl forced out of the plane of the quinone ring system (Wang, *et al.*, 1996). Some of the strain was relieved in the closed, lactone structure **1.7**.

Computational methods have been used to identify the contributors to the high lactonization rate of the trimethyl lock (Karaman, 2009). These computations suggested that the difference in ground-state free energy between trimethyl lock **1.1** and lactone **1.2** was only 7 kcal/mol, accounting for only a 10^6-fold increase in the rate of lactonization. Thus, relief of strain could not be the only factor influencing the rate of lactonization. It has been proposed that proximity also contribute to rate-enhancement (Bruice and Pandit, 1960)

1.2   Trimethyl Lock Prodrugs

The utilization of the trimethyl lock in bioreversible derivatives of drugs was pioneered in the laboratory of Ronald Borchardt, a former Cohen postdoctorate. A bioreversible derivative, or prodrug, is used to modify undesirable properties of a parent drug, such as poor solubility, bioavailability, or stability while maintaining desirable properties, such as therapeutic activity (Sinkula and Yalkowsky, 1975). Vital to the performance of prodrugs is bioreversibility; the parent drug must be released at the appropriate rate under physiological conditions.

Although many bioreversible options exist for modifying an alcohol—such as conjugation as esters, phosphates, or sulfates—few are available for an amine. Amides, formed from the acylation of amines, hydrolyze too slowly to be useful prodrugs unless the amide happens to be a substrate for a specific peptidase (Amsberry, *et al.*, 1991). Consequently, amide formation is not a general strategy to produce amine prodrugs. One notable exception, hydroxyamide **1.13** (Figure 1.5), lactonizes with a half-life estimated to be 1 min (Amsberry and Borchardt, 1990). Appendage of a variety of functional groups to the hydroxyl prevents the lactonization reaction. The rate of decomposition of the amide becomes dependent on the lability of the introduced functionality. Thus, the trimethyl lock is a general method to reversibly mask amines with tunable kinetics.

The potential use of the trimethyl lock in prodrugs is displayed in the acetyl ester of the trimethyl lock **1.12** (Figure 1.5), which releases *p*-methoxyaniline **1.14** upon

lactonization. This pro-prodrug has good *in vitro* stability—its half-life in phosphate buffered saline is 4039 min. Porcine liver esterase hydrolyzes the acetyl ester and releases *p*-methoxyaniline with a half-life of only 12 min. Trimethyl lock **1.12** is cleaved in plasma with $t_{1/2} = 54$ min, which can be overcome by the esterase inhibitor diisopropylfluorophosphate ($t_{1/2} = 475$ min) (Amsberry, *et al.*, 1991). Key features of this prodrug are its good buffer stability and its rapid bioreversibility.

The elegance of the trimethyl lock is in its modularity. Most of the synthetic effort is exerted in parallel to the molecule of interest. As a result, appending the trimethyl lock can be as easy as a peptide conjugation. Additionally, one triggering moiety can be exchanged for another to alter spatial and temporal aspects of lactonization (Amsberry, *et al.*, 1991).

1.2.1 Cyclic Peptide Prodrugs Improve Bioavailability and Enzymatic Stability

The benefits of trimethyl lock amide prodrugs are evident in cyclic peptide prodrug **1.15** (Figure 1.6) (Wang, *et al.*, 1997). The increased steric bulk of the peptidic ester **1.15**, compared to acetyl ester **1.12** slowed the rate of ester hydrolysis in human plasma from $t_{1/2} = 508$ min to 54 min, providing a means to tune the peptide-release rate (Amsberry, *et al.*, 1991; Wang, *et al.*, 1997). A significant advantage in using a cyclic prodrug became apparent when comparing the stability of the cyclic peptide **1.15** to its linear counterpart. The linear peptide was degraded by peptidases in plasma with a half-life of only 3.7 min. Moreover, the linear peptide had poor oral bioavailability. In Caco-2 cells, an *in vitro* model of intestinal mucosa, the linear peptide permeated a monolayer of

cells 70-fold less efficiently than the cyclic peptide. Whereas some of the poor permeation by the linear peptide was a result of enzymatic degradation, peptidase inhibitors did not enhance permeation to the level of the cyclic peptide (Wang, *et al.*, 1997).

The trimethyl lock provided a potential means to utilize peptides as pharmaceuticals. Biologically active peptides could be made resistant to enzymatic degradation and be made permeable to the intestinal mucosa through cyclization. Importantly, the trimethyl lock accomplished the release of free peptides, with no residual atoms from a protecting group.

1.2.2 PEG Prodrugs

The cytotoxic nature of chemotherapeutics, often used in the treatment of cancer, necessitates careful dosing to prevent harmful side effects. Chemotherapeutics kill normal cells to an appreciable extent that may not vary much from their ability to kill cancerous cells. This ratio of toxic to therapeutic concentrations of a drug is called the therapeutic index, and is usually low for chemotherapeutics. Ideally, a drug is dosed such that the time that a drug is above the therapeutic concentration is maximized, while the time above the toxic concentration is minimized.

Some of the barriers to effective drug plasma concentrations are renal filtration, metabolism, toxicity, solubility, and specificity. Derivatives of drugs may be synthesized to overcome some of these barriers. There are two main types of derivatives, reversible and irreversible. Irreversible derivatives typically modify pharmacokinetic properties

without affecting a drug's activity, because the derivative cannot be cleaved. Some applications stipulate a drug's activity to be blocked until being activated with temporal-spatial control, requiring a reversible derivative, also known as a prodrug. Reversible and irreversible derivatives must be accommodating to the various types of functionalities that may be present in drugs.

Poly(ethylene glycol), or PEG, is a water-soluble, flexible polymer that has been used to improve the properties of pharmaceuticals. Appending a small molecule drug to a high molecular weight polymer has two main effects: decreased renal clearance and increased tumor retention (Maeda, *et al.*, 2001). Polymers are too large to fit through the renal filtration slits and therefore cannot be cleared by the kidneys. Rapid renal elimination dictates frequent dosing and produces steep fluctuations in the plasma concentration of a drug over time, thus it is harder to maintain an effective, non-toxic concentration. Extending the circulation time of a drug abates the fluctuations in its plasma concentration. On the other hand, increased tumor retention of a polymer is explained by the enhanced permeability and retention (EPR) effect (Maeda, *et al.*, 2001). Tumors may have greater vascular permeability and reduced lymphatic drainage compared to normal tissues leading to an accumulation of macromolecules (Greenwald, *et al.*, 2000). Thus, PEG conjugates can potentially lower the required dose of a drug since the conjugate would accumulate at the desired site.

PEG conjugates, alone, may not alleviate all obstacles to dosing a chemotherapeutic. The locally high concentration of a chemotherapeutic at the injection site may cause adverse effects, thus presenting a limitation to the administered dose and possibly the

efficacy. A drug may be inactivated to prevent mechanism-based toxicity, but any modification must be reversible to maintain efficacy. A bioreversible PEG-conjugate has the potential to evade renal filtration, to accumulate in a tumor, and to increase therapeutic index owing to the active drug only being released at the desired location.

Greenwald and coworkers synthesized PEG derivatives of the cytotoxic drug daunorubicin **1.17** (Table 1.1) with cleavable trimethyl lock linkers (Greenwald, *et al.*, 2000). PEG (40 kDa) was conjugated to different amino acid spacers and then appended to the trimethyl lock through a labile ester bond. Upon hydrolysis, unmodified daunorubicin was released. As expected, some of the daunorubicin PEG-trimethyl lock conjugates showed improved efficacy over daunorubicin alone in balb/c mice with subcutaneous Madison lung carcinoma. The modularity of the trimethyl lock allowed many derivatives to be synthesized that varied in half-life in rat plasma from 12 to >1440 min. Daunorubicin, alone, was effective when administered intraperitoneally (i.p.); however, it was lethal in 17% of the mice. Daunorubicin had no efficacy or toxicity when administered intravenously (i.v.), presumably because it was rapid cleared by the kidneys. Compound **1.18**, containing an alanine ester spacer had a plasma half-life of 114 min and was modestly effective when dosed i.p. or i.v, with no observed toxicity. Compounds with shorter half-lives were toxic when dosed i.p., but not i.v. — compound **1.19**: $t_{1/2}$ = 12 min, 83% lethal i.p.; compound **1.20**: $t_{1/2}$ = 66 min, 66% lethal i.p. The compound with the greatest efficacy contained an aminopropionic ester linker and incorporated *ortho* steric hindrance into the trimethyl lock (compound **1.21**) to increase

the plasma half-life to 480 min. When dosed i.v., mean tumor volume was only 31.6% relative to that of the control.

Curiously, neither *in vitro* IC_{50} nor plasma half-life correlated well with *in vivo* efficacy. It was apparent that an important feature of the trimethyl lock was its modularity. Many derivatives could be synthesized, in parallel, and tested *in vivo* to determine the most efficacious compound with the lowest toxicity.

1.2.3 Oral Bioavailability in Ganciclovir Prodrug

Ganciclovir is a DNA polymerase inhibitor that is used to treat cytomegalovirus (CMV) infections. Interestingly, ganciclovir, itself, is a prodrug, and must be phosphorylated by viral thymidine kinase for activity. Ganciclovir has very poor oral bioavailability, and requires large doses to have efficacy (Dillon, *et al.*, 1996).

Maag and coworkers synthesized a pro-pro-prodrug of ganciclovir incorporating the trimethyl lock to improve its bioavailability (compound **1.22**, Figure 1.7) (Dillon, *et al.*, 1996). Their strategy was somewhat atypical in that they used the trimethyl lock to mask an alcohol, effectively adding two ester bonds where the hydrolysis of one ester triggered rapid scission of the second. Two ganciclovir derivatives were synthesized and oral bioavailability was measured in rats. Free ganciclovir had a bioavailability of 3.6%, while the acetyl trimethyl lock ester **1.22** had a bioavailability of 15.6%. The benzyl trimethyl lock ester **1.23**, which was more enzymatically stable than the acetyl trimethyl lock ester **1.22**, was not bioavailable, meaning no free ganciclovir was detected in the plasma. This control confirmed that acetyl ester hydrolysis did not occur before absorption.

Additionally, it meant that the trimethyl lock trigger must have led to the release of free ganciclovir, not hydrolysis of the trimethyl lock ester directly.

In the time since publication by Maag and coworkers, Roche Global Development received FDA approval in 2001 for valganciclovir, a valine ester of the same hydroxyl that was modified in ganciclovir. Valganciclovir has an oral bioavailability of approximately 60% in humans (NDA 21-304). The success of valganciclovir demonstrates the importance of considering many options when developing bioreversible drug derivatives.

1.2.4 Water-Soluble Prodrugs of Paclitaxel and Other Chemotherapeutics

Taxol (generic name paclitaxel), a natural product from the western yew, is a cytotoxic drug specific to cancerous cells (Wani, *et al.*, 1971). Unfortunately, paclitaxel is poorly soluble in water and requires solubilizing agents, such as polyethoxylated castor oil and ethanol, which may lead to much of the adverse effects of the formulation (Rowinsky, *et al.*, 1990). Attempts had been made to generate more soluble derivatives of paclitaxel, including phosphorylation of the C-2' or C-7 hydroxyl positions (compounds **1.24** and **1.25**, Figure 1.8) (Vyas, *et al.*, 1993). While the authors were successful in increasing the solubility of paclitaxel, the phosphate moieties could not be hydrolyzed by alkaline phosphatase or by plasma, resulting in no efficacy against tumors. It was speculated that the phosphates were too hindered by the paclitaxel ring core to be good substrates for phosphatases.

The same laboratory synthesized the analogous derivatives of paclitaxel that contained phosphate trimethyl locks (**1.26** and **1.27**) in the place of phosphates **1.24** and **1.25** (Nicolaou, *et al.*, 1996b; Ueda, *et al.*, 1993). The rationale was that a pendant trimethyl lock would be more accessible to phosphatases and be rapidly cleaved to release active paclitaxel. Aryl phosphates generally should be more labile than a phosphate of a secondary or tertiary alcohol. Both phosphate trimethyl lock derivatives had vastly enhanced water solubility, >10 mg/mL compared to approximately 2 μg/mL at 37 °C for unmodified paclitaxel (Dordunoo and Burt, 1996). Both derivatives were able to be cleaved by alkaline phosphatase *in vitro*, but strangely, were resistant to cleavage in plasma. Binding of the drug to albumin in serum possibly sequestered it from phosphatases. Despite this result, compound **1.27** displayed comparable efficacy to paclitaxel against the M109 tumor model in mouse xenografts, and required no solubilizing agents in its formulation.

The same phosphate trimethyl lock was applied to a novel antitumor analog of combretastatin A-4 (**1.28**, Figure 1.8) (Nam, *et al.*, 2003). Improving water solubility led to an increase from 59% to 75% in the inhibition rate of the mean tumor volume versus controls of subcutaneous 3LL tumors in BDF1 mice. The efficacy of compound **1.28** approached that of etoposide (79%), an approved chemotherapeutic, but displayed little toxicity, corroborated by weight gain of the mice.

The trimethyl lock was utilized to improve water solubility, and potentially the toxicity profile, of paclitaxel and combretastatin A-4, by introducing a labile phosphate moiety. The phosphate trimethyl lock conferred similar cleavage profiles regardless of

what position it was used to mask, effectively insulating solubilization from lability. A water-soluble formulation of paclitaxel, Abraxane (paclitaxel bound to albumin), was approved by the FDA in 2005 for the treatment of metastatic breast cancer in patients that had failed combination chemotherapy (NDA 21-660).

1.2.5 Tissue Specificity Conferred by Trimethyl Lock Prodrugs

Borchardt and coworkers developed a trimethyl lock derivative that was activated not by hydrolysis, but by reduction of a quinone **1.29** (Figure 1.9) to a hydroquinone (**1.30**) for use in amide prodrugs (Amsberry and Borchardt, 1991). Reduction to the hydroquinone led to rapid lactonization, similar to other trimethyl lock compounds. Contrary to other trimethyl locks, primary aromatic amides were not stable due to conjugate addition of the amidic nitrogen into the quinone, thereby forming a fused ring system (Nicolaou, *et al.*, 1996a).

Release of a prodrug in a reducing environment would be quite beneficial for tumor-specificity. Many tumors have higher expression of reductase enzymes as well as lower oxygen tension than normal cells (Lee, *et al.*, 1998). Temporary inactivation of a cytotoxic drug with a labile quinone trimethyl lock could potentially increase the therapeutic index by targeting the drug specifically to tumors (Naughton, 2001).

Weerapreeyakul and coworkers extensively studied the quinone trimethyl lock system in its ability to cross lipid bilayers, and to be activated through reduction (Gharat, *et al.*, 2001; Weerapreeyakul, *et al.*, 2007). Quinone trimethyl lock derivatives of four cytotoxic compounds (**1.32–1.35**) isolated from fungi were synthesized. Their cytotoxicity was

tested against various reducing and non-reducing cell lines *in vitro*. While the cytotoxicity was lower toward normal cells, unfortunately, cytotoxicity was also reduced toward cancerous cells. Some evidence indicated that the quinone trimethyl lock was, indeed, being reduced, hence there might have been more efficacy *in vivo*, warranting further experiments. This construct may be amenable to gene-directed enzyme prodrug therapy (GDEPT) or antibody-directed enzyme prodrug therapy (ADEPT) utilizing DT-diaphorase, nitroreductase, or other reductases (Denny, 2002; Fu, *et al.*, 2005; Knox, *et al.*, 1993).

1.3 Trimethyl Lock Fluorogenic Enzyme Substrates

Fluorescence of the xanthene dye, rhodamine 110 (**1.37**, Figure 1.10), has been masked through acylation of its amines (Leytus, *et al.*, 1983). Modification of the acyl groups, for example, by incorporating various amino acid sequences has generated numerous peptidase substrates (**1.36**) (Beija, *et al.*, 2009). Raines and coworkers sought to develop novel fluorescent esterase substrates, but were limited by the requirement of an amide linkage to mask the fluorescence of rhodamine 110 (Chandran, *et al.*, 2005). The trimethyl lock (**1.38**) provided a convenient means to achieve esterase-mediated amide bond cleavage, thereby expanding the scope of reactions that could trigger fluorescence development. Since the initial publication of compound **1.38**, numerous fluorescent substrates have been developed. Fluorescence development can be triggered

through a variety of enzymatic and non-enzymatic methods, including hydrolysis, oxidation, reduction, and photocleavage, which will be discussed below.

1.3.1 Esterase-Activated Fluorophores

Figure 1.11 depicts the activation of rhodamine trimethyl lock **1.38** by non-specific esterases that was developed in our laboratory (Chandran, *et al.*, 2005). Acylation of the amine groups of rhodamine 110 removed electron density from the conjugated system and led to lactone formation through nucleophilic attack of the carboxylate into the quinonemethide-like carbon. This lactone formation interrupted the conjugation across the ring system, and therefore reduced the quantum yield to 0. Hydrolysis of one of the amides allowed the amine to donate electron density back into the ring, which opened the lactone and partially restored fluorescence. Hydrolysis of the second amide fully restored fluorescence, equivalent to the initial value of rhodamine 110 (**1.37**). This system was perfectly adapted for use as a fluorogenic enzyme substrate.

Lorey and coworkers found that desymmetrization of rhodamine 110 by appending only one peptidase substrate resulted in simplified (one-hit) kinetics and allowed functionalization of the second amine with biological handles (Lorey, *et al.*, 2002). Our laboratory adapted this strategy, substituting peptidase substrates for the trimethyl lock to generate esterase substrates (**1.39** and **1.40**, Figure 1.12), and found that functionalizing the second amine with a urea, as opposed to an amide, led to higher quantum yields of the product fluorophore (Lavis, *et al.*, 2006a). Additionally, mono(trimethyl lock) rhodamines displayed faster rates of fluorescence generation following esterase activation

than did di(trimethyl lock) rhodamines. Despite a potentially greater fluorescence increase following a second cleavage for di(trimethyl lock) systems, the intermediate zwitterionic rhodamine derivative was a poorer substrate. As a result, utilizing mono(trimethyl lock) rhodamines permitted the remaining urea to be functionalized with maleimide or succinimide linkers (**1.39** and **1.40**) for conjugation to biomacromolecules (Lavis, *et al.*, 2006a; Watkins, *et al.*, 2009). These substrates were used to track the internalization of exogenously applied proteins into esterase containing endosomes,(Chao, *et al.*, 2010; Lavis, *et al.*, 2006a; Turcotte, *et al.*, 2009) to label expressed proteins specifically using the HaloTag system (Promega) (Watkins, *et al.*, 2009), or to image the trafficking of cell-surface receptors using polymers containing multivalent recognition elements (Mangold, *et al.*, 2008).

While other fluorogenic and chromogenic substrates for esterases are available, such as fluorescein diacetate, methylumbelliferyl acetate, and *p*-nitrophenyl acetate, they suffer from two main setbacks: poor stability, and pH-sensitivity (Lavis, *et al.*, 2006a; Levine, *et al.*, 2008). The amine-derivatives rhodamine 110, aminomethyl coumarin, or *p*-nitroaniline eliminate pH sensitivity; however, direct acylation of these compounds is not bioreversible by esterases. Acylation through installation of the trimethyl lock to form a stable amide linkage masks the signal of these compounds and is labile to esterases. The acetyl ester of the trimethyl lock has much greater chemical stability to hydrolysis than do the acetyl esters of fluorescein, methylumbelliferone, or *p*-nitrophenol, presumably due to a higher pK_a of the conjugate acids of the leaving groups after hydrolysis

(trimethyl lock ≈ 10.3 versus 6.3, 7.8, and 7.1 respectively) (Lavis, *et al.*, 2006a; Lavis, *et al.*, 2006b; Levine, *et al.*, 2008).

Additionally, our laboratory was able to mask the fluorescence of aminomethyl coumarin and cresyl violet with the same esterase-cleavable trimethyl lock to generate blue and red excited fluorgenic esterase substrates (**1.41** and **1.42**, Figure 1.13) (Lavis, *et al.*, 2006b). We also synthesized a chromogenic esterase substrate **1.43** by masking *p*-nitroaniline with the trimethyl lock, generating a potential high throughput screening agent with greater *in vitro* stability than *p*-nitrophenyl acetate (Levine, *et al.*, 2008).

1.3.2 DT-Diaphorase Fluorogenic Substrates

Huang and coworkers have developed fluorogenic substrates for a tumor-enriched enzyme, DT-diaphorase, utilizing the quinone trimethyl lock (Huang and Lin, 2006; Huang, *et al.*, 2008). DT-diaphorase is a quinone reductase that may be upregulated in cancer cells, and has become a popular target for high-throughput screening for drug discovery. A di(quinone trimethyl lock) rhodamine 110 derivative **1.44** (Figure 1.14) was synthesized that could be used to search for high-affinity DT-diaphorase substrates. In addition, a long-wavelength coumarin derivative **1.45** (λ_{em} = 595 nm) was masked with a single quinone trimethyl lock to improve upon the two-hit kinetics of the di(trimethyl lock) rhodamine 110 substrate **1.44** and to broaden the scope of applications.

In addition to its individual importance, DT-diaphorase requires NADH as a cofactor, thus it can be used in coupled assays for enzymes that generate NADH, such as dehydrogenases. Huang and coworkers used either of the two novel DT-diaphorase

substrates to assay glucose-1-dehydrogenase, glucose-6-phosphate dehydrogenase/phosphoglucomutase, or 3-hydroxybutyrate dehydrogenase. Of note, the assays were insensitive to atmospheric oxygen concentrations, distinguishing them from known coupled assays for these enzymes.

1.3.3 Cytochrome P450 Fluorogenic Substrate

Cytochrome P450 enzymes (P450) are the principal metabolizers of pharmaceuticals and environmental toxins. As such, understanding their activity and regulation is important to pharmacology, oncology, and toxicology. P450 enzymatic activity is typically measured using chromatographic methods. The available fluorogenic substrates, 7-ethoxycoumarin and 7-ethoxyresorufin, are oxidatively dealkylated by P450 enzymes to yield a fluorescent molecule; however, the substrates possess a small amount of fluorescence, resulting in high background (Farinas, *et al.*, 2001).

Our laboratory synthesized an ethyl ether of the trimethyl lock to serve as a substrate for the cytochrome P450 isozyme CYP1A1 (Yatzeck, *et al.*, 2008). The trimethyl lock masked the fluorescence of rhodamine 110 through an amide linkage (**1.46**, Figure 1.15), circumventing the problem of partial masking of fluorescence by direct alkylation of coumarin or resorufin. The mechanism of fluorescence development is depicted in Figure 1.15. CYP1A1 employed its iron protoporphyrin IX to activate molecular oxygen, inserting a single oxygen atom onto the carbon adjacent to the ether oxygen of the trimethyl lock substrate. The generated hemiacetal **1.47** spontaneously decomposed to

acetaldehyde and the free trimethyl lock **1.48**, which rapidly lactonized with concomitant release of the fluorescent rhodamine **1.49** (Farinas, *et al.*, 2001; Yatzeck, *et al.*, 2008).

CYP1A1 is mainly localized to the lungs, where it is believed to metabolize many compounds found in cigarette smoke into potent carcinogens (Houlston, 2000). Cigarette smoke induces the expression of CYP1A1, as does the toxin 2,3,7,8-tetrachlorodibenzo-*p*-dioxin (TCDD), a contaminant in the defoliant Agent Orange. Utilizing substrate **1.46**, induction of CYP1A1 could be visualized *in cellulo* in lung adenocarcinoma cell line A549. Additionally, inhibition of CYP1A1 activity could be observed after the addition of resveratrol, a putative anticancer agent. Substrate **1.46** has many potential applications in medicinal chemistry, biotechnology, and diagnostics due to the significance of the P450 enzymes.

1.3.4 Alkaline Phosphatase Substrates

Alkaline phosphatase from *Escherichia coli* is a widely used enzyme for enzyme-linked immunosorbant assays (ELISAs) and as a model for other phosphomonoesterases (Cleland and Hengge, 2006; Porstmann, *et al.*, 1985). Phosphate exhibits potent product inhibition on alkaline phosphatase, $K_i \approx 1$ μM, which explains the wide variation of kinetic data in the literature (O'Brien and Herschlag, 2002). Assays of alkaline phosphatase activity must be sensitive enough to detect product at concentrations much lower than 1 μM. Fluorogenic and luminogenic assays are preferable due to higher sensitivity, yet, many common phosphatase substrates are subject to the same limitations as the esterase substrates discussed above: two-hit kinetics, chemical instability and pH-

sensitivity (Robinson and Willcox, 1969). To improve upon these properties, the phosphate trimethyl lock was appended to amine-containing reporters, such as aminoluciferin (Zhou, *et al.*, 2008) or morpholinourea rhodamine (Levine and Raines, 2011).

Aminoluciferin is oxidized by luciferase in the presence of oxygen and ATP through a process that emits energy as light, and can be used for coupled bioluminogenic assays. Masking the amino group of aminoluciferin generates a molecule that is not a substrate for luciferase (**1.50** Figure 1.16). Hydrolysis of the masking group by alkaline phosphatase releases free substrate that can be measured utilizing a coupled luminescence assay. A common substrate, 6-luciferin phosphate is prone to non-enzymatic hydrolysis, a result of the low pK_a of the conjugate acid of the leaving group, luciferin. The luciferin released prior to the addition of alkaline phosphatase leads to high background luminescence in luciferase assays. Phosphate trimethyl lock substrate **1.50** contains a stable amide linkage, eliminating background signal.

The same principles for improving luminescent alkaline phosphatase substrates can also be applied to fluorogenic substrates. Morpholinourea rhodamine, as discussed above, emits bright, pH-insensitive fluorescence at wavelengths useful for biological assays. Compound **1.51** improves upon the properties of similar fluorogenic phosphatase substrates, such as fluorescein diphosphate and methyl umbelliferyl phosphate. Additionally, compound **1.51** can be used for continuous assays of alkaline phosphatase activity.

1.4 Biological Switches

1.4.1 Modulating Subcellular Localization

The ability to toggle the function of a peptide or protein in cells has the potential to be a powerful tool in chemical biology. Photoswitching increases the scope of possibilities even further by imparting temporal control onto cellular functions. In an elegant manner, Otaka and coworkers incorporated the trimethyl lock design into a photoactivated "nucleocytoplasmic shuttle peptide" (**1.52**, Figure 1.17) (Shigenaga, *et al.*, 2007). They were able to shift the subcellular localization of a peptide from the nucleus to the cytoplasm by exposing cells to UV light.

The key to this strategy was the bifunctionalization of the trimethyl lock by α-amination of its carbonyl, essentially transforming the trimethyl lock into a non-native *o*-hydroxyphenylalanine derivative. The phenoxide was masked with an *o*-nitrobenzyl ether, a UV-photocleavable moiety. The N-terminus of the trimethyl lock amino acid was elaborated with a cationic cell penetrating peptide (CPP) sequence and nuclear localization signal (NLS). The cleavable C-terminus was conjugated to a complex peptide. The first amino acid, serine was modified through an O-acyl isopeptide incorporating half of functionally suppressed nuclear export signal (NES) and a fluorescent marker (FITC). The second half of the NES was conjugated through a native peptide bond to the C-terminus of the serine.

Addition of peptide **1.52** (Figure 1.18) to a cell resulted in internalization, due to the CPP, after which it diffused throughout the cytoplasm and the nucleus, due to the NLS.

Upon UV-irradiation, the nitrobenzyl ether was cleaved, releasing the free phenoxide, which rapidly lactonized to release cleaved-peptides **1.53** and **1.54**. An O–N acyl shift of **1.54** generated the functional NES **1.55** resulting in exclusion of the peptide from the nucleus.

Additional derivatives of this system were developed to allow cleavage with two-photon infrared light, as opposed to UV cleavage, which may be toxic to cells (Shigenaga, *et al.*, 2010c). A FRET-based assay was developed to determine the optimal amino acid sequence to accelerate the cleavage reaction (Shigenaga, *et al.*, 2009). Finally, an enantioselective synthesis of the non-natural trimethyl lock amino acid was developed to improve its functionality by eliminating the inappropriate enantiomer (Shigenaga, *et al.*, 2010b).

1.4.2 Triggered DNA Release

Otaka and coworkers utilized their bifunctionalized trimethyl lock to synthesize not only cleavable peptides, as discussed above, but also cleavable peptide nucleic acids (PNAs) (Shigenaga, *et al.*, 2010a). PNAs are polymers with repeating nucleotide bases that are linked by a polyamide backbone, as opposed to the native (deoxy)ribose–phosphate backbone (Nielsen, *et al.*, 1991). PNAs are capable of hybridizing with native DNA or RNA to form stable conjugates, which may be able to cross cell membranes. Delivery of DNA or RNA into a cell is necessary for gene therapy, transfection, and RNAi. Viruses are sometimes used for nucleic acid delivery, but there is a chance of infecting the host cells or delivering parts of the viral genome in addition to the desired

oligonucleotides. Development of chemical means to selectively deliver DNA or RNA to cells with high efficiency is a valuable goal.

Otaka and coworkers added a short PNA sequence to both termini of their trimethyl lock amino acid **1.56** (Figure 1.19). In this derivative, the trigger was not photocleavage, but was thiol-promoted cleavage of a *p*-nitrosulfonyl ester. The PNA trimethyl lock, containing eight thymine bases, was hybridized to nonadeoxyadenosine. Upon cleavage of the *p*-nitrosulfonyl ester by thiols, the resultant phenol lactonized to release 4 of the 8 PNA monomers, lowering the T_m from 25 °C to below 10 °C. Free nonadeoxyadenosine was released. Thiols such as glutathione are abundant in the cytoplasm of cells, hence compounds similar to PNA construct **1.56** may be able to selectively deliver oligonucleotides to cells and then release them upon cellular internalization.

1.4.3 Redox-Triggered Contents Release from Liposomes

Liposomes are artificial vesicles of lipid bilayers that can encapsulate a drug to enhance drug targeting and delivery (Guo and Szoka, 2003). Two requirements of successful liposome–drug formulations are: (1) the drug must not be released by the liposome prematurely and (2) the drug must be released at therapeutic concentrations at the target tissue. These two requirements are not mutually excusive; increasing liposome stability decreases premature release but hampers therapeutic release. A triggered release system provides the means to satisfy both conditions.

Common mechanisms of triggered release from liposomes include pH-triggered and reduction-triggered release (Guo and Szoka, 2003). As endosomes mature, the pH is

lowered from 7.4 in plasma to as low as 5.5 in late endosomes (Gruenberg and Maxfield, 1995). Chemical changes or cleavage reactions induced by lowered pH in these compartments can trigger liposome disruption and release of contents. Reduction by thiols in the cytoplasm of cells is another mechanism of triggered release. Redox-triggered release, independent of thiols, is attractive because solid tumors are believed to have increased reductase activity and increased reducing potential, as discussed above (Lee, *et al.*, 1998).

McCarley and coworkers devised a liposome delivery system that could release its contents after entering a reducing environment, such as a solid tumor (**1.57**, Figure 1.20) (Ong, *et al.*, 2008). A quinone trimethyl lock was used to N-acylate dioleylphosphatidylethanolamine (DOPE), modifying both the charge and the shape of the lipid. *N*-Acylated DOPE formed liposomes which encapsulated a self-quenching fluorophore. Upon reduction of the quinone trimethyl lock, the developed hydroquinone lactonized to release DOPE, allowing a transition in the lipids from lamellar to inverted micellar phase (Siegel and Epand, 1997). The instability introduced by DOPE led to decomposition of the liposomes, releasing the contents, measured by an increase in fluorescence upon relief of self-quenching.

The stability of the trimethyl lock caged liposomes was utilized to mediate drug delivery by modulating the identity, and hence, the behavior of lipids. Contents-release was triggered by an endogenous signal and would have the potential to encapsulate chemotherapeutics in the future. Besides its application in drug delivery, this lipid system can be used as a research tool to study membrane dynamics and trafficking.

1.5   Solid-Phase Synthesis Resin Linkers

1.5.1 Peptide Synthesis Resin Cleaved Under Mildly Reducing Conditions

Merrifield's synthesis of the entire enzyme ribonuclease A, composed of 124 amino acids, paved the way for solid phase synthesis as an invaluable chemical tool (Gutte and Merrifield, 1971). Since then, the synthesis of non-natural peptides, PNAs and oligonucleotides has placed an ever-increasing demand for the development of new solid phase resins. In particular, resins that can be cleaved orthogonally in the presence of protecting groups, or delicate functional groups are required for the litany of experiments that researchers seek to perform.

Wang and coworkers developed a new solid phase synthesis resin, based on the quinone trimethyl lock (**1.61**, Figure 1.21), that could be cleaved using mild reducing agents, a reaction that was orthogonal to common protecting groups (Zheng, *et al.*, 1999). The trimethyl lock was bifunctionalized by performing a Claisen rearrangement of allyl hydroquinone **1.58**. Upon protection of the hydroquinone **1.59** hydroxyl and oxidation of the olefin over three steps, the generated carboxylic acid was reacted with a polystyrene linker containing a benzyl amine functionality to generate compound **1.60**. Removal of the protecting group followed by oxidation to the quinone yielded the resin **1.61**.

The trimethyl lock, normally conjugated to the *N*-terminus of a peptide, is not compatible with solid-phase peptide synthesis, in which conjugation reactions proceed in a C-to-N direction. As a result, this system was designed for the synthesis of C-terminal

modified peptides to convert the carboxyl functionality of the resin to an amine. The resin was charged with *N*-Boc-ethanolamine, which was incorporated into the C-termini of the synthesized peptides.

The key feature of this resin **1.61** was the mechanism of peptide cleavage. Sodium hydrosulfite, a mild reducing agent, reduced the quinone trimethyl lock to the hydroquinone, which lactonized to release the ethanolamine-modified peptide. *N*-terminal Boc protecting groups survived the cleavage process, indicative of the utility of this resin. An additional attractive attribute, the cleavage reaction progress could be monitored colorimetrically by observing the disappearance of the yellow quinone.

Wang and coworkers had success in developing a reductively cleavable resin that could release an unmodified C-terminal peptide (Shan, *et al.*, 2000). It was believed that utilizing a trimethyl lock that released a peptide based on nucleophilic substitution rather than acyl substitution would be compatible with generating unmodified peptides. To accomplish this, compound **1.62**, containing a free hydroxyl that could be conjugated as an ester with amino acids, was designed based on the some of the earliest trimethyl lock work (Borchardt and Cohen, 1972a). Unfortunately, this compound was not stable, and underwent intramolecular nucleophilic attack of the free alcohol to the conjugated olefin (as in **1.63**) or the carbonyl (as in **1.64**, Figure 1.21). This complication was overcome by charging the alcohol **1.65** with the first amino acid prior to oxidation of hydroquinone **1.66** to quinone **1.67**. Due to the oxidation step, peptides which could be synthesized were limited to those that did not contain cysteine or methionine in the C-terminal position. Cleavage of the peptide from the trimethyl lock required two steps: reduction to

the hydroquinone **1.68** followed by cyclization to **1.69** initiated by the addition of tetrabutyl ammonium fluoride (TBAF). The additional steps were not detrimental, as all synthetic steps and cleavage reactions proceeded with high yield.

Wang and coworkers developed two trimethyl locks that can potentially be used as resins for solid-phase synthesis of C-terminal modified and unmodified peptides. Peptides were cleaved under mildly reducing conditions, allowing sensitive functionalities and protecting groups to be incorporated.

1.5.2 Oligonucleotide Synthesis Resin for Synthesis of 3'-Phosphorothioate Monoesters

The synthesis of 3'-phosphate and phosphorothioate modified oligonucleotides is important for elucidating enzymatic mechanisms, synthesizing circular oligonucleotides, and appending reporter molecules (Cheruvallath, *et al.*, 2003). Many of the existing methods for the syntheses of these compounds require multiple deprotection steps or harsh conditions. Ravikumar and coworkers developed a solid phase resin for the synthesis of 3'-phosphorothioate oligonucleotides that could be cleaved in a single step using ammonia.

The trimethyl lock was modified such that it was conjugated to an oligonucleotide through a phosphoester bond (**1.70**, Figure 1.22). Upon cleavage of the ester, cyclization proceeded by intramolecular nucleophilic substitution, with concomitant release of the 3'-phosphorothioate oligonucleotide. This trimethyl lock was similar to **1.67**, described in the previous section (Borchardt and Cohen, 1972a; Shan, *et al.*, 2000); although, the rate

of reaction here was promoted by the favorable leaving group, phosphate or phosphorothioate, and proceeded spontaneously. Resin **1.70** provided a novel method for the practical synthesis of 3′-phosphorothioate oligonucleotides.

1.6 Conclusions

The trimethyl lock has been employed in medical, chemical, biochemical, and biological applications. The trimethyl lock provides excellent stability of conjugates until a desired triggering reaction occurs, then rapidly undergoes scission. The modularity, ease of synthesis, and predictable kinetics are major benefits of the trimethyl lock. It is an important addition to the toolbox of prodrug strategies, providing helpful insights into stability, bioavailability, specificity, and solubility. Incredibly, the trimethyl lock can be used to synthesize peptides, make them bioavailable, trace their cellular internalization with fluorophores, and switch their function once inside cells. We anticipate that the list of trimethyl lock applications will continue to expand due to its versatility.

Acknowledgements

Figure 1.1   Structure of the trimethyl lock and mechanism of lactonization

X   = O,NH
R^1 = labile moiety
R^2 = drug, peptide, fluorophore
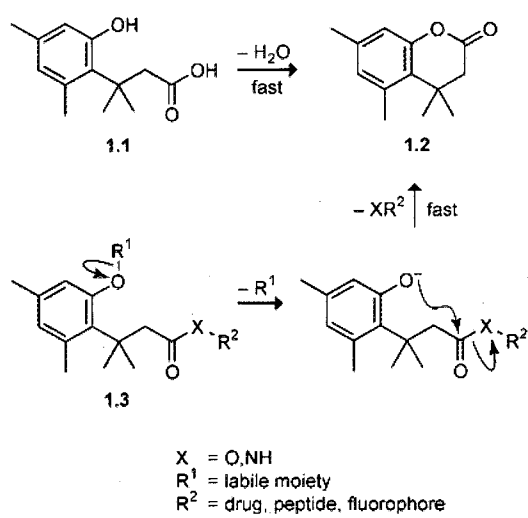
Figure 1.2   Rate acceleration in the trimethyl lock system

1.4	**1.5**	**1.6**	**1.1**
1.00	1.05	4400	10^{11}

Lactonization rate constant (rel.)
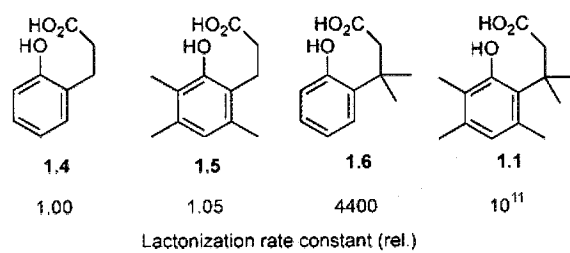
Figure 1.3   1969 model for oxidative phosphorylation. Adapted from (Thanassi and

Cohen, 1969).
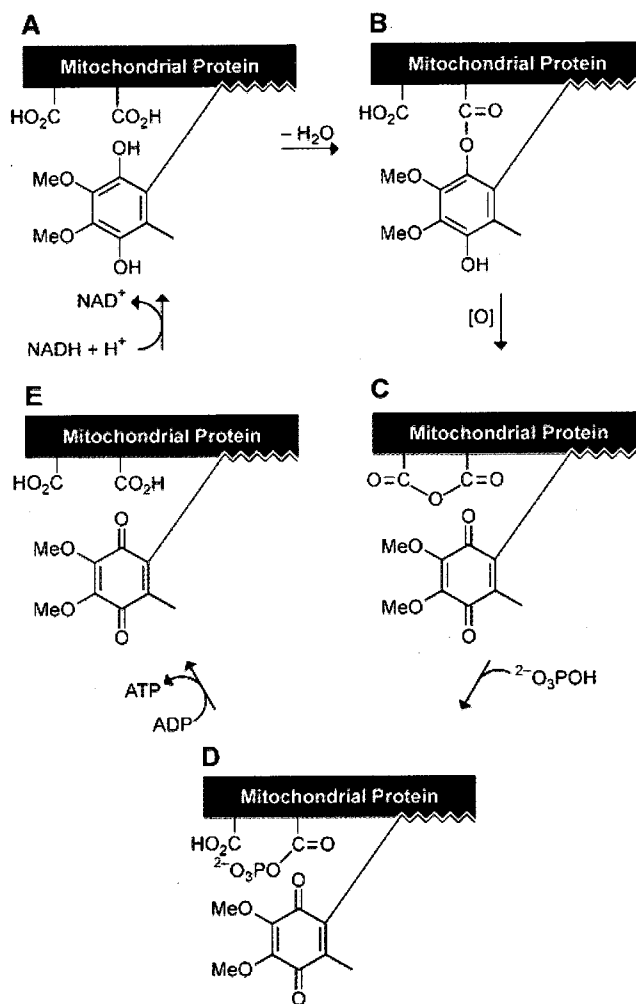
Figure 1.4   Quinone trimethyl locks with solved crystal structures

1.7

1.8 R = OH
1.9 R = NHCH$_2$Ph
1.10 R = N(CH$_3$)CH$_2$Ph
1.11 R = NHPhF
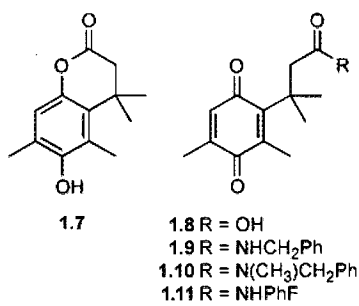
Figure 1.5   Esterase-activated prodrug

1.12

1.13

1.2

1.14
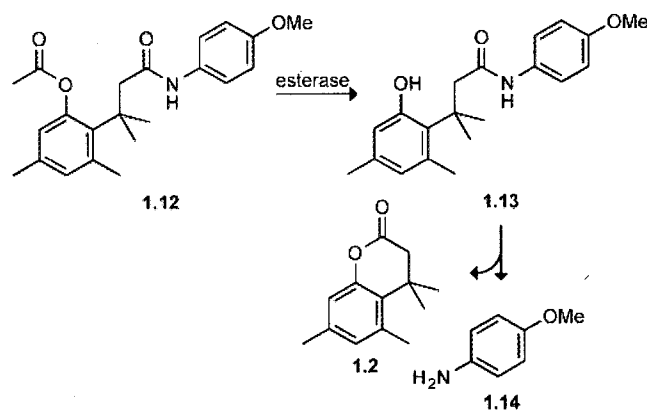
Figure 1.6   Cyclic-peptide prodrug based on the trimethyl lock

1.15   esterase   **1.16**   **1.2**

$$H_3\overset{+}{N}-Trp-Ala-Gly-Gly-Asp-Ala\cdot CO_2^-$$
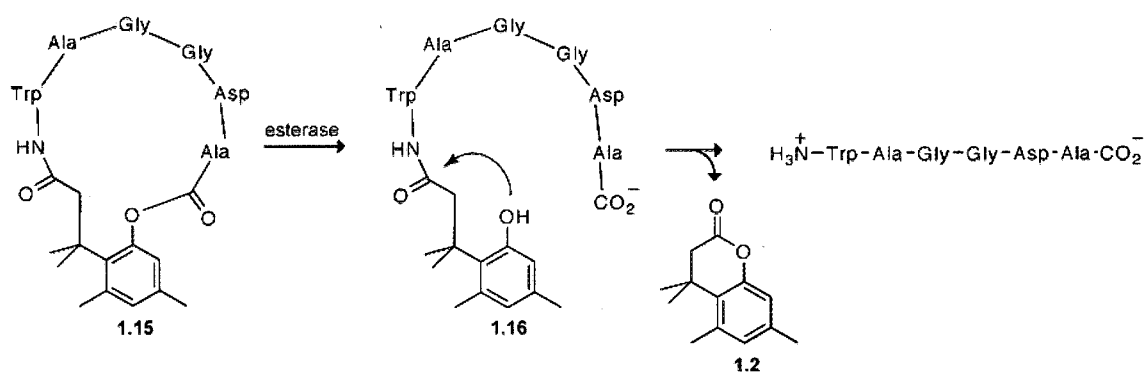
Figure 1.7   Bioavailability is increased in trimethyl lock ganciclovir prodrugs
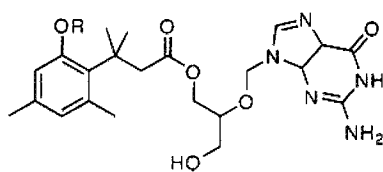
1.22 R = Ac

1.23 R = Bn

Figure 1.8   Phosphate prodrugs of paclitaxel and combretastatin A-4 to increase

solubility
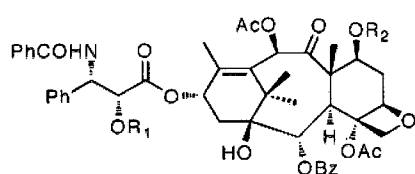
1.24 R$_1$ = P$_i$, R$_2$ = H
1.25 R$_1$ = H, R$_2$ = P$_i$
1.26 R$_1$ = TML, R$_2$ = H
1.27 R$_1$ = H, R$_2$ = TML

1.28 R$_3$ = TML

TML =

P$_i$ = $\{$—PO$_3{}^{2-}$
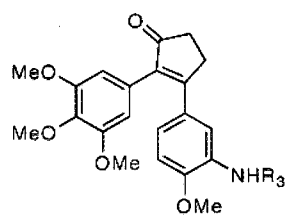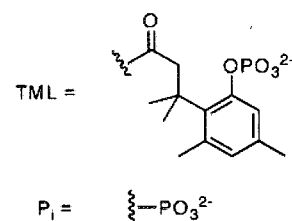
Figure 1.9 Mechanism of quinone trimethyl lock activation and structure of cytotoxic

prodrugs

1.29

reduction

1.30

1.31   1.7

HX—Drug

X = O, NH

R =

1.32

1.33

1.34

1.35
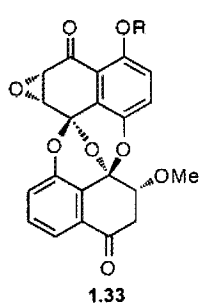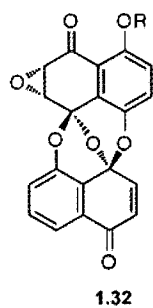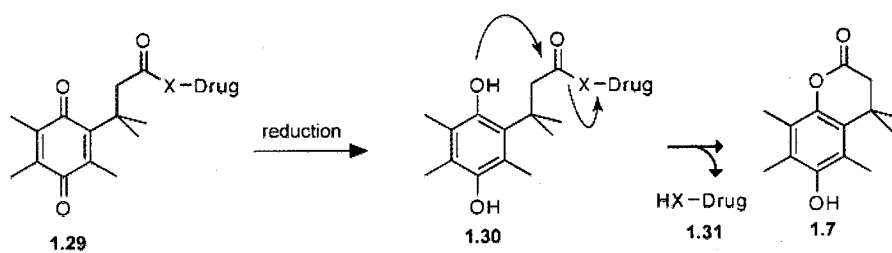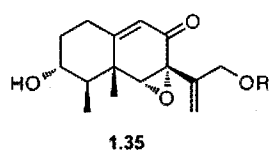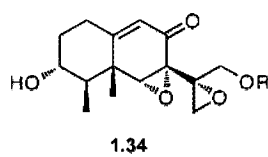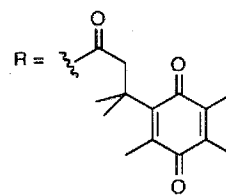
Figure 1.10   Fluorogenic enzyme substrates based on rhodamine 110

1.36 → **1.37** (peptidase)

1.38 → (esterase) **1.2** + acetate
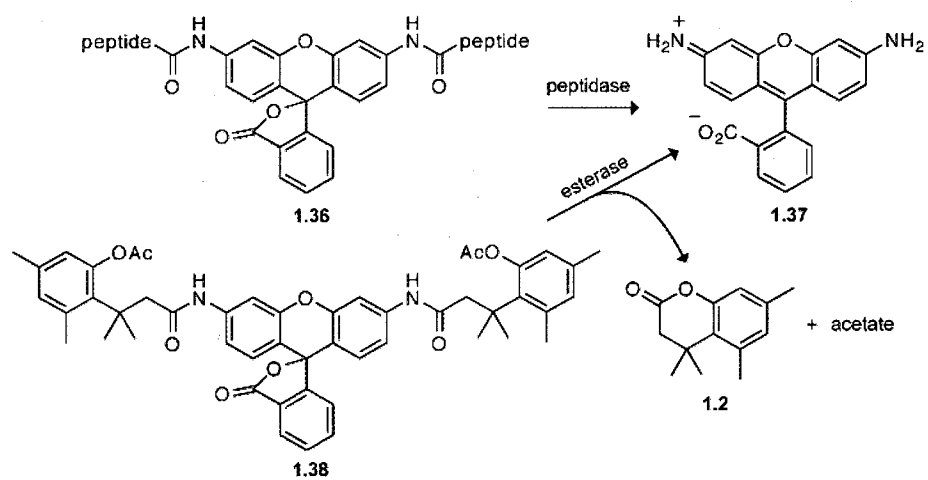
Figure 1.11   Fluorescence development in rhodamine 110 trimethyl lock esterase

substrate **1.38**

1.38

1.2

1.37
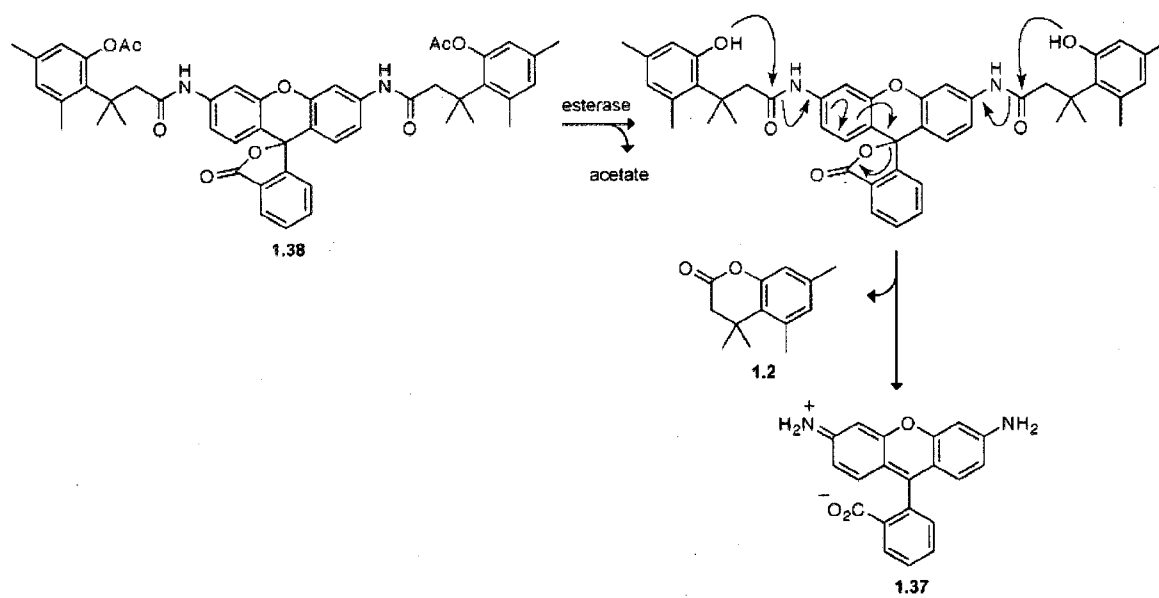
Figure 1.12   Mono(trimethyl lock) rhodamines incorporating biological handles
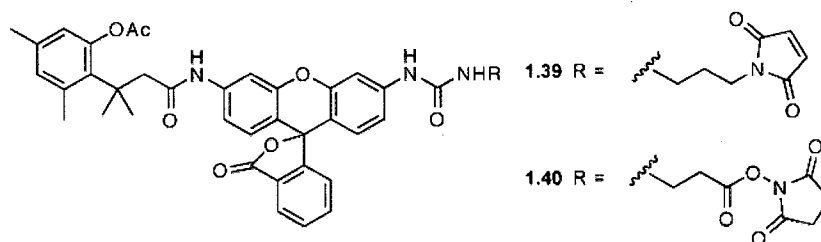
Figure 1.13   Fluorogenic and chromogenic esterase substrates

1.41

1.42

1.43
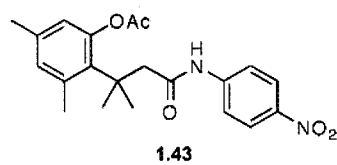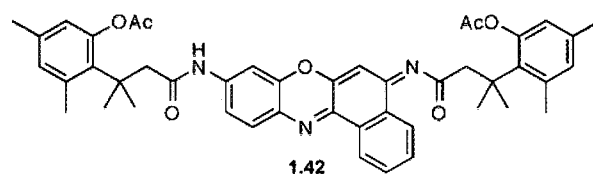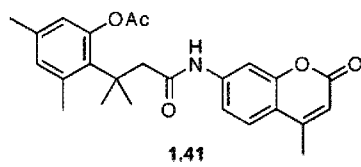
Figure 1.14   Fluorogenic DT-diaphorase substrates

1.44

1.45
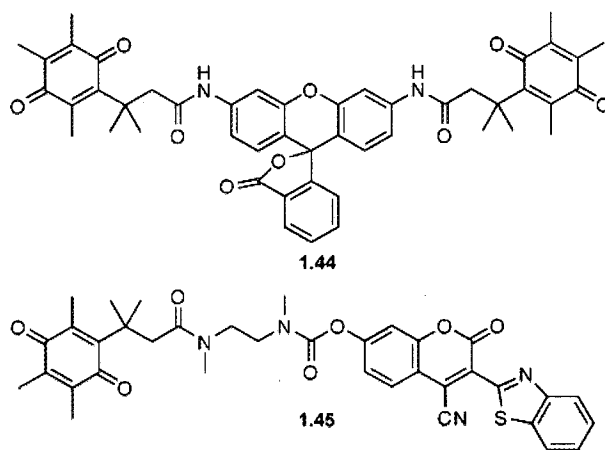
Figure 1.15   Cytochrome P450 substrate and mechanism of fluorescence development

CYP1A1

NADPH+2H⁺ NADP⁺
+   +
O₂   H₂O

1.46

1.47

acetaldehyde

1.49

1.2

1.48
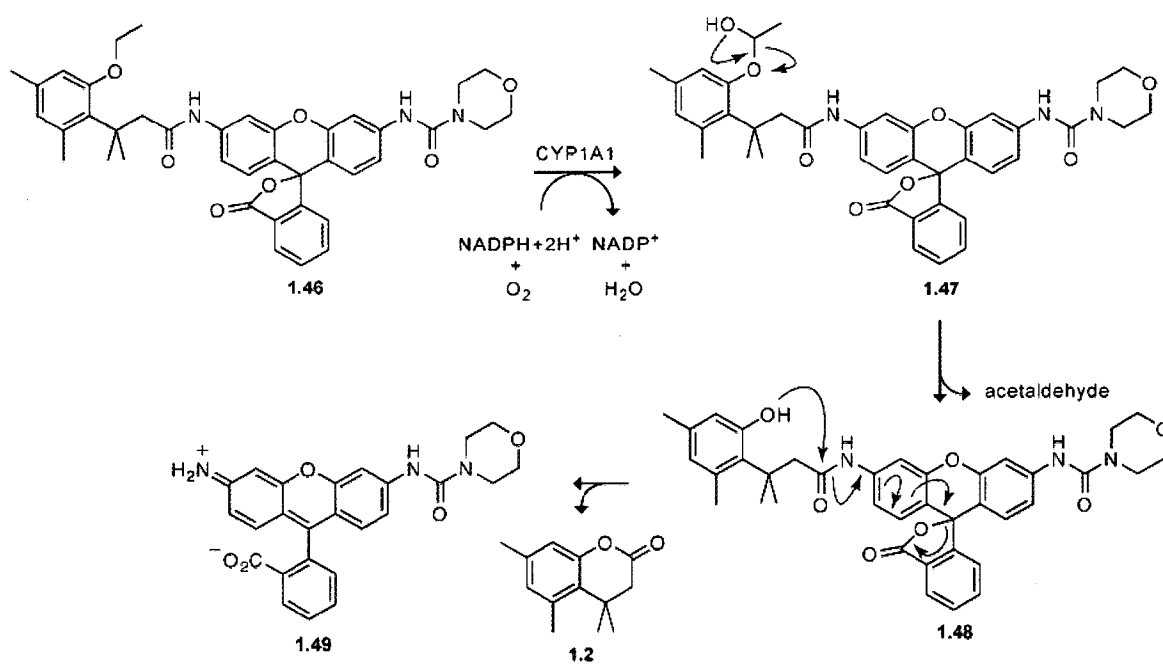
Figure 1.16   Alkaline phosphatase substrates utilizing a phosphate trimethyl lock

1.50

1.51
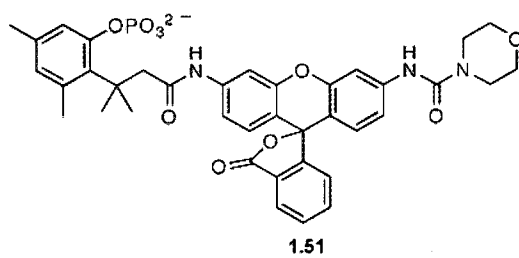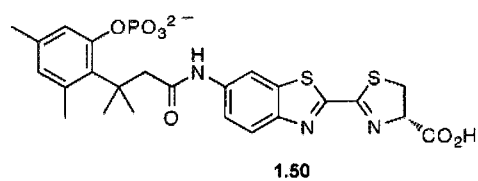
Figure 1.17 Nucleocytoplasmic shuttle peptide. *o*-NB, *ortho*-nitrobenzyl; FTC,

fluorescein isothiocyanate; CPP, cell penetrating peptide; NLS, nuclear

localization signal; NES, nuclear export signal.

FTC—Abu—LARLF—O

H—RRRRRRRR—KRKRR—NH

CPP   NLS

1.52

UV-irradiation →

H—RRRRRRRR—KRKRR

1.53

FTC—Abu—LARLF—O

H₂N / ALGV—NH₂

1.54

O-N acyl shift

FTC—Abu—LARLFSALGV—NH₂

NES

1.55
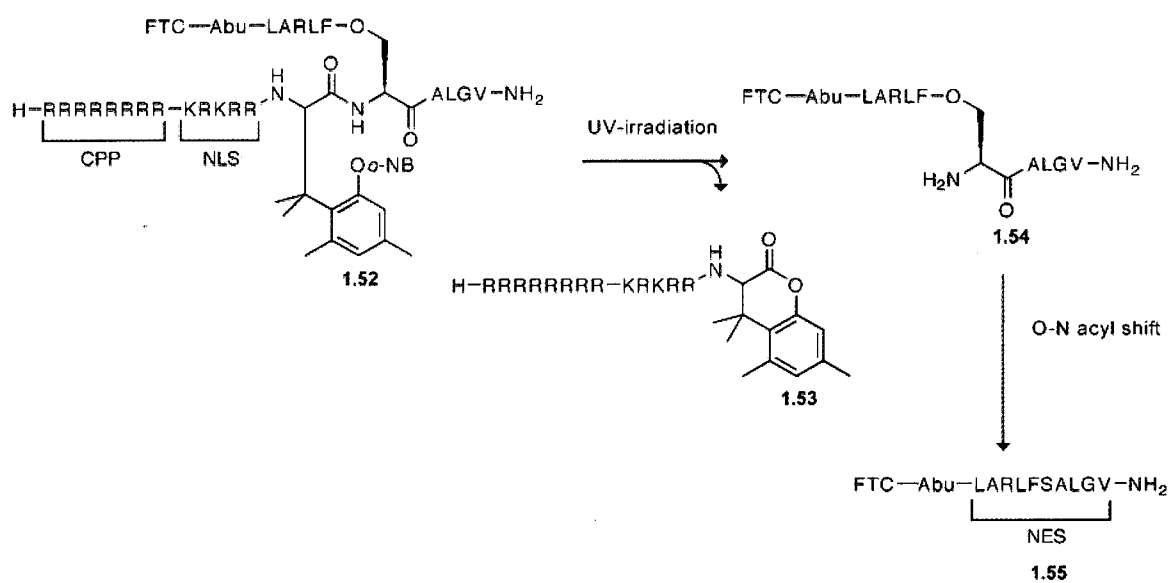
Figure 1.18 Modulating the subcellular localization of the nucleocytoplasmic shuttle

peptide. Confocal microscopy of CHO-K1 cells incubated with **1.52**. UV

(−): cells that had been treated with **1.52**. UV (+): cells that had been

treated with **1.52**, then exposed to ultraviolet light for 4 minutes, then

incubated an additional 1 hour at 37 °C. UV (+) +LMB: Before an

additional 1 hour incubation, cells were treated with leptomycin B.

Reproduced from (Shigenaga *et al.*, 2007).

| FTC | Hoechst | Merge | Phase contrast |

UV (−)

UV (+)

UV (+)
+LMB

Bar = 50 μm
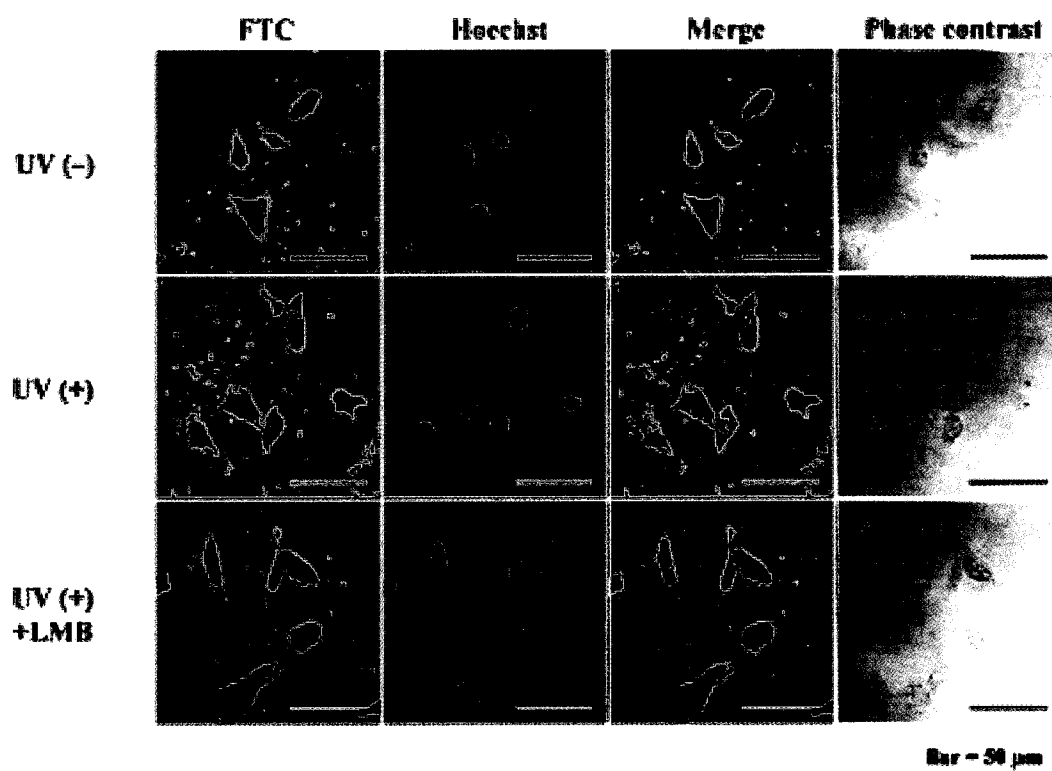
Figure 1.19   DNA delivery utilizing cleavable peptide nucleic acid. *p*NS, *para-*

nitrosulfonyl; PNA, peptide nucleic acid.

1.56

thiol-mediated
cleavage

Released DNA
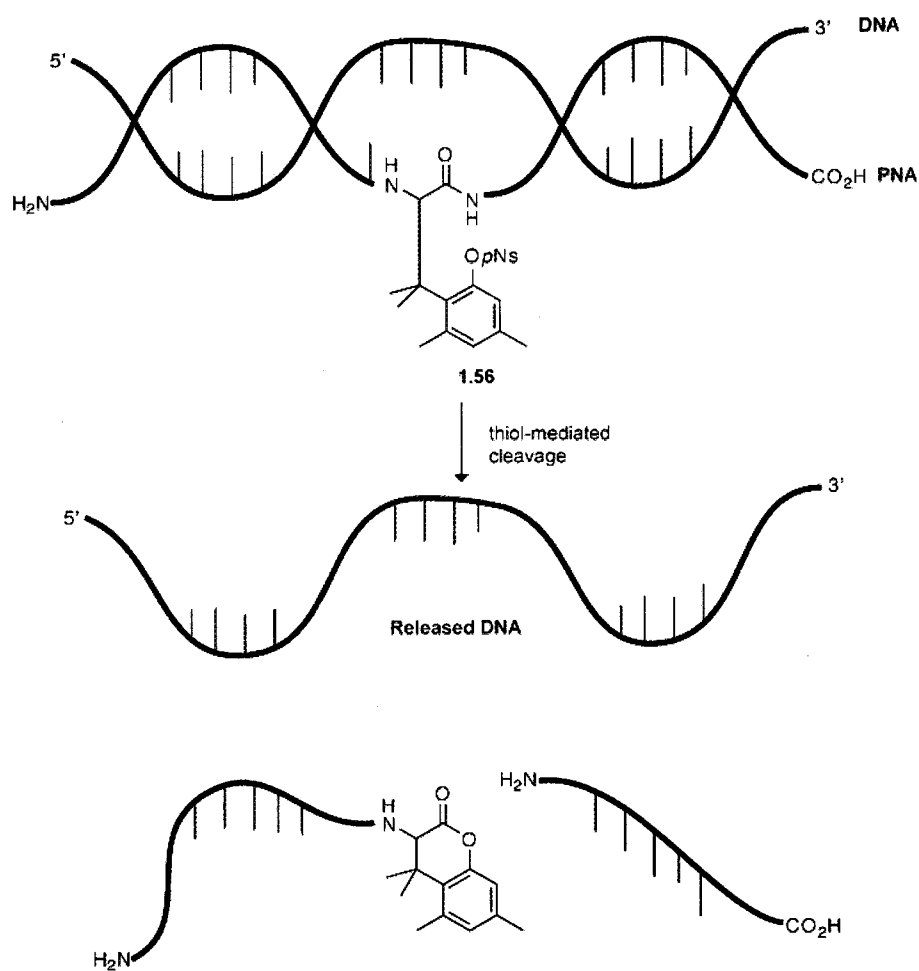
Figure 1.20   Quinone trimethyl lock DOPE for triggered release of contents from

liposomes

1.57
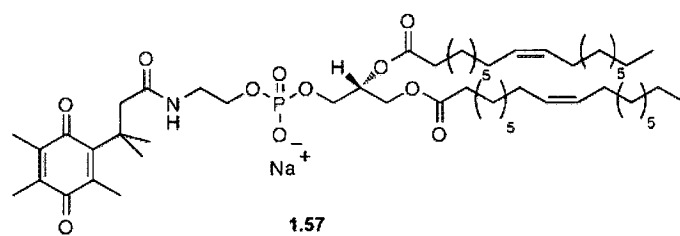
Figure 1.21   Solid-phase synthesis resins cleaved by reduction. Sphere, polystyrene

resin support.
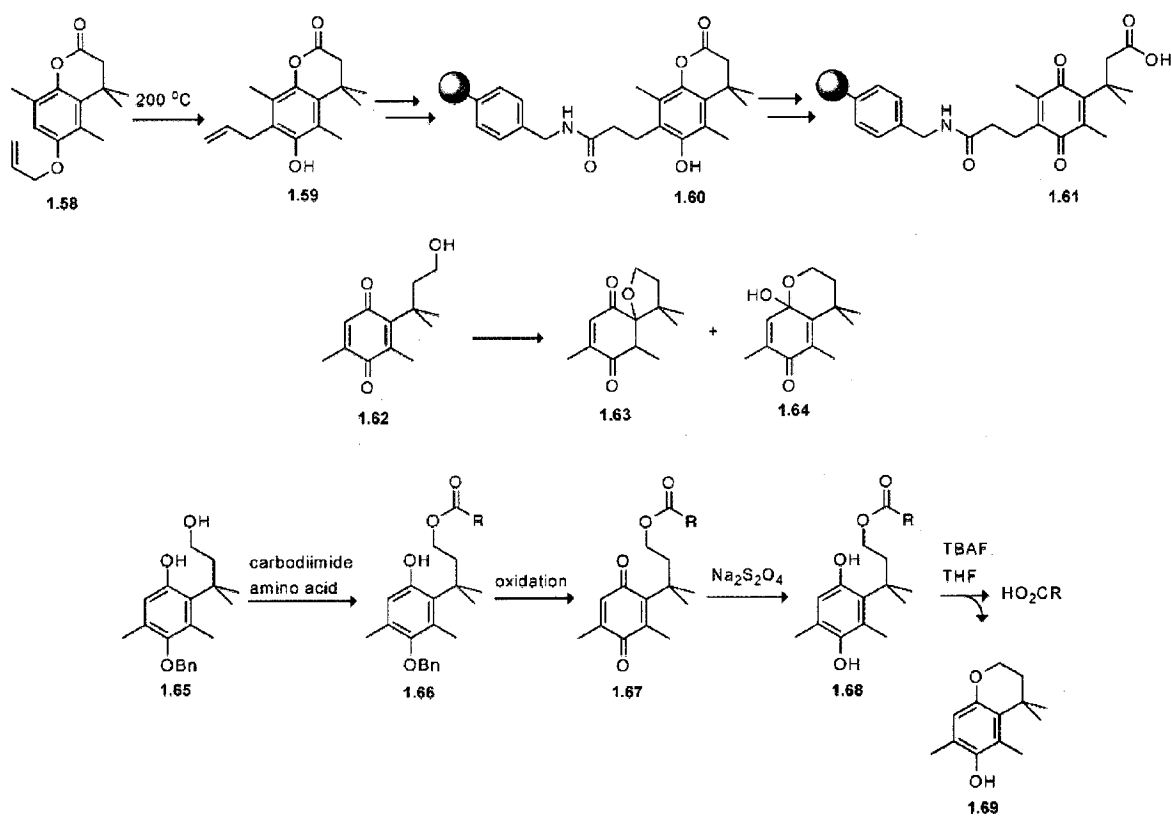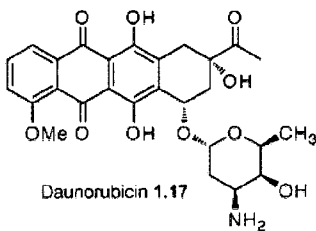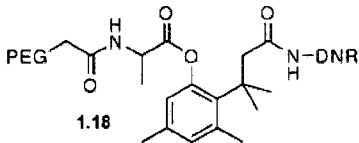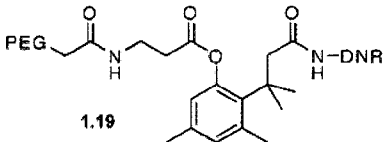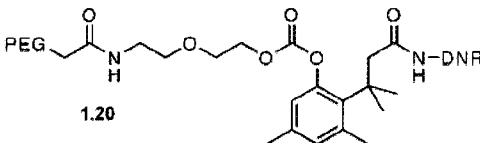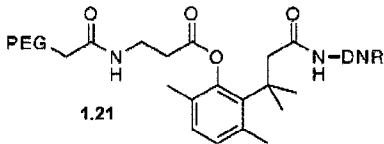
Figure 1.22 Solid phase oligonucleotide synthesis resin. Oligo, oligonucleotide; CNE,

cyanoethyl; Sphere, Pharmacia HL-30 primer resin.
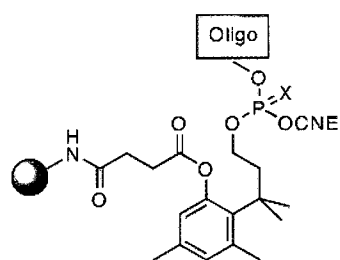
1.70 X = O, S

Table 1.1 PEG prodrugs of daunorubicin. $t_{1/2}$, half-life. IC_{50} was measured in P388/0

cell line. Percent treatment over control (%T/C) was the mean tumor

volume of M109 murine Madison lung carcinoma subcutaneous

xenografts in balb/c mice after treatment. i.p., intraperitoneal; i.v.,

intravenous; DNR, daunorubicin.

Compound	$t_{1/2}$ (min) Rat Plasma	IC_{50} (nM) P388/0	M109 (%T/C) i.p. (% Lethality)	M109 (%T/C) i.v.
Daunorubicin 1.17	---	3	44.8 (17%)	117.0
1.18	114	43	62.8 (0%)	92.5
1.19	12	203	101.2 (83%)	63.7
1.20	66	142	57.1 (66%)	118.4
1.21	480	411	114.8 (0%)	31.6

CHAPTER 2

Trimethyl Lock: A Stable Chromogenic

Substrate for Esterases

2.1   Abstract

p-Nitrophenyl acetate is the most commonly used substrate for detecting the catalytic

activity of esterases, including those that activate prodrugs in human cells. This substrate

is unstable in aqueous solution, limiting its utility. Here, a stable chromogenic substrate

for esterases is produced by the structural isolation of an acetyl ester and *p*-nitroaniline

group using a trimethyl lock moiety. Upon ester hydrolysis, unfavorable steric

interactions between the three methyl groups of this *o*-hydroxycinnamic acid derivative

encourage rapid lactonization to form a hydrocoumarin and release *p*-nitroaniline. This

"prochromophore" could find use in a variety of assays.

2.2   Introduction

Prodrug strategies have been employed to improve the properties of potential small-molecule chemotherapeutic agents, including their solubility, stability, organ selectivity, duration of action, and bioavailability (Amsberry and Borchardt, 1990; Testa and Mayer, 2003). Recently, our research group reported on the use of the "trimethyl lock" prodrug strategy as the basis for a new class of latent fluorophores (Chandran, *et al.*, 2005; Lavis, *et al.*, 2006a; Lavis, *et al.*, 2006b). The trimethyl lock is an *o*-hydroxycinnamic acid derivative in which severe steric repulsion between three methyl groups leads to rapid lactonization to form a hydrocoumarin with consequent release of an alcohol or amine (Borchardt and Cohen, 1972a; Dillon, *et al.*, 1996; Milstien and Cohen, 1972). In our latent fluorophores, the trimethyl lock was inserted between a labile functional group and a fluorescent dye. The isolation of the labile group and dye led to a marked improvement in chemical stability with the retention of enzymatic reactivity.

To exploit further the utility and modularity of the trimethyl lock system, we have designed a chromogenic esterase substrate, **2.1**. Although chromogenic substrates lack the level of sensitivity of fluorogenic substrates (Yatzeck, *et al.*, 2008), the simplicity and low cost of a spectrophotometer is a notable advantage. The utility of *p*-nitrophenyl acetate (**2.2**, *p*NPA), the most often-used esterase substrate, is diminished by a number of unfavorable properties, especially the pH-sensitivity of its chromophoric properties and its notorious chemical instability (Hartley and Kilby, 1954; Menger and Ladika, 1987). The hydrolysis product of **2.2**, *p*-nitrophenol (*p*NP), has a pK_a of 7.0 and an absorbance

spectrum that exhibits a hypsochromic shift (blue shift) below pH 8 (Oldfield, *et al.*, 1990). The pH optimum (pH 6.5–8.0) of pig liver esterase (PLE; EC 3.1.1.1), the most often-used esterase, encompasses the pK_a of pNP, such that a small pH change during an assay with pNPA as a substrate leads to inaccurate results (Barker and Jencks, 1969; Junge and Heymann, 1979). A notable improvement to the chemical stability of pNP-based esterase substrates involves using acyloxymethyl ethers in place of the acetate esters (Leroy, *et al.*, 2003; Sicart, *et al.*, 2007). Although this substitution endows increased chemical stability, the pH-sensitivity of the pNP chromophore remains problematic. Here, we report on the synthesis and characterization of a novel prochromophore that utilizes the trimethyl lock and overcomes the limitations of pNPA and other esterase substrates.

2.3   Results and Discussion

2.3.1 pH-Sensitivity of Chromophores

To overcome an intrinsic problem of *p*NP, we chose to use *p*-nitroaniline (*p*NA) as the chromophore in an esterase substrate. In contrast to *p*NP, *p*NA does not have a pK_a value in the physiologic range, and its absorbance spectrum is constant from pH 4–10 (Figure 2.1). Derivatization of *p*NA to make a nitroanilide confers a hypsochromic shift in its absorbance spectrum, enabling it to be used for spectrophotometric assays (Lowe and Yuthavong, 1971).

2.3.2 Synthesis of a Prochromophore 2.1

To prepare prochromophore **2.1**, we followed the route used by Amsberry and coworkers to synthesize the trimethyl lock precursor (Amsberry, *et al.*, 1991). Condensation with *p*-nitroaniline to form an amide bond was difficult, presumably due to steric constraints in the trimethyl lock substrate and the low nucleophilicity of the aromatic amine. Traditional peptide coupling reagents such as EDC and DIC led to poor yields, but formation of the acid chloride *in situ* under neutral conditions using Ghosez's reagent, which is an α-chloroenamine, followed by the addition of *p*-nitroaniline and pyridine, was ultimately successful (Scheme 2.1) (Furstner and Weintritt, 1998; Haveaux, *et al.*, 1979).

2.3.3 Spectroscopic Properties

As expected (Lowe and Yuthavong, 1971), the spectrum of **2.1** (λ_{max} = 322 nm) (Figure 2.2) displays a hypsochromic shift relative to pNA (λ_{max} = 383 nm). We performed our kinetics assays at 410 nm, where the absorbance of the substrate is negligible (ε_{410} = ~0 $M^{-1}cm^{-1}$) but that of the pNA product is high (ε_{410} = 10,681 $M^{-1}cm^{-1}$) (Lyublinskaya, *et al.*, 1974).

2.3.4 Chemical Stability

Stability in aqueous solution is an important property for enzymatic substrates, particularly those for hydrolases. It is well established that pNPA (**2.2**) hydrolyzes spontaneously in neutral buffer (Hartley and Kilby, 1954; Menger and Ladika, 1987), and that the rate of its hydrolysis increases in the presence of proteins or amino acids, especially those with free amino or phenolic groups (Hartley and Kilby, 1954). pNPA has even been used as an acetylating agent to modify cysteine and lysine residues in proteins (Park, *et al.*, 1966). Accordingly, the use of pNPA as an esterase substrate requires the performance of numerous control experiments to ensure that pNP is being produced by the putative catalyst in a truly catalytic manner (Park, *et al.*, 1961). Moreover, the use of pNPA is not amenable to any assay requiring long incubation times or low enzyme concentrations (Wolf, *et al.*, 2006).

As shown in Figure 2.3, prochromophore **2.1** was remarkably stable in phosphate-buffered saline (PBS) containing bovine serum albumin (BSA) whereas **2.2** was hydrolyzed completely in a few hours. This large difference in stability is likely due, in

part, to the difference in the pK_a of the leaving groups, as pNP is a much better leaving group (pK_a 7.0) than is the electron-rich phenol of the trimethyl lock (*e.g.*, *o*-methylphenol has a pK_a of 10.28) (Fickling, *et al.*, 1959; Lavis, *et al.*, 2006a).

2.3.5 Enzymatic Reactivity

Next, we compared prochromophore **2.1** and **2.2** as substrates for PLE (Figure 2.4). The addition of the trimethyl lock moiety rendered **2.1** to be less soluble than pNA, and 10% v/v DMSO was used as a cosolvent for all kinetic assays. The value of the Michaelis constant for **2.1** ($K_M = 14$ μM) was substantially lower than that for **2.2** ($K_M = 0.54$ mM). The active site of the human homologue of PLE is 10–15 Å deep within a hydrophobic pocket, and the increased size and hydrophobicity of **2.1** could contribute to the decreased K_M value (Fleming, *et al.*, 2005). We have noticed a similar inverse relationship between the molecular size and K_M value of our fluorogenic esterase substrates (Chandran, *et al.*, 2005; Lavis, *et al.*, 2006a; Lavis, *et al.*, 2006b). The value of the second-order rate constant for the turnover of **2.1** ($k_{cat}/K_M = 3.0 \times 10^5$ M^{-1}s^{-1}) was within an order of magnitude of that for **2.2** ($k_{cat}/K_M = 2.2 \times 10^6$ M^{-1}s^{-1}).

2.4 Conclusions

We have synthesized an improved chromogenic esterase substrate by incorporating the trimethyl lock. Adopting this prodrug strategy led to superior chemical stability while maintaining high enzymatic reactivity. These attributes could be useful in numerous

contexts, including high-throughput screens and directed evolution of esterases and lipases (Schmidt, *et al.*, 2004; Schmidt and Bornscheuer, 2005), and the *de novo* discovery of new catalysts for ester-bond hydrolysis (Hecht, *et al.*, 2004; Wei and Hecht, 2004). The modular design of this substrate enables its tailoring to confer reactivity with other enzymes. For example, replacing the acetyl group with a phosphoryl group could yield a substrate superior to *p*-nitrophenyl phosphate, which like *p*NPA suffers from deleterious chemical instability.

2.5 Experimental Section

2.5.1 General

Dichloromethane was drawn from a Baker CYCLE-TAINER solvent-delivery system. All other reagents were from Aldrich Chemical (Milwaukee, WI) or Fisher Scientific (Hanover Park, IL), and were used without further purification.

Thin-layer chromatography was performed by using aluminum-backed plates coated with silica gel containing F_{254} phosphor, and was visualized by UV illumination or developed with ceric ammonium molybdate stain. Flash chromatography was performed on open columns with silica gel-60 (230–400 mesh).

PBS contained (in 1.00 L) KCl (0.20 g), KH_2PO_4 (0.20 g), NaCl (8.0 g), and $Na_2HPO_4 \cdot 7H_2O$ (2.16 g) and had pH 7.4.

2.5.2 Spectroscopy

NMR spectra were obtained with a Bruker DMX-400 Avance spectrometer at the National Magnetic Resonance Facility at Madison (NMRFAM). Electron-impact mass spectra were obtained using a Waters (Micromass) AutoSpec™ (Beverly, MA) mass spectrometer at the Mass Spectrometry Facility in the Department of Chemistry. UV–visible spectrophotometric measurements were made at the University of Wisconsin–Madison Biophysics Instrumentation Facility (BIF) with a Cary 400 UV–visible spectrophotometer from Varian (Palo Alto, CA) equipped with sample stirring and a thermostatted cuvette holder set at 25 °C, using a circulating water bath. Cuvettes were glass or quartz from Starna Cells (Atascadero, CA). Compounds were prepared as stock solutions in DMSO. PLE (163 kDa) was from Sigma Chemical (St. Louis, MO; product number E2884) as a suspension in $(NH_4)_2SO_4$ (3.2 M), and was diluted to appropriate concentrations in PBS before use. Kinetic parameters were calculated with the programs Microsoft Excel 2000 and GraphPad Prism 4.

2.5.3 Prochromophore 2.1

3-(2'-Acetoxy-4',6'-dimethylphenyl)-3,3-dimethylpropanoic acid (Amsberry, et al., 1991) (100 mg, 0.38 mmol) was dissolved in anhydrous CH_2Cl_2 (1.0 mL). 1-Chloro-N,N,2-trimethylpropenylamine (55 μL, 0.42 mmol) in CH_2Cl_2 (0.2 mL) was added quickly, and the reaction mixture was stirred under Ar(g) for 3 h at 0 °C. The reaction progress was followed by TLC (30% v/v EtOAc in hexanes) after quenching a small aliquot with MeOH to generate the methyl ester. 4-Nitroaniline (105 mg,

0.76 mmol) and anhydrous pyridine (50 μL) were dissolved in CH_2Cl_2 (1.0 mL), and the resulting solution was added to the reaction mixture, which was then stirred at ambient temperature overnight. The reaction mixture was partitioned between CH_2Cl_2 and water. The layers were separated, and the aqueous phase was extracted with CH_2Cl_2. The combined organic layers were washed with saturated brine, and dried over anhydrous $MgSO_4(s)$. Solvent was removed under reduced pressure, and the residue was purified by column chromatography (silica gel, 20% v/v EtOAc in hexanes) to yield **2.1** as a white crystalline solid (62 mg; 43%, 2 steps). ^1H NMR (400 MHz, $CDCl_3$) δ: 8.06 (d, J = 9.2 Hz, 2H), 7.82 (br s, 1H), 7.34 (d, J = 9.2 Hz, 2H), 6.74 (s, 1H), 6.65 (s, 1H), 2.52 (s, 2H), 2.32 (s, 3H), 2.36 (s, 3H), 2.23 (s, 3H), 1.72 ppm (s, 6H). ^{13}C NMR (100 MHz, $CDCl_3$) δ: 173.2, 170.3, 150.4, 144.3, 143.2, 139.4, 137.6, 133.4, 132.9, 125.0, 123.6, 118.6, 51.3, 40.8, 32.5, 25.7, 22.1, 20.3 ppm. HRMS (EI): m/z 405.1577 $[M+Na]^+$ ($[C_{21}H_{24}N_2O_5Na]$ = 405.1578).
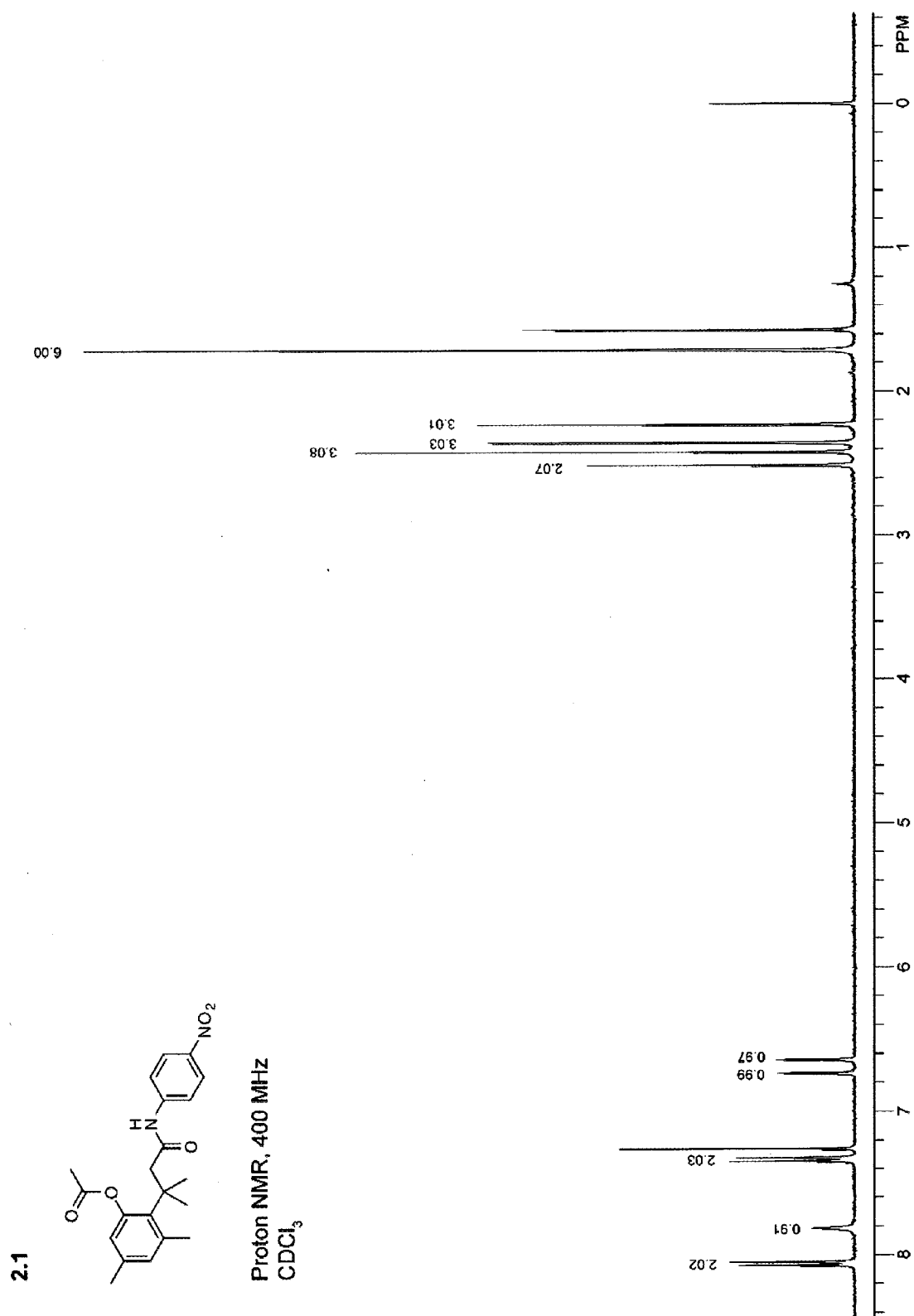
2.1
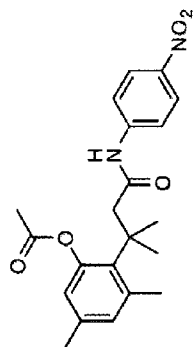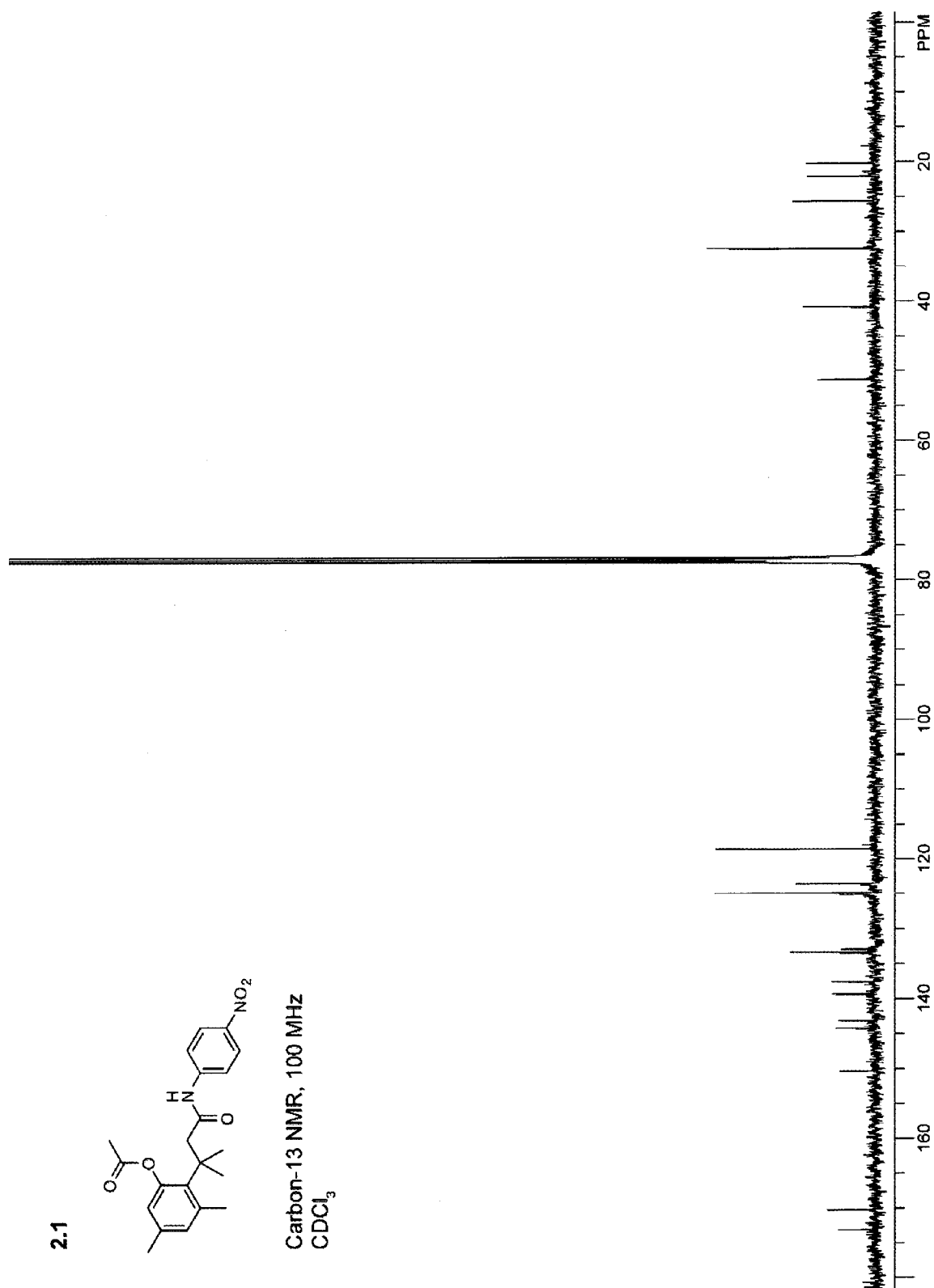
Proton NMR, 400 MHz
CDCl$_3$

2.1

Carbon-13 NMR, 100 MHz
CDCl$_3$

Scheme 2.1   Route for the synthesis of prochromophore **2.1**, and putative mechanism

for the activation of prochromophore **2.1** and *p*-nitrophenyl acetate

(*p*NPA; **2.2**) by an esterase.
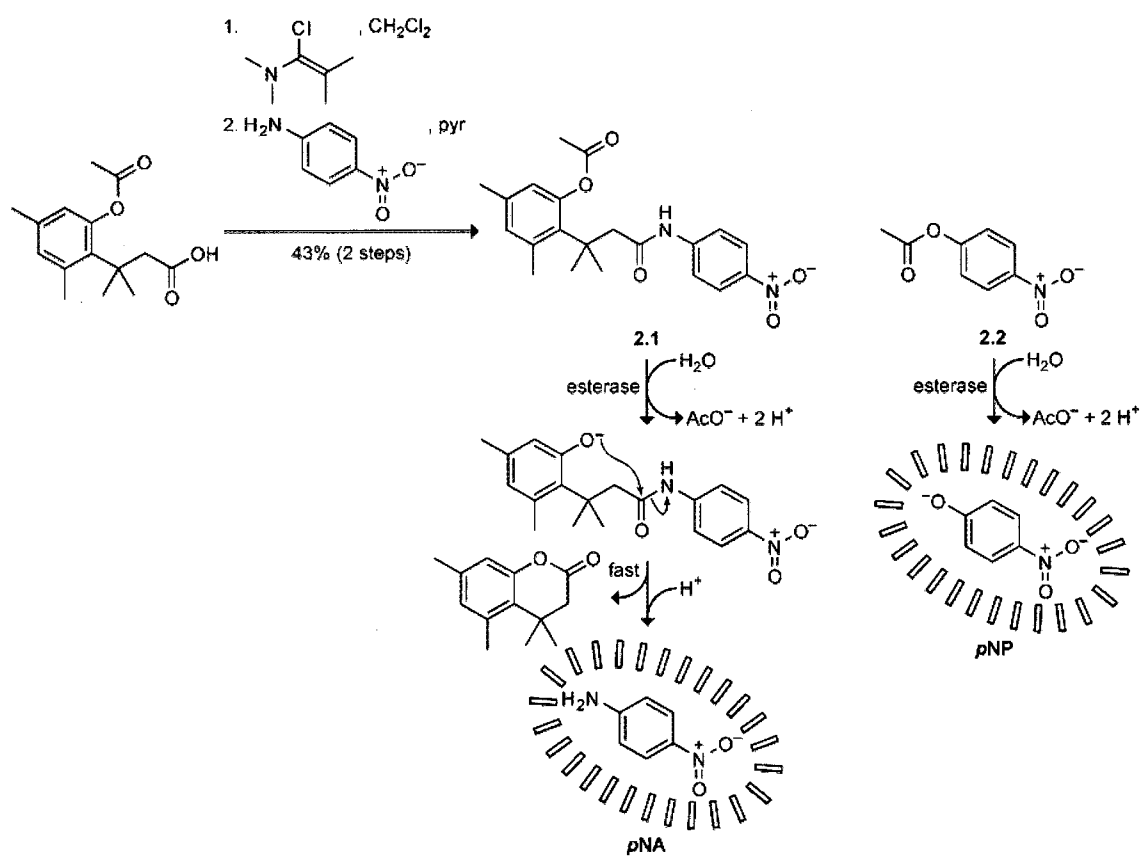
Figure 2.1   pH-Sensitivity of the extinction coefficients at 410 nm of p-nitroaniline

(pNA) and p-nitrophenol (pNP). Measurements were made in triplicate in

PBS adjusted to the appropriate pH. The observed pK_a of pNP was 7.0.
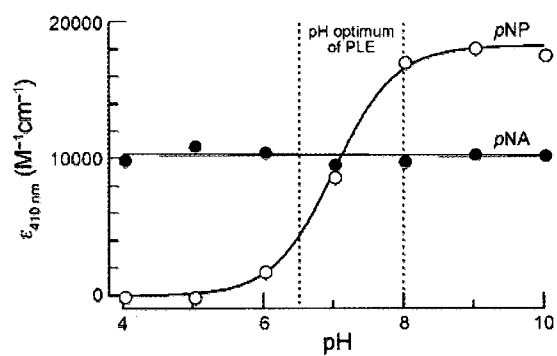
Figure 2.2 (A) Absorbance spectra of prochromophore **2.1** and its hydrolysis product,

p-nitroaniline (*p*NA), in PBS (pH 7.4). (B) Absorbance spectra of

p-nitrophenyl acetate (*p*NPA; **2.2**) and its hydrolysis product,

p-nitrophenol (*p*NP) in PBS (pH 7.4).
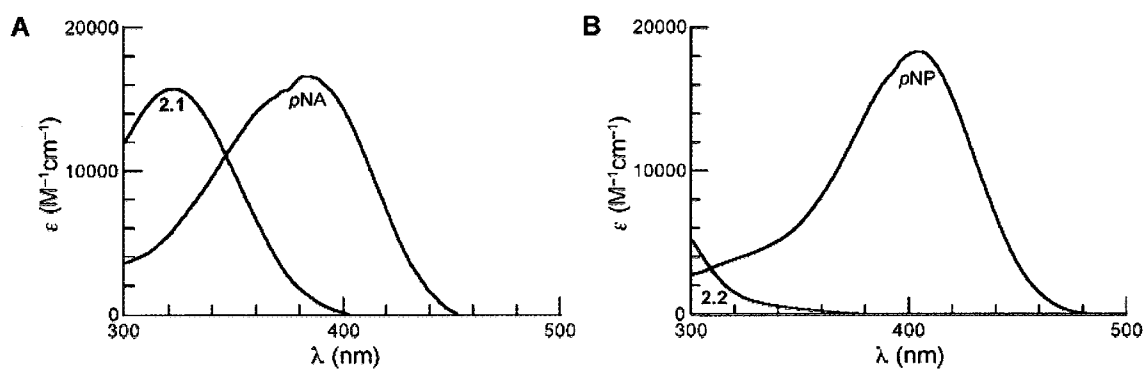
Figure 2.3 Time course for the mean change in the absorbance at 410 nm of

prochromophore **2.1** (13 μM) and *p*-nitrophenyl acetate (**2.2**) (13 μM) in

PBS containing BSA (1.0 mg/mL). Three separate experiments were

performed, and absorbance measurements were made in triplicate.
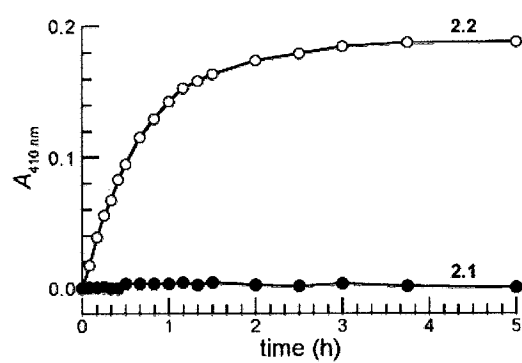
Figure 2.4 (A) Saturation curve for the hydrolysis of prochromophore **2.1**

(33→0.5 µM) by PLE (0.25 µg/mL) in PBS (pH 7.7) containing DMSO

(10% v/v) and monitored at $\lambda = 410$ nm; $k_{cat}/K_M = 3.0 \times 10^5$ $M^{-1}s^{-1}$ and

$K_M = 14$ µM. Data points are the mean of triplicate determinations. (B)

Saturation curve for the hydrolysis of pNPA (**2**; 266→4 µM) by PLE

(0.25 µg/mL) in PBS (pH 7.7) containing DMSO (10% v/v) and

monitored at $\lambda = 410$ nm; $k_{cat}/K_M = 2.2 \times 10^6$ $M^{-1}s^{-1}$ and $K_M = 0.54$ mM.

Data points are the mean of triplicate determinations.
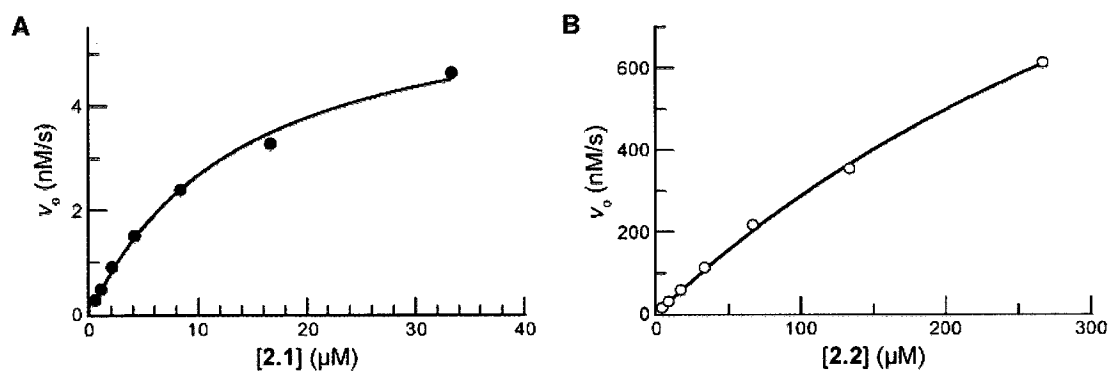
CHAPTER 3

Sensitive Fluorogenic Substrate

for Alkaline Phosphatase

3.1   Abstract

Alkaline phosphatase serves as both a model enzyme for studies on the mechanism and kinetics of phosphomonoesterases and as a reporter in enzyme-linked immunosorbent assays (ELISAs) and other biochemical methods. The tight binding of the enzyme to its inorganic phosphate product leads to strong inhibition of catalysis and confounds measurements of alkaline phosphatase activity. We have developed an alkaline phosphatase substrate in which the fluorescence of rhodamine is triggered upon P–O bond cleavage in a process mediated by a "trimethyl lock". Although this substrate requires a second, non-enzymatic step to manifest fluorescence, we demonstrated that the first, enzymatic step limits the rate of fluorogenesis. The substrate enables the activity of alkaline phosphatase to be measured with high sensitivity and accuracy. Its attributes are ideal for enzymatic assays of alkaline phosphatase for both basic research and biotechnological applications.

3.2 Introduction

Alkaline phosphatase (EC 3.1.3.1) is a prototypical phosphomonoesterase (Cleland and Hengge, 2006; Coleman, 1992; Millán, 2006) that is used often in enzyme-linked immunosorbent assays (ELISAs) and other biochemical methods (Porstmann, *et al.*, 1985). Despite its frequent study and widespread use, determining rate constants for catalysis by alkaline phosphatase is difficult. This difficulty arises largely from the high affinity of alkaline phosphatase for its product, inorganic phosphate. For example, the well-known enzyme from *Escherichia coli* is inhibited with $K_i \approx 1$ μM (Snyder and Wilson, 1972). In typical spectrophotometric assays for alkaline phosphatase, the concentration of inorganic phosphate saturates the enzyme before a measurable signal is observable, limiting accuracy. Fluorometric assays using aryl phosphates can overcome this limitation. Still, known fluorogenic substrates, such as fluorescein diphosphate (Huang, *et al.*, 1999), are hampered by chemical instability, two-hit kinetics, and pH-dependent fluorescence (Robinson and Willcox, 1969).

Rhodamine 110 is a xanthene dye first synthesized by Maurice Ceresole over a century ago (Ceresole, 1887). Its fluorescence is bright and pH-insensitive, and its emission and excitation wavelengths are ideal for biological assays (Lavis and Raines, 2008). To adapt rhodamine 110 as a reporter of enzymatic catalysis, we have employed the "trimethyl lock" as a trigger that couples fluorescence generation to a designated chemical reaction (Chandran, *et al.*, 2005; Lavis, *et al.*, 2006a; Lavis, *et al.*, 2006b; Yatzeck, *et al.*, 2008). The trimethyl lock is an *o*-hydroxydihydrocinnamic acid derivative in which steric

interactions between three methyl groups leads to rapid lactonization to a dihydrocoumarin ring (**3.3**, Scheme 3.1) with concomitant release of an alcohol or amine (Borchardt and Cohen, 1972a; Milstien and Cohen, 1972; Nicolaou, *et al.*, 1996b). The scission of a labile bond to the phenolic oxygen enables the manifestation of fluorescence (Chandran, *et al.*, 2005; Lavis, *et al.*, 2006a; Lavis, *et al.*, 2006b; Yatzeck, *et al.*, 2008). Here, we describe how the trimethyl lock can enable the fluorescence of rhodamine 110 to report on P–O bond cleavage catalyzed by alkaline phosphatase.

3.3 Experimental Section

3.3.1 General

Dichloromethane was drawn from a Baker CYCLE-TAINER solvent-delivery system. All other reagents were from Aldrich Chemical (Milwaukee, WI) or Fisher Scientific (Hanover Park, IL), and were used without further purification.

Thin-layer chromatography was performed by using aluminum-backed plates, coated with silica gel containing F_{254} phosphor, and was visualized by ultraviolet illumination, or developed with ceric ammonium molybdate stain. Flash chromatography was performed on open columns with silica gel-60 (230–400 mesh).

NMR spectra were obtained with a Bruker DMX-400 Avance spectrometer at the National Magnetic Resonance Facility at Madison (NMRFAM). Mass spectrometry was performed using a Micromass LCT (electrospray ionization, ESI) mass spectrometer at the Mass Spectrometry Center in the Department of Chemistry.

3.3.2 Synthesis of Substrate 1

3-[2'-(Dibenzylphophono)oxy-4',6'-dimethylphenyl]-3,3-dimethylpropionic acid

(Nicolaou, *et al.*, 1996b) (**3.5**, 326 mg, 0.676 mmol) was dissolved in anhydrous CH_2Cl_2

(2.0 mL) in a flame-dried, 25-mL round-bottom flask. 1-Chloro-$N,N,2$-

trimethylpropenylamine (98 μL, 0.75 mmol) in CH_2Cl_2 (0.4 mL) was added quickly, and

the reaction mixture was stirred under Ar(g) for 3 h. The reaction progress was followed

by TLC (50% v/v EtOAc in hexanes) after quenching a small aliquot with MeOH to

generate the methyl ester. Rhodamine **3.4** (Lavis, *et al.*, 2006a) (150 mg, 0.34 mmol) and

anhydrous pyridine (109 μL, 1.35 mmol) were dissolved in CH_2Cl_2 (2.0 mL), and the

resulting solution was added to the reaction mixture, which was then stirred overnight.

The reaction mixture was partitioned between CH_2Cl_2 and water. The organic layer was

washed with 50 mL of 1 N HCl, water, 5% w/v sodium bicarbonate, water, and brine.

The organic phase was dried over Na_2SO_4(s) and filtered, and the solvent was removed

under reduced pressure. The residue was purified by silica gel chromatography (7:2:1

EtOAc/CH_2Cl_2/hexanes), followed by a second column (7:2:1 EtOAc/CH_2Cl_2/toluene) to

give phosphotriester **3.6** as a white solid (161 mg; 52%). ^{1}H NMR (400 MHz, CDCl$_3$) δ:

8.86 (s, 1H), 7.98 (d, J = 7.3 Hz, 1H), 7.63 (ddd, J = 8.3, 7.1, 1.0 Hz, 1H), 7.58 (ddd, J =

8.3, 7.5, 1.1 Hz, 1H), 7.50 (d, J = 1.8 Hz, 1H), 7.40 (d, J = 2.2 Hz, 1H), 7.37–7.34 (m,

10H), 7.09 (d, J = 7.6 Hz, 1H), 6.94 (dd, J = 8.7, 1.8 Hz, 1H), 6.90 (s, 1H), 6.84 (dd, J =

8.8, 1.8 Hz, 1H), 6.67 (s, 1H), 6.64 (d, J = 8.6 Hz, 1H), 6.63 (s, 1H), 6.55 (d, J = 8.7 Hz,

1H), 5.21–5.09 (m, 4H), 3.73 (t, J = 4.7 Hz, 4H), 3.49 (t, J = 4.6 Hz, 4H), 2.72 (d, J =

13.0 Hz, 1H), 2.65 (d, J = 12.9 Hz, 1H), 2.43 (s, 3H), 2.09 (s, 3H), 1.68 (s, 3H), 1.66 ppm

(s, 3H). ^{13}C NMR (100 MHz, CDCl$_3$) δ: 170.7, 169.9, 154.7, 153.4, 152.0, 151.7, 150.2,

141.2, 140.9, 139.6, 137.0, 135.1, 135.0, 132.5, 132.2, 129.8, 129.1, 128.9, 128.8, 128.5,

128.4, 128.3, 128.1, 126.6, 125.0, 124.2, 119.5, 115.6, 115.4, 113.4, 113.2, 107.6, 107.4,

83.3, 70.6, 66.6, 50.1, 44.4, 41.0, 32.4, 25.8, 20.4 ppm. ^{31}P NMR (162 MHz, CDCl$_3$) δ: –

6.20 ppm. HRMS (ESI) m/z: 930.3125 [M+Na]$^+$ ([C$_{52}$H$_{50}$N$_3$O$_{10}$PNa] = 930.3127).

A three-neck flask was chilled to –15 °C in an ice bath saturated with sodium

chloride. Phosphotriester **3.6** (20 mg, 0.022 mmol) and 10% Pd/C (2 mg, 0.002 mmol Pd)

were added, and a septum was placed in the center neck. A flow-control adapter, with a

Teflon stopcock and ground-glass joint, was secured to one neck of the flask to enable

attachment of either vacuum tubing or a balloon. The final neck was covered with a

septum, an Ar(g) line was affixed, and the flask was flushed with Ar(g). Methanol (10

mL) was added and the solution was allowed to cool. The flask was evacuated with a

vacuum pump before attachment of a balloon filled with H$_2$(g). Evacuation, followed by

reintroduction of H$_2$(g), was repeated two more times. The reaction was allowed to stir,

covered in foil, under H$_2$(g) for 2 h. Reaction progress was monitored by TLC (7:1:1:1

EtOAc/H$_2$O/AcOH/MeOH). Upon completion, the palladium was rapidly removed by

filtration through a pad of celite. Ammonium acetate (7.0 mg, 0.091 mmol) was added to

the filtrate, and the solvent was removed under reduced pressure. The residue was

purified by column chromatography using Sephadex LH-20 as the stationary phase and

1:1 MeOH/H$_2$O as the mobile phase. The product-containing fractions were combined, and the organic solvent was removed under reduced pressure. Water was removed by lyophilization to yield substrate **3.1** as a white powder (11 mg; 66%). ^{1}H NMR (400 MHz, CD$_3$OD) δ: 8.00 (d, J = 7.3 Hz, 1H), 7.78–7.72 (m, 1H), 7.71–7.66 (m, 1H), 7.56 (d, J = 1.3 Hz, 1H), 7.45 (d, J = 1.9 Hz, 1H), 7.33 (s, 1H), 7.16 (d, J = 7.2 Hz, 1H), 7.09 (dd, J = 8.5, 1.9 Hz, 1H), 6.95 (dd, J = 9.2, 1.3 Hz, 1H), 6.60 (d, J = 8.5 Hz, 1H), 6.54 (d, J = 8.5 Hz, 1H), 6.50 (s, 1H), 3.70 (t, J = 4.6 Hz, 4H), 3.52 (t, J = 4.5 Hz, 4H), 2.94 (s, 2H), 2.40 (s, 3H), 2.14 (s, 3H), 1.74 ppm (s, 6H). ^{13}C NMR (100 MHz, CD$_3$OD) δ: 174.3, 171.5, 157.4, 154.5, 153.1, 152.7, 144.4, 143.7, 142.5, 138.6, 137.3, 136.7, 131.4, 131.2, 130.4, 129.0, 128.7, 125.6, 125.3, 121.0, 117.4, 117.2, 114.8, 114.7, 114.0, 108.9, 108.6, 84.8, 67.7, 50.8, 45.6, 42.4, 33.9, 26.0, 20.5 ppm. ^{31}P NMR (162 MHz, CD$_3$OD) δ: –4.12 ppm. HRMS (ESI): m/z 726.2245 [M–H]$^-$ ([C$_{38}$H$_{37}$N$_3$O$_{10}$P] = 726.2222).

3.3.3 Spectroscopy Methods

Absorption measurements were made with a Cary model 50 spectrometer from Varian. Fluorometric measurements were with a QuantaMaster1 photon-counting spectrofluorometer from Photon Technology International, equipped with sample stirring. Stock solutions of rhodamine **3.4** and p-nitrophenol were in DMSO; stock solutions of substrate **3.1** were in MeOH. Stock solutions of monosodium phosphate and p-nitrophenyl phosphate (**3.5**) were in 0.10 M MOPS, pH 8.0, containing NaCl (0.50 M). Stock solutions were diluted, such that the final organic solvent concentration did not

exceed 1% v/v for alkaline phosphatase assays. MOPS buffers were adjusted to the appropriate pH by adding either 1.0 M HCl or 1.0 M NaOH. *E. coli* alkaline phosphatase (2 × 47 kDa (Sun, *et al.*, 1999)) was obtained from Sigma–Aldrich (Product No. P4069) as a solution in buffered aqueous glycerol. All assays and standard curves were performed in triplicate, and uncertainties were expressed as the standard deviation.

3.3.4 Fluorometric Assay with Substrate 3.1

Substrate **3.1** was diluted to appropriate concentrations and added to 2.0 mL of MOPS buffer, pH 8.0. Reactions were initiated by the addition of alkaline phosphatase to a final concentration of 13 ng·mL^{-1} (0.14 nM). Product formation was measured by fluorescence (λ_{ex} = 496 nm, λ_{em} = 520 nm). Fluorescence units were converted to product concentration by using a standard curve made with rhodamine **3.4**. Initial velocities were calculated ensuring that the total product concentration did not exceed 0.5 µM.

3.3.5 Rate-Determining Step in Fluorogenesis

For substrate **3.1** to be useful in evaluating alkaline phosphatase activity, the rate-determining step for fluorogenesis must be the enzyme-catalyzed hydrolysis step, not the spontaneous lactonization step. The rate constant for trimethyl lock lactonization had been measured previously (Nicolaou, *et al.*, 1996b), but not in the context of a continuous assay for an enzyme-catalyzed reaction. Accordingly, we used two distinct assays to assess whether the rate of fluorogenesis reports on alkaline phosphatase activity.

*Chromogenic Assay with Substrate **3.1** and p-Nitrophenyl Phosphate at pH 7 and 8.*

Substrate **3.1** or *p*-nitrophenyl phosphate was diluted to appropriate concentrations and added to 1.0 mL of MOPS buffer at pH 7.0 or 8.0. Reactions were initiated by the addition of alkaline phosphatase to a final concentration of 25 ng·mL^{-1} (0.27 nM). Product formation was measured by the absorbance at 496 nm of rhodamine **3.4**, and that at 410 nm of *p*-nitrophenol (Scheme 3.1). Extinction coefficients were obtained from standard curves at pH 7.0 or 8.0.

*Malachite Green Assay with Substrate **3.1**.* Malachite green color reagent was prepared essentially as described previously (Baykov, *et al.*, 1988). Briefly, concentrated sulfuric acid (60 mL) was added to water (300 mL), and the resulting solution was cooled to room temperature. Malachite green oxalate (440 mg, 0.95 mmol) was dissolved in this solution. On the day of its use, the color reagent was made by adding 2.5 mL of 7.5% w/v ammonium molybdate to 10 mL of the malachite green solution. Due to the low concentrations of inorganic phosphate generated during the assay, surfactant was omitted from this reagent, as the color development reaction at phosphate concentrations <10 μM was slow in the presence of surfactant (data not shown).

Substrate **3.1** was dissolved in 1.8 mL of 0.10 M MOPS, pH 8.0, containing NaCl (0.50 M). Alkaline phosphatase was added to a final concentration of 25 ng^{-1}·mL (0.27 nM). The production of rhodamine **3.4** was monitored by its absorbance at 496 nm (*t* = 0 and 360 s). The production of phosphate was determined by removing aliquots (800 μL) from the reaction mixture (*t* = 0 and *t* = 600 s), quenching with 200 μL of color reagent in a new cuvette, and reading the absorbance at 630 nm after 3 min to allow the color to

develop completely. Extinction coefficients were determined by generating standard

curves for rhodamine **3.4** and monosodium phosphate.

3.6

Proton NMR, 400 MHz
CDCl$_3$

3.6

Carbon-13 NMR, 100 MHz
CDCl$_3$

3.6

Phosphorus-31 NMR, 162 MHz
$CDCl_3$

PPM

Proton NMR, 400 MHz
CD$_3$OD

3.1

PPM

5.87

2.93
2.93

1.89

4.08
4.00

1.01
0.97
0.94

1.08
0.96
1.04

0.96
0.95
0.93

0.97
0.96

0.93

Carbon-13 NMR, 100 MHz
CD₃OD

3.1

112

3.1

Phosphorus-31 NMR, 162 MHz
CD$_3$OD

-40 PPM

-20

0

20

40

60

80

100
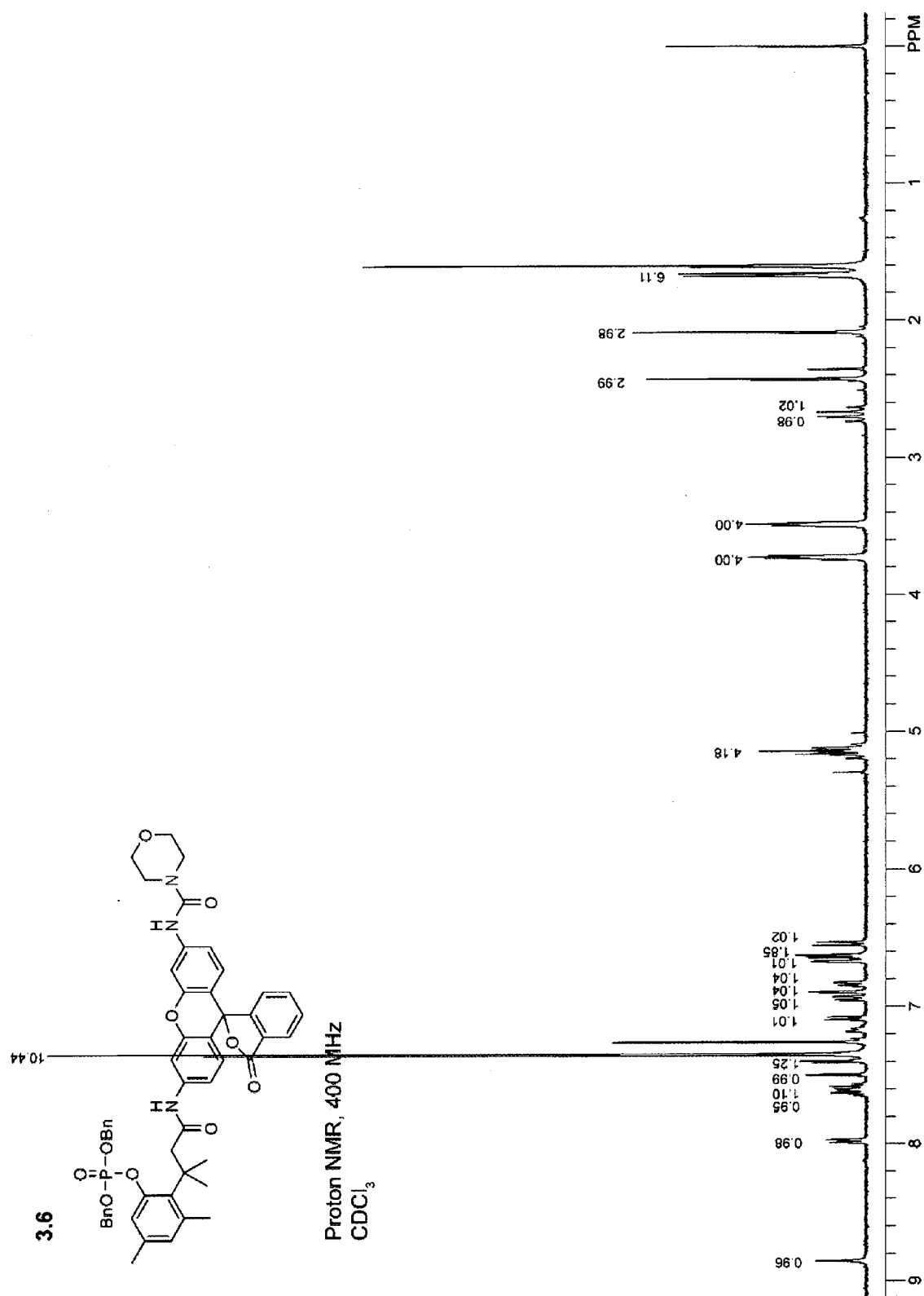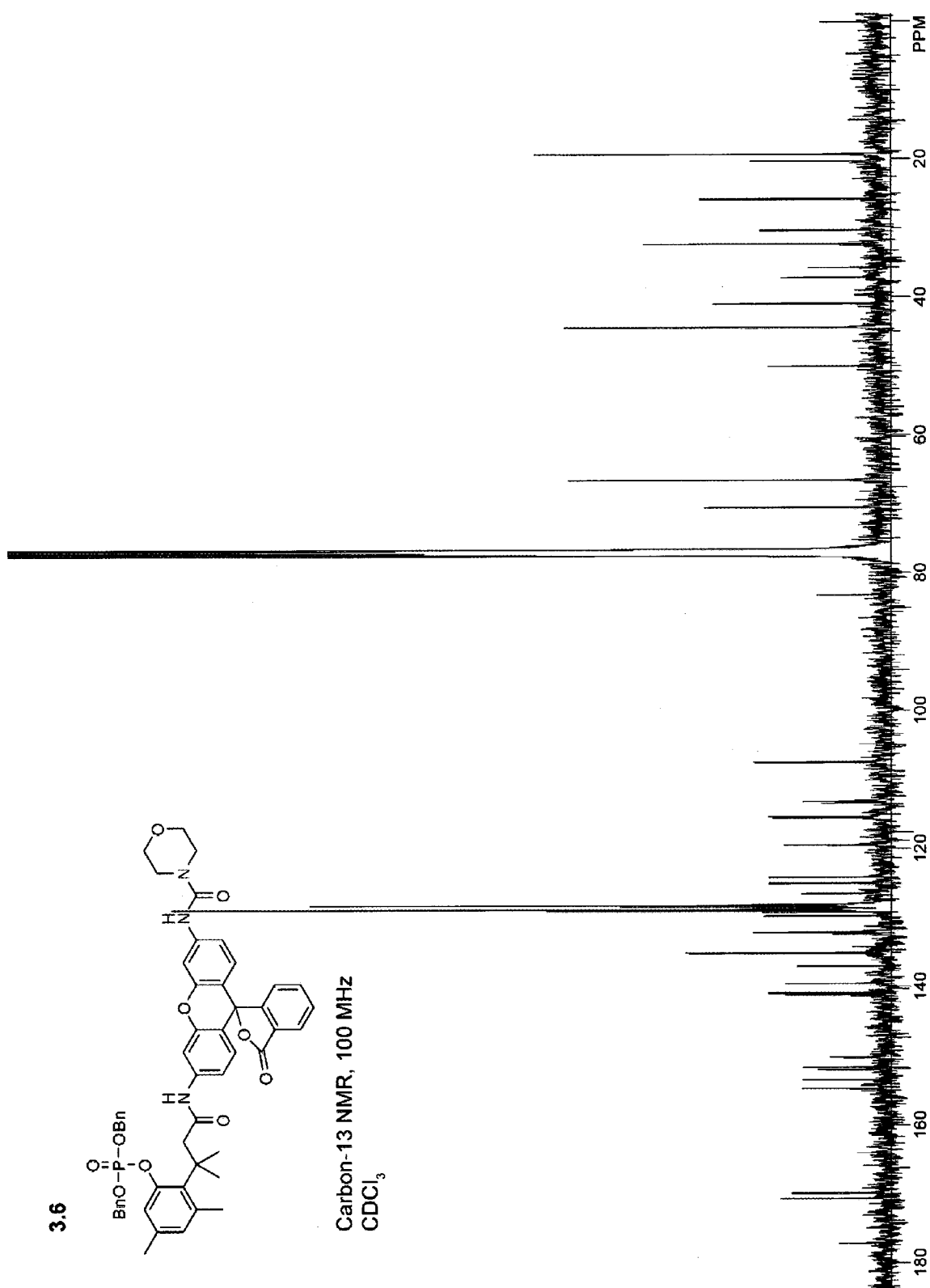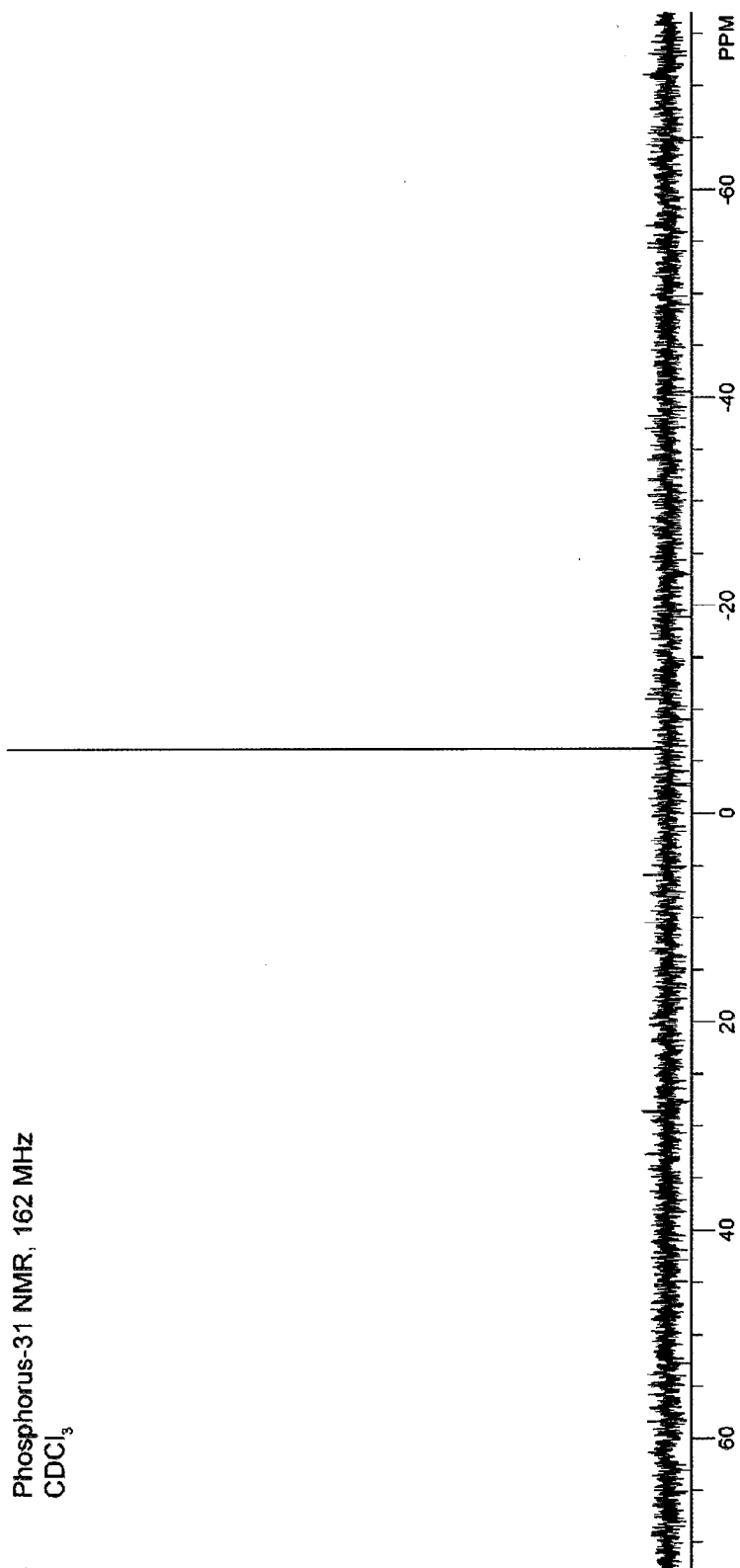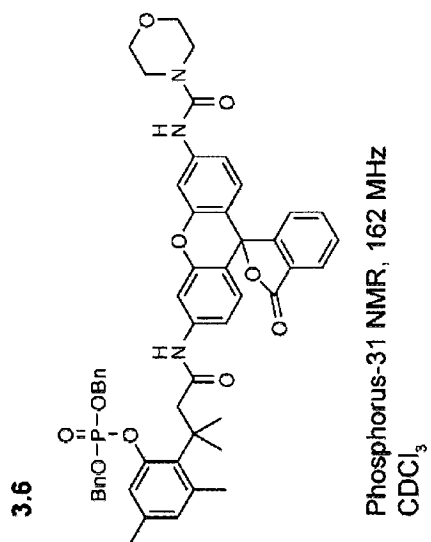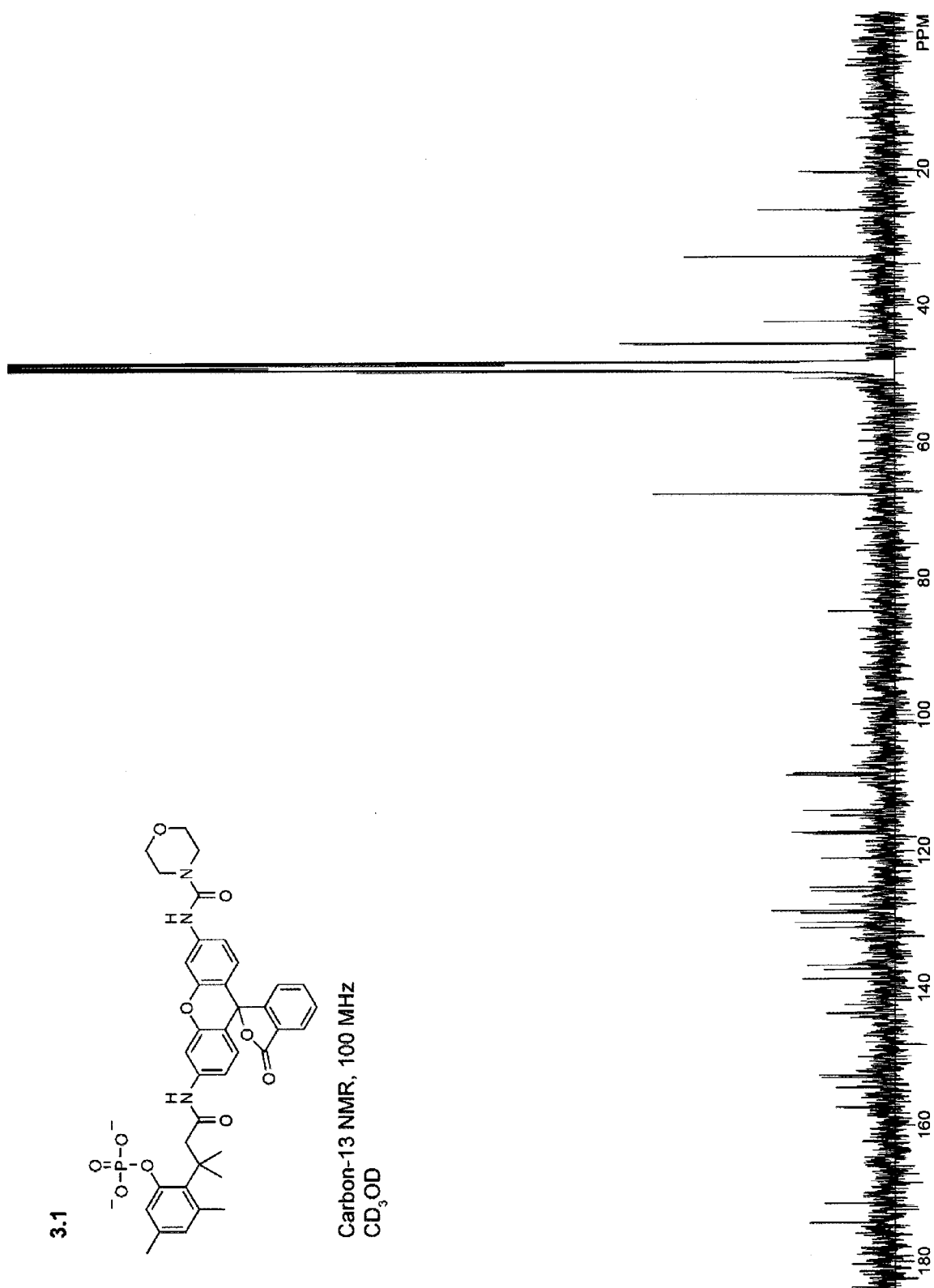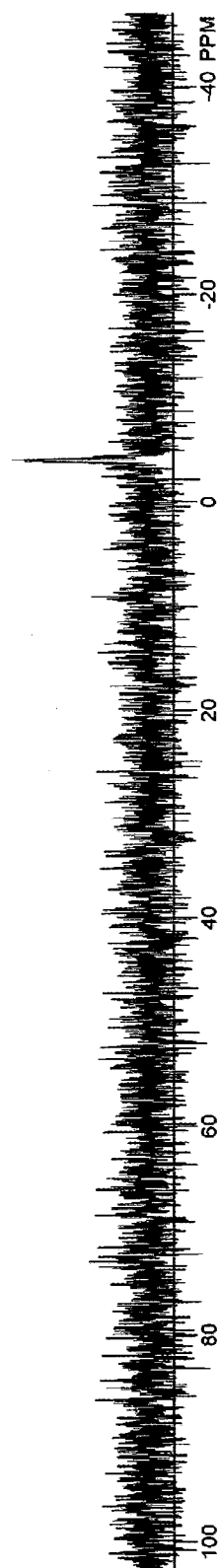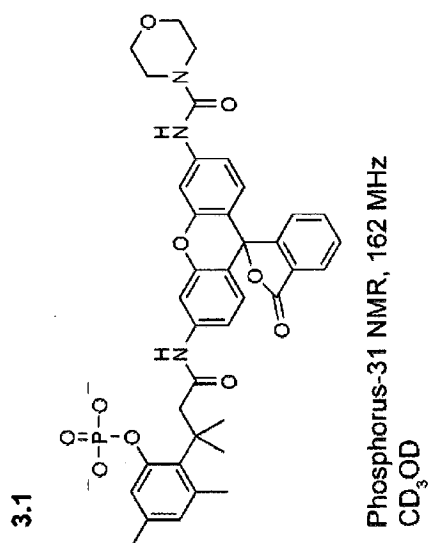
3.4 Results and Discussion

3.4.1 Synthesis of Substrate 3.1

Our strategy for the synthesis of a fluorogenic substrate for alkaline phosphatase is shown in Scheme 3.2. We had described rhodamine **3.4** previously (Lavis, *et al.*, 2006a). Acid **3.5** was synthesized by a known procedure (Nicolaou, *et al.*, 1996b). Our attempts to couple the poorly nucleophilic rhodamine **3.4** with sterically hindered acid **3.5** failed with standard carbodiimides, mixed anhydrides, and acid chlorides. Only acid-chloride formation *in situ*, using an α-chloroenamine under neutral conditions (Haveaux, *et al.*, 1979; Levine, *et al.*, 2008), followed by the addition of morpholinourea rhodamine and pyridine, led to successful coupling. This reaction produced an acceptable yield of 52%, despite the poor solubility of morpholinourea rhodamine in dichloromethane. The benzyl protecting groups were removed by hydrogenolysis in methanol, and substrate **3.1** was purified as its diammonium salt.

3.4.2 Fluorometric Assay for Alkaline Phosphatase

A Michaelis–Menten kinetic analysis of catalysis by alkaline phosphatase was performed using substrate **3.1** (Figure 3.1). The hydrolysis of **3.1** yields equimolar inorganic phosphate, dihydrocoumarin **3.3**, and rhodamine **3.4** (Scheme 3.1). Rhodamine **3.4**, which has an extinction coefficient of 48,600 $M^{-1}cm^{-1}$ and a quantum yield of 0.49 (Lavis, *et al.*, 2006a), can be detected by fluorescence spectroscopy at concentrations «1 μM, which is the inhibition dissociation constant of inorganic

phosphate for *E. coli* alkaline phosphatase (O'Brien and Herschlag, 2002). Even for the highest substrate concentrations assayed herein, the highest measured product concentration reached only 0.3 μM. Thus, the high sensitivity of substrate **3.1** can provide accurate kinetic data by ensuring that inorganic phosphate does not attain inhibitory concentrations.

3.4.3 Rate-Determining Step for Alkaline Phosphatase-Catalyzed Hydrolysis of Substrate 3.1

As shown in Scheme 3.1, two steps are required for the generation of fluorescence from substrate **3.1**: (1) enzyme-catalyzed P–O bond cleavage to release phenol **3.2** and inorganic phosphate, and (2) nonenzymatic lactonization of phenol **3.2** with concomitant release of morpholinourea rhodamine **3.4**. For substrate **3.1** to provide a valid report of alkaline phosphatase activity, the rate of nonenzymatic lactonization must be faster than that of enzyme-catalyzed P–O bond cleavage.

We used two methods to verify that the rate-determining step of fluorescence generation from substrate **3.1** is indeed the enzymatic step. First, we compared the effect of pH on the steady-state kinetic parameters for the production of rhodamine **3.4** with that for the production of *p*-nitrophenol from *p*-nitrophenyl phosphate (which does not entail a nonenzymatic step). Then, we measured independently the rate of fluorogenesis and the rate of inorganic phosphate production.

3.4.4 Comparison of Substrate 3.1 to p-Nitrophenyl Phosphate at pH 7 and 8

In addition to its utility as a latent fluorophore, substrate **3.1** can also be employed as a latent chromophore, as rhodamine **3.4** has robust absorbance at 496 nm. Alkaline phosphatase is often assayed by monitoring its ability to catalyze the hydrolysis of another latent chromophore, *p*-nitrophenyl phosphate, to form *p*-nitrophenol (Scheme 3.1), which has a conjugate base with absorbance at 410 nm. Unlike with substrate **3.1**, P–O bond cleavage of *p*-nitrophenyl phosphate generates a chromophore in a single step (Cleland and Hengge, 2006). Accordingly, a comparison of these two chromogenic substrates can be used to assess the rate-determining step for the production of rhodamine **3.4** from substrate **3.1**.

The steady-state kinetic parameters for the hydrolysis of different aryl phosphates by *E. coli* alkaline phosphatase determined at pH 7 should vary in a constant manner when determined at pH 8 (Cleland and Hengge, 2006; Hull, *et al.*, 1976; O'Brien and Herschlag, 2002). This variance would be confounded if lactonization, rather than hydrolysis, were rate-determining for fluorogenesis from substrate **3.1**. The value of k_{cat} for the alkaline phosphatase-catalyzed hydrolysis of *p*-nitrophenyl phosphate is known to increase by ~3-fold from pH 7 to 8 (Sun, *et al.*, 1999). Accordingly, we assayed the ability of alkaline phosphatase to generate chromophores from substrate **3.1** and *p*-nitrophenyl phosphate at pH 7 and 8.

We found that the alkaline phosphatase-catalyzed hydrolysis of both substrate **3.1** and *p*-nitrophenyl phosphate varied with pH (Table 3.1). Importantly, both substrates showed a ~3-fold increase in k_{cat} and a ~5-fold increase in K_M at pH 8 compared to pH 7. This

correlation suggests that the enzymatic step limits the rate of fluorogenesis from substrate

3.1. There is, however, a caveat.

Lactonization of phenol **3.2** required deprotonation of the phenolic hydroxyl group

($pK_a \approx 10.3$ (Borchardt and Cohen, 1972a); Scheme 3.1). A pH shift from 7.0 to 8.0

results in a 10-fold increase in the deprotonated form, and should increase the rate of

lactonization by 10-fold. Consequently, some of the observed ~3-fold increase in k_{cat} at

pH 8.0 (Table 3.1) could be due to an increase in the rate of lactonization. Accordingly,

we devised an assay to monitor the hydrolysis and lactonization reactions of substrate **3.1**

simultaneously.

3.4.5 Comparison of Fluorogenesis and Inorganic Phosphate Production

Alkaline phosphatase catalyzes the hydrolysis of substrate **3.1** to inorganic phosphate

and phenol **3.2**, neither of which has measurable absorbance. Malachite green, however,

forms a complex with phosphate and molybdate (Figure 3.1), generating an intense green

color (Baykov, *et al.*, 1988; Chang, *et al.*, 2008; Itaya and Ui, 1966). We found that the

concentrations of inorganic phosphate (malachite green assay) and rhodamine **3.4**

(chromogenesis assay) increased at the same rate upon hydrolysis of substrate **3.1** by

alkaline phosphatase (Figure 3.2). These data, like the comparative pH-dependent rates,

indicate that the enzymatic step is rate-determining for fluorogenesis from substrate **3.1**,

and validate this substrate as a reporter of alkaline phosphatase activity.

3.5 Conclusions

We have generated a sensitive fluorometric substrate that can be used to assay alkaline phosphatase activity without the risk of product inhibition by inorganic phosphate. We have shown that the rate-determining step of fluorogenesis from this substrate is enzyme-catalyzed hydrolysis. We anticipate that substrate **3.1** would be useful for other phosphatases as well, and could achieve widespread use in ELISAs and other assays that employ phosphatases.

Scheme 3.1   Alkaline phosphatase substrates. Unmasking of trimethyl lock substrate

3.1 with alkaline phosphatase requires two steps: an enzymatic step with

phosphatase, and a chemical lactonization step. Comparison of substrate

3.1 to two other assays, *p*-nitrophenyl phosphate and malachite green

determined that the enzymatic step is rate-determining.

p-nitrophenyl phosphate

phosphatase

$HPO_4^{2-} + H^+$

p-nitrophenol

$\lambda_{ab} = 410$ nm

3.1

phosphatase

$HPO_4^{2-} + H^+$

molybdate
malachite green

phosphomolybdate
•
malachite green

$\lambda_{ab} = 630$ nm

3.2

3.3

H^+

3.4

$\lambda_{ab} = 496$ nm
$\lambda_{em} = 520$ nm
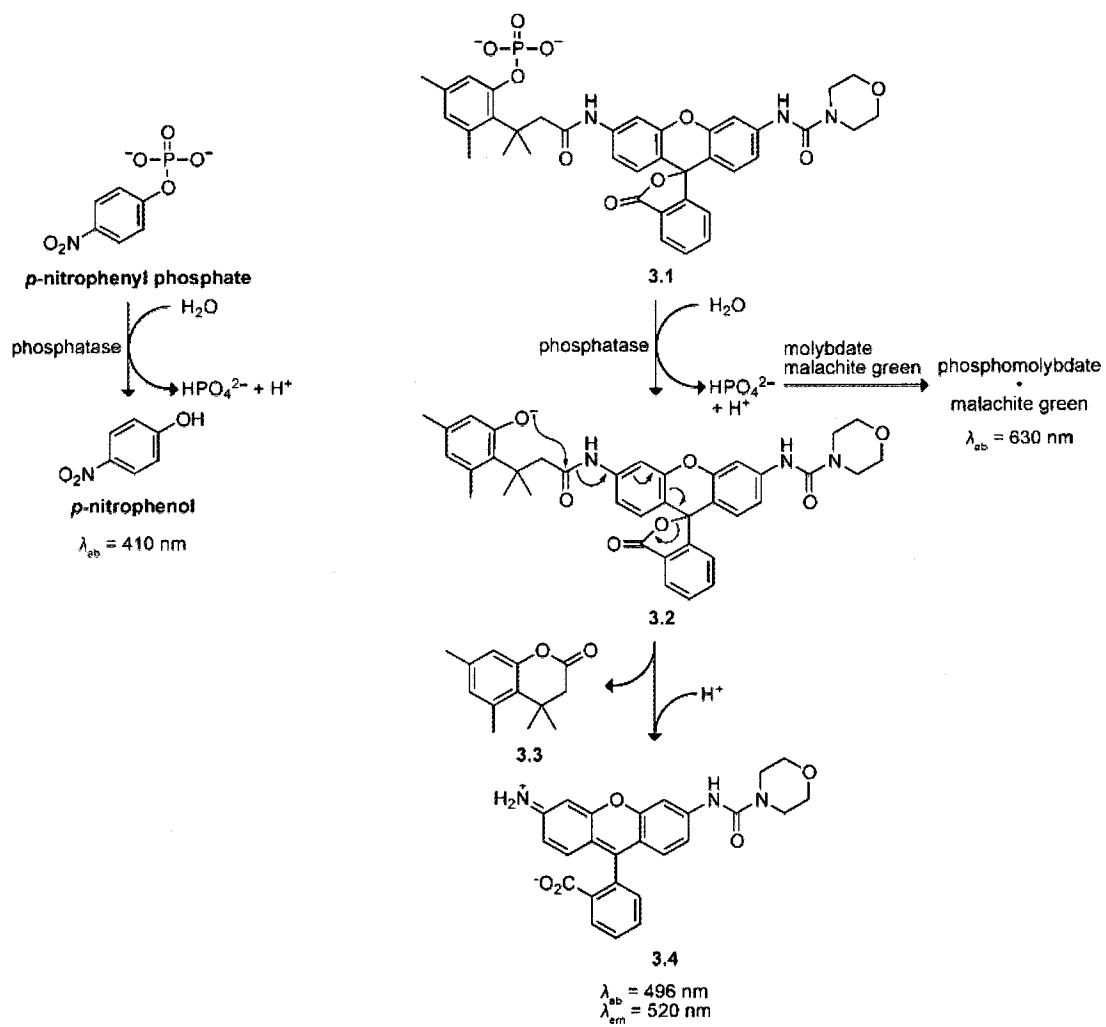
Scheme 3.2   Route for the synthesis of substrate **3.1.**

3.5

1.
2.

3.4

pyr

52% (2 steps)

3.6

1. H₂, Pd/C, MeOH
2. NH₄OAc

66% (2 steps)

3.1
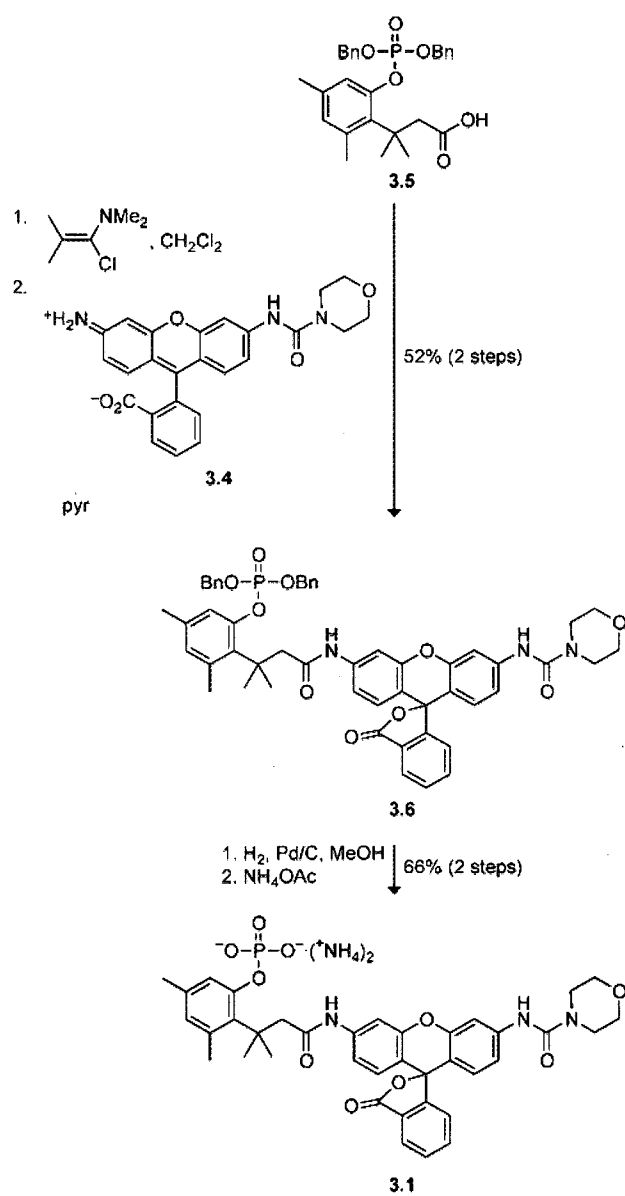
Figure 3.1   Catalysis of the hydrolysis of substrate **3.1** by alkaline phosphatase, as

monitored by fluorescence spectroscopy. Assays were performed in 0.10

M MOPS buffer, pH 8.0, containing NaCl (0.50 M), substrate **3.1** (0.31–

120 μM), and *E. coli* alkaline phosphatase (13 ng·mL^{-1}, which was added

at t = 30 s). Reactions were monitored by the change in fluorescence at

λ_{em} = 520 nm upon excitation at λ_{ex} = 496 nm. Michaelis–Menten analysis

(inset): k_{cat} = (7.3 ± 0.4) s^{-1}, k_{cat}/K_M = (3.3 ± 0.5) × 10^5 M^{-1}s^{-1}.

Uncertainties are expressed as the standard deviation of three experiments.
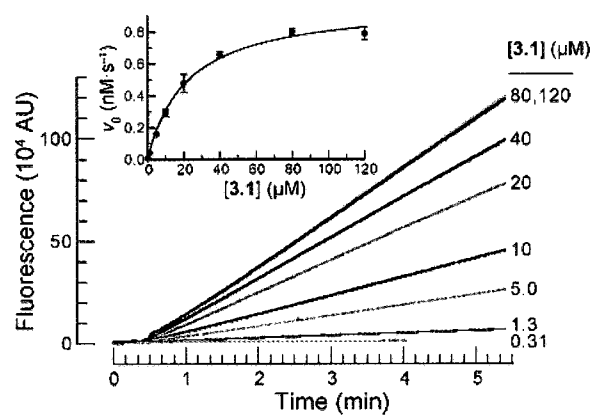
Figure 3.2 Catalysis of the hydrolysis of substrate **3.1** by alkaline phosphatase, as

monitored by absorbance spectroscopy and a malachite green assay for

inorganic phosphate. Michaelis–Menten plots for the serial dilution of

substrate **3.1** (128→5.9 μM) with *E. coli* alkaline phosphatase (25 ng·mL⁻

^{1}) in 0.10 M MOPS buffer, pH 8.0, containing NaCl (0.50 M). Product

formation was measured by the absorbance of rhodamine **3.4** at 496 nm

(●): $k_{cat} = (13 \pm 1)$ s^{-1}, $k_{cat}/K_M = (5.0 \pm 1.2) \times 10^5$ M^{-1}s^{-1}; or by a malachite

green assay for inorganic phosphate (○): $k_{cat} = (10 \pm 2)$ s^{-1}, $k_{cat}/K_M = (6.9 \pm$

$3.6) \times 10^5$ M^{-1}s^{-1}. Uncertainties are expressed as the standard deviation of

three experiments.
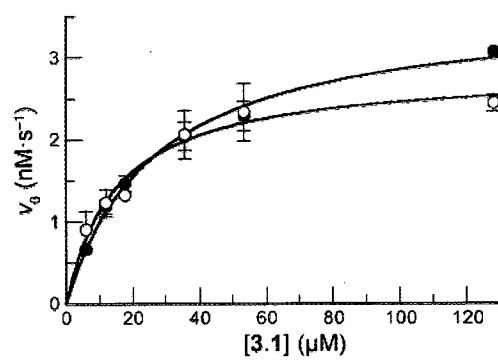
Table 3.1. Alkaline phosphatase assay of p-nitrophenyl phosphate and substrate **3.1** at pH 7 and 8.

	p-nitrophenyl phosphate			Substrate **3.1**		
	k_{cat} (s^{-1})	K_M (µM)	k_{cat}/K_M (M^{-1}s^{-1})	k_{cat} (s^{-1})	K_M (µM)	k_{cat}/K_M (M^{-1}s^{-1})
pH 8.0	118 ± 2	4.6 ± 0.4	$(2.6 \pm 0.2) \times 10^7$	13 ± 1	26 ± 6	$(5.0 \pm 1.2) \times 10^5$
pH 7.0	35 ± 1	1.0 ± 0.1	$(3.4 \pm 0.5) \times 10^7$	4.7 ± 0.5	5.4 ± 2.5	$(8.6 \pm 4.2) \times 10^5$
Ratio	3.3 ± 0.1	4.5 ± 0.8	0.75 ± 0.13	2.9 ± 0.4	4.9 ± 2.6	0.58 ± 0.32

Kinetic parameters ($\pm$ SD) were determined by monitoring reactions in 0.10 M MOPS buffer containing NaCl (0.50 M) and *E. coli* alkaline phosphatase (25 ng·mL^{-1}) with spectrophotometry (p-nitrophenyl phosphate, $\lambda = 410$ nm; substrate **3.1**, $\lambda = 496$ nm).

CHAPTER 4

A Profluorophore Headgroup-Modified Lipid

to Assay Constitutive Cellular Endocytosis

4.1   Introduction

Endocytosis is the key regulator of macromolecular internalization in eukaryotic cells (Conner and Schmid, 2003). Extracellular proteins do not enter cells through membrane transporters, as small molecule metabolites or ions do, but must be internalized by endocytosis. Endocytosis is the process of plasma membrane invagination and fusing to pinch off a lipid bilayer vesicle in the interior of a cell. Many endocytic pathways operate in parallel. The most well studied pathway, clathrin-mediated endocytosis, occurs constitutively in all cell types and generally involves binding of a ligand to a receptor prior to internalization (Conner and Schmid, 2003). Caveolin-mediated endocytosis is characterized by vesicles enriched in glycosphingolipids, cholesterol, and the integral membrane protein, caveolin (Thomsen, *et al.*, 2002). These pathways allow delivery of essential nutrients into cells, for example, iron via transferrin, and cholesterol via lipoprotein particles. Alternatively, the endocytic system may be hijacked by pathogens and their toxins, such as influenza, cholera toxin, and diphtheria toxin (Chinnapen, *et al.*, 2007; Lakadamyali, *et al.*, 2004; Murphy, 2011).

Endocytosis directly influences cell signaling, disruption of which is a hallmark of cancer (Hanahan and Weinberg, 2011). Endocytosis regulates a signaling receptor's concentration and activity by transporting it to and from the plasma membrane (Mosesson, *et al.*, 2008). Additionally, inappropriate trafficking is associated with loss of cellular polarity in cancer, a precursor to metastasis. Responsible for the maintenance of cell polarity, cadherins may be inappropriately routed away from cell-cell junctions in

cancer. The dissolved junctions would lead to enhanced endocytosis due to the greater exposed surface area of the membrane. Insights into the differences in endocytosis between cancerous cells and normal cells may lead to novel treatment options. Some pancreatic-type ribonucleases (RNases) are specifically cytotoxic to cancer cells (Leland and Raines, 2001; Makarov and Ilinskaya, 2003; Rutkoski, *et al.*, 2005; Turcotte, *et al.*, 2009). When applied exogenously, RNases are internalized by receptor-independent endocytosis, after which they escape from the endosomes to the cytoplasm where they degrade cellular RNA. The mechanism of cancer-specific cytotoxicity has not been elucidated, but may be a result of differences in endocytosis.

Lipid dynamics may be assayed using fluorescent lipid probes (Maier, *et al.*, 2002). Due to the relatively small molecular weight of lipids compared to the size of the probes, fluorescent labeling may alter the function of a lipid. Typically, a fluorescent probe is conjugated to a lipid in one of two locations: the head group, or the fatty acyl chain. The position of labeling depends on the assay that is to be performed and on the chemical nature of the fluorophore (Maier, *et al.*, 2002). Modification of the head group is not desirable if the head group is important for function, for example, phosphatidylserine in apoptosis. Consideration of whether the probe fluoresces in an aqueous or lipid environment is essential.

Two examples of fluorescent membrane probes are N-(lissamine rhodamine B sulfonyl)phosphatidylethanolamine (N-Rh-PE) and N-(3-triethylammoniumpropyl)-4-(4-dibutylamino)styryl)pyridinium dibromide (FM 1-43). N-Rh-PE is a headgroup-modified lipid that is constitutively fluorescent and has high background fluorescence

(Kok, *et al.*, 1990). Extensive washing is required to remove the non-specifically bound and soluble molecules. N-Rh-PE is typically used in conjunction with a second fluorescent lipid in liposomes which undergo Förster resonance energy transfer (FRET) upon membrane fusion and lipid mixing. This type of fluorophore cannot measure endocytosis because it is not possible to exclusively label either endosomes or the plasma membrane.

One advantage of FM 1-43 is that it is a membrane-intercalated fluorophore that is only fluorescent when membrane bound (Cochilla, *et al.*, 1999; Rea, *et al.*, 2004). This property reduces the background fluorescence in solution, yet FM 1-43 does not show a change in fluorescence intensity when localized in either the endosome or cell membrane. FM 1-43 is predominantly used for exocytosis assays of secretory vesicles at neuron synapses. In these assays, the dye is added to neurons and allowed to be endocytosed where it is stored in synaptic vesicles. The remaining dye in the outer cell membrane is washed away. A stimulus that causes depolarization of the neuron leads to exocytosis of the vesicles and transfer of the dye back to the cell membrane. The rate of exocytosis is measured as a decrease in fluorescence in the neuron cell membrane after destaining with fresh media. This method is not generally applicable to other cell types unless exocytosis is stimulus dependent, for example in pituitary endocrine tissues (Brumback, *et al.*, 2004; Cochilla, *et al.*, 1999). As with N-Rh-PE, FM 1-43 cannot be used to assay endocytosis. Both dyes stain the cellular membrane in addition to endosomes, limiting their use in quantifying internalization (Kok, *et al.*, 1990; Rea, *et al.*, 2004). Similarly to exocytosis, endosome recycling can be measured by alternating staining and destaining with N-[N-

(7-nitro-2,1,3-benzoxadiazol-4-yl)-ε-aminohexanoyl]-sphingosylphosporylcholine (C$_6$-NBD-SM) (Hao and Maxfield, 2000; Mayor, *et al.*, 1993).

Endocytosis has been quantified by assaying the uptake of soluble enzymes, such as horseradish peroxidase, and staining with colorimetric substrates (Steinman and Cohn, 1972). The approximate surface area of endosomal membranes could be observed and measured over time to calculate a rate of endocytosis. We hoped to convert this tedious process into an objective assay for endocytosis by utilizing a headgroup-modified profluorophore lipid. A profluorophore would have no background fluorescence, and would be able to label endosomes independently of the plasma membrane; therefore, the rate of endocytosis would be directly proportional to the amount of fluorescence generated over time. The synthesis and characterization of this profluorophore lipid is described below.

4.2   Results and Discussion

4.2.1 Synthesis of Lipid 4.3

Profluorophore **4.1** (Scheme 4.1) (Lavis, *et al.*, 2006a) was conjugated to the head group of the non-native lipid 1,2-dihexadecanoyl-*sn*-glycero-3-phosphothioethanol (**4.2**; DPPTE; Avanti Polar Lipids). DPPTE contained a thiol which underwent a conjugate addition reaction with the maleimide of profluorophore **4.1**. This reaction proceeded smoothly in chloroform with triethylamine to produce **4.3** in 66% isolated yield.

Lipid **4.3** contains a trimethyl lock that can be activated by non-specific esterases (Amsberry and Borchardt, 1990; Lavis, *et al.*, 2006a). The trimethyl lock is a prodrug strategy in which steric interactions between three interlocking methyl groups lead to rapid lactone formation to produce dihydrocoumarin **4.5** with concomitant release of an amine. Acylation of the fluorophore rhodamine with the trimethyl lock results in masking of its fluorescence (Chandran, *et al.*, 2005). Esterase-catalyzed hydrolysis of acetyl ester **4.3** produces phenol **4.4**, which undergoes rapid lactonization to release the fluorescent **4.6** and dihydrocoumarin **4.5**. Previously, profluorophore **4.1** has been appended to proteins or biological ligands to assay the endocytosis of ribonucleases (Chao and Raines, 2011; Lavis, *et al.*, 2006a; Turcotte, *et al.*, 2009) or the internalization of cell surface receptors (Mangold, *et al.*, 2008).

Headgroup-modified lipids are incorporated from solution into cell membranes (Kok, *et al.*, 1990). Addition of lipid **4.3** to cells in which endocytosis has been arrested at low temperature, should lead to uptake into the plasma membrane. Endocytosis is initiated with warming, leading to an increase in fluorescence as profluorophore **4.3** becomes exposed to non-specific esterases in endosomes. Measuring the rate of endocytosis over time by this method should be simplified compared to other methods, as there is no pre-equilibrium binding of the substrate to the cell membranes before endocytosis occurs.

*4.2.2 Microscopy of Lipid **4.3** Endocytosis*

As shown in Figure 4.1, lipid **4.3** displayed a punctate staining pattern in HeLa cells incubated at 37 °C for 3 hours. This pattern was not observed in unlabeled cells, nor in

labeled cells incubated at 4 °C for 3 hours. A punctate staining pattern was evidence for vesicular localization of the fluorescence. The increase in fluorescence was dependent on endocytosis, indicated by the lack of fluorescence in cells that were never warmed.

Lipid **4.3** partially colocalized with LysoTracker Red, a marker of acidic vesicles (Figure 4.2A). As expected, upon initiation of endocytosis, some vesicles fused with late endosomes or lysosomes. Colocalization of lipid **4.3** and LysoTracker Red could be observed in these subcellular compartments. In contrast, lipid **4.3** did not colocalize with a fluorescently tagged transferrin conjugate (Figure 4.2B–C). Transferrin, a well-characterized marker of recycling endosomes, was added either at the initiation of endocytosis, or after 2 hours; however, neither condition resulted in colocalization.

The lack of colocalization with transferrin might be explained by an absence of the esterases responsible for unmasking of **4.3** in early or recycling endosomes. Chao *et al.* showed that RNase A, labeled with profluorophore **4.1**, did colocalize with transferrin; therefore, esterase activity must have been present in those compartments (Chao and Raines, 2011). Alternatively, lipid **4.3** was not trafficked through recycling endosomes. Some lipids are known to accumulate in specific subcellular compartments, not disperse freely throughout all membranes (Maier, *et al.*, 2002). It was possible that lipid **4.3** did not label recycling endosomes. If recycling were occurring, unmasked **4.6** would be expected to be transported back to the plasma membrane. The results showed that plasma membrane fluorescence was never observed in labeled cells allowed to incubate at 37 °C for 24 hours (Figure 4.3). Based on these results, it was believed that lipid **4.3** was

unmasked in late endosomes and lysosomes, but did not enter the recycling endosome pathway.

4.2.3 Time Course of Endocytosis in HeLa Cells

HeLa cells were labeled in the cold with lipid **4.3** and then incubated for various times at 37 °C. There was an increase in the mean fluorescence per cell over time Figure 4.4). Cells that were incubated for 3 hours possessed a mean fluorescence per cell approximately 4.5-fold higher than cells that were not warmed. This result was in agreement with the microscopy data, which showed that cells had an increase in fluorescence after 3 hours of incubation. Warming of the cells initiated endocytosis, resulted in lipid **4.3** internalization, and subsequently resulted in hydrolysis by non-specific esterases to release fluorescent-lipid **4.6**.

Previous studies typically expressed endocytosis rates as the time it took to endocytose an equivalent of the entire surface area of the cell membrane. For example, the surface area of the membrane of the amoeba *Dictyostelium discoideum*, or of mouse macrophage and L cells were internalized completely every 0.75, 0.53, and 1.85 hours respectively (Thilo and Vogel, 1980). The rate of fluorescence increase in this study could not be correlated to the amount of membrane surface area endocytosed because the initial quantity of the non-fluorescent lipid **4.3** in the plasma membrane could not be determined. Attempts were made to unmask lipid **4.3** *in situ* with mammalian and bacterial esterases, or with small molecules such as hydrazine, hydroxylamine and trimethylamine oxide; however, none were successful. It was believed that relatively

large esterases were unable to penetrate the extracellular matrix—a cellular structure not present inside endosomes where unmasking did occur. Future work will focus on determining the extent of membrane labeling with the profluorophore.

4.2.4 Quantifying Endocytosis Between a Matched Cancerous and Normal Cell Line by Flow Cytometry

Human tissue culture cell lines HTB-126 and HTB-125 are matched breast cancer and normal cell lines obtained from the same patient (An, *et al.*, 2008). Comparing endocytosis between the two may provide insights into the regulation of cell growth, signal transduction, and susceptibility to chemotherapeutics. It is difficult to predict *a priori* what alterations in endocytosis are present in cancerous cells. Cells that are not growing are expected to maintain the surface area of their membrane by balancing endocytosis and exocytosis processes (Mayor and Pagano, 2007). The rates of each might reflect turnover of cell-surface receptors. In cancerous cells that are growing, the balance might be shifted away from endocytosis processes, which in turn might lead to less down-regulation of growth and mitogenic receptors. While the ratios of endocytosis to exocytosis may be predicted, the overall rates are less transparent. We are interested in explaining the cancer selectivity of the chemotherapeutic ribonucleases, which must be endocytosed for efficacy. Perhaps bulk endocytosis rates are increased in cancerous cell lines.

We have assayed the cancerous line, HTB-126, utilizing our endocytosis assay and quantifying fluorescence increase by flow cytometry. The increase in fluorescence over 3

h of incubation at 37 °C was approximately 7-fold (2.33–16.8), which was similar to the increase in HeLa cells of 4.5-fold. We are currently optimizing this assay to analyze HTB-125 concurrently with HTB-126.

4.3 Experimental Section

4.3.1 General

All reagents, unless noted, were from Aldrich Chemical (Milwaukee, WI) or Fisher Scientific (Hanover Park, IL), and were used without further purification. Thin-layer chromatography was performed by using aluminum-backed plates coated with silica gel containing F_{254} phosphor, and was visualized by UV illumination or developed with ceric ammonium molybdate stain. Flash chromatography was performed on open columns with silica gel-60 (230–400 mesh).

NMR spectra were obtained with a Bruker DMX-400 Avance spectrometer at the National Magnetic Resonance Facility at Madison (NMRFAM). Mass spectrometry was performed with an Applied Biosystems MDS SCIEX 4800 matrix assisted laser desorption ionization time of flight (MALDI TOF) mass spectrometer at the Mass Spectrometry Facility in the Biotechnology Center, University of Wisconsin–Madison.

4.3.2 Synthesis of Lipid 4.3

Maleimidourea rhodamine (Lavis, *et al.*, 2006a) (**4.1**, 20 mg, 0.026 mmol) was added to a flame dried 10 mL round bottom flask, that had been flushed with Ar(g), and was

dissolved in anhydrous chloroform (5 mL). Anhydrous triethylamine (20 μL, 0.14 mmol) was added, followed by 1,2-dihexadecanoyl-*sn*-glycero-3-phosphothioethanol, sodium salt (Avanti Polar Lipids, Alabaster, AL; **4.2**, 20 mg, 0.027 mmol). The reaction was stirred for 3 hours under Ar(g) covered in foil. Reaction progress was monitored by thin layer chromatography (10% methanol in DCM). Upon completion, the solvent was evaporated under reduced pressure and the residue was placed under high vacuum overnight. The crude product was purified by silica gel chromatography (10–15% methanol in DCM) to yield **4.3** as a white powder (26 mg, 66%). ^{1}H NMR (400 MHz, CDCl$_3$) δ: 8.52 (bs, 1H), 7.94 (d, J = 6.3 Hz, 1H), 7.79 (s, 1H), 7.64–7.50 (m, 2H), 7.39 (s, 2H), 7.05 (d, J = 6.9 Hz, 1H), 6.97 (bs, 1H), 6.76 (s, 1H), 6.64–6.56 (m, 2H), 6.51 (t, J = 7.2 Hz, 2H), 6.13 (s, 1H), 5.20 (s, 1H), 4.35 (d, J = 10.8 Hz, 1H), 4.15–3.86 (m, 6H), 3.52–3.40 (m, 2H), 3.24–2.92 (m, 7H), 2.87–2.75 (m, 1H), 2.63–2.57 (m, 2H), 2.41 (s, 3H), 2.34 (s, 3H), 2.28–2.15 (m, 7H), 1.64 (s, 6H), 1.56–1.46 (m, 4H), 1.33–1.14 (m, 48H), 0.87 (t, J = 6.2 Hz, 6H) ppm. ^{13}C NMR (100 MHz, CDCl$_3$) δ: 178.5, 175.4, 174.0, 173.7, 172.1, 170.4, 170.0, 156.0, 153.0, 151.8, 151.7, 150.1, 142.5, 140.1, 139.0, 137.3, 135.4, 133.2, 133.1, 129.9, 128.3, 126.5, 125.0, 124.2, 123.5, 115.4, 114.7, 114.0, 111.6, 107.6, 106.0, 83.6, 70.6, 65.3, 63.9, 62.9, 50.9, 40.3, 39.6, 37.0, 36.5, 34.4, 34.2, 32.1, 30.2–29.2, 27.1, 26.7, 25.7, 25.1, 25.0, 22.8, 22.0, 20.3, 14.3 ppm. ^{31}P NMR (162 MHz, CDCl$_3$) δ: −1.7 ppm. MS (MALDI): m/z 1487.75 [M+H]$^+$ ([C$_{80}$H$_{113}$O$_{17}$N$_4$NaPS]$^+$ = 1487.75).

4.3.3 Mammalian Cell Culture

HeLa, HTB-125, and HTB-126 cells were from the American Type Culture Collection (ATCC, Manassas, VA). HeLa cells were grown in Dulbecco's Modified Eagle Medium (DMEM) containing fetal bovine serum (FBS; 10% v/v), penicillin (100 units/mL) and streptomycin (100 μg/mL). HTB-125 cells were grown in Hybri-Care Medium supplemented with sodium bicarbonate (1.5 g/L), mouse epidermal growth factor (30 ng/mL), FBS (10% v/v), penicillin (100 units/mL) and streptomycin (100 μg/mL). HTB-126 cells were cultured in DMEM supplemented with bovine insulin (10 μg/mL), FBS (10% v/v), penicillin (100 units/mL), and streptomycin (100 μg/mL). Media and supplements were from Invitrogen (Carlsbad, CA), Sigma Aldrich (Milwaukee, WI) or ATCC. Cells were cultured at 37 °C in a humidified incubator containing $CO_2(g)$ (5% v/v).

4.3.4 Microscopy

Imaging was performed using a Nikon Eclipse TE2000-U laser scanning confocal microscope equipped with a Zeiss AxioCam digital camera. A blue-diode laser was used to provide excitation at 408 nm, and emission light was passed through a 35-nm band-pass filtered centered at 450 nm. An argon-ion laser was used to provide excitation at 488 nm, and emission light was passed through a 40-nm band-pass filter centered at 515 nm. A HeNe laser was used to provide excitation at 543 nm, and emission light was passed through a 75-nm band-pass filter centered at 605 nm.

HeLa cells were plated 24 hours prior to experiments at a density of 1×10^5 cells in 1-cm diameter glass bottom dishes (Electron Microscopy Sciences, Hatfield, PA) in 1 mL DMEM Complete Growth Medium. On the day of the experiments, all cells, media, and pipette tips were pre-cooled to 4 °C for two hours. Next, the cells were washed with serum-free DMEM (3 × 1 mL). Stock solutions of lipid **4.3** (50 mM in DMSO) were diluted to 10 mM with absolute ethanol. From this stock, 1 µL was added to 500 µL of serum-free DMEM, which was then vigorously vortexed, and applied to the HeLa cells. Vehicle treated cells were treated with 500 µL serum-free DMEM containing 1 µL ethanol. The labeling reaction was allowed to proceed for 3 hours at 4 °C, after which, the cells were washed with serum-free DMEM (3 × 1 mL). Cells were incubated for the given amount of time at 37 °C. LysoTracker Red (Invitrogen) was used to stain acidic vesicles at a concentration of 50 nM for the final 20 minutes of incubation at 37 °C. Endocytic marker AlexaFluor 594–transferrin (Invitrogen) was incubated for either 1 or 3 hours at 37 °C with profluorophore **4.3** labeled HeLa cells at a concentration of 1 µM. Nuclear counterstaining was performed with Hoechst 33342 (Invitrogen) at a concentration of 2 µg/mL for the final 5 minutes at 37 °C. Cells were washed with serum-free DMEM prior to imaging.

4.3.5 Flow Cytometry

Flow cytometry was performed in the University of Wisconsin Carbone Cancer Center using a FACSCalibur instrument equipped with a 488 argon-ion air cooled laser (Becton Dickinson, Franklin Lakes, NJ). Fluorescence emission light was passed through

a 30-nm band pass filter centered at 530 nm. Cell lines were plated 24 hours prior to

experiments at a density of 3×10^5 cells in T-25 tissue culture flasks (BD Biosciences) in 6

mL of their respective media, described above in "Mammalian Cell Culture". On the day

of the experiments, all cells, media, and pipette tips were pre-cooled to 4 °C for two

hours. Next, the cells were washed with serum-free DMEM (3 × 1 mL). Stock solutions

of lipid **4.3** (50 mM in DMSO) were diluted to 10 mM with absolute ethanol. This stock

solution in ethanol was added to serum-free DMEM to a final concentration of 20 μM,

and was vigorously vortexed. The media was removed from the cells and was replaced

with 1 mL of the labeling solution. Vehicle treated cells were treated with 1 mL serum-

free DMEM containing 2 μL ethanol. The labeling reaction was allowed to proceed for 3

hours at 4 °C, after which, the cells were washed with serum-free DMEM (3 × 1 mL).

Cells were incubated for the given amount of time at 37 °C. Cells were washed with

DPBS (1 mL; Invitrogen) and treated with trypsin/EDTA (0.25% w/v; 750 μL) for 5

minutes at 37 °C. The trypsin was neutralized with DMEM containing FBS (10% v/v;

750 μL), and the cells were pelleted by centrifugation (5 minutes at 400 × g). The

supernatant was decanted and the pellet was resuspended in 1 mL DPBS, and then

centrifuged (5 minutes at 400 × g). The supernatant was decanted and the pellet was

resuspended and fixed with 100 μL of a 2% solution of formaldehyde for 30 minutes

covered in foil. This solution was diluted up to 1 mL with DPBS, and was centrifuged (5

minutes at 400 × g). The supernatant was decanted and the pellet was resuspended in 1

mL DPBS. The suspension was strained through a 35 μm filter into a polystyrene flow

cytometry test tube (BD Biosciences). The fixed cells were stored on ice until analyzed

(approximately 1-4 hours). The mean fluorescence per cell was determined for 10,000

cells and analyzed using Flowjo software.

4.3

Proton NMR, 400 MHz
CDCl₃

144

4.3

Carbon-13 NMR, 100 MHz
CDCl₃

4.3
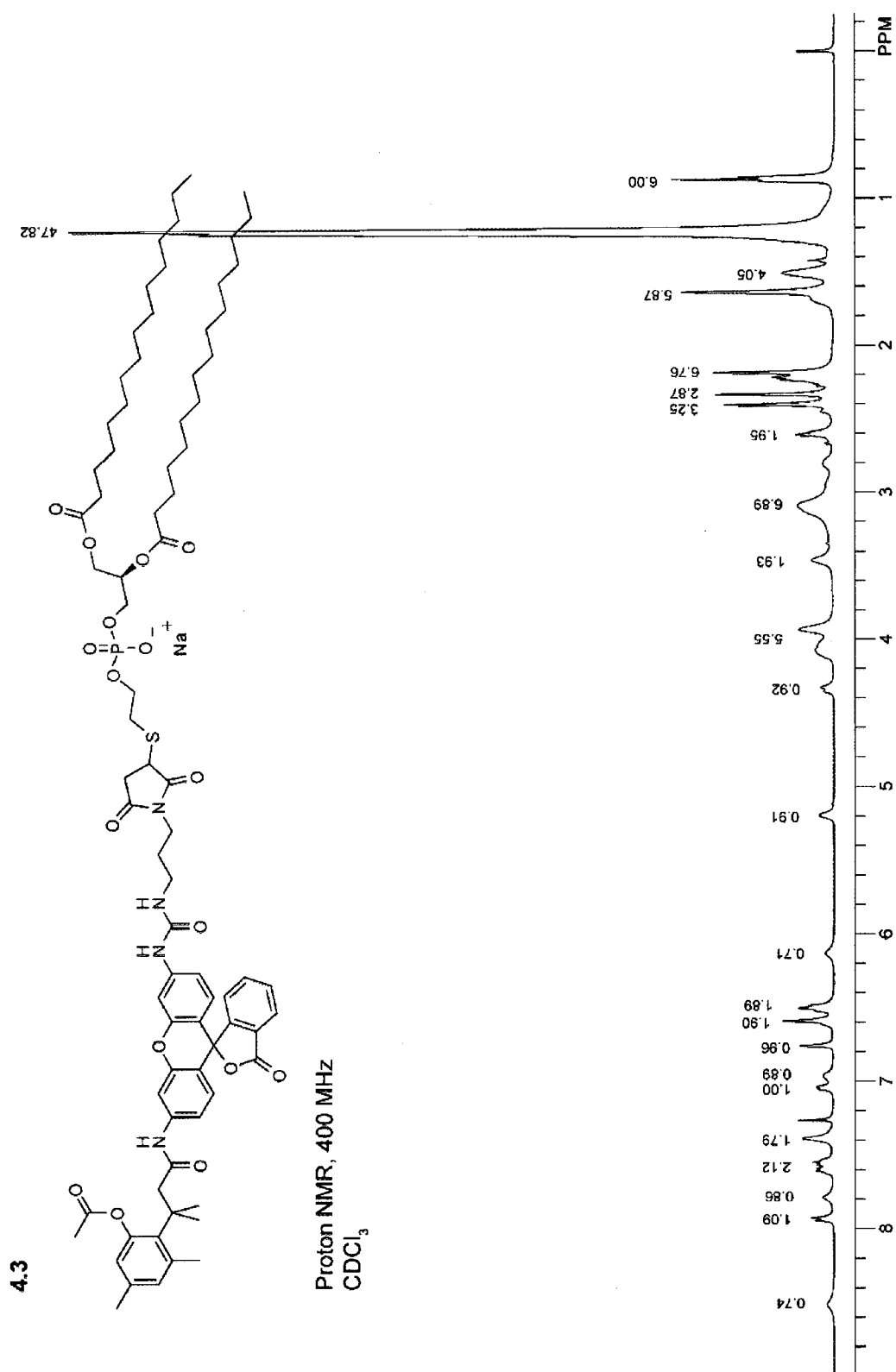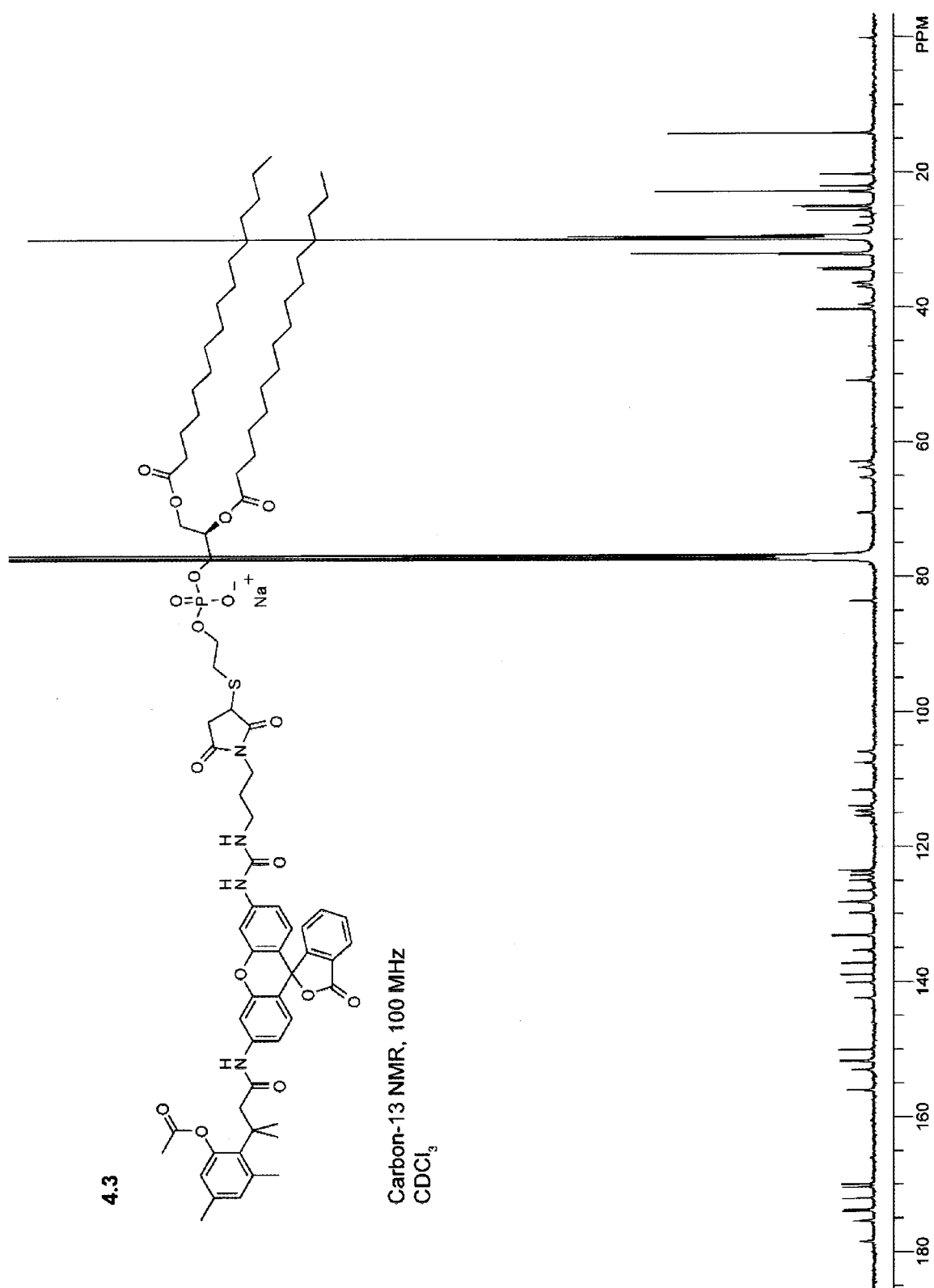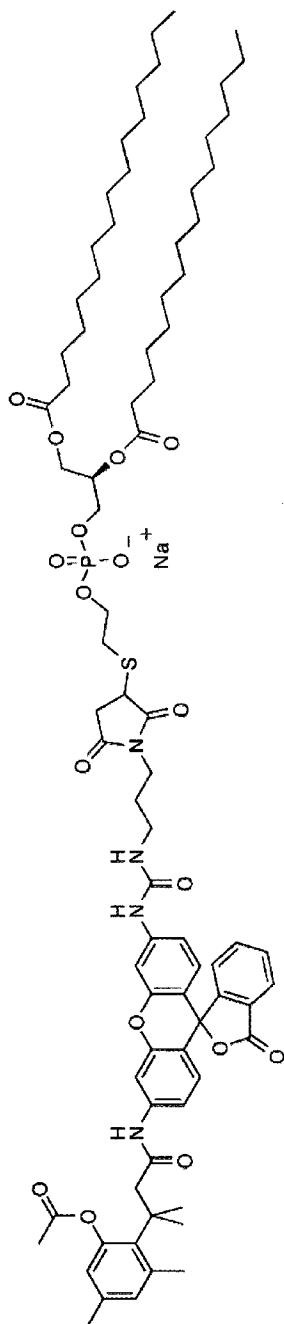
Phosphourus-31 NMR, 162 MHz
CDCl$_3$
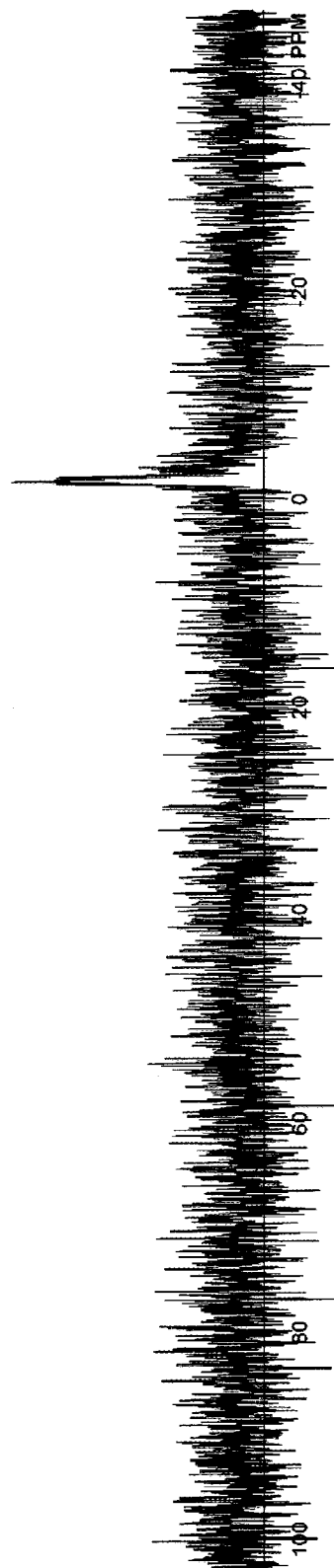
4.4 Conclusions

We have synthesized a headgroup-modified lipid that can be incorporated into the plasma membrane, and that becomes fluorescent upon initiation of endocytosis. The lipid is trafficked to late endosomes and lysosomes and does not enter the recycling endosome pathway. The increase in fluorescence can be monitored over time by flow cytometry and we believe this assay will be amenable to quantifying differences in endocytosis between cancerous and normal cell lines.

Scheme 4.1 Synthesis of lipid **4.3** and mechanism of esterase-mediated fluorescence

development
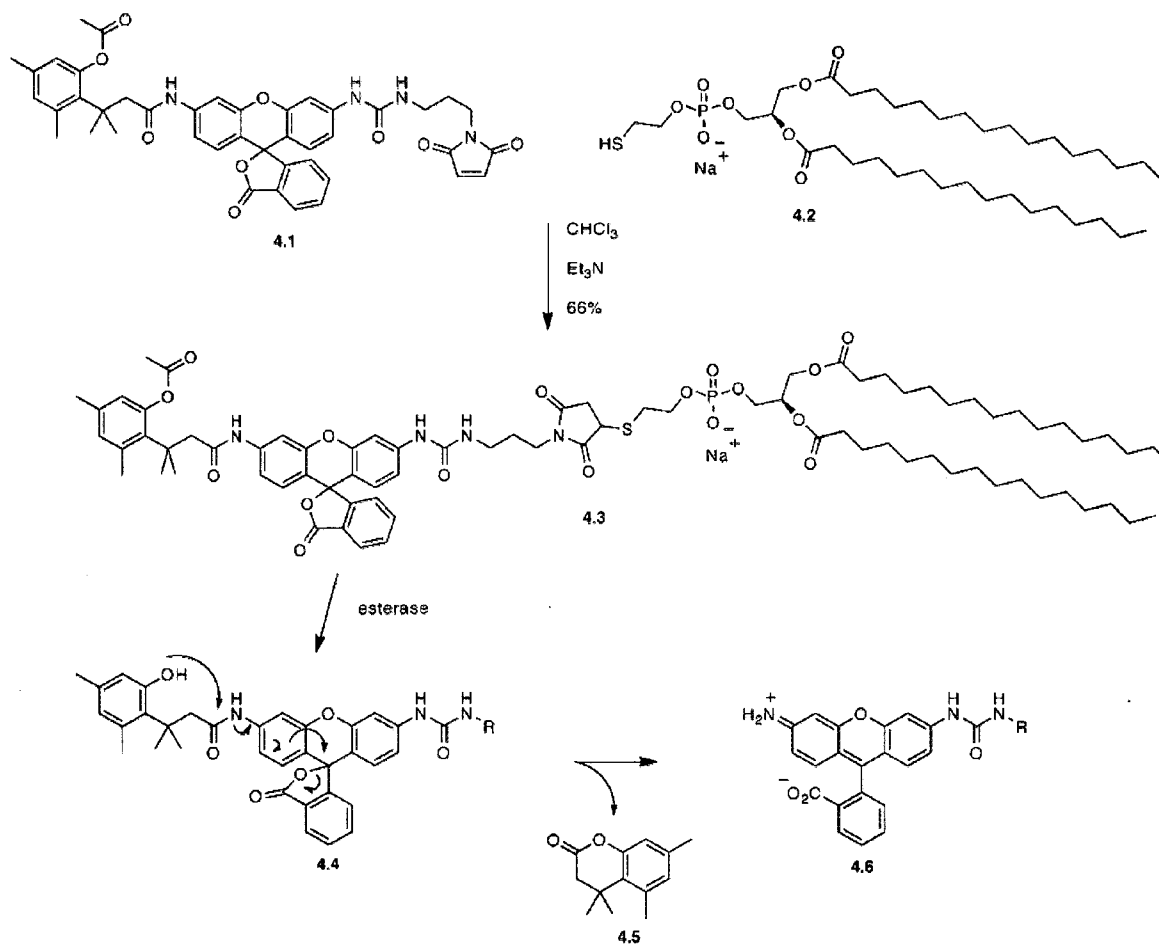
Figure 4.1   Endocytosis of lipid **4.3** imaged by confocal microscopy. HeLa cells were

labeled for 3 hours at 4 °C with 20 µM lipid **4.3** or vehicle. Cells were

washed with fresh serum-free media, then endocytosis was initiated by

warming to 37 °C for 3 hours. (A–C) HeLa cells labeled with 20 µM lipid

4.3. (A) HeLa cells labeled at 4 °C but not warmed. (B) Cells labeled at 4

°C, then incubated at 37 °C for 3 hours. (C) Cells labeled at 4 °C, then

incubated an additional 3 hours at 4 °C. (D–E) Unlabeled HeLa cells

(vehicle treated). (D) Cells treated with vehicle at 4 °C. (E) Cells treated

with vehicle at 4 °C then incubated 3 hours at 37 °C. Blue, Hoechst

33342; Green, unmasked lipid **4.3** (lipid **4.6**); Upper panels, confocal

images; Lower panels, transillumination; Scale bars, 20 µm.

Time = 0 hours

Time = 3 hours

4 °C

37 °C

4 °C

A

B

C

Lipid 4.3 (20 μM)

D

E

Vehicle Treated
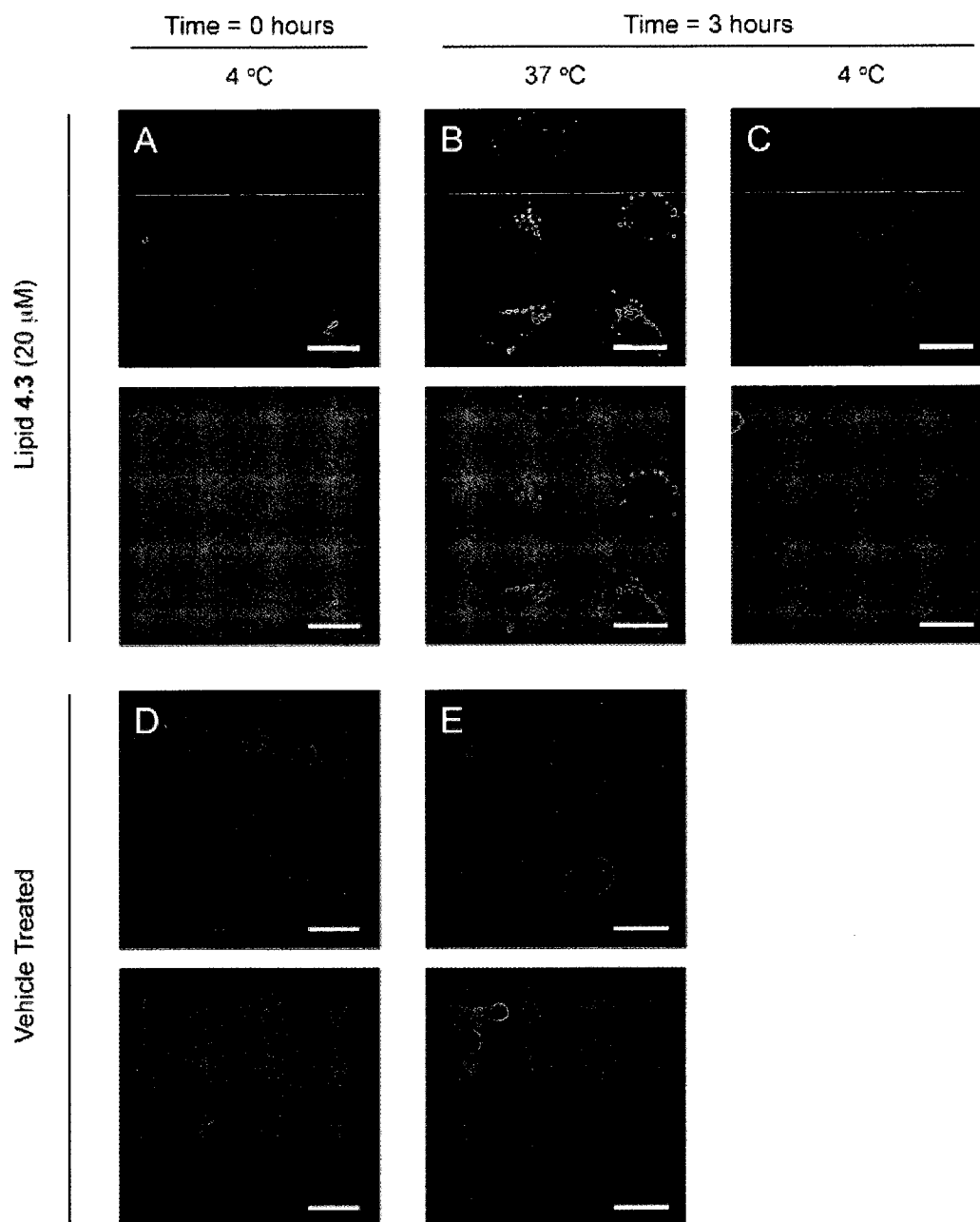
Figure 4.2   Lipid **4.3** colocalizes with LysoTracker Red, but not transferrin. HeLa

cells were labeled for 3 hours at 4 °C with 20 μM lipid **4.3**. Cells were

washed with fresh serum-free media, then endocytosis was initiated by

warming to 37 °C for 3 hours. (A) LysoTracker Red (50 nM) was added

for the final 20 minutes of incubation at 37 °C. (B) AlexaFluor 594–

transferrin conjugate (1 μM) was added at the initiation of endocytosis

(time = 0 h). (C) AlexaFluor 549–transferrin conjugate was added for the

final 1 hour of incubation at 37 °C (time = 2 h). Images were obtained by

confocal microscopy. Blue, Hoechst 33342; Green, unmasked lipid **4.3**

(lipid **4.6**); Red, LysoTracker Red or AlexaFluor 594–transferrin; Scale

bars, 20 μm.

| Endocytic Marker | Lipid **4.3** (green) | Merge |

Lysotracker Red (red): **A**

Transferrin (red) Added at t = 0 h: **B**

Transferrin (red) Added at t = 2 h: **C**
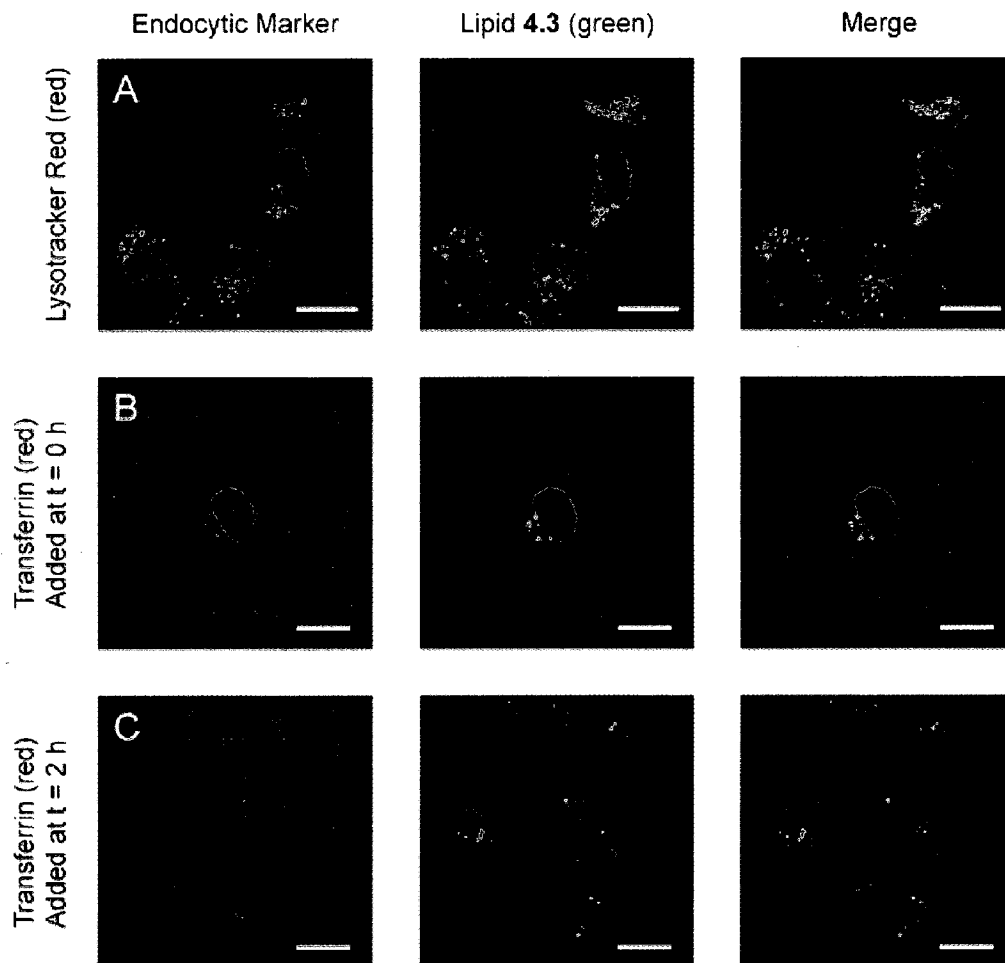
Figure 4.3 Fluorescence of the plasma membrane is not observed after 24 hours of

endocytosis. HeLa cells were labeled for 3 hours at 4 °C with 20 μM lipid

4.3 or vehicle. Cells were washed with fresh serum-free media, then

endocytosis was initiated by warming to 37 °C for 24 hours. (A) Vehicle

treated cells. (B) HeLa cells labeled with 20 μM lipid **4.3**. Blue, Hoechst

33342; Green, unmasked lipid **4.3** (lipid **4.6**); Upper panels, confocal

images; Lower panels, transillumination; Scale bars, 20 μm.

Vehicle Treated   Lipid **4.3** (20 μM)
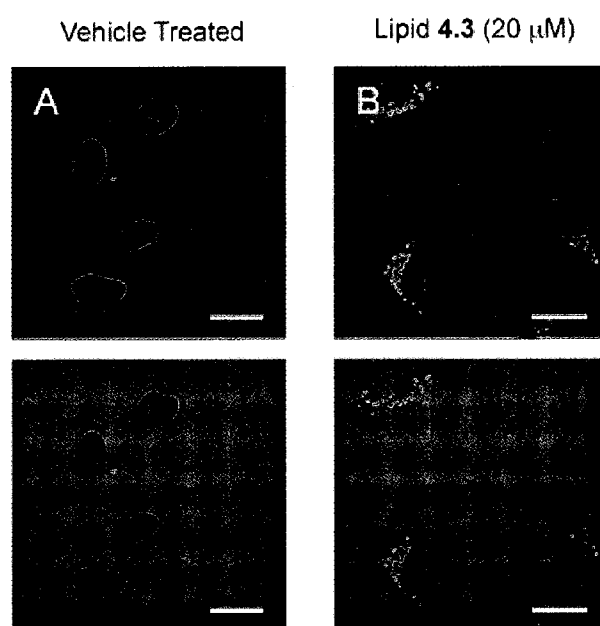
Figure 4.4   Time course of endocytosis in HeLa cells. HeLa cells were labeled for 3

hours at 4 °C with 20 μM lipid **4.3**. Cells were washed with fresh serum-

free media, then endocytosis was initiated by warming to 37 °C for

various times. Cells were fixed with formaldehyde and then analyzed by

flow cytometry. Uncertainties were expressed as the standard deviation.
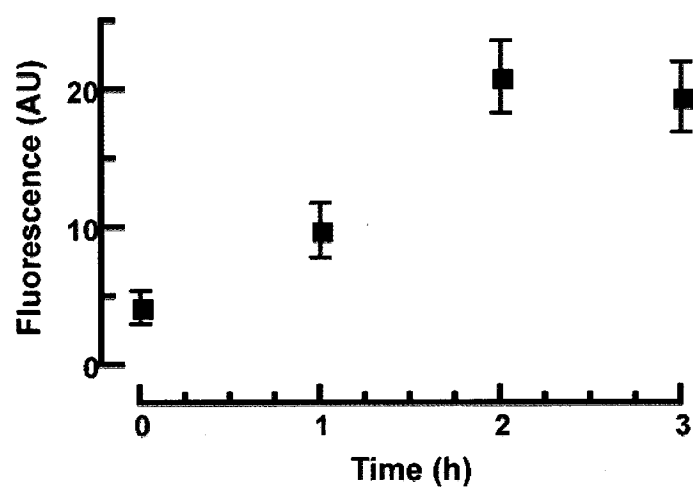
CHAPTER 5

Future Directions

5.1   Bifunctional Trimethyl Lock Linker

As described throughout, the trimethyl lock is used to temporarily mask fluorophores, peptides, or drugs. Most of these applications involve masking a single molecule. Shigenaga developed a bifunctional trimethyl lock that could be incorporated into the center of a peptide (CHAPTER 1) (Shigenaga, *et al.*, 2007). The peptide was cleaved photolytically to alter the function of the peptide *in cellulo*. The ability to temporarily link two molecules with a triggered release mechanism would be beneficial in numerous applications.

M.T. Borra of the Raines laboratory sought to target cytotoxic ribonuclease specifically to colon cancer cells by engineering a ribonuclease–single chain antibody fusion protein. Ribonucleases must be internalized to the cytoplasm of cells to have efficacy (Turcotte, *et al.*, 2009). The fusion protein was able to target cancer cells and was taken up into endosomes but never displayed any cytotoxicity. It was theorized that while ribonucleases could escape endosomes, the fusion protein might not have been able. If there were a way to link a ribonuclease to an antibody to target cancer cells, in a manner that after endocytosis the linkage would be severed, perhaps the ribonuclease would translocate to the cytoplasm resulting in cell death.

We propose to synthesize a trimethyl lock that is functionalized by two protein-reactive handles that would be cleaved by a user defined enzymatic reaction. Additionally, this strategy would be amenable to systems other than ribonucleases, to

provide targeted delivery of proteins, peptides, or drugs to cells. The trimethyl lock is a bioreversible modification that would leave no residual trace on the molecules that it delivers.

5.2   Photoactivatable Headgroup-Modified Lipid

In CHAPTER 4, a profluorophore headgroup-modified lipid was used to assay the rates of endocytosis in cancerous and normal cells. The readout of the assay was fluorescence change per cell over time, which was comparable within a single assay, but could not be normalized to the results of other types of assays. Ideally, the rate of endocytosis would be expressed as the surface area of membrane internalized per unit time. This type of output was not possible for our assay, because the initial concentration of profluorophore lipid incorporated into the membrane could not be determined. Attempts were made to unmask the profluorophore *in situ* but none were successful. Importantly, addition of esterases to the outside of labeled cells did not result in unmasking. This lack of reactivity was most likely due to the steric bulk of the extracellular matrix, preventing the esterases from being closely associated with the cell membrane.

A number of strategies were considered to determine the amount of profluorophore lipid incorporation. The cell membrane could be labeled with the unmasked fluorophore lipid at the same concentration as the masked fluorophore lipid. This would provide an estimate of the efficiency of uptake of the lipid into cells; however, the polarity of the masked and unmasked fluorophores were significantly different. We would not have

confidence that the efficiency of labeling was similar for the two. Another option would be to conjugate two fluorophores to the lipid: a masked profluorophore, and an unmasked fluorophore that emitted at a different wavelength. This ratiometric profluorophore would allow the concentration of the lipid to be measured at any time during the assay. Fluorescent probes tend to be large molecules and adding a second fluorophore to the lipid might alter its stereoelectronics significantly. It was believed that a lipid of that nature would not be incorporated into a membrane because the headgroup would be too large and hydrophilic.

The method with the most likely chance of success would be to synthesize a profluorophore headgroup-modified lipid that would be activated by UV light. The unmasking of this profluorophore would not be affected by the steric bulk of the plasma membrane or extracellular matrix. Unmasking could be performed with great temporal control and specificity. Two types of photoactivatable lipids are foreseeable: one that could be unmasked by UV light and esterases, or one that could be unmasked only by UV light but would be similar in structure to the previously developed esterase-activated profluorophore lipid. The former would be incorporated into cells in the cold and then would be endocytosed upon warming to give the typical increase in fluorescence signal. To determine the initial concentration, cells that were labeled in the cold would be exposed to UV light. The latter would be incorporated into a parallel cell population to the esterase-activated substrate, at the same concentration. Unmasking of the photoactivatable lipid by UV light would give a reasonable estimate of the concentration in the second cell population if the structures of the two lipids were similar.

A profluorophore lipid substrate that could be activated by UV light or esterases might be synthesized by conjugating **B.1** (APPENDIX B) to DPPTE (CHAPTER 4). **B.1** is a rhodamine derivative that is masked with a photocleavable *o*-nitrobenzyl carbamate. Some carbamates are susceptible to hydrolysis by esterases. This is apparent in **A.18** (APPENDIX A), a similar carbamate that is unmasked in the endosomes of HeLa cells. Drawbacks of this method would be that the carbamate may not fully mask the fluorescence of rhodamine, leading to a small amount of background fluorescence. Benefits would include that a single substrate would be able to determine the rate of endocytosis.

A profluorophore lipid substrate that would only be unmasked by UV light might be synthesized by appending an *o*-nitrobenzyl group to the phenol of the trimethyl lock. The trimethyl lock would then mask the fluorescence of rhodamine through an amide linkage, which would not be susceptible to esterase-mediated hydrolysis. This substrate would have less background fluorescence, but there would be more error in determining the concentration of the esterase-cleaved lipid.

5.3   Basis for Cancer Cell Selectivity of Cytotoxic Ribonucleases

Once methods become available to assay the endocytosis and translocation of cytotoxic ribonucleases and the endocytosis of membranes, we would have the tools necessary to begin to elucidate the mechanism of cancer cell specificity of those cytotoxic ribonucleases. One hypothesis is that ribonucleases bind more tightly to the membrane of cancer cells. Another is that they are internalized better in cancer cells,

either through endocytosis or translocation. Future work might focus on determining the rates of endocytosis and translocation of a ribonuclease in a panel of cancerous and normal cell lines, as well as the rates of constitutive endocytosis, and correlating the results to the potency of ribonuclease cytotoxicity against those cell lines. Any insights into differences between cancerous and normal cells may lead to more effective treatments with ribonucleases or, alternatively, novel treatment targets may be realized.

APPENDIX A

Fluorogenic Assay for Monitoring Cytoplasmic Translocation of Pancreatic-

Type Ribonucleases

A.1 Introduction

The pancreatic-type ribonucleases (RNases) superfamily of secreted enzymes catalyze the degradation of ribonucleic acid (RNA) (Raines, 1998). Several pancreatic-type ribonucleases have been shown to be selectively toxic to cancerous cells, when compared to non-cancerous cells (Rutkoski, *et al.*, 2005). One RNase in this family, Onconase (ONC), is in clinical trials for the treatment of malignant mesothelioma (Turcotte, *et al.*, 2009).

The presumed mechanism of cytotoxicity is shown in Figure A.1 (Turcotte, *et al.*, 2009). Briefly, a cationic RNase binds to the anionic cell surface where it is endocytosed in a receptor-independent manner. The RNase then crosses a lipid bilayer to escape the endosome through a process referred to as translocation. Once in the cytoplasm, RNases that evade the ribonuclease inhibitor protein (RI) degrade cellular RNA leading to apoptosis. RI-evasive RNases can be naturally occurring, in the case of ONC, or engineered variants of mammalian RNases, such as DRNG RNase A (Rutkoski, *et al.*, 2005).

The current biochemical technology permits the measurement of the binding, endocytosis (Lavis, *et al.*, 2006a), and RI-evasion steps in the mechanism (Lavis, *et al.*, 2007). Cytotoxicity is an indication of achievement of all steps of RNase internalization. Turcotte *et al.* shows that while the cytotoxicity conferred by a particular RNase variant ranges widely, there are only small differences in values obtained for each individual step

in the mechanism. Importantly, no trends are observed relative to cytotoxicity. These findings point to translocation as, perhaps, the decisive step of RNase-mediated cytotoxicity (Turcotte, *et al.*, 2009).

Development of a fluorogenic assay for translocation is challenging for a number of reasons. Firstly, a masked substrate must be stable in aqueous buffers. Secondly, it must not be unmasked in endosomes, and finally, it must be activated in the cytoplasm. The fluorogenic assay for endocytosis developed by Lavis *et al.* can be used as a model to overcome the first challenge of aqueous stability (Lavis, *et al.*, 2006a). Endosomes are a harsh environment for a masked fluorophore. The pH in an endosome or lysosome can be as low as 5.5 (Gruenberg and Maxfield, 1995). Complicating assay development, there are countless poorly characterized enzymes present in endosomes that may hydrolyze a fluorophore. Unmasking of the fluorophore in the cytoplasm requires an enzyme that is not also present in endosomes. Many current substrates are activated by hydrolytic enzymes, which are more likely to be present in endosomes.

To overcome these challenges, we proposed to utilize bacterial enzymes to activate profluorophores in the cytoplasm of mammalian cells. Many bacterial enzymes have activities that are absent in mammalian cells. It was presumed that a substrate designed to be unmasked by one of these bacterial enzymes would remain intact in the endosomes of mammalian cells. The bacterial enzyme could be transfected into the cytoplasm of mammalian cells to specify the location of substrate unmasking.

A.2   Results and Discussion

A.2.1 β-Lactamase Substrate

Substrate **A.1** (Scheme A.1), or a variant containing a maleimide for conjugation to ribonucleases (Figure A.2) would be activated by the hydrolytic enzyme β-lactamase. β-lactamase has been used extensively as a reporter in bacterial systems. The ampicillin resistance gene, TEM1 from *E. coli*, encodes a β-lactamase that is commonly used for selection screening in cultures. Only recently has β-lactamase begun to be used as a reporter in mammalian cells (Gao, *et al.*, 2003). β-lactamase from TEM1 is a small (29 kDa) monomer that efficiently cleaves both penicillin and cephalosporin derivatives (Campbell, 2004). Constructs lacking a signal sequence are available, allowing sole localization of β-lactamase to the cytoplasm of transfected cells. Both β-lactamase substrates and products are non-toxic, and activity of β-lactamase is orthogonal in mammalian cells.

Many β-lactamase substrates are currently used in the laboratory and in the clinic; however, substrates that satisfy all the requirements to measure translocation of ribonucleases—sensitivity, stability, and a handle for bioconjugation—are not available. Nitrocefin, a substrate used clinically to diagnose β-lactam resistant bacterial colonies, has two significant drawbacks. It is a chromogenic substrate, which lacks sensitivity and it is susceptible to nonspecific hydrolysis by serum (O'Callaghan, *et al.*, 1972). Alternatively, there are two general types of fluorogenic β-lactamase substrates. β-lactamase substrates that utilize Förster resonance energy transfer (FRET) tend to have a

small dynamic range and poor solubility. Substrates that release a masked fluorophore have a much better dynamic range, but are less stable (Qureshi, 2007). The trimethyl lock may be used to improve the stability of a substrate by forming a stable amide bond to an amine-based fluorophore.

The proposed mechanism of fluorescence development is portrayed in Figure A.2. The β-lactamase substrate is conjugated to a ribonuclease variant containing a free cysteine through a maleimide handle. β-lactamase hydrolyzes the amide bond of the cephalosporin moiety. Upon hydrolysis, the amine that is produced no longer participates in amidic resonance, and its lone pairs are free to donate into the conjugated olefin system. This leads to elimination of the phenoxide of the trimethyl lock, which rapidly lactonizes to release the unmasked rhodamine. Translocation of ribonuclease to the cytoplasm is a slow process, meaning the measured increase in fluorescence over time is dependent on the rate of translocation, rather than the rate of β-lactamase–catalyzed hydrolysis, or subsequent unmasking steps (Lavis, *et al.*, 2006a).

A.2.2 β-Lactamase Substrate Synthesis

Retrosynthetic analysis, (Scheme A.1) shows that β-lactamase substrate **A.1** may be synthesized by peptide bond conjugation of **A.2** with morpholinourea rhodamine (Lavis, *et al.*, 2006a). Olefin **A.2** may be synthesized from its two halves through an olefin cross metathesis reaction. Key intermediate **A.4** may be synthesized in a three steps from known trimethyl lock precursor **A.5** (Amsberry and Borchardt, 1990).

Unfortunately, the key synthetic step, the olefin cross metathesis reaction could not be completed. The use of Grubb's 2nd generation ruthenium catalyst could not overcome the electron poor nature of conjugated, terminal alkene of cephalosporin **A.3**. Further experiments revealed that the catalyst became ligated to **A.3** in an unproductive manner and was not able to catalyze the cross metathesis reaction. A preformed complex of the catalyst with **A.3** showed no activity when a known ring closing metathesis substrate was added, although the reaction proceeded if no **A.3** was added.

As shown in Scheme A.2, olefin **A.4** was converted into vicinal diol **A.9** by protecting the carboxylic acid as a methyl ester and performing a syn-dihydroxylation with catalytic osmium tetroxide in the presence of stoichiometric trimethylamine oxide. **A.9** was oxidatively cleaved with sodium periodate to the aldehyde, which was not stable and was therefore reacted immediately in a Wittig reaction with phosphonium ylide **A.10**. Various methods were attempted to remove the methyl ester protecting group from **A.11**, including base hydrolysis with lithium hydroxide, sodium hydroxide, potassium trimethyl silanolate, or trimethyltin hydroxide. Reactions resulted in no product formation or destruction of the cephalosporin core. For this reason, **A.4** was protected as the trimethylsilyl ethyl ester. Attempted cleavage of this ester with tetrabutylammonium fluoride or potassium fluoride resulted in decomposition of the cephalosporin.

If the proposed β-lactamase substrate synthesis could have been completed, **A.1** would have faced the challenge of endosomal stability. Both β-lactamase and endosomes were hydrolytic, presenting less selectivity in where the substrate would be unmasked.

Due to difficulty in this synthesis and foreseeable risk, the synthesis of substrate **A.1** was abandoned for an enzyme substrate that would be activated by reduction, not hydrolysis.

A.2.3 Nitroreductase Substrate

Many of the same properties of β-lactamase that are ideal towards developing a marker of ribonuclease translocation hold for the enzyme nitroreductase (NTR). NTR is a 24 kDa flavoenzyme from *E. coli* that catalyzes the reduction of aryl nitro groups to hydroxylamines and amines (Anlezark, *et al.*, 1992). A crystal structure has been determined and substrate specificity is well known (Parkinson, *et al.*, 2000). Importantly, the NTR gene has been codon-optimized for mammalian cells and functionally expressed at high levels (Grohmann, *et al.*, 2009). Expression in mammalian cells renders the cells sensitive to the cytotoxic effects of the prodrug CB1954, which has a nitro group that must be reduced for it to be effective (Bridgewater, *et al.*, 1995). Nitroreductase activity is not normally present in mammalian cells, so transfection of NTR should limit its activity to the cytoplasm. One mammalian reductase, a subtype of DT-diaphorase that is similar to NTR, is limited to Walker 256 rat carcinoma cells, but the nitroreductase activity is not expected to be present in endosomes (Knox, *et al.*, 1988).

NTR substrate **A.14** (Scheme A.3) contains a *p*-nitrobenzylcarbamate (Sykes, *et al.*, 2000), which masks the fluorescence of morpholinourea rhodamine (Lavis, *et al.*, 2006a). Reduction of the nitro group—which is electron withdrawing and contains no lone pair electrons—to hydroxylamine **A.15**—which is electron donating and contains lone pair electrons—results in elimination of a carbamic acid and iminoquinone methide **A.16**.

Carbamic acids rapidly hydrolyze in water, decomposing to carbon dioxide and releasing a free amine, in this case releasing the fluorescent morpholinourea rhodamine **A.17**.

Compound **A.14** was assayed as a substrate for NTR utilizing fluorescence spectroscopy. Addition of NADH, a required cofactor, to compound **A.14** and NTR in phosphate buffered saline (PBS) resulted in an increase in fluorescence. The hydrophobic nature of compound **A.14** led to limited solubility and aggregation in aqueous solution, a result that can be seen in the Michaelis—Menten plot (Figure A.3) as a decrease in initial velocity at high substrate concentrations. After conjugation of this substrate to a ribonuclease, aggregation would no longer be a hindrance.

The stability of substrate **A.14** was measured in PBS and HeLa cell lysate to determine if untransfected cells possessed nitroreductase activity. After 8 hours, much less than 0.1% had become fluorescent indicating no native nitroreductase activity. Exogenous NADH was added as a supplement to account for any oxidation that may have occurred while preparing the cell lysate, but no difference in fluorescence was observed.

Substrate **A.18** (Scheme A.4), containing a maleimide handle for conjugation to ribonucleases, was synthesized from known starting materials in a 70% yield. Human RNase 1 P19C, a variant containing a free cysteine, was recombinantly expressed and purified from *E. coli*. Substrate **A.18** was conjugated to the free cysteine of RNase 1 P19C. A plasmid containing the mammalian codon-optimized nfsB (NTR) gene and the gene encoding for red fluorescent protein, mCherry, separated by an internal ribosomal entry site (IRES), was transfected into HeLa cells. The mCherry was utilized as a control

for transfection; any cell that appeared red must also contain NTR due to the nature of the IRES.

Twenty four hours after transfection, the RNase 1–Substrate **A.18** conjugate was added exogenously to the media and allowed to incubate at 37 °C for 17 hours. The results are shown in Figure A.4. Cells that neither had conjugate **A.18**–P19C–RNase 1 applied nor had NTR transfected showed only nuclear staining (Figure A.4A). Untransfected cells that had conjugate added displayed green punctate staining but no red or green fluorescence in the cytoplasm (Figure A.4B). Some cells that were transfected had red cytoplasmic staining due to mCherry expression (Figure A.4C). When ribonuclease conjugate was added to transfected cells, green punctate fluorescence was observed in cells that had red cytoplasmic (Figure A.4D). Green punctate fluorescence was also present in cells that did not have a red cytoplasm, although it could not be determined if those cells were successfully transfected with NTR by this method.

The punctate staining pattern result indicated that ribonuclease conjugate **A.18** was unmasked primarily in endosomes, and no cytoplasmic staining was evident. The green staining was present in cells regardless of whether they were transfected. This suggested that either nitroreductase activity was present in the endosomes of HeLa cells, or more likely, another enzyme was degrading substrate **A.18** to produce the fluorescent rhodamine. Carbamates possess some enzymatic lability, from which free rhodamine would be released.

Compound **A.21** (Scheme A.5) was synthesized as a NTR substrate that did not contain a carbamate linkage. Masking of the fluorescence of rhodamine required

acylation, hence, the p-nitrobenzylamine of rhodamine would not be expected to have decreased fluorescence. The trimethyl lock was appended to mask the fluorescence of rhodamine while increasing enzymatic stability and susceptibility to NTR. p-Nitrobenzyl ether trimethyl lock **A.21** was synthesized as shown in Scheme A.5. This compound effectively split the carbamate group of substrate **A.14** (Scheme A.3) into an ether and an amide, two physiologically stable linkages.

Unfortunately, compound **A.21** did not display an increase in fluorescence in the presence of NTR and NADH. Perhaps the trimethyl lock was too sterically encumbered to fit into the active site of NTR. A second possibility was that reduction of the nitro group of compound **A.21** did occur, but due to the relatively poor leaving group ability of a phenol, compared to a carbamic acid, iminoquinone methide formation was not favorable under physiologic conditions.

A.2.4 Other NTR Substrates

Another attempt to synthesize a marker of ribonuclease translocation was to utilize the quinone trimethyl lock (Amsberry and Borchardt, 1991). Benzoquinones are known to be substrates for NTR as well as DT-diaphorase (Bridgewater, *et al.*, 1995; Ernster, 1967). Substrate **A.23** (Scheme A.6) was based on the substrates developed by Huang and coworkers, but contained only one trimethyl lock to enable conjugation of the fluorophore to a ribonuclease (Huang and Lin, 2006; Huang, *et al.*, 2008). Reduction of the quinone trimethyl lock by thiols was a concern and its stability was tested.

Unfortunately, compound **A.23** was completely degraded within minutes upon addition to PBS regardless of the presence or absence of thiols in the buffer.

Compound **A.30** (Scheme A.7), was similar to the trimethyl lock and relied on a lactamization process to release a masked fluorophore. This compound was based upon that of Hu and coworkers (compound **A.31**), which contained a *gem*-dimethyl moiety, but not a third methyl group (Hu, *et al.*, 2000; Jiang, *et al.*, 2002). Subsequent to reduction of the nitro group, nucleophilic attack of the amine on the carbonyl of **A.32** led to lactamization to **A.33**. Hu and coworkers showed that scission of an ester occurred spontaneously but that scission of an amide did not occur under physiologic conditions. It was believed that synthesizing a variant of **A.31** that more closely resembled the trimethyl lock, **A.30**, would spontaneously lactamize following nitro reduction, including scission of amides.

A synthesis of the trimethyl lock variant **A.30** was attempted (Scheme A.7). 3-Nitro-*o*-xylene (**A.24**) was acylated with diethyl oxalate and oxidatively decarboxylated to form 2-methyl-6-nitrophenylacetic acid **A.25**. The carboxylic acid was protected as the methyl ester **A.26**. Dialkylation was attempted using methyl iodide with a variety of bases and solvents, such as potassium *tert*-butoxide and sodium hydride in THF, DMF, HMPA, and in the presence of 18-crown-6 ether. No conditions provided the desired product **A.28**. Due to steric hindrance, only the monomethyl product **A.27** was able to be synthesized.

Even if compound **A.30** could be synthesized, there was no literature precedent for reduction of its nitro group enzymatically. All studies on the lactamization reaction utilized chemical reduction as the trigger. Compound **A.35** (Scheme A.8), similar to

compound **A.14** above, was not a substrate for NTR, suggesting that *p*-nitro aromatics may be substrates, but *o*-nitro aromatics may not be.

A.3   Experimental Section

A.3.1 General

Dichloromethane (DCM), tetrahydrofuran (THF), and dimethyl formamide (DMF) were drawn from a Baker CYCLE-TAINER solvent-delivery system. All other reagents were from Aldrich Chemical (Milwaukee, WI) or Fisher Scientific (Hanover Park, IL), and were used without further purification. PBS contained (in 1.00 L) KCl (0.20 g), KH_2PO_4 (0.20 g), NaCl (8.0 g), and $Na_2HPO_4 \cdot 7H_2O$ (2.16 g) and had pH 7.4.

Thin-layer chromatography was performed by using aluminum-backed plates coated with silica gel containing F_{254} phosphor, and was visualized by UV illumination or developed with ceric ammonium molybdate stain. Flash chromatography was performed on open columns with silica gel-60 (230–400 mesh).

NMR spectra were obtained with a Bruker DMX-400 Avance spectrometer at the National Magnetic Resonance Facility at Madison (NMRFAM). Mass spectrometry was performed using a Micromass LCT (electrospray ionization, ESI) mass spectrometer at the Mass Spectrometry Center in the Department of Chemistry.

A.3.2 Synthesis of A.6

Compound **A.5** (Amsberry and Borchardt, 1990) (5.0 g, 24 mmol) was added to a flame dried 500 mL pear shaped flask and dissolved in 250 mL dry acetone (HPLC grade). Potassium iodide (7.92 g, 48.0 mmol), allyl bromide (10.2 mL, 120 mmol), and potassium carbonate (6.63 g, 48 mmol) were added and the reaction mixture was refluxed overnight. The reaction became yellow and a fine, white precipitate formed. TLC (20% EtOAc in hexanes) showed only partial reaction progress. An additional two equivalents of allyl bromide (4.1 mL, 48 mmol) was added and the reaction was refluxed overnight. After reaction completion, as monitored by TLC, the mixture was concentrated under reduced pressure and then partitioned between 300 mL each of H_2O and ether. The organic phase was collected and washed with saturated brine (100 mL). The organic phase was dried over magnesium sulfate and filtered, then evaporated under reduced pressure. The crude product was purified by silica gel chromatography (20% EtOAc in hexanes) to afford 3.35 g (56%) **A.6** as yellow oil. ^{1}H NMR (400 MHz, CDCl$_3$) δ: 6.58 (s, 1H), 6.54 (s, 1H), 6.11 (m, 1H), 5.42 (d, J = 16.8 Hz, 1H), 5.27 (d, J = 10.1 Hz, 1H), 4.53 (d, J = 5.1 Hz, 2H), 3.54 (t, J = 6.7 Hz, 2H), 2.49 (s, 3H), 2.26–2.17 (m, 5H), 1.54 (s, 6H), 1.07 (bs, 1H) ppm. ^{13}C NMR (100 MHz, CDCl$_3$) δ: 158.5, 137.7, 136.1, 133.9, 131.2, 127.7, 117.5, 112.7, 69.9, 61.5, 45.7, 40.0, 32.4, 26.0, 20.9 ppm. HRMS (ESI): *m/z* 271.1661 [M+Na]$^{+}$ ([C$_{16}$H$_{24}$O$_2$Na]$^{+}$ = 271.1669).

A.3.3 Synthesis of A.7

Pyridinium chlorochromate (PCC; 2.61 g 12.1 mmol) was suspended in 40 mL dry

DCM in a flame dried 250 mL round bottom flask. **A.6** (1.5 g, 6.1 mmol) was dissolved

in 30 mL dry DCM and was added to the reaction dropwise. The reaction was stirred for

3 hours. Upon completion, monitored by TLC (20% EtOAc in hexanes), the reaction

mixture was poured onto a short plug of silica gel, which was eluted with DCM to obtain

a yellow oil. The crude product was purified by silica gel chromatography (15% EtOAc

in hexanes) to afford a yellow oil (1.17 g; 79%). ^{1}H NMR (400 MHz, CDCl$_3$) δ: 9.52 (t, J

= 2.5 Hz, 1H), 6.58 (s, 1H), 6.57 (s, 1H), 6.12–6.05 (m, 1H), 5.40 (d, J = 16.5 Hz, 1H),

5.28 (d, J = 10.8 Hz, 1H), 4.53 (d, J = 5.8 Hz, 2H), 2.99 (d, J = 2.5 Hz, 2H), 2.51 (s, 3H),

2.24 (s, 3H), 1.59 (s, 6H) ppm.

A.3.4 Synthesis of A.4

A.7 (1.0 g, 4.1 mmol) was dissolved in 72 mL of *tert*-butanol in a 500 mL pear

shaped flask. 2-methyl-2-butene (18 mL, 170 mmol) was added to the solution.

Monosodium phosphate hydrate (3.93 g, 28.5 mmol) and sodium chlorite (technical

grade; 3.31 g, 36.6 mmol) were dissolved in 30 mL water and added dropwise to the

reaction mixture while allowing the yellow color that was formed after each addition to

disappear before the next addition. The reaction was stirred for 30 minutes, at which time

reaction progress was determined by TLC. The workup procedure for TLC was as

follows: a few drops of the reaction mixture were added to 1 mL of 1:1 EtOAc/H$_2$O, the

TLC plate was spotted from the upper organic phase (20% EtOAc in hexanes). The organics were evaporated from the reaction mixture under reduced pressure. The remaining aqueous solution was extracted with EtOAc (3 × 50 mL). The organic phases were combined and washed with saturated brine (100 mL), then dried over magnesium sulfate and filtered. The filtrate was evaporated and the residue purified by silica gel chromatography (20% EtOAc in hexanes) to yield a white solid (1.0 g; 94%). ^{1}H NMR (400 MHz, CDCl$_3$) δ: 10.2 (bs, 1H), 6.56 (s, 1H), 6.53 (s, 1H), 6.15–6.03 (m, 1H), 5.39 (d, J = 17.1 Hz, 1H), 5.26 (d, J = 10.8 Hz, 1H), 4.51 (d, J = 4.5 Hz, 2H), 3.03 (s, 2H), 2.50 (s, 3H), 2.23 (s, 3H), 1.61 (s, 6H) ppm.

A.3.5 Synthesis of A.8

A.4 (600 mg, 2.3 mmol) was added to a 50 mL round bottom flask and dissolved in toluene/MeOH (4:1, 20 mL). TMS-diazomethane (1.3 mL, 2.5 mmol) was added dropwise. A bright yellow color developed and gas evolution from the solution was observed. After 2 hours, the reaction was analyzed by TLC (10% EtOAc in hexanes) and was determined to be complete. Concentrated AcOH (120 μL) was added to quench the reaction. The solution was evaporated under reduced pressure to give **A.8** as an oil (629 mg; 99%). ^{1}H NMR (400 MHz, CDCl$_3$) δ: 6.56 (s, 1H), 6.53 (s, 1H), 6.17–6.05 (m, 1H), 5.41 (d, J = 16.8 Hz, 1H), 5.27 (d, J = 10.7 Hz, 1H), 4.53 (d, J = 5.3 Hz, 2H), 3.49 (s, 3H), 3.00 (s, 2H), 2.52 (s, 3H), 2.22 (s, 3H), 1.61 (s, 6H) ppm.

A.3.6 Synthesis of A.9

A.8 (200 mg, 0.72 mmol) was dissolved in THF/H$_2$O (2:1, 6 mL) in a 50 mL round bottom flask. Osmium tetroxide (4% solution in water; 92 µL, 0.014 mmol) was added to the solution, followed by trimethylamine oxide (97 mg, 0.87 mmol). The reaction was stirred overnight. Reaction progress was monitored by TLC (70% EtOAc in hexanes). Upon completion, the reaction mixture was partitioned between H$_2$O (20 mL) and EtOAc (40 mL). The organic phase was collected and then washed with saturated sodium metabisulfite (40 mL). The aqueous phase was extracted with additional EtOAc (40 mL) and the organic phases were combined, and washed with saturated brine (100 mL). The organic phase was added to 1 g of Fluorosil. The slurry was filtered through a pad of celite and the filtrate was evaporated under reduced pressure. The crude product was purified by silica gel chromatography (50% EtOAc in hexanes) to yield a colorless viscous oil (169 mg; 75%). ^{1}H NMR (400 MHz, CDCl$_3$) δ: 6.56 (s, 1H), 6.53 (s, 1H), 4.30 (d, J = 2.3 Hz, 1H), 4.25–4.18 (m, 1H), 4.11–3.99 (m, 2H), 3.87–3.79 (m, 1H), 3.78–3.70 (m, 1H), 3.54 (s, 3H), 3.00 (d, J = 13.3 Hz, 1H), 2.93 (d, J = 13.3 Hz, 1H), 2.51 (s, 3H), 2.28 (t, J = 5.6 Hz, 1H), 2.23 (s, 3H), 1.66 (s, 3H), 1.59 (s, 3H) ppm. HRMS (ESI): *m/z* 333.1666 [M+Na]$^+$ ([C$_{17}$H$_{26}$O$_5$Na]$^+$ = 333.1673).

A.3.7 Synthesis of A.11

Phosphonium salt **A.10** was synthesized as described (Ko, *et al.*, 1996). Vicinal diol **A.9** (160 mg, 0.51 mmol) was dissolved in THF/H$_2$O (2:1, 6 mL) in a 10 mL round bottom flask. Sodium periodate (327 mg, 1.53 mmol) was added. A white precipitate

formed. The solution was stirred for 25 minutes. The reaction was transferred to a separatory funnel. The product was extracted with H_2O (25 mL) and DCM (25 mL). The organic phase was washed with saturated brine (50 mL), dried over sodium sulfate, and filtered. The filtrate, was set aside.

Meanwhile **A.10** (857 mg, 1.02 mmol) was dissolved in 30 mL DCM in a 100 mL round bottom flask. NaOH (1 M, 10 mL) was added and the solution turned dark brown/red. The reaction was stirred for 25 minutes, after which the mixture was poured into a separatory funnel. The organic phase was washed with saturated brine (50 mL), dried over sodium sulfate, and filtered. The filtrate was combined with the filtrate of the above reaction in a 100 mL round bottom flask. The reaction was stirred under Ar(g) overnight. Reaction progress was monitored by TLC (6:2.5:1.5) hexanes/EtOAc/DCM). Upon completion, the solvent was evaporated under reduced pressure and the residue was purified by silica gel chromatography (6:2.5:1.5 hexanes/EtOAc/DCM) to give **A.11** as a yellowish solid (123 mg; 34%). ^{1}H NMR (400 MHz, CDCl$_3$) δ: 7.41–7.24 (m, 7H), 6.86 (d, J = 7.9 Hz, 2H), 6.54 (s, 1H), 6.38 (s, 1H), 6.31 (d, J = 11.2 Hz, 1H), 6.10 (d, J = 9.0 Hz, 1H), 5.97–5.88 (m, 1H), 5.85–5.79 (m, 1H), 5.16 (s, 2H), 4.98 (d, J = 3.0 Hz, 1H), 4.42–4.34 (m, 1H), 4.23–4.16 (m, 1H), 3.76 (s, 3H), 3.68 (d, J = 16.5 Hz, 1H), 3.61 (d, J = 15.0 Hz, 1H), 3.53–3.44 (m, 4H), 3.29 (d, J = 18.7 Hz, 1H), 2.94 (d, J = 15.0 Hz, 1H), 2.87 (d, J = 13.5 Hz, 1H), 2.5 (s, 3H), 2.21 (s, 3H), 1.56 (s, 6H) ppm. HRMS (ESI): m/z [M+Na]$^+$ = 735.2708 ([C$_{40}$H$_{44}$N$_2$O$_8$SNa]$^+$ = 735.2711).

A.3.8 Synthesis of A.14

Morpholinourea rhodamine (Lavis, *et al.*, 2006a) (50 mg, 0.11 mmol) was dissolved in dry THF in a flame dried 10 mL round bottom flask, that had been flushed with Ar(g). 4-nitrobenzyl chloroformate (49 mg, 0.23 mmol), pyridine (19 μL, 0.23 mmol), and dimethylaminopyridine (1 mg, 0.011 mmol) were added and the reaction was left under foil for 3 days. Reaction progress was followed by TLC (1:7:2 hexanes/EtOAc/DCM). Upon completion, the reaction mixture was transferred to a separatory funnel and partitioned between DCM and 10% citric acid solution in water (50 mL). The organic phase was collected and washed with saturated sodium bicarbonate, followed by saturated brine (50 mL each). The organic phase was dried of sodium sulfate, filtered and dried under reduced pressure. The residue was purified by silica gel chromatography (1:7:2 hexanes/EtOAc/DCM) to obtain a white solid (39 mg; 56%). ^{1}H NMR (400 MHz, CDCl$_3$) δ: 8.16 (d, $J = 7.1$ Hz, 2H), 7.98 (d, $J = 7.1$ Hz, 1H), 7.70 (s, 1H), 7.68–7.56 (m, 2H), 7.50 (d, $J = 8.7$ Hz, 2H), 7.43 (s, 1H), 7.37 (s, 1H), 7.12–7.00 (m, 3H), 6.89 (d, $J = 8.6$ Hz, 1H), 6.65 (d, $J = 8.6$ Hz, 1H), 6.57 (d, $J = 9.5$ Hz, 1H), 5.24 (s, 2H), 3.67 (m, 4H), 3.48 (m, 4H) ppm. ^{13}C NMR (100 MHz, CDCl$_3$) δ: 170.3, 155.0, 153.2, 152.9, 151.9, 151.7, 147.7, 143.5, 141.5, 140.1, 135.6, 130.0, 128.6, 128.3, 126.3, 125.1, 124.2, 123.9, 115.8, 114.5, 113.5, 112.7, 107.8, 106.6, 83.5, 66.6, 65.5, 44.4 ppm. HRMS (ESI): *m/z* 645.1576 [M+Na]$^+$ ([C$_{33}$H$_{26}$N$_4$O$_9$Na]$^+$ = 645.1592).

A.3.9 Synthesis of A.18

To a flame dried, 50 mL round bottom flask that had been flushed with Ar(g) was added maleimidourea rhodamine (Lavis, *et al.*, 2006a) (50 mg, 0.10 mmol). 5 mL of THF was added. 4-nitrobenzyl chloroformate (42 mg, 0.20 mmol) was dissolved in 3 mL dry THF and added to the reaction mixture followed by pyridine (16 μL, 0.20 mmol) and dimethylaminopyridine (1 mg, 0.01 mmol). The reaction was stirred under foil and Ar(g) for 40 hours. Reaction progress was monitored by TLC (80% EtOAc in hexanes). Upon completion, the reaction mixture was transferred to a separatory funnel. 1 N HCl (50 mL) was added, and was extracted with EtOAc (2 × 50 mL). The organic phases were combined and were washed with 50 mL each H_2O, and saturated brine. The organic phase was dried over sodium sulfate and evaporated under reduced pressure. The residue was purified by silica gel chromatography (70% EtOAc in hexanes) to give a white solid (47 mg; 70%). ^{1}H NMR (400 MHz, $CDCl_3$) δ: 8.15 (d, J = 8.1 Hz, 2H), 8.00 (d, J = 7.4 Hz, 1H), 7.78 (s, 1H), 7.67–7.57 (m, 2H), 7.50 (d, J = 8.1 Hz, 2H), 7.40 (s, 1H), 7.31 (s, 1H), 7.16–7.07 (m, 3H), 6.98 (d, J = 8.7 Hz, 1H), 6.69–6.63 (m, 3H), 6.59 (d, J = 7.4 Hz, 1H), 5.73 (t, J = 6.0 Hz, 1H), 5.24 (s, 2H), 3.55 (t, J = 6.0 Hz, 2H), 3.17 (m, 2H), 1.75 (m, 2H) ppm. ^{13}C NMR (100 MHz, $CDCl_3$) δ: 171.1, 170.6, 155.4, 153.2, 153.1, 151.8, 151.6, 147.8, 143.3, 141.8, 140.2, 135.7, 134.3, 130.1, 128.9, 128.6, 128.4, 126.3, 125.2, 124.2, 123.9, 115.3, 113.4, 111.9, 107.3, 106.8, 106.6, 84.1, 65.9, 37.2, 35.2, 29.0 ppm. HRMS (ESI): m/z 712.1685 [M+Na]$^+$ ($[C_{36}H_{27}N_5O_{10}Na]^+$ = 712.1651).

A.3.10 Synthesis of A.19

A.5 (Amsberry and Borchardt, 1990) (1.0 g, 4.8 mmol), 4-nitrobenzyl bromide (1.14 g, 5.28 mmol), potassium iodide (1.58 g, 9.60 mmol), and potassium carbonate (1.33 g, 9.60 mmol) were added to a flame dried 100 mL round bottom flask. Acetone (50 mL) was added and the reaction was refluxed overnight under foil. Reaction progress was monitored by TLC (30% EtOAc in hexanes). The solvent was evaporated under reduced pressure. The residue was extracted with ether (75 mL) and H_2O (75 mL). The organic phase was washed with 10% sodium thiosulfate solution in H_2O (100 mL), then H_2O (100 mL), then saturated brine (100 mL). The organic phase was dried over sodium sulfate, filtered, and the filtrate was evaporated under reduced pressure. The residue was purified by silica gel chromatography (20% EtOAc in hexanes) to give a yellowish white solid (777 mg; 47%). ^{1}H NMR (400 MHz, CDCl$_3$) δ: 8.26 (d, J = 8.3 Hz, 2H), 7.62 (d, J = 8.4 Hz, 2H), 6.60 (s, 1H), 6.58 (s, 1H), 5.17 (s, 1H), 3.56 (t, J = 7.3 Hz, 2H), 2.52 (s, 3H), 2.22 (s, 3H), 2.17 (t, J = 7.2 Hz, 2H), 1.54 (s, 6H), 1.02 (bs, 1H) ppm. ^{13}C NMR (100 MHz, CDCl$_3$) δ: 158.3, 147.7, 145.0, 138.1, 136.4, 131.4, 128.4, 128.0, 123.1, 112.9, 70.2, 61.3, 45.7, 40.0, 32.4, 26.0, 20.8 ppm. HRMS (ESI): m/z 366.1661 [M+Na]$^+$ ([C$_{20}$H$_{25}$NO$_4$Na]$^+$ = 366.1676).

A.3.11 Synthesis of A.20

A.19 (300 mg, 0.87 mmol) was dissolved in 50 mL acetone (HPLC grade) in a 100 mL round bottom flask. Jones reagent was made up as follows: chromium trioxide (0.70 g, 7.0 mmol) was dissolved in 0.6 mL concentrated sulfuric acid and then diluted up to

2.5 mL with H$_2$O. 500 µL of this solution (1.4 mmol) was added dropwise to the reaction mixture. The solution turned green over time. The reaction was stirred for 2 hours. The reaction was quenched with isopropanol (5 mL). The chromate salts were filtered off and the filtrate was dried under reduced pressure. The residue was partitioned between EtOAc and H$_2$O (50 mL). The layers were separated and the aqueous layer was extracted with two additional washings of EtOAc (50 mL). The combined organic phases were washed with H$_2$O (50 mL) then saturated brine (50 mL). The organic phase was dried over sodium sulfate, filtered, and the filtrate was evaporated under reduced pressure to get a brown/white solid. The crude product was recrystallized from 2:1 hexanes/EtOAc to provide a yellowish solid (104 mg; 33%). ^{1}H NMR (400 MHz, CDCl$_3$) δ: 8.24 (d, J = 8.7 Hz, 2H), 7.60 (d, J = 8.4 Hz, 2H), 6.59 (s, 1H), 6.56 (s, 1H), 5.16 (s, 2H), 2.95 (s, 2H), 2.52 (s, 3H), 2.21 (s, 3H), 1.62 (s, 6H) ppm. ^{13}C NMR (100 MHz, CDCl$_3$) δ: 177.2, 157.9, 147.7, 144.9, 138.2, 136.5, 130.0, 128.4, 128.0, 124.1, 112.6, 70.0, 47.2, 39.8, 31.9, 25.7, 20.9 ppm. HRMS (ESI): m/z 356.1496 [M–H]$^-$ ([C$_{20}$H$_{22}$NO$_5$]$^-$ = 356.1503).

A.3.12 Synthesis of A.26

A.25 (Tang, *et al.*, 2000) (5.0 g, 25.6 mmol) was added to a flame dried 250 mL round bottom flask. Anhydrous MeOH (80 mL) was added, then concentrated sulfuric acid (2.7 mL, 51 mmol) was added dropwise. Reaction progress was followed by TLC (30% EtOAc in hexanes). The solvent was concentrated under reduced pressure. The residue was transferred to a separatory funnel, DCM (40 mL) was added, and washed with 1 N NaOH (2 × 100 mL). The organic phase was dried over magnesium sulfate,

filtered, and the filtrate was evaporated under reduced pressure to provide a brown oil

that crystallized upon standing. The crystals were washed with cold 10% EtOAc in

hexanes and dried (3.93 g, 73%). ^{1}H NMR (400 MHz, CDCl$_3$) δ: 7.82 (d, J = 8.2 Hz, 1H),

7.47 (d, J = 7.4 Hz, 1H), 7.34 (t, J = 7.7 Hz, 1H), 3.94 (s, 2H), 3.73 (s, 3H), 2.42 (s, 3H)

ppm. ^{13}C NMR (100 MHz, CDCl$_3$) δ: 170.3, 140.2, 135.1, 131.5, 127.9, 127.8, 122.9,

52.4, 34.6, 20.5 ppm. HRMS (ESI): m/z 232.0590 [M+Na]$^+$ ([C$_{10}$H$_{11}$NO$_4$Na]$^+$ =

232.0581).

A.3.13 Synthesis of A.27

A.26 (1.0 g, 4.8 mmol) was added to an oven dried, three neck flask that had been

flushed with Ar(g). Methyl iodide (1.5 g, 10.6 mmol) and 18-crown-6 ether (317 mg, 1.2

mmol) were added. Anhydrous THF (60 mL) was added and the flask was cooled to –78

°C in a dry ice/acetone bath. A 1 M solution of potassium *tert*-butoxide (5.2 mL, 5.26

mmol) was added via dropping funnel. The solution turned dark blue. The reaction was

allowed to warm to room temperature and was stirred for 2 hours. Reaction progress was

monitored by TLC with the following workup: a few drops from the reaction were added

to saturated ammonium chloride in water (1 mL) and EtOAc (0.5 mL) was added. TLC

was spotted from the upper organic layer (40% EtOAc in hexanes). The reaction was

cooled to –78 °C and saturated ammonium chloride was added, which froze. The flask

was warmed to room temperature and extracted with DCM (100 mL). The organic phase

was washed with H$_2$O (100 mL) then saturated brine (100 mL). The organic phase was

dried over magnesium sulfate, filtered, and the filtrate was evaporated under reduced

pressure to produce a brown oil. The oil was purified by silica gel chromatography (30% EtOAc in hexanes) to produce a slightly green oil, which crystallized upon drying to produce a white crystals (619 mg; 58%). ^{1}H NMR (400 MHz, $CDCl_3$) δ: 7.73 (d, J = 8.0 Hz, 1H), 7.44 (d, J = 7.7 Hz, 1H), 7.30 (t, J = 7.7 Hz, 1H), 4.09 (q, J = 7.4 Hz, 1H), 3.66 (s, 3H), 2.41 (s, 3H), 1.61 (d, J = 6.9 Hz, 3H) ppm. HRMS (ESI): m/z 246.0743 [M+Na]$^+$ ([$C_{11}H_{13}NO_4Na$]$^+$ = 246.0737).

A.3.14 Spectroscopy Methods

Absorption measurements were made with a Cary model 50 spectrometer from Varian. Fluorometric measurements were with a QuantaMaster1 photon-counting spectrofluorometer from Photon Technology International, equipped with sample stirring. Stock solutions of **A.14** were made in DMSO and were diluted to appropriate concentrations for assays such that the final DMSO concentration did not exceed 0.5%. Stock solutions of NADH and NTR (MW = 24,000; Sigma Catalog #N9284) were made in PBS. **A.14** was added to 2 mL PBS in 1 cm path-length poly(methyl methacrylate) cuvettes (final concentration 0.03–27.2 μM), followed by the addition of NTR (10 nM). Reactions were initiated by the addition of NADH (500 μM). Product formation was monitored by fluorescence (λ_{ex} = 496 nm; λ_{em} = 520 nm) and product concentration was calculated utilizing a standard curve generated from morpholinourea rhodamine (Lavis, *et al.*, 2006a).

A.3.15 P19C RNase 1 Purification and Labeling

P19C RNase 1 was purified and labeled as described previously (Johnson, *et al.*, 2007) with the following modifications: A plasmid encoding P19C RNase 1 was obtained from R.J. Johnson. The labeling reaction was performed with a ten-fold excess of **A.18** in PBS containing 10% dimethyl formamide. Protein concentration was determined using a bicinchoninic assay. Degree of labeling was determined by unmasking a known amount of conjugate with excess NTR and NADH, and calculating the concentration by fluorescence spectroscopy compared to a standard curve of morpholinourea rhodamine.

A.3.16 Mammalian Cell Culture

HeLa cells were from the American Type Culture Collection (Manassas, VA) and were grown in DMEM containing FBS (10% v/v), penicillin (100 units/mL) and streptomycin (100 µg/mL). Media and supplements were from Invitrogen (Carlsbad, CA). Cells were cultured at 37 °C in a humidified incubator containing $CO_2(g)$ (5% v/v).
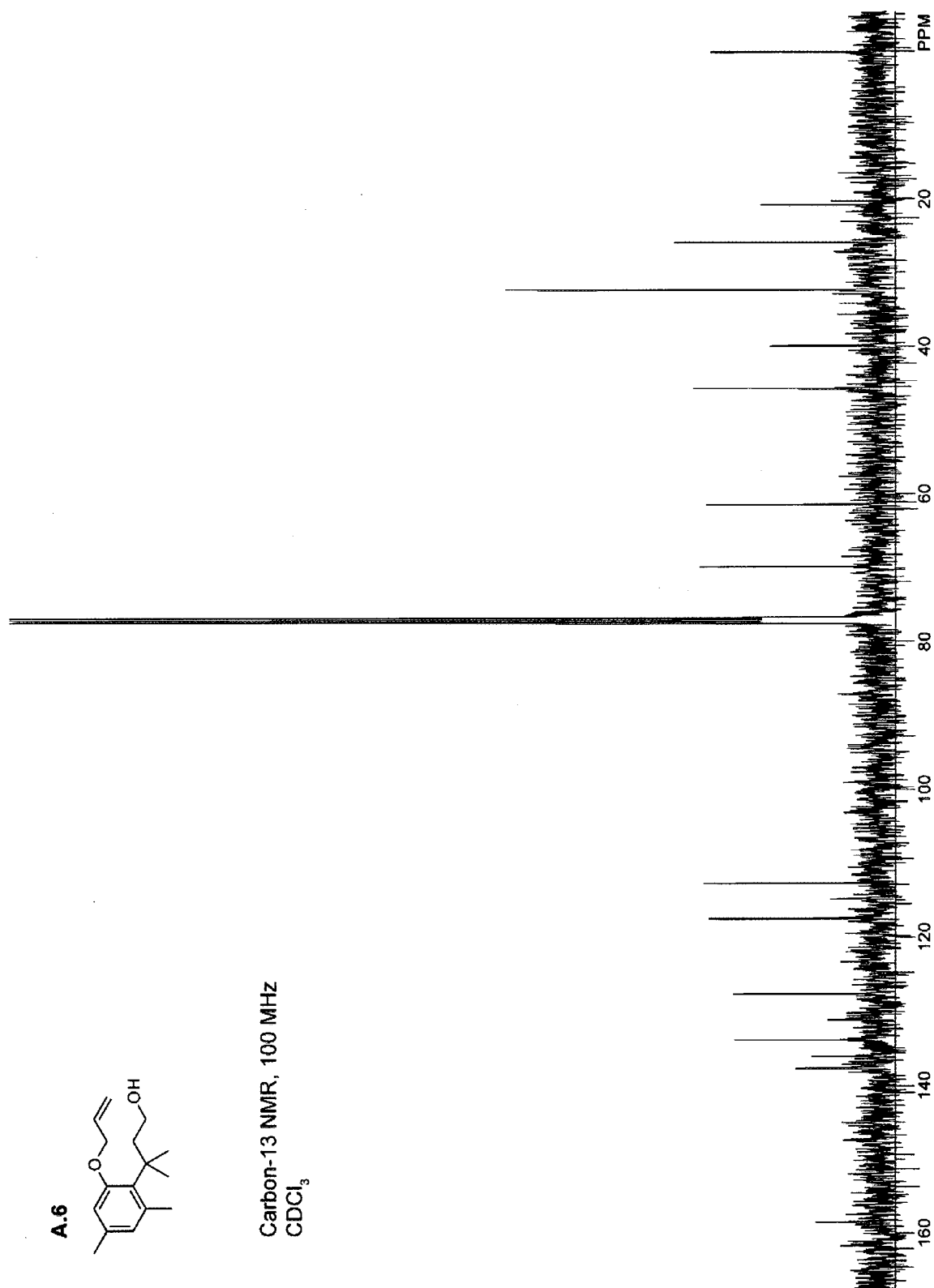
A.3.17 Microscopy

The internalization of **A.18**–P19C RNase 1 conjugates were monitored in live HeLa cells by confocal microscopy on a Nikon Eclipse TE2000-U laser scanning confocal microscope equipped with a Zeiss AxioCam digital camera. Excitation at 408 nm was provided by a blue-diode laser, and emission light was passed through a filter centered at 450 nm with a 35-nm band-pass. Excitation at 488 nm was provided by an argon-ion laser, and emission light was passed through a filter centered at 515 nm with a 40-nm
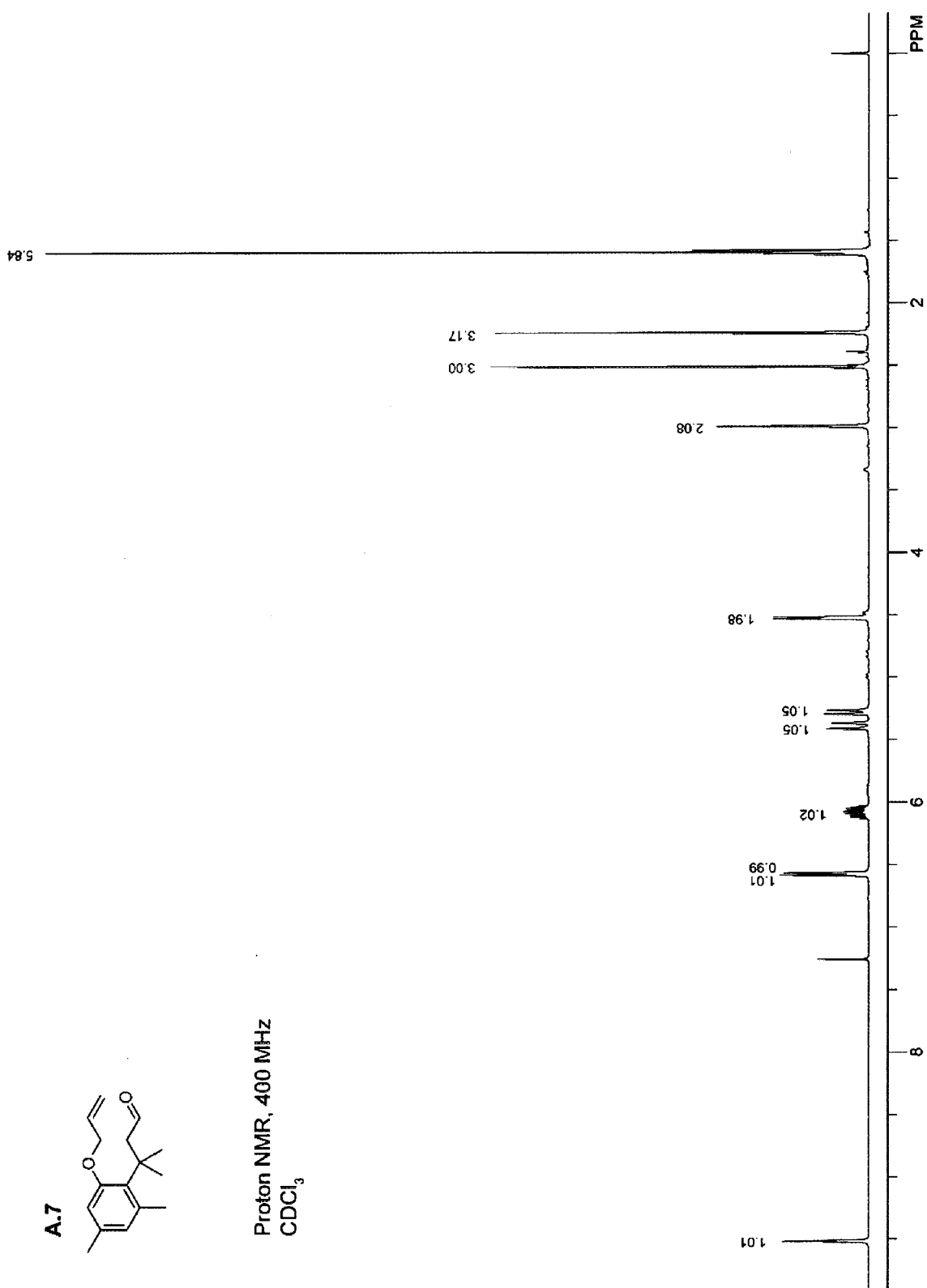
band-pass. Excitation at 543 nm was provided by a HeNe laser, and emission light was passed through a filter centered at 605 nm with a 75-nm band-pass. HeLa cells were plated on 8-well microscope slides at a density of 5×10^4 cells/well in 200 μL DMEM 24 hours prior to transfection. Plasmid pCAG-616-IRES-mCherry, containing the nfsB gene, was a gift from L.D. Lavis (Janelia Farm). The plasmid was transfected using the transfection reagent, Lipofectamine 2000 (Invitrogen). The **A.18**–P19C RNase 1 conjugate was added to the cells in fresh media 24 hours after transfection at a concentration of 5 or 10 μM. Internalization was imaged after 17 hours. Nuclear counterstaining was performed using Hoechst 33342 (Invitrogen).
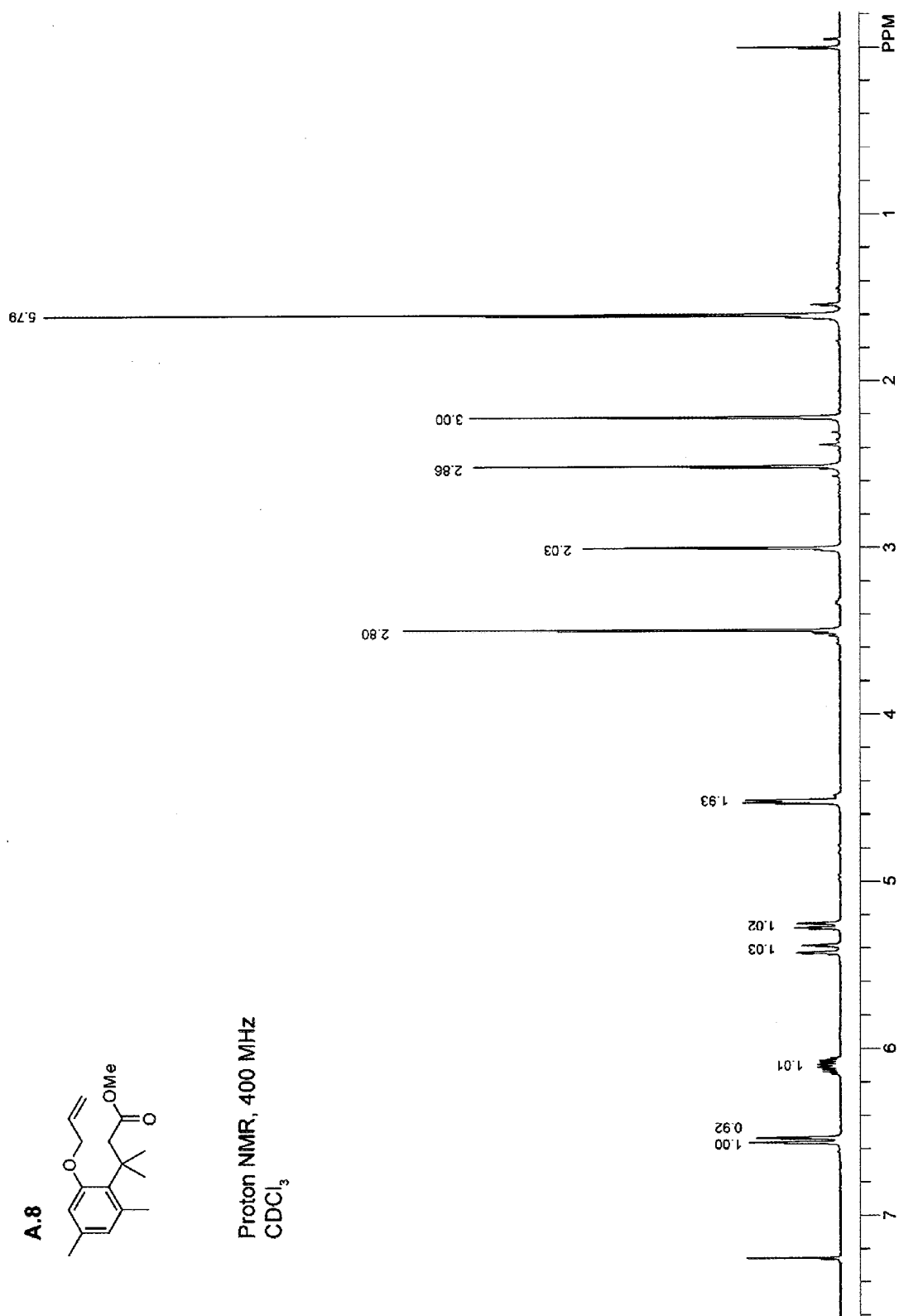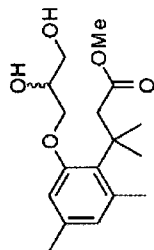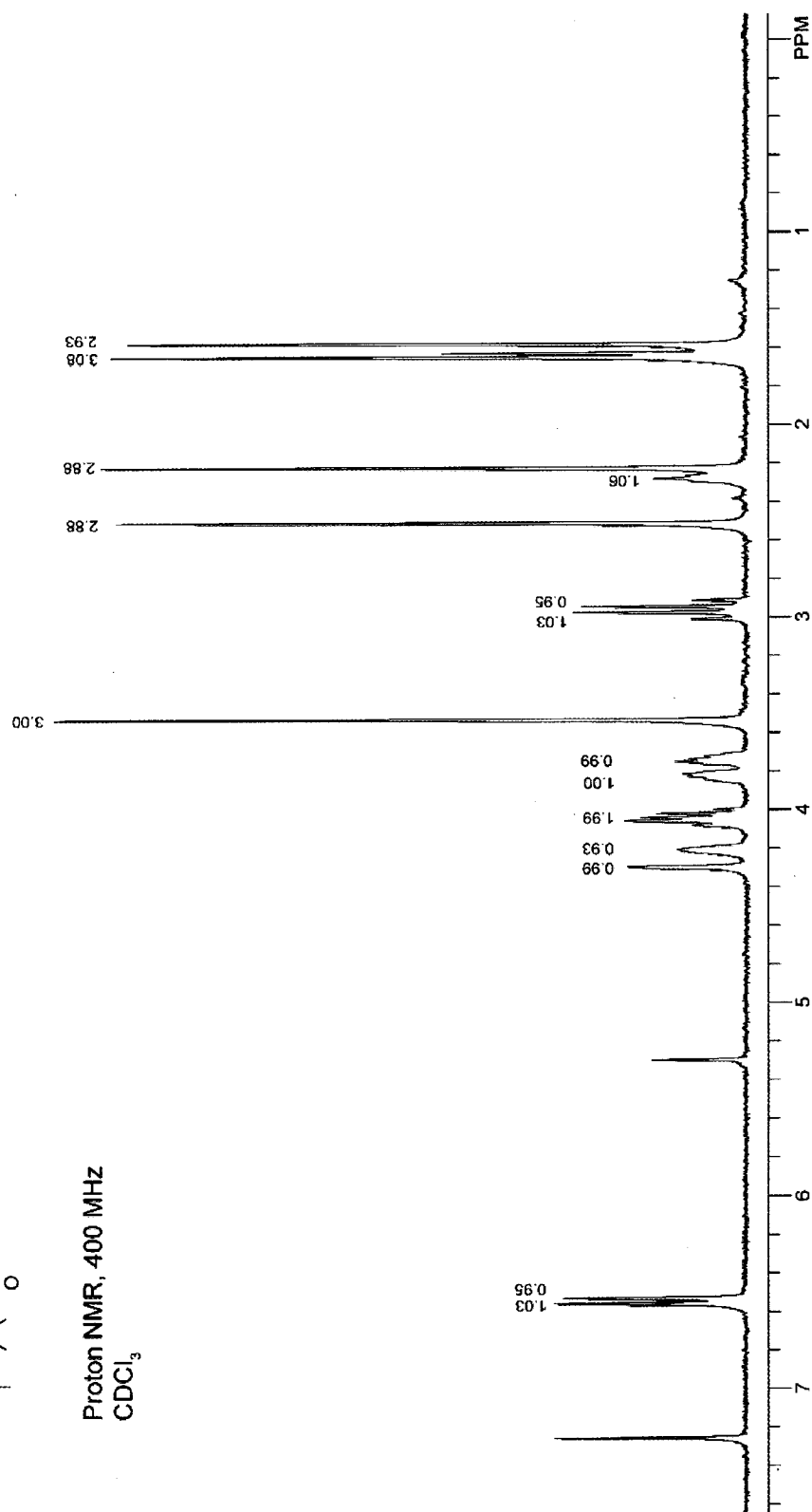
A.6

Proton NMR, 400 MHz
CDCl$_3$

6.93
5.44
2.86
2.00
2.06
1.06
1.08
1.02
0.92
1.03
0.88

PPM

A.6

Carbon-13 NMR, 100 MHz
CDCl$_3$

PPM

5.84

3.17

3.00

2.08

1.98

1.05
1.05

1.02

0.99
1.01

1.01

A.7

Proton NMR, 400 MHz
CDCl$_3$

A.4

Proton NMR, 400 MHz
CDCl$_3$

6.14

2.95

2.81

2.00

1.84

1.01
1.00

0.98

0.96
0.90

PPM

A.8

Proton NMR, 400 MHz
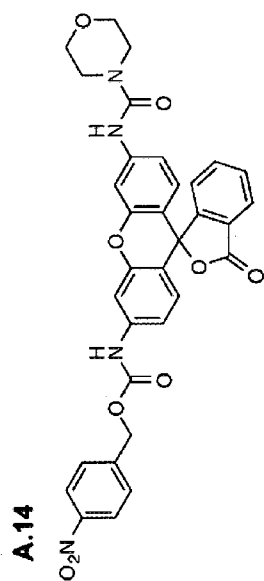CDCl$_3$

PPM
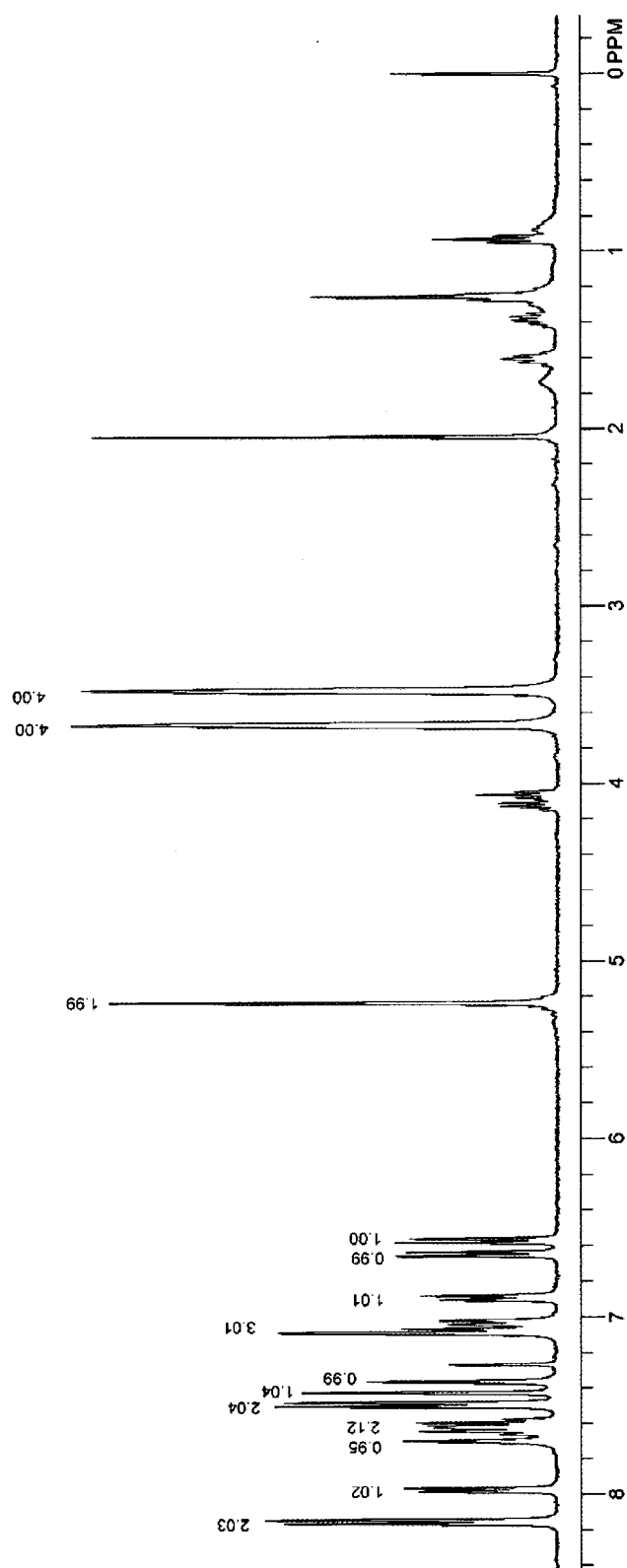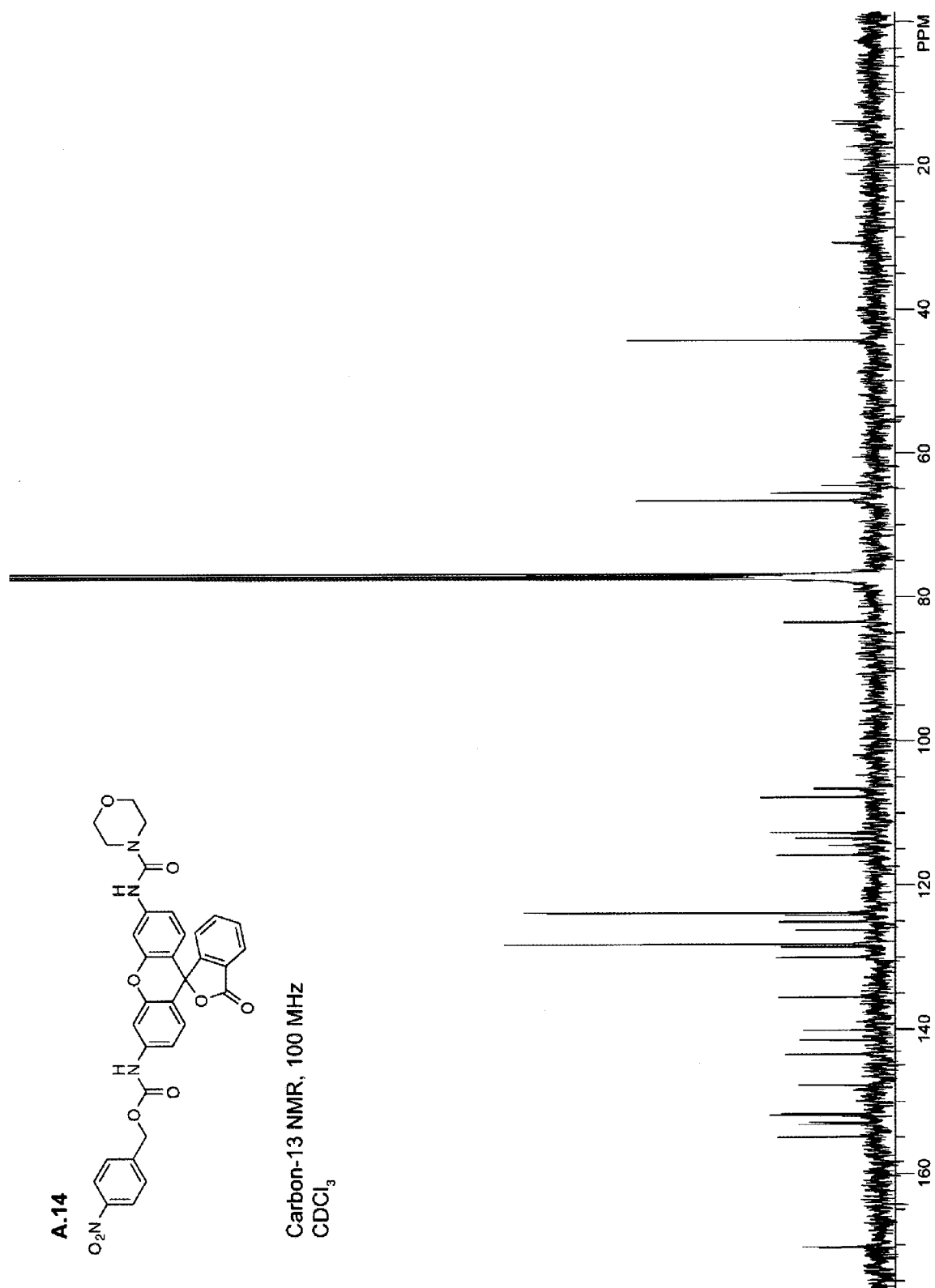
6.79

3.00
2.86
2.03
2.80
1.93
1.02
1.03
1.01
0.92
1.00
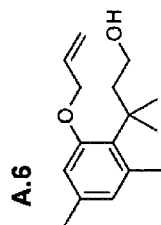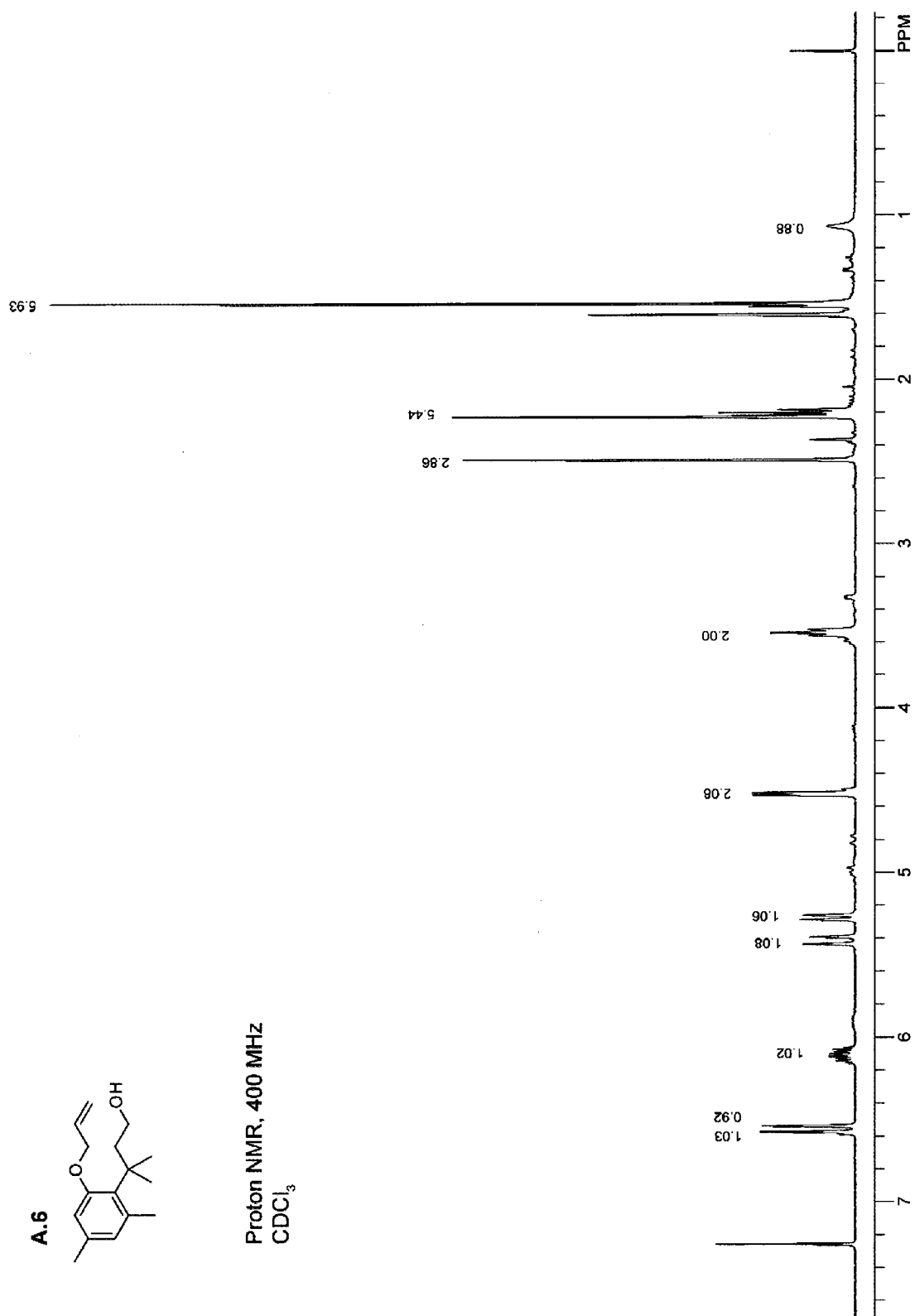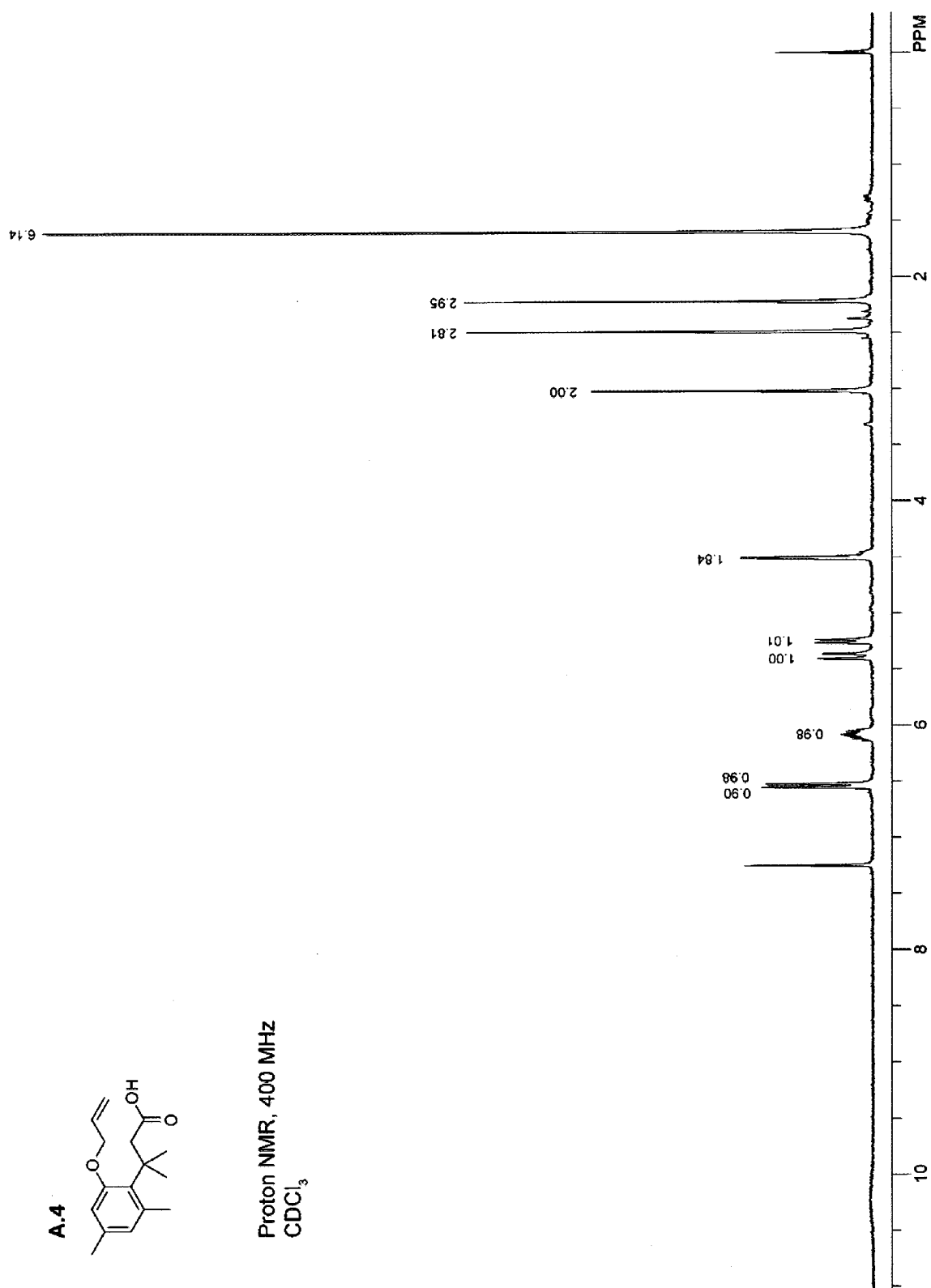
A.9

Proton NMR, 400 MHz
CDCl₃

A.11

Proton NMR, 400 MHz
CDCl₃

A.14

Proton NMR, 400 MHz
CDCl₃

A.14
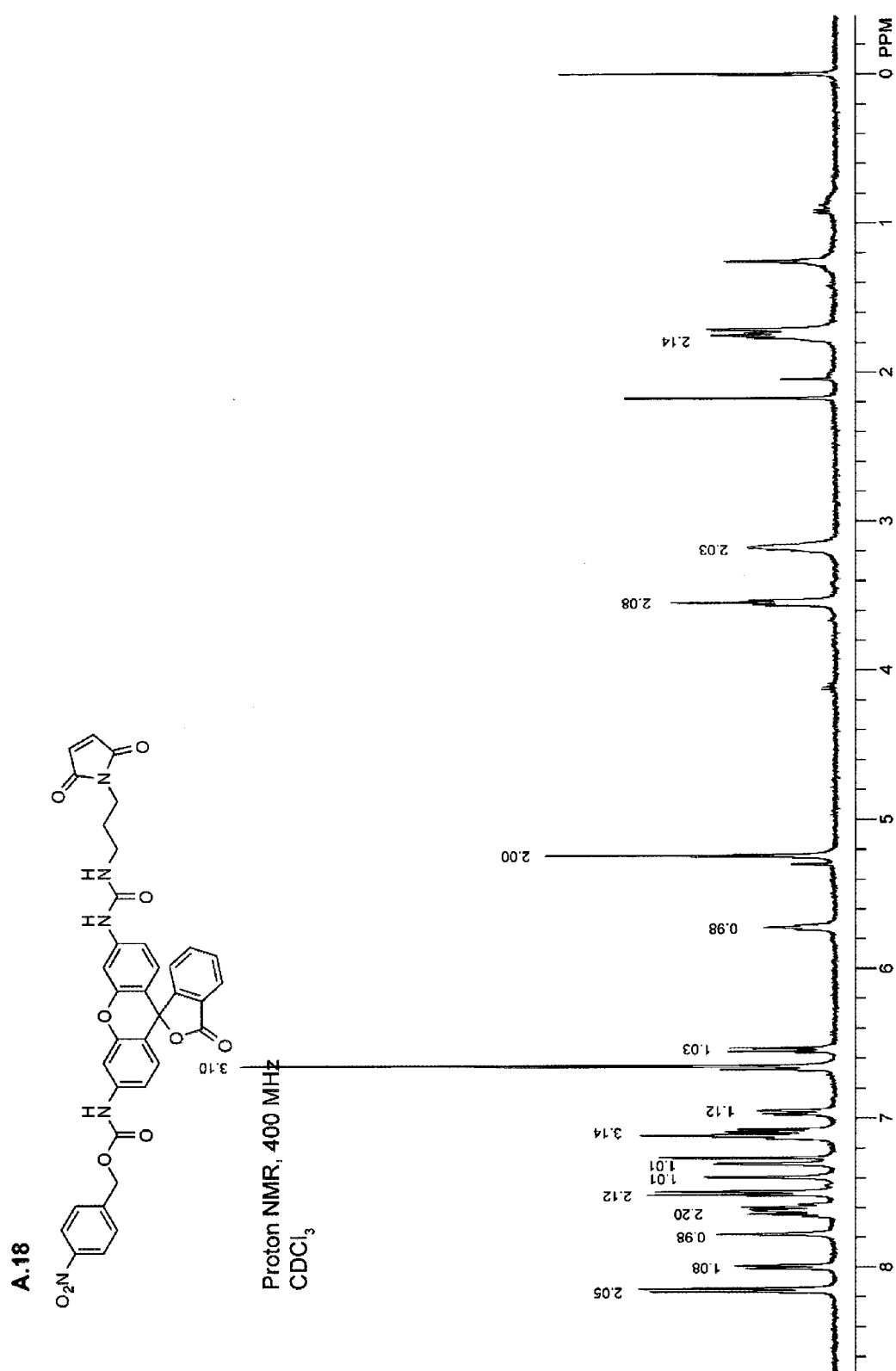
Carbon-13 NMR, 100 MHz
CDCl$_3$

A.18

Proton NMR, 400 MHz
CDCl₃

198
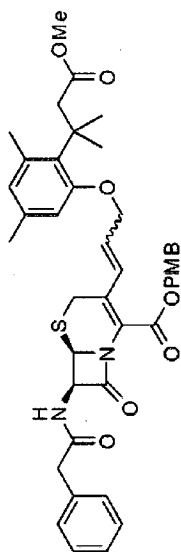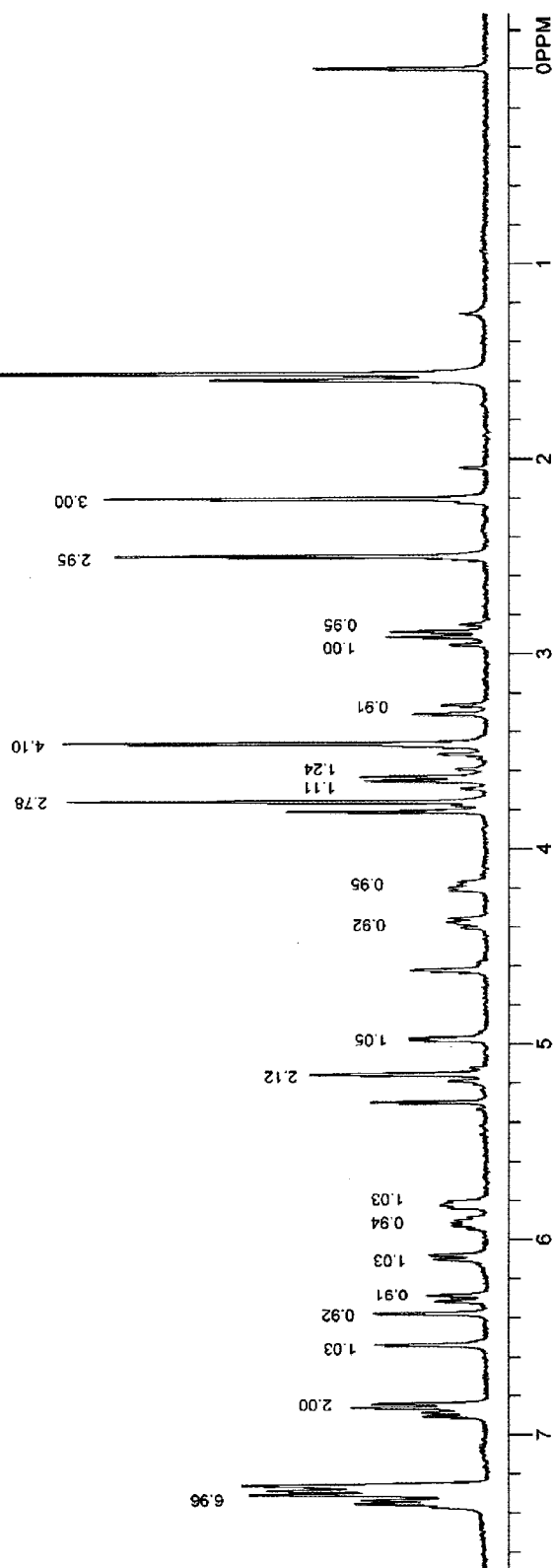
A.18

Carbon-13 NMR, 100 MHz
CDCl$_3$

A.19

Proton NMR, 400 MHz
CDCl$_3$
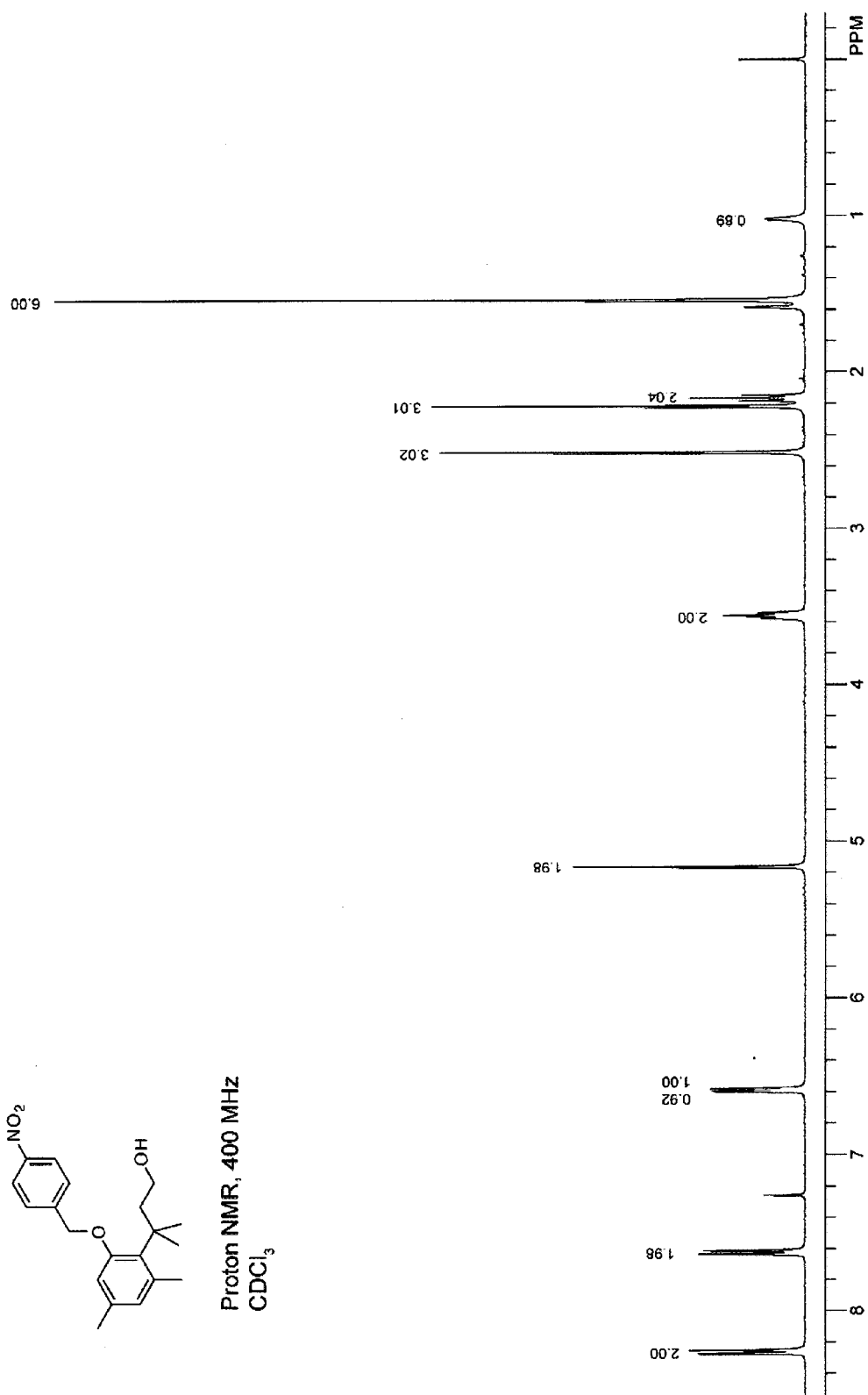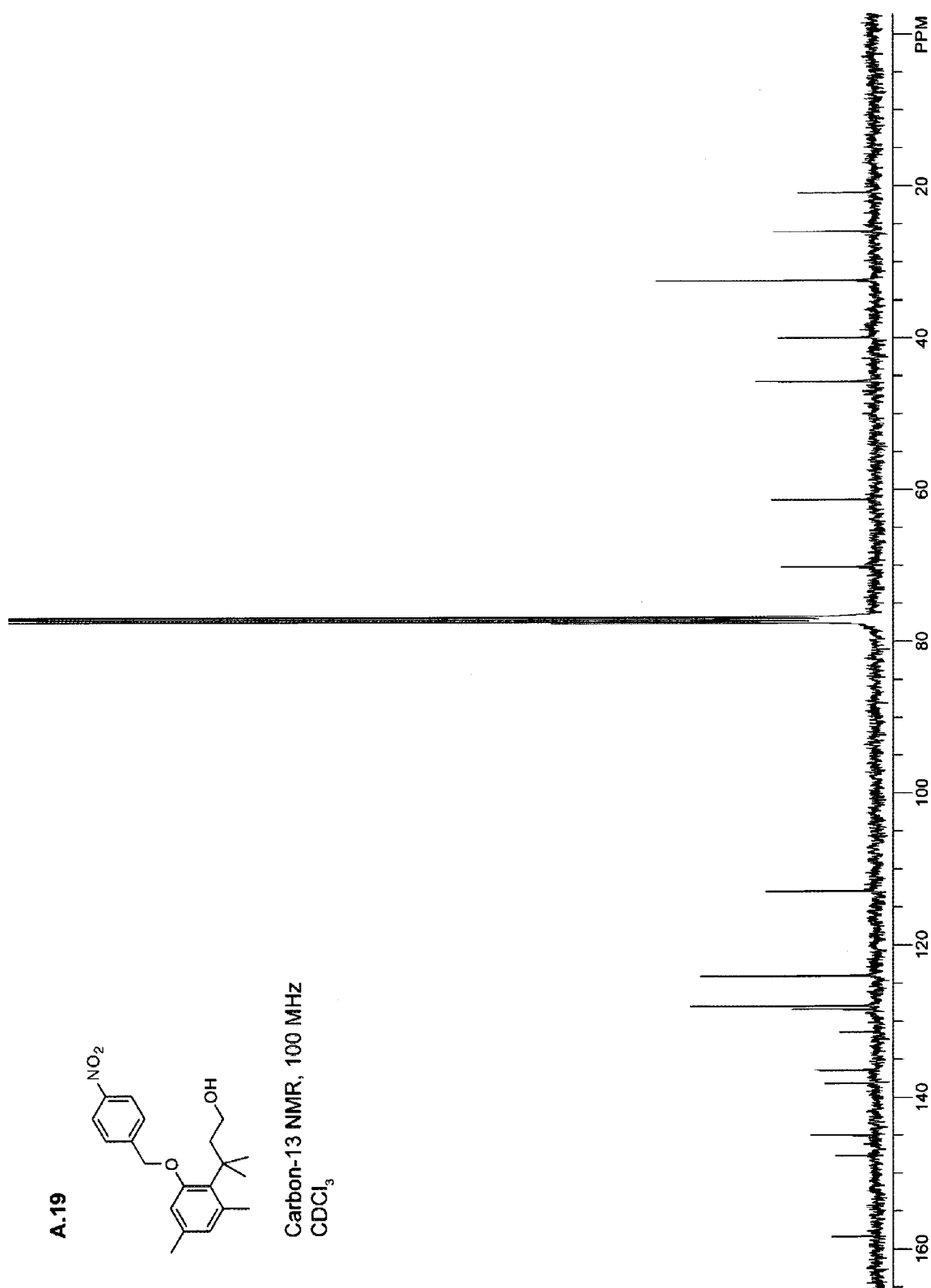
200

A.19

Carbon-13 NMR, 100 MHz
CDCl$_3$

PPM

6.08

3.11

3.03

2.00

1.97

0.96
1.02

1.99
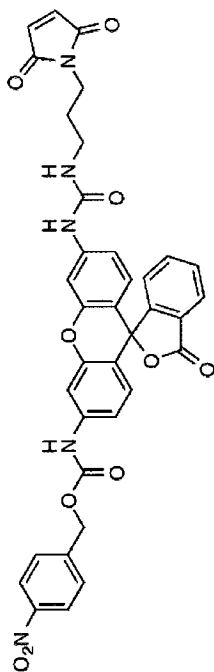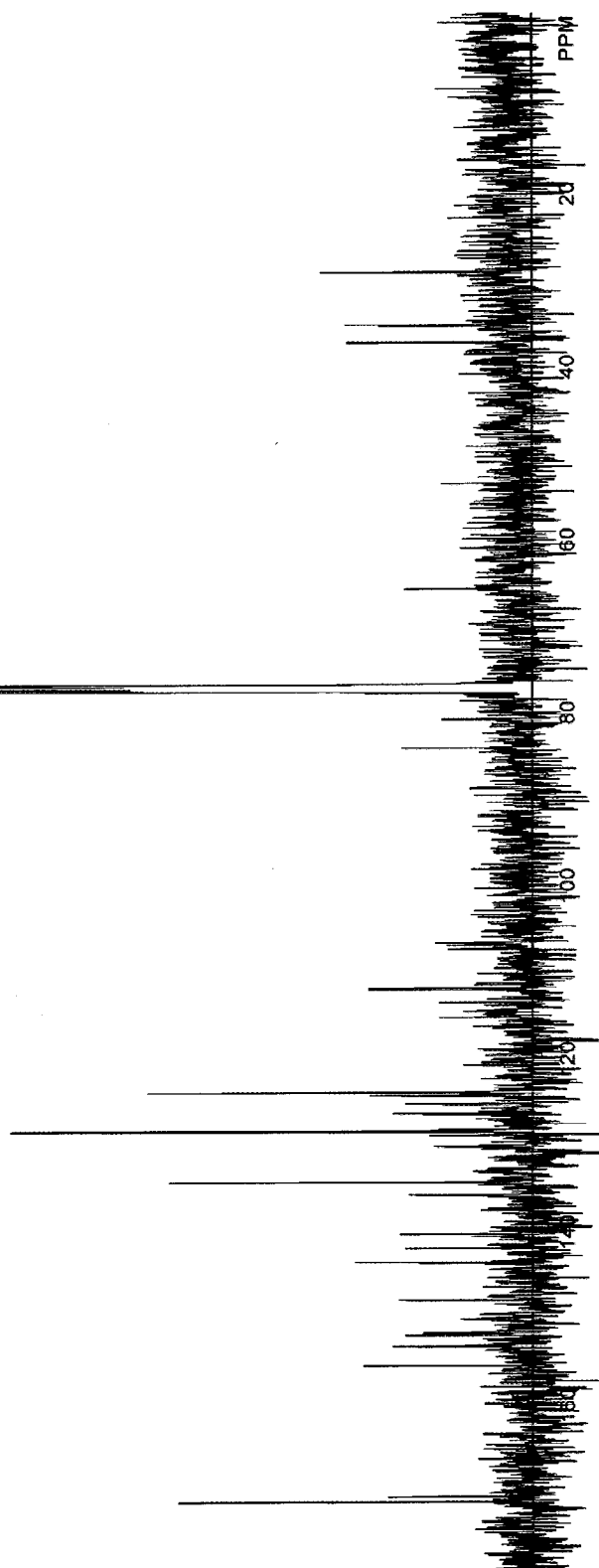
2.03

A.20

Proton NMR, 400 MHz
CDCl$_3$

202

A.20

Carbon-13 NMR, 100 MHz
CDCl$_3$

A.26

NO₂

COOMe

Proton NMR, 400 MHz
CDCl₃

3.04

3.00

2.03

0.98
1.00

1.00

PPM

A.26

NO₂ / COOMe structure
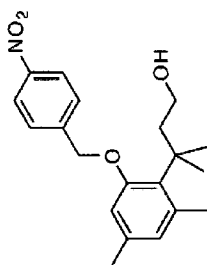
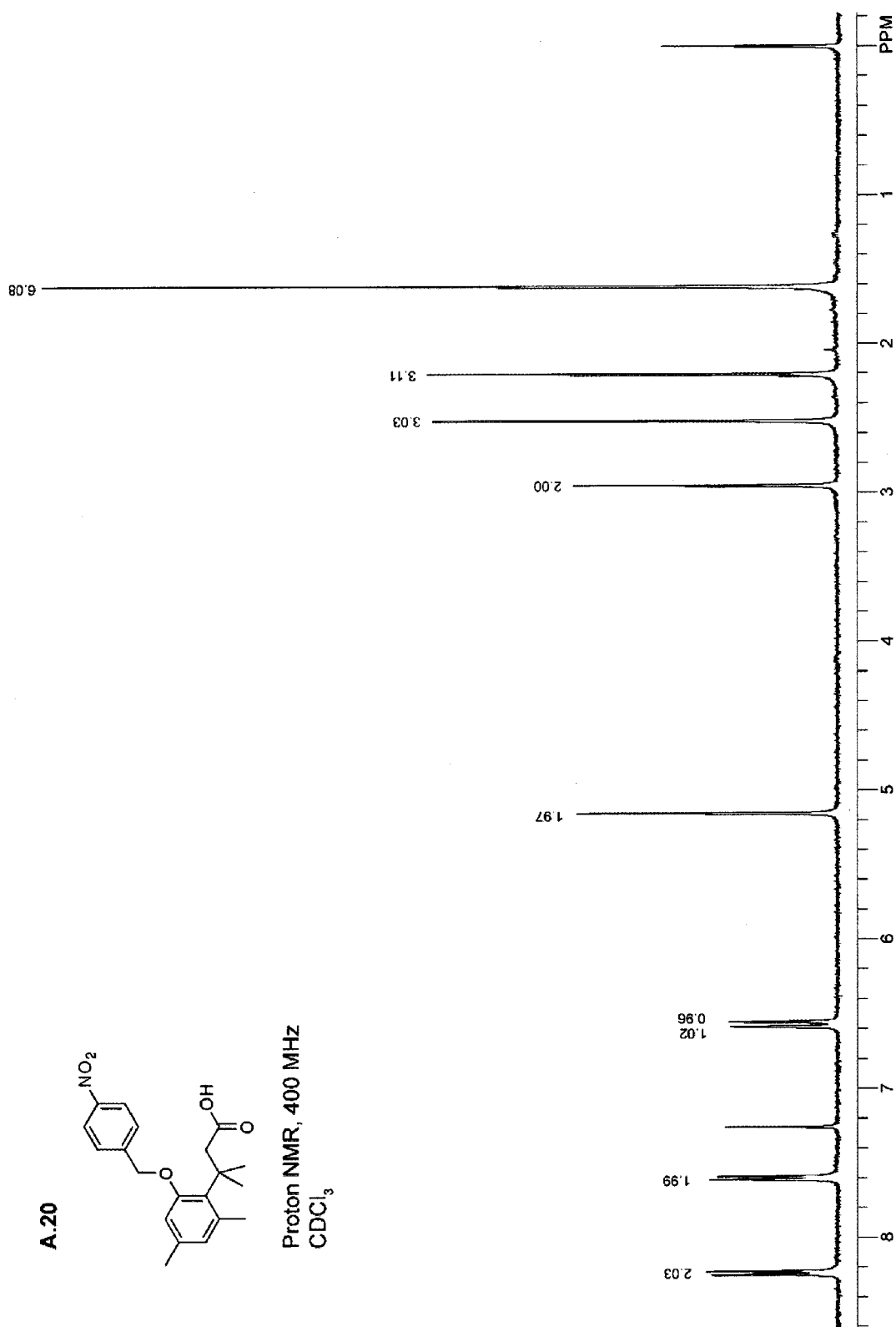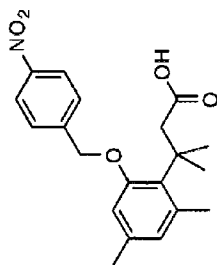Carbon-13 NMR, 100 MHz
CDCl₃

PPM

20

40

60

80

100

120

140

160

A.27

Proton NMR, 400 MHz
CDCl$_3$

PPM

3.01

3.08

3.01

1.03

1.02
1.00

0.99
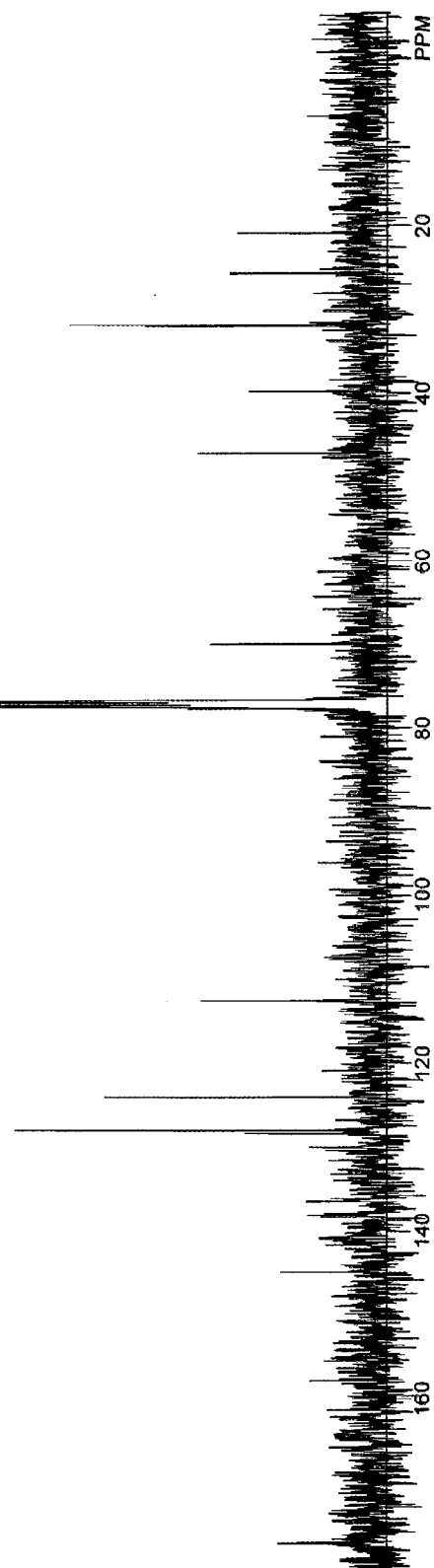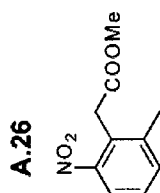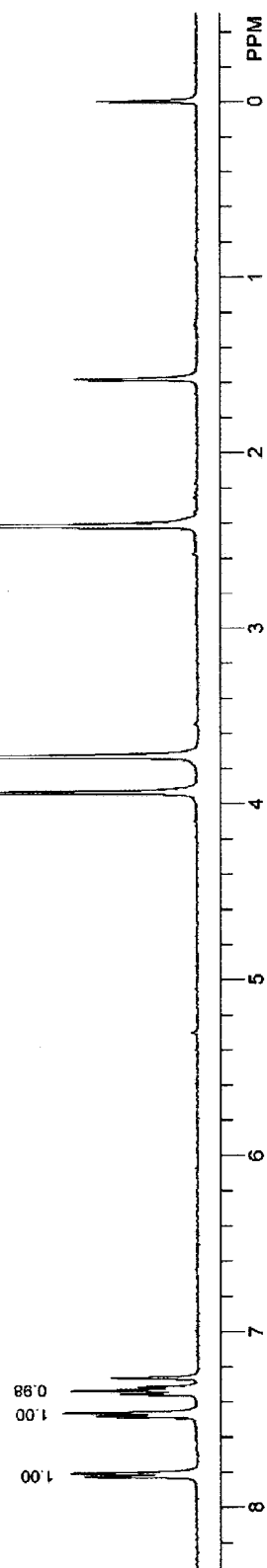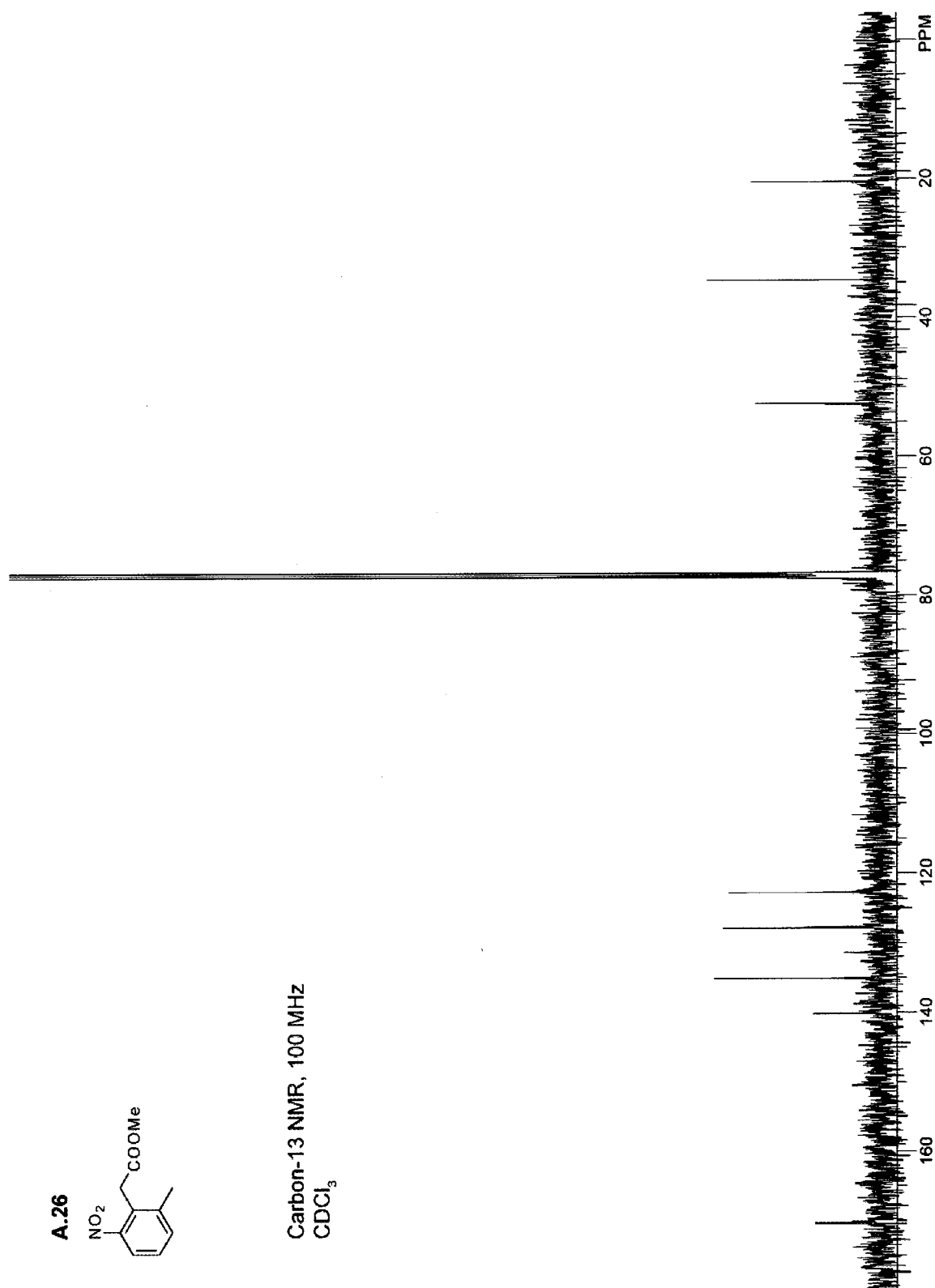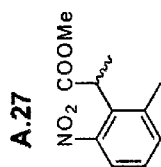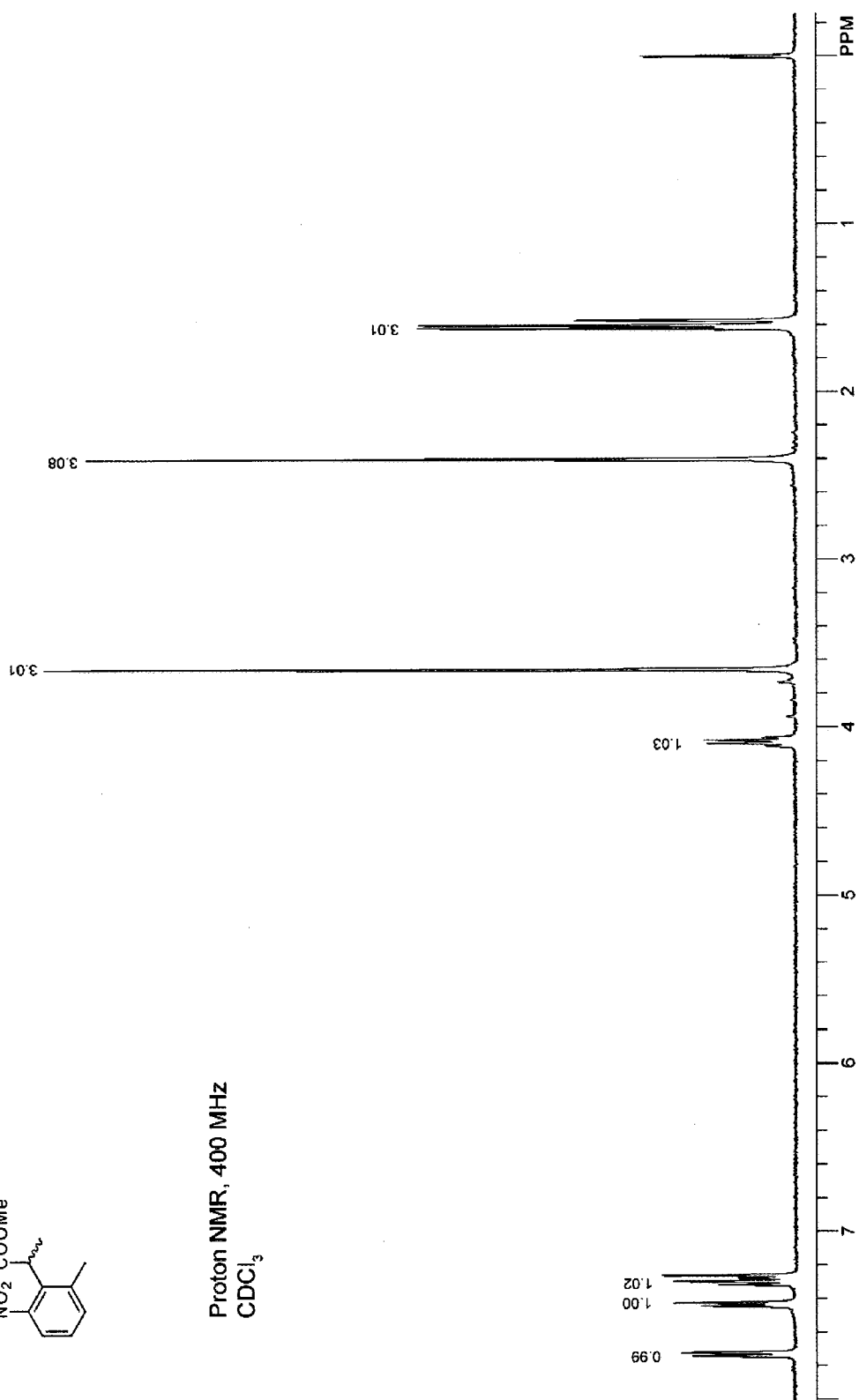
A.4 Conclusions

A fluorogenic substrate for NTR was synthesized and conjugated to a ribonuclease, which subsequently was applied to HeLa cells that were transfected with NTR. The fluorophore was unmasked in endosomes, not in the cytoplasm, as was desired. The unmasking was likely a result of the carbamate linkage utilized to mask the fluorescence of rhodamine. Other attempts to synthesize NTR substrates, or β-lactamase substrates were unsuccessful. The ability to assay the translocation step of cytotoxic ribonuclease cellular internalization would provide insight into the mechanism of cancer selectivity of these proteins.

Scheme A.1   Retrosynthesis of β-lactamase substrate **A.1**.

A.1

A.2

A.3

A.4

A.5
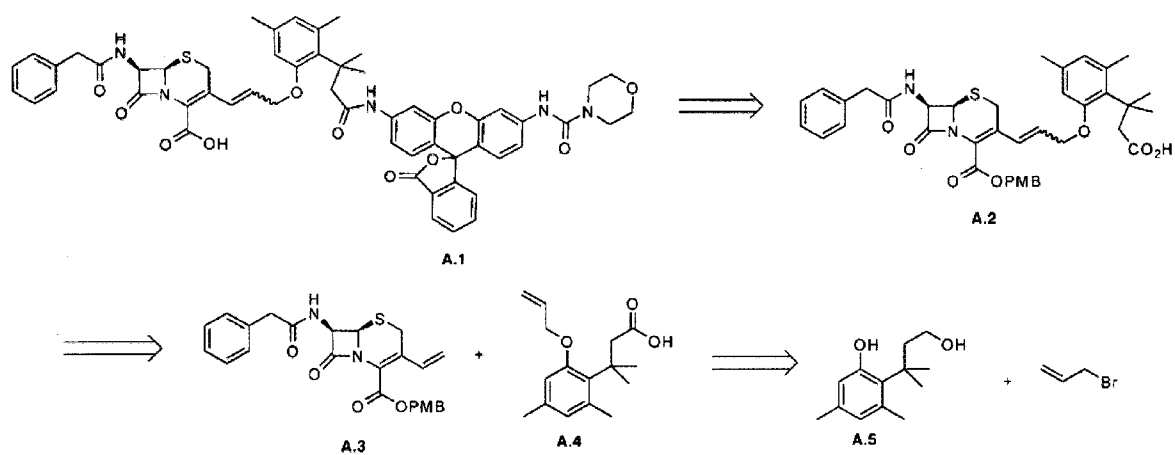
Scheme A.2 Attempted synthetic scheme for the synthesis of β-lactamase substrate

A.1.
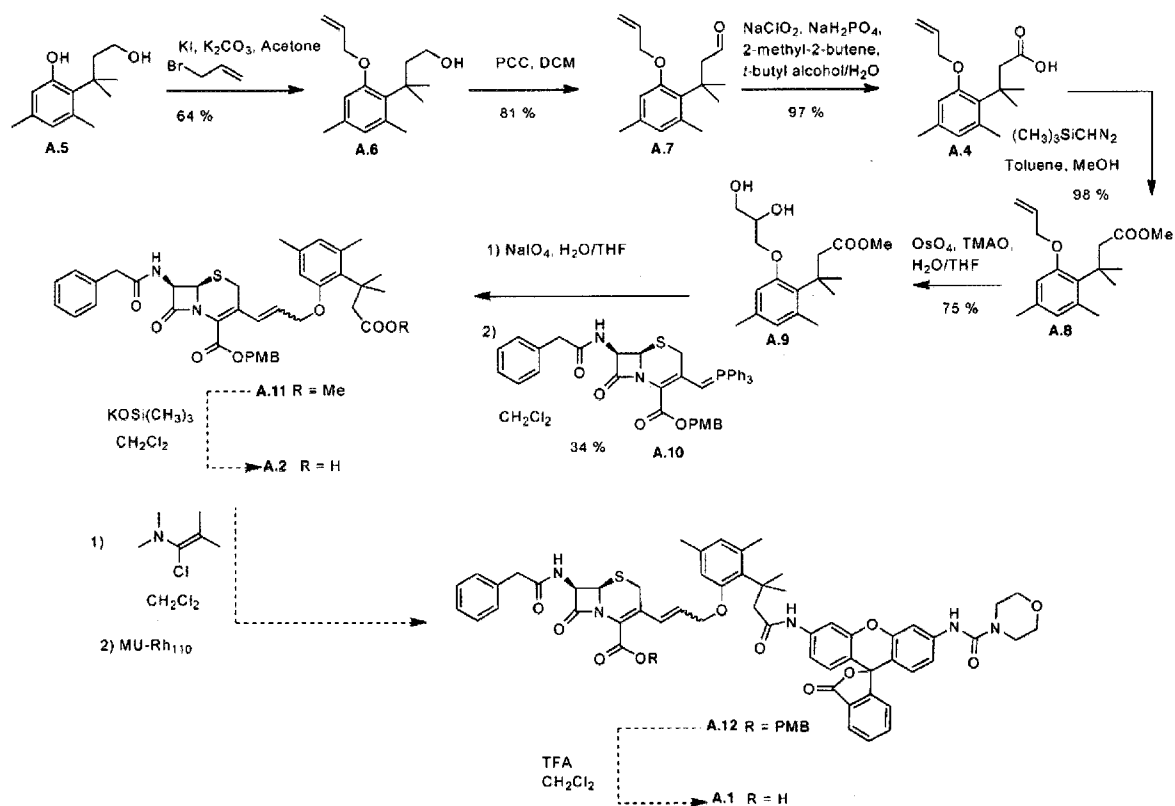
Scheme A.3   Synthesis of NTR substrate **A.14** and mechanism of fluorescence

generation.
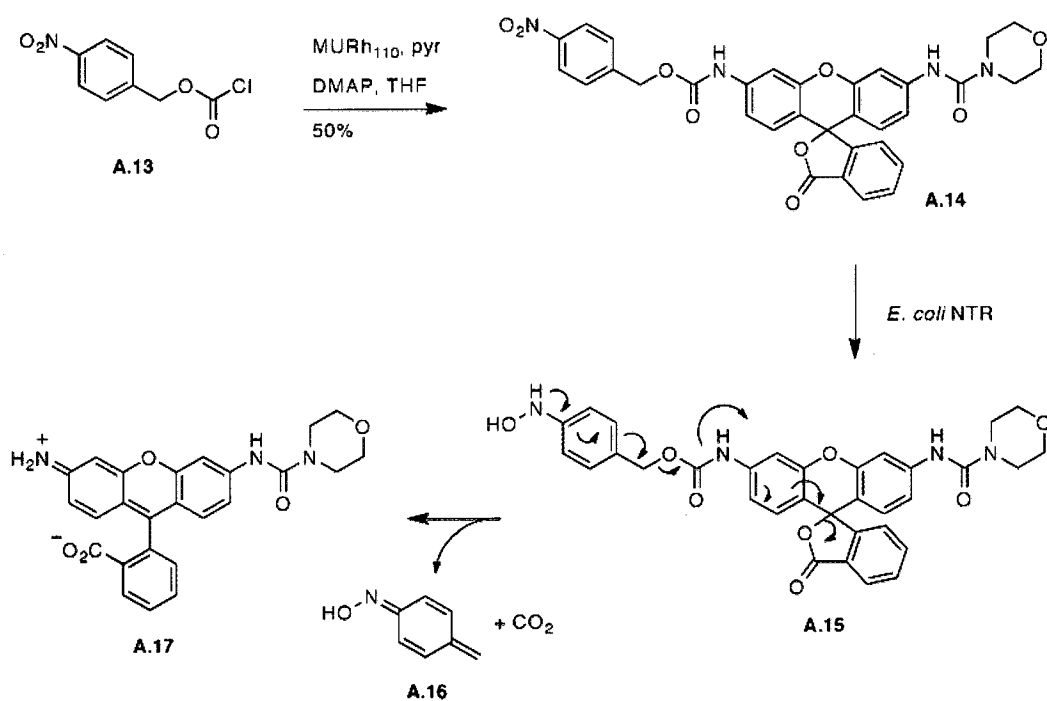
Scheme A.4 Synthesis of NTR substrate **A.18** containing a maleimide handle.

A.13   MalURh₁₁₀, pyr / DMAP, THF / 70%   A.18
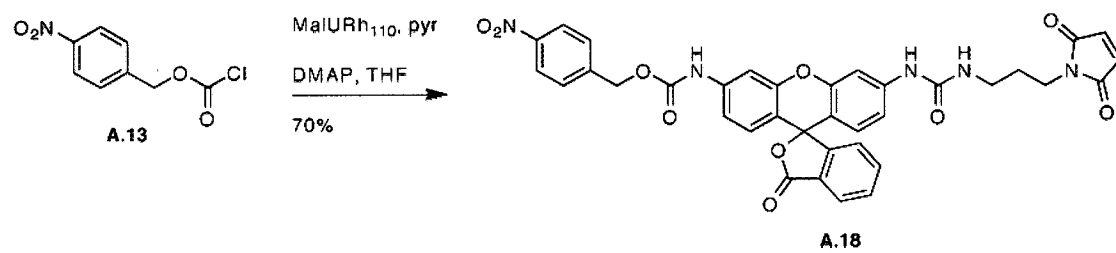
Scheme A.5 Synthesis of *p*-nitrobenzyl trimethyl lock rhodamine derivative **A.21**.
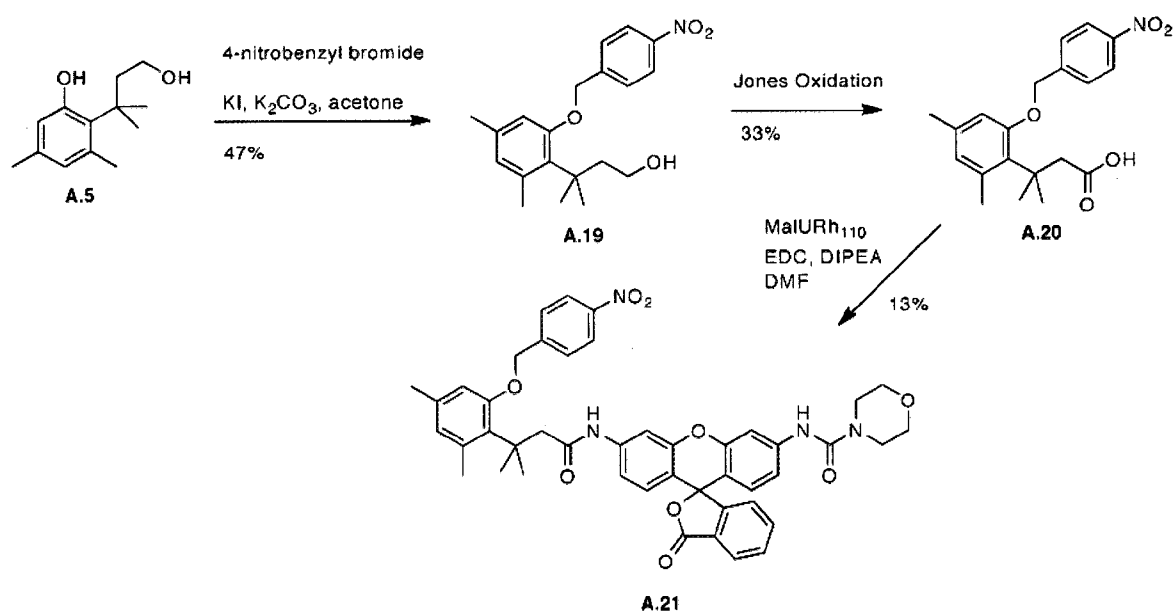
Scheme A.6 Synthesis of quinone trimethyl lock rhodamine derivative **A.23**.

A.22

MURh₁₁₀, EDC
pyr, DMF

38%

A.23
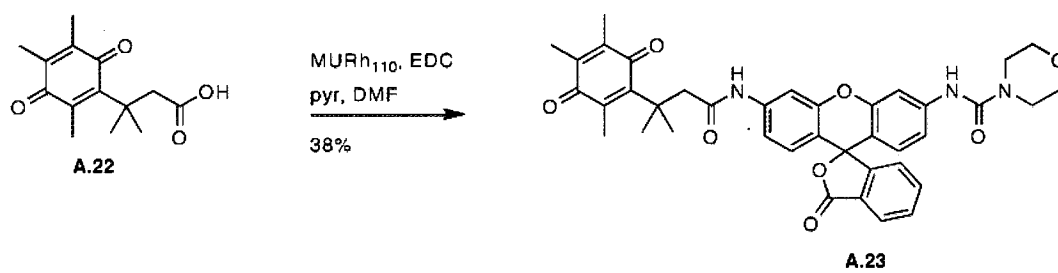
Scheme A.7   Attempted synthesis of nitro trimethyl lock rhodamine derivative **A.30**.
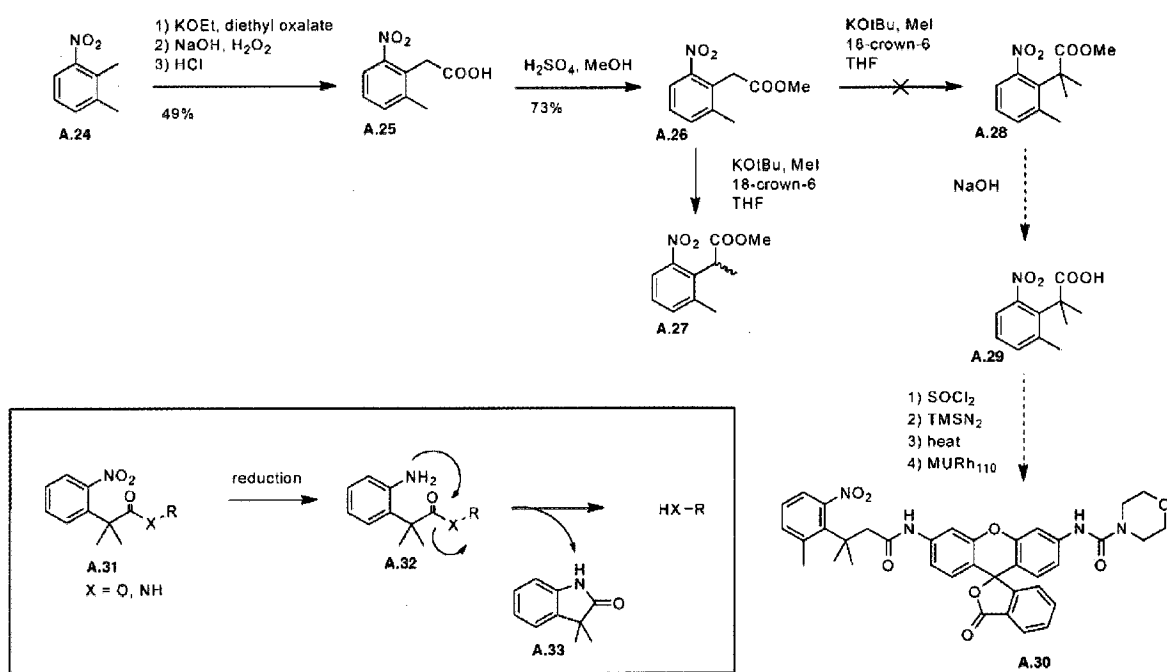
Scheme A.8 Synthesis of *o*-nitrobenzyl carbamate rhodamine derivative **A.35**.

A.34

MURh$_{110}$, pyr

DMAP, THF

26%

A.35
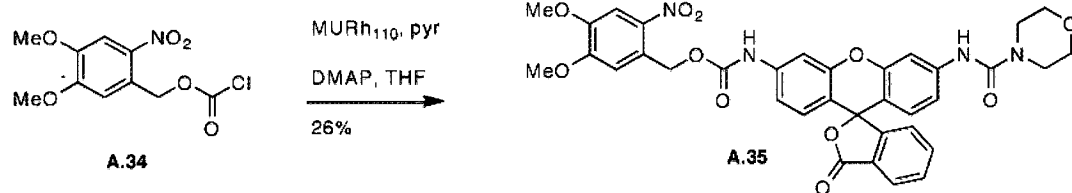
Figure A.1 Mechanism of ribonuclease internalization and cytotoxicity. Arrows below

indicate the methods that can be used to assay individual steps.

Reproduced from Turcotte *et al.* 2009.
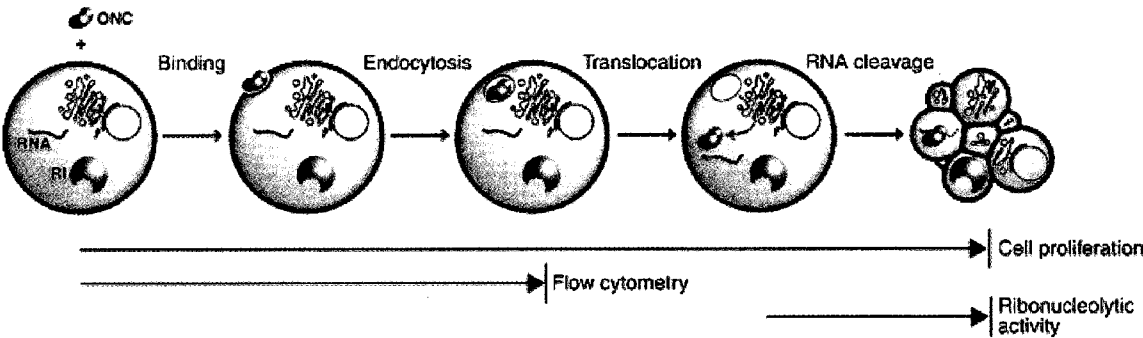
Figure A.2   Mechanism of fluorescence development in β-lactamase substrate. β-lactamase cleaves the β-lactam bond (shown in red) of a substrate that is conjugated to a ribonuclease (blue bean) upon entry into the cytoplasm. The generated amine initiates an elimination reaction to release free trimethyl lock phenoxide. The trimethyl lock undergoes lactonization to release the fluorophore rhodamine (green) that remains conjugated to a ribonuclease.

β-lactamase
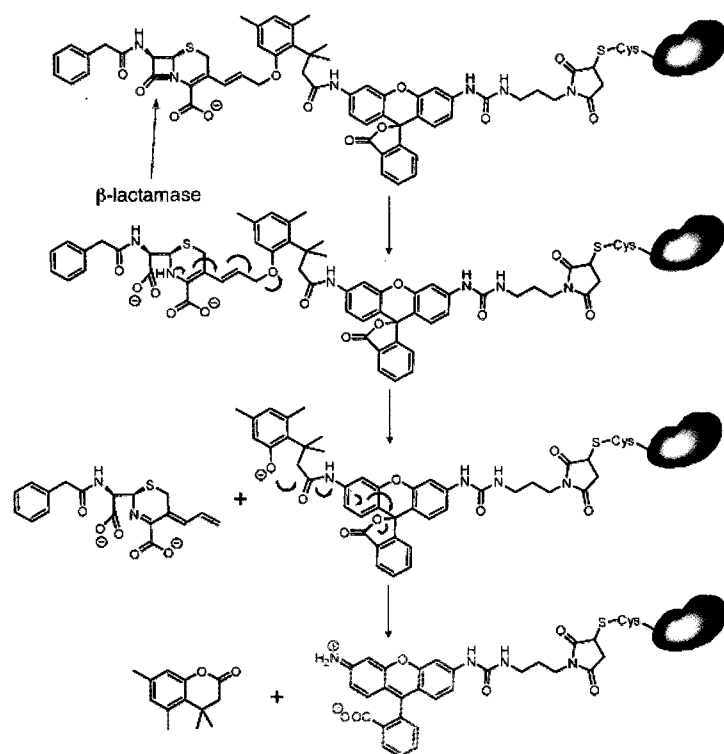
Figure A.3   Catalysis of reduction of **A.14** by NTR. Assays were performed in PBS

pH 7.4, containing **A.14** (0.03–27.2 μM), NADH (500 μM), and *E. coli*

NTR (10 nM). Reactions were initiated by the addition of NADH at $t = 90$

s. Inset: Michaelis–Menten plot. v_o, initial velocity; [E], enzyme

concentration.
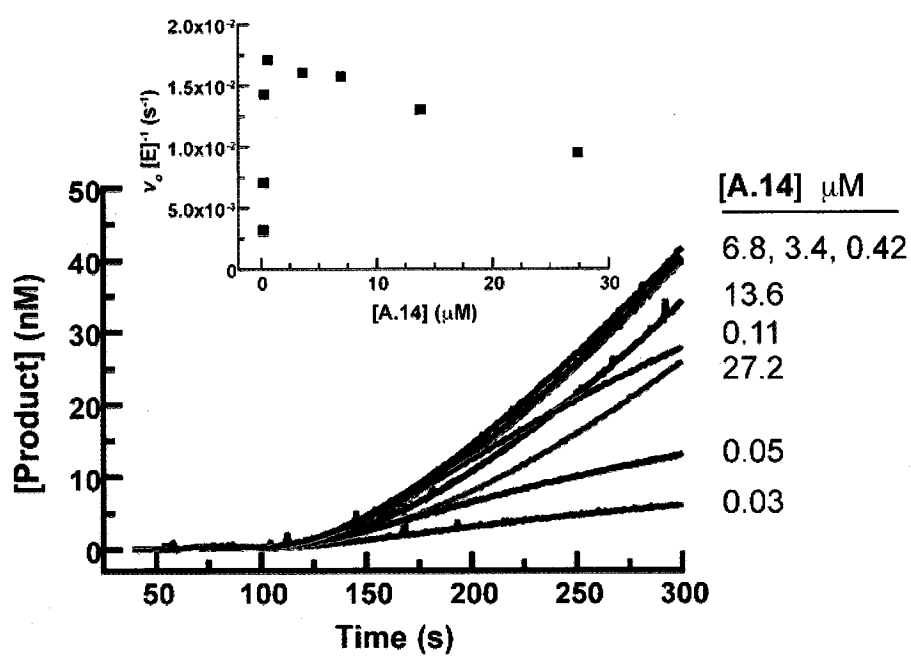
Figure A.4   Microscopy of ribonuclease internalization. HeLa cells were transfected with NTR and mCherry. Profluorophore **A.18**–RNase 1 P19C conjugate was added to the cells 24 hours after transfection. Images were captured 17 hours after addition of the conjugate. Cells were counterstained with Hoechst 33342 (blue); mCherry (red); unmasked conjugate (green). Scale bars are 20 μm. (A) Untransfected HeLa cells. (B) 5 μM conjugate added to untransfected HeLa cells. (C) HeLa cells transfected with NTR and mCherry. (D) 5 μM conjugate added to transfected cells.

Vehicle

A.18-RNase1 P19C (5 μM)
(rhodamine = green)

Untransfected

A

B

NTR transfected
(mCherry = red)

C

D
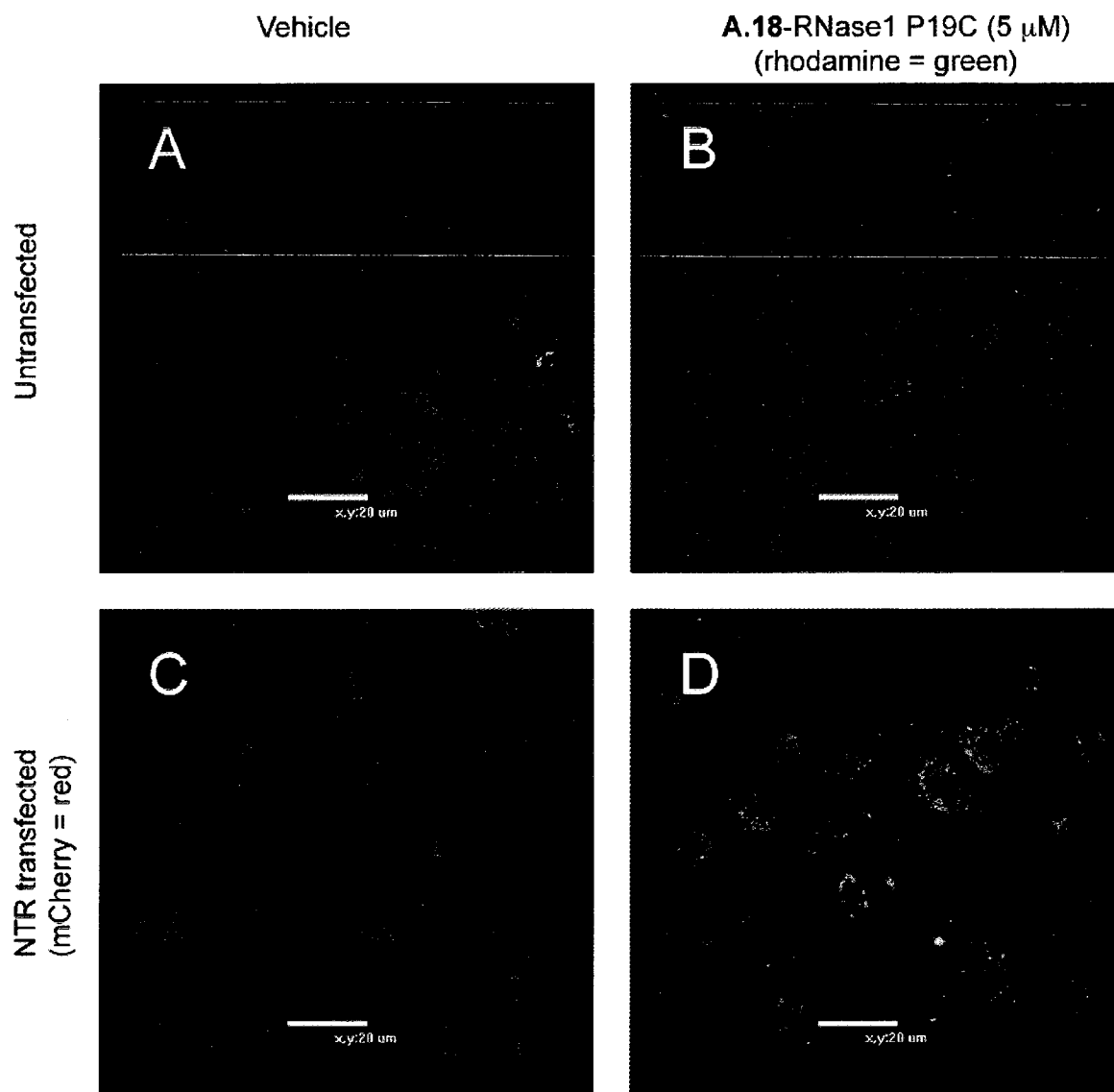
APPENDIX B

Photoactivatable Rhodamine

Collaboration with the laboratory of M.T. Zanni
Department of Chemistry, University of Wisconsin–Madison
Contribution: Design and synthesis of photoactivatable rhodamine **B.1**

B.1   Introduction

Amyloid diseases are a significant cause of morbidity and mortality in humans. The prevalence of Alzheimer's disease in people older than 70 years old in the United States is nearly 10% (Brookmeyer, *et al.*, 2011). Type 2 diabetes mellitus has a prevalence of approximately 24% in the same population and is the sixth leading cause of death in the United States (Danaei, *et al.*, 2009). Both of these diseases are strongly linked to a specific type of misfolded and aggregated protein called amyloid (Westermark, *et al.*, 2011).

Amyloid peptides and proteins are difficult to study due to numerous factors. Many of the amyloid-forming peptides are small peptide hormones containing little secondary structure (Westermark, *et al.*, 2011). Amyloid peptides interconvert among monomers, unfolded states, and multimeric states, which may be intracellular or extracellular, and soluble or insoluble (Strasfeld, *et al.*, 2009; Westermark, *et al.*, 2011). The exact structures of amyloids are elusive due to poorly organized secondary structure and transient protein–protein interactions.

While most of the toxicity of amyloids has been attributed to their soluble polymeric fibril form, some researchers believe that there is a soluble oligomeric state that forms pores in cell membranes (Westermark, *et al.*, 2011). The oligomeric states are poorly defined, and might range from trimers to octamers. The pores are believed to be donut-shaped, which allow ions to pass through the cell membrane, leading to cell death.

The laboratory of M.T. Zanni in the Department of Chemistry at the University of Wisconsin–Madison proposed a method to accurately assess the oligomeric states of amyloid pores using single-molecule fluorescence techniques. The method required a photoactivatable profluorophore to be conjugated to the amyloid protein monomers. The monomers would be allowed to form oligomeric structures in solution. Exposure of one oligomeric pore to a carefully titrated intensity of UV irradiation would activate a single profluorophore on one monomer. This event could be observed by single-molecule microscopy. Subsequently, the activated fluorophore would be photobleached. Photoactivation and photobleaching of the same oligomer would be repeated until no fluorescence is observed with activation. The number of iterations would indicate the number of monomers in each oligomeric pore complex.

B.2   Results and Discussion

B.2.1 Synthesis of B.1

The fluorophore maleimidourea rhodamine (Lavis, *et al.*, 2006a) was reacted with 4,5-dimethoxy-2-nitrobenzyl chloroformate with pyridine and catalytic *N,N*-dimethylaminopyridine to afford **B.1** in 22% isolated yield. This photoactivatable rhodamine was adapted from compound **A.35** (Scheme A.8, APPENDIX A), a molecule that was originally synthesized to be a nitroreductase substrate. We had concerns that **A.35** would be photocleavable, a property undesirable for a nitroreductase substrate.

When approached by the Zanni laboratory, we recognized the potential of this system to be applied to amyloid peptides.

B.2.2 Photoactivation of **B.1**

Compound **B.1** was spotted on a TLC plate and was eluted with 70% ethyl acetate in hexanes. The product spot (R_f = 0.2) absorbed short-wave UV light (254 nm) and did not fluoresce under long-wave UV light (365 nm). Exposure of the spot to short-wave UV light for 5 minutes converted the spot such that it fluoresced green under long-wave light. A fluorescent spot was not observed on a corresponding TLC plate that was kept in the dark for 5 minutes.

If **B.1** was spotted on a TLC plate and exposed to short-wave UV light for 5 minutes prior to elution with 70% ethyl acetate in hexanes, two spots became visible. A spot at R_f = 0.2 absorbed short-wave UV light and did not fluoresce under long-wave UV. A second spot, which remained on the baseline, emitted green fluorescence under long-wave UV light. The TLC mobility of the baseline spot was consistent with maleimidourea rhodamine, the expected product of photocleavage. This fluorescence provided evidence that **B.1** could be cleaved by UV light to generate a fluorescent molecule.

D.G. Ha of the Zanni laboratory quantified the photoactivation of **B.1** in solution by irradiating the sample with the middle of the 2 mW laser lines (408, 488, or 532 nm) for 20 minutes in 10 mM Tris HCl buffer (pH 7.5). The samples irradiated at 488 and 532 nm had an identical fluorescence emission spectrum as the non-irradiated sample (Figure B.1). There was a small amount of background fluorescence at 525 nm. Irradiation of **B.1**

at 408 nm resulted in a greater than 5-fold increase in the fluorescence intensity at 525 nm. The small amount of background fluorescence might be due to fluorescent impurities, such as maleimidourea rhodamine, and could be removed by HPLC purification or by photobleaching prior to assaying the amyloid proteins. If the background fluorescence were due to the presence of the carbamate linker in **B.1**, then a photoactivatable rhodamine containing an amide linker based on the trimethyl lock could be synthesized (discussed in CHAPTER 5).

Work is currently being done to conjugate **B.1** to amyloid proteins. These protein conjugates will be oligomerized and the number of monomers per oligomer will be counted by single-molecule fluorescence microscopy. These experiments could provide great insight into prevalent diseases like Alzheimer's and type 2 diabetes mellitus.

B.3   Experimental Section

B.3.1 General

Tetrahydrofuran (THF) was drawn from a Baker CYCLE-TAINER solvent-delivery system. All other reagents were from Aldrich Chemical (Milwaukee, WI) or Fisher Scientific (Hanover Park, IL), and were used without further purification. PBS contained (in 1.00 L) KCl (0.20 g), KH_2PO_4 (0.20 g), NaCl (8.0 g), and $Na_2HPO_4 \cdot 7H_2O$ (2.16 g) and had pH 7.4.

Thin-layer chromatography was performed by using aluminum-backed plates coated with silica gel containing F_{254} phosphor, and was visualized by UV illumination or

developed with ceric ammonium molybdate stain. Flash chromatography was performed on open columns with silica gel-60 (230–400 mesh).

NMR spectra were obtained with a Bruker DMX-400 Avance spectrometer at the National Magnetic Resonance Facility at Madison (NMRFAM). Mass spectrometry was performed with an Agilent mass spectrometer with electrospray ionization (ESI), a mass selective detector (MSD), and time of flight (TOF) mass analyzer at the Mass Spectrometry Facility in the Biotechnology Center, University of Wisconsin–Madison.

B.3.2 Synthesis of B.1

All steps in the following synthesis were conducted with minimal lighting and covered in aluminum foil when possible. Maleimidourea rhodamine (Lavis, *et al.*, 2006a) (50 mg, 0.10 mmol) was added to a flame dried, 50-mL round-bottom flask that had been flushed with Ar(g) and was dissolved in 5 mL of THF. 4,5-dimethoxy-2-nitrobenzyl chloroformate (55 mg, 0.20 mmol) was dissolved in 3 mL of dry THF and added to the reaction mixture, followed by pyridine (16 µL, 0.20 mmol) and dimethylaminopyridine (1 mg, 0.01 mmol). The reaction was stirred under Ar(g) and covered in foil for 40 h. Reaction progress was monitored by TLC (70% EtOAc in hexanes). Upon completion, the reaction mixture was transferred to a separatory funnel. 1 N HCl (50 mL) was added, and the resulting solution was extracted with EtOAc (2 × 50 mL). The organic phases were combined and were washed with 50 mL each of H_2O and saturated brine. The organic phase was dried over sodium sulfate and evaporated under reduced pressure. The residue was purified by silica gel chromatography (70% EtOAc in hexanes) to give a

white solid (16 mg; 22%). ^{1}H NMR (400 MHz, CDCl$_3$) δ: 7.99 (d, J = 7.4 Hz, 1H), 7.88 (s, 1H), 7.67–7.58 (m, 3H), 7.41 (s, 1H), 7.30 (s, 1H), 7.17–6.95 (m, 5H), 6.69–6.62 (m, 3H), 6.54 (d, J = 8.5 Hz, 1H), 5.76 (t, J = 6.1 Hz, 1H), 5.55 (s, 2H), 3.96–3.88 (m, 6H), 3.56 (t, J = 6.2 Hz, 2H), 3.23–3.14 (m, 2H), 1.82–1.75 (m, 2H) ppm. ^{13}C NMR (100 MHz, CDCl$_3$) δ: 171.2, 170.6, 155.4, 153.7, 153.2, 153.1, 151.8, 151.5, 148.4, 141.8, 140.3, 139.9, 135.7, 134.3, 130.1, 128.8, 128.3, 127.3, 126.4, 125.2, 124.3, 115.3, 114.6, 113.4, 111.8, 110.8, 108.3, 107.0, 106.6, 84.3, 64.2, 56.7, 56.5, 37.2, 35.3, 29.1 ppm. HRMS (ESI): m/z 750.2041 [M+H]$^+$ ([C$_{38}$H$_{32}$N$_5$O$_{12}$]$^+$ = 750.2047).
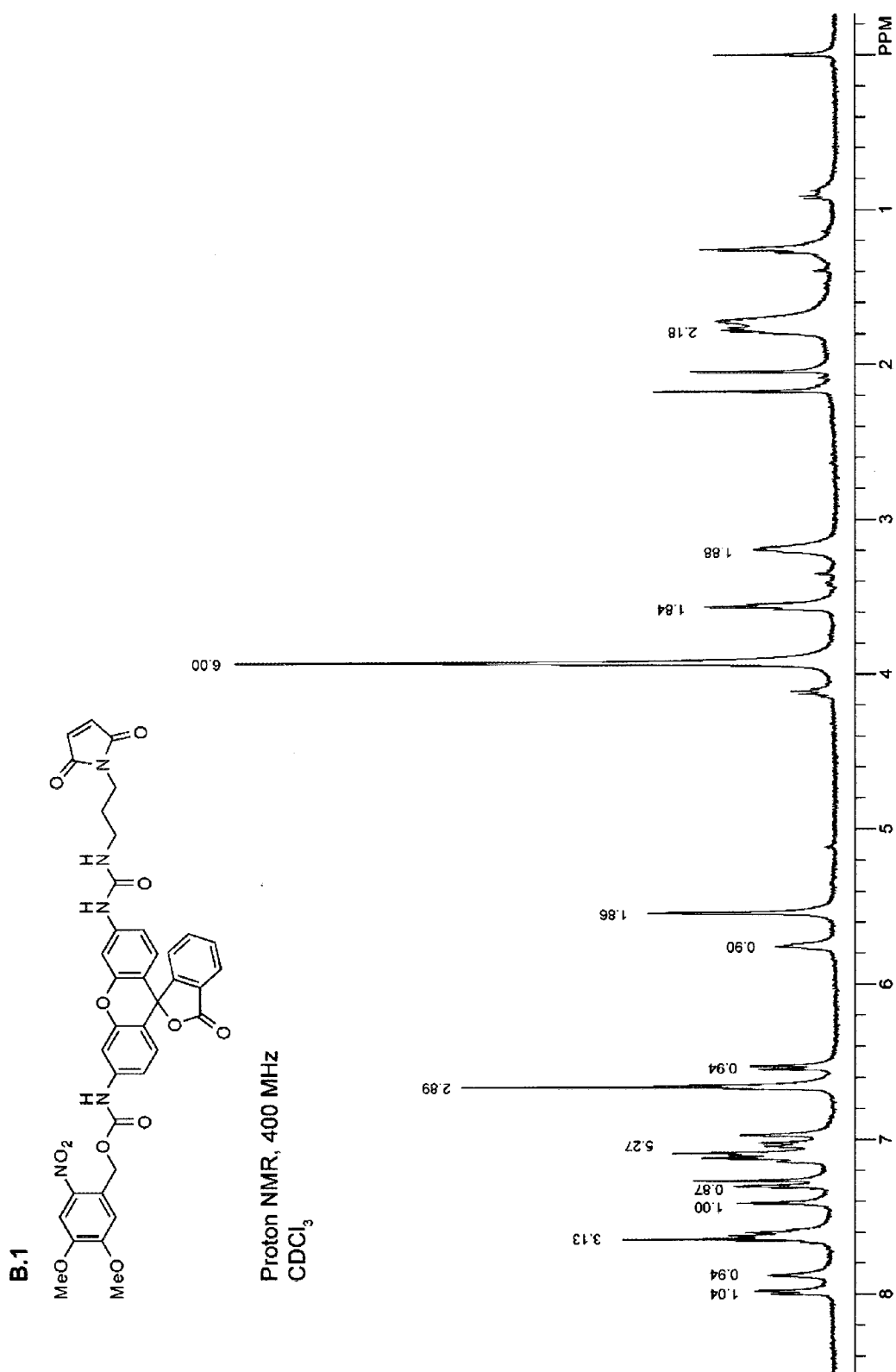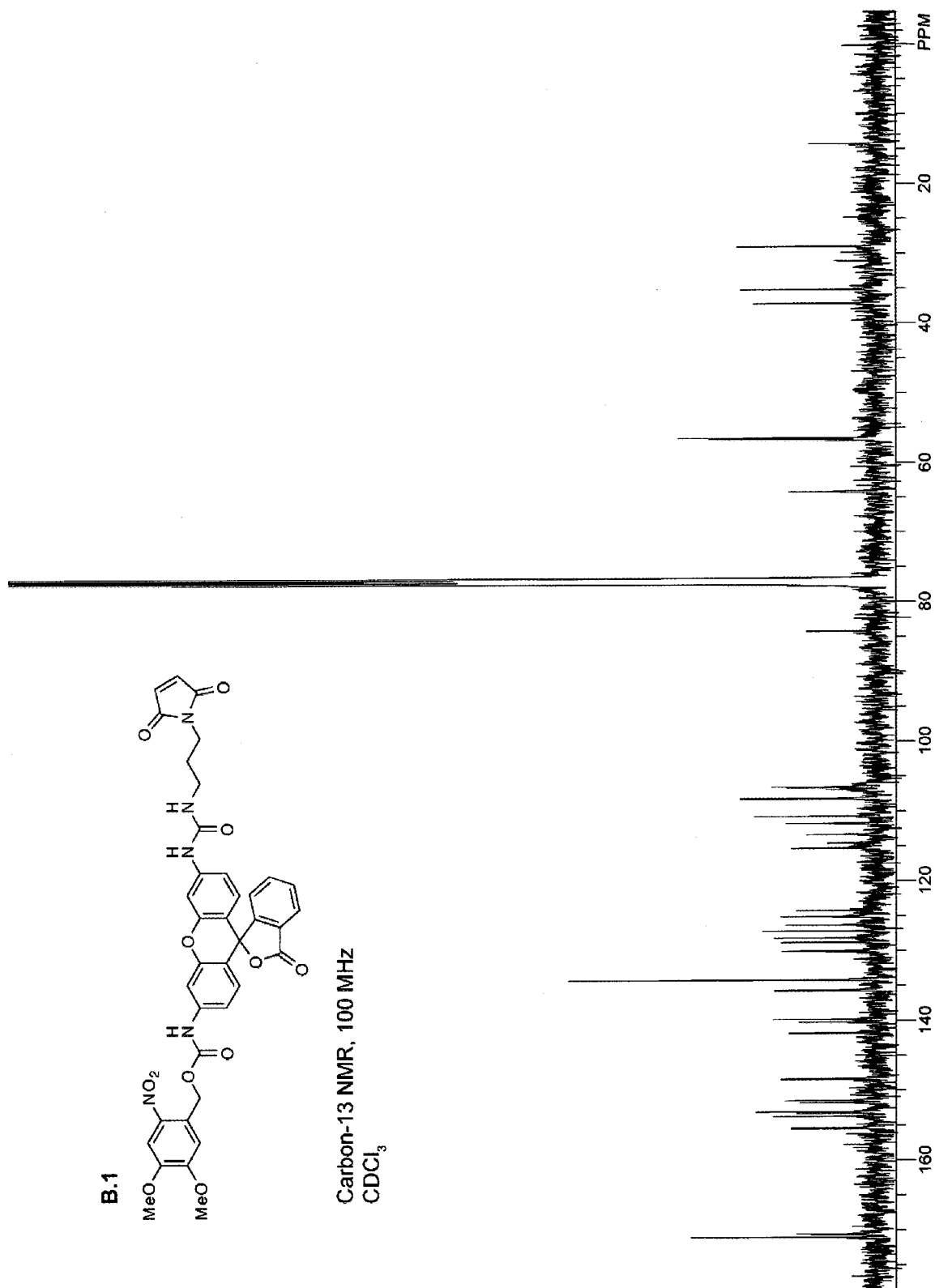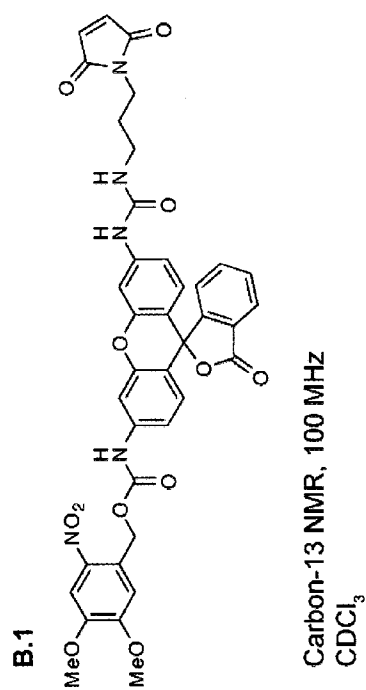
B.1

Proton NMR, 400 MHz
CDCl$_3$

B.1

Carbon-13 NMR, 100 MHz
CDCl$_3$

Acknowledgments

Scheme B.1   Synthesis of photoactivatable rhodamine fluorophore **B.1**

B.1
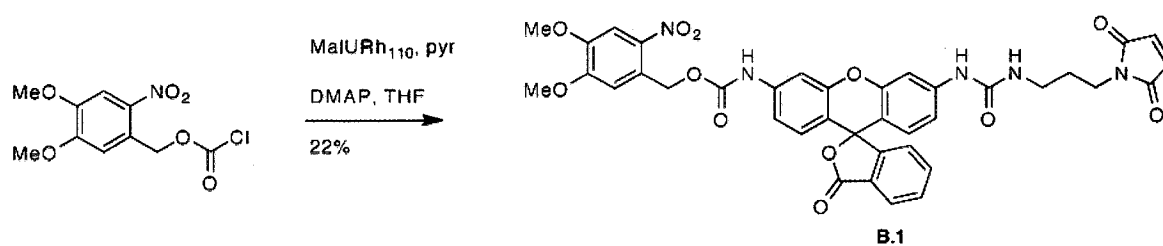
Figure B.1   Fluorescence emission spectra of **B.1** photoactivation. **B.1** was irradiated

with the middle of the 2 mW laser lines at 405, 488 or 532 nm for 20

minutes in 10 mM Tris buffer, pH 7.5. The fluorescence emission spectra

were measured with excitation at 488 nm. Control, sample was placed in

the dark for 20 minutes. Figure adapted from data collected by D. G. Ha in

the laboratory of M. T. Zanni.
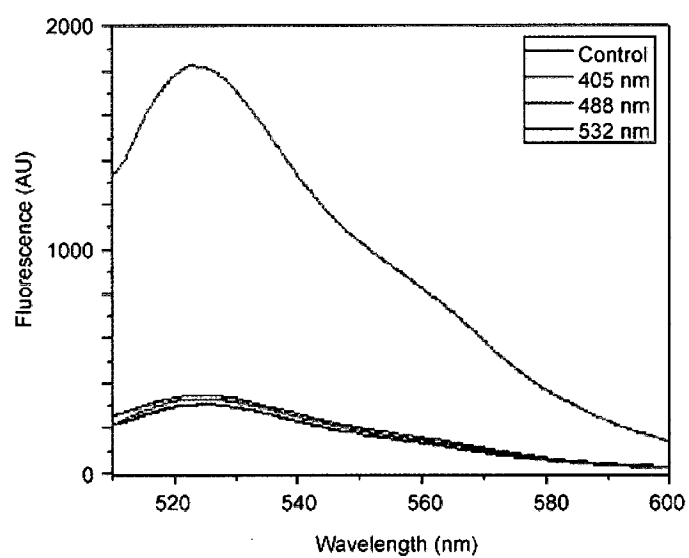
APPENDIX C

Blue-Shifted Fluorogenic Esterase Substrate

to Monitor Ribonuclease Endocytosis

C.1 Introduction

As described in Appendix A, some pancreatic-type ribonuclease variants are selectively toxic to cancerous cells. The mechanism of cytotoxicity is currently under investigation, but is believed to occur as shown in Figure A.1 (Turcotte, *et al.*, 2009). In order to be cytotoxic, a ribonuclease must first be internalized by endocytosis (Haigis and Raines, 2003); however, the mechanism of endocytosis may vary for different ribonuclease homologs, such as bovine RNase A, human RNase 1, and amphibian Onconase (Chao and Raines, 2011). Moreover, cell-penetrating peptides may be internalized by additional mechanisms, that may include non-endocytic mechanisms.

Lavis *et al.* developed a profluorophore (**C.1**) that could track the endocytosis of ribonucleases (Lavis, *et al.*, 2006a). This profluorophore, a trimethyl lock-based esterase substrate that contained a maleimide handle for conjugation to a free cysteine ribonuclease variant, became fluorescent upon exposure to non-specific esterases in endosomes. Fluorescence generation could be monitored visually, by confocal microscopy, or quantitatively, by flow cytometry. Due to the numerous endocytic pathways, the exact mechanism of ribonuclease internalization could not be determined. A second profluorophore, differing in wavelength than rhodamine (**C.1**), would be necessary to perform colocalization experiments of ribonuclease with protein markers of specific endosomal pathways.

A blue-shifted fluorophore (**C.2**), incorporating the same esterase-activated trimethyl lock as **C.1** had been synthesized previously (Lavis, *et al.*, 2006b). The fluorescence

emission wavelengths of aminomethyl coumarin underwent a hypsochromic shift upon acylation of the amine with the trimethyl lock. Aminomethyl coumarin had comparable fluorescence intensity to the rhodamine derivative used to track ribonuclease endocytosis. One caveat was that profluorophore **C.2** did not have a maleimide handle for conjugation to ribonuclease.

Profluorophore **C.7** was designed to be a derivative of **C.2** that contained a maleimide. The goal was to perform experiments in which one biomolecule was labeled with **C.7** and another type was labeled with **C.1** to look for colocalization of the two fluorophores in the same endosomes. For example, ribonucleases could be tested against cell penetrating peptides, or other endocytic markers such as transferrin and cholera toxin. Perhaps insights into the specific endosomal pathway taken by ribonucleases could be gained. The synthesis, spectroscopic properties, esterase kinetics, and *in cellulo* endocytosis of a blue-shifted profluorophore are described herein.

C.2   Results and Discussion

C.2.1 Synthesis of Soluble Blue-Shifted Esterase Substrates

Modification of coumarin fluorophores may result in a shift in the absorbance or fluorescence spectra. Therefore, two soluble derivatives, **C.8** and **C.9** were synthesized to accurately determine the effects of adding a triazole moiety to the fluorogenic esterase substrate that had been previously developed, **C.2** (Lavis, *et al.*, 2006b). **C.3** was synthesized following the methods of Cürten *et al.*, and van Berkel *et al.* (Cürten, *et al.*,

2005; van Berkel, *et al.*, 2009). Conversion of trimethyl lock **C.4** to its acid chloride using Ghosez's reagent followed by the addition of **C.3** and pyridine yielded **C.5**. Both **C.3** and **C.5** underwent azide–alkyne cylcoaddition reactions with propargyl alcohol to yield water soluble molecules **C.8** and **C.9**, respectively. **C.9** was expected to be hydrolyzed by non-specific esterases to generate **C.8**, with a concomitant shift in fluorescence wavelengths.

C.2.2 Absorbance and Fluorescence Spectra

Esterase substrate **C.9** displayed a hypsochromic shift of approximately 50 nm in the maximum wavelength of fluorescence relative to its presumed product, **C.8**. The difference in the absorbance wavelength maxima between the two compounds was much less, only 20 nm. Both shifts would provide opportunities to image one compound in the presence of the other using microscope optical filter sets.

The extinction coefficient and quantum yield of **C.8** were larger than **C.9** ($\varepsilon = 31,200$ vs. $26,100$ M^{-1} cm^{-1}; $\Phi = 0.50$ vs. 0.13 respectively; Figure C.2). The difference in extinction coefficient and quantum yield was unexpected because azides **C.3** and **C.5** had similar fluorescence intensities. The fluorescence intensities of triazoles **C.8** and **C.9** would be beneficial for imaging because the product of the profluorophore would have greater fluorescence intensity. In fact, the fluorescence intensity of **C.8** was similar to that of morpholinourea rhodamine, a substrate used to image ribonuclease endocytosis.

C.2.3 Esterase-Mediated Hydrolysis of C.9

C.9 was assayed for its ability to be converted to **C.8** by esterase-catalyzed

hydrolysis. It was presumed that hydrolysis of the acetyl ester of **C.9** would release the

free phenoxide of the trimethyl lock, leading to rapid lactonization with concomitant

release of fluorescent **C.8** (Amsberry and Borchardt, 1990; Lavis, *et al.*, 2006b). Indeed,

C.9 was a substrate for a non-specific esterase, porcine liver esterase (PLE; Figure C.3).

The K_M of 5.1 µM and k_{cat}/K_M of 1.5×10^5 $M^{-1}s^{-1}$ were consistent with the published

values for **C.2** ($K_M = 8.2$ µM; $k_{cat}/K_M = 2.5 \times 10^5$ $M^{-1}s^{-1}$) (Lavis, *et al.*, 2006b).

Importantly, the rate of catalysis was also consistent with that of **C.1**, a substrate known

to be a marker of endocytosis of ribonucleases (Lavis, *et al.*, 2006a).

C.2.4 Synthesis of Maleimide C.7 Conjugated to Ribonuclease

C.7 was synthesized by a copper-catalyzed azide-alkyne cycloaddtion between **C.5**

and maleimide **C.6** (Royer, *et al.*, 2008). This "click" reaction proceeded in 60% yield.

The maleimide blue-shifted profluorophore **C.7** was conjugated to P19C RNase 1, a

ribonuclease containing a free cysteine. Additionally, **C.1** was conjugated to a second

sample of P19C RNase 1 to generate a green profluorophore conjugate. The degree of

RNase labeled was approximately 70% for both **C.1** and **C.7**. The fluorescence spectra of

the conjugates and the conjugates unmasked by PLE were similar to those shown in

Figure C.2.

C.2.5 Microscopy of Ribonuclease 1 Conjugates

With both profluorophores in hand, the spectral wavelengths were determined to be compatible with confocal microscopy optical filter sets. The large bathochromic shift displayed by **C.7**, upon esterase-mediated unmasking, provided a convenient means to specifically image the emission of the unmasked fluorophore compared to **C.7**. Additionally, the unmasked fluorophore could be excited more efficiently than **C.7** presenting an even greater specificity between the two. The unmasked **C.7** and unmasked **C.1** had a large difference in excitation and emission spectra and could be imaged independently with no bleed-through between fluorescence channels. DRAQ5, a nuclear stain with far-red emission, was chosen for this experiment. Typically used nuclear stains, for example DAPI and Hoechst 33342, have overlapping spectra with unmasked **C.7**.

RNase 1 conjugated to **C.1** or **C.7** was applied to the media of HeLa and was allowed to be endocytosed for 3 hours at 37 °C. As expected, endocytosis of RNase 1 conjugated to **C.1** could be detected by confocal microscopy (Figure C.4B) (Lavis, *et al.*, 2006a); however, **C.7** endocytosis could not be observed (Figure C.4A). Multiple combinations of filter sets were selected to attempt to improve the signal to background fluorescence. Both band-pass and long-pass filters were tried, but neither resulted in a fluorescence signal above background.

The endocytosis assay was repeated using an epifluorescence microscope to increase the amount of emitted light that would reach the detector. In HeLa cells to which no conjugate was added, a bright perinuclear staining pattern was evident (Figure C.4C).

The same staining pattern was observed in cells where RNase 1 **C.7** conjugate was added (Figure C.4D), signifying that the background fluorescence of HeLa cells was higher than the increase in fluorescence of **C.7** upon endocytosis. Fluorescence of RNase 1 **C.1** conjugate was visible as a punctate staining pattern by epifluorescence (Figure C.4E). Although **C.1** and **C.7** had similar fluorescence intensities, only **C.1** could be visualized *in cellulo*. It was known that autofluorescence (fluorescence due to cellular cofactors and biomolecules) should be higher at lower wavelengths. Unfortunately, the autofluorescence was so high that it obscured any fluorescence signals produced by **C.7**.

C.3 Experimental Section

C.3.1 General

Dichloromethane (DCM), tetrahydrofuran (THF), and dimethyl formamide (DMF) were drawn from a Baker CYCLE-TAINER solvent-delivery system. All other reagents were from Aldrich Chemical (Milwaukee, WI) or Fisher Scientific (Hanover Park, IL), and were used without further purification. PBS contained (in 1.00 L) KCl (0.20 g), KH_2PO_4 (0.20 g), NaCl (8.0 g), and $Na_2HPO_4 \cdot 7H_2O$ (2.16 g) and had pH 7.4.

Thin-layer chromatography was performed by using aluminum-backed plates coated with silica gel containing F_{254} phosphor, and was visualized by UV illumination or developed with ceric ammonium molybdate stain. Flash chromatography was performed on open columns with silica gel-60 (230–400 mesh).

NMR spectra were obtained with a Bruker DMX-400 Avance spectrometer at the National Magnetic Resonance Facility at Madison (NMRFAM). Mass spectrometry was performed using a Micromass LCT (electrospray ionization, ESI) mass spectrometer at the Mass Spectrometry Center in the Department of Chemistry.

C.3.2 Synthesis of C.5

C.3 was synthesized as described (Cürten, *et al.*, 2005; van Berkel, *et al.*, 2009). **C.5** (Amsberry and Borchardt, 1990) (500 mg, 1.89 mmol) was dissolved in 10 mL dry DCM in a flame-dried 100 mL round bottom flask that had been flushed with Ar(g). The flask was cooled to 0 °C in an ice bath and 1-chloro-N,N,2-trimethyl-1-propenylamine (275 μL, 2.08 mmol) was added in 1 mL dry DCM. The reaction was stirred at 0 °C for 2 hours. Next, **C.3** (408 mg, 1.89 mmol) and pyridine (305 μL, 3.78 mmol) were dissolved in 10 mL anhydrous THF and were added to the reaction mixture. The reaction was allowed to warm to room temperature, and was stirred overnight, under Ar(g), and covered in foil. Reaction progress was monitored by TLC (50% EtOAc in hexanes). Upon completion, the solvent was evaporated under reduced pressure and the residue was purified by silica gel chromatography (50% EtOAc in hexanes) to produce a white, crystalline solid (633 mg; 72%). ^{1}H NMR (400 MHz, CDCl$_3$) δ: 7.82 (bs, 1H), 7.36–7.29 (m, 2H), 7.17 (dd, J = 8.6, 2.0 Hz, 1H), 6.75 (s, 1H), 6.64 (s, 1H), 6.37 (s, 1H), 4.49 (s, 2H), 2.56 (s, 2H), 2.43–2.35 (m, 6H), 2.24 (s, 3H), 1.70 (s, 6H) ppm. ^{13}C NMR (100 MHz, CDCl$_3$) δ: 172.7, 170.2, 160.7, 154.5, 150.2, 148.5, 142.2, 139.1, 137.4, 133.2,

132.9, 124.1, 123.5, 115.6, 112.9, 112.5, 106.9, 51.1, 50.7, 40.6, 32.3, 25.6, 22.1, 20.3

ppm. HRMS (ESI): m/z 485.1810 [M+Na]$^+$ ([C$_{25}$H$_{26}$N$_4$O$_5$Na]$^+$ = 485.1796).

C.3.3 Synthesis of C.7

C.5 (50 mg, 0.11 mmol) was added to a scintillation vial and dissolved in 2:1

THF/H$_2$O (3 mL). **C.6** (Royer, *et al.*, 2008) (15 mg, 0.11 mmol) was added, followed by

copper sulfate pentahydrate (2.7 mg, 0.011 mmol) and sodium ascorbate (9.0 mg, 0.044

mmol). The reaction was warmed to 40 °C and stirred for 24 hours covered in foil.

Reaction progress was followed by TLC (2% MeOH in DCM). Upon completion, the

reaction mixture was partitioned between EtOAc and H$_2$O (25 mL each) in a separatory

funnel. The organic phase was collected and the aqueous phase was extracted with

additional EtOAc (20 mL). The combined organic phases were washed with saturated

brine (50 mL), and dried over sodium sulfate. The suspension was filtered and the filtrate

was evaporated under reduced pressure. The crude product was purified by silica gel

chromatography (5% MeOH in DCM), then by a second column (1–3% MeOH in DCM).

The combined fractions were evaporated to yield a white solid (39 mg; 60%). ^{1}H NMR

(400 MHz, CD$_2$Cl$_2$) δ: 7.61 (bs, 1H), 7.47 (d, J = 1.9 Hz, 1H), 7.40 (d, J = 8.7 Hz, 1H),

6.97 (dd, J = 8.8, 2.1 Hz, 1H), 6.75 (s, 1H), 6.72 (s, 2H), 6.67 (s, 1H), 5.78 (s, 1H), 5.60

(s, 2H), 4.78 (s, 2H), 2.54 (s, 2H), 2.39 (s, 3H), 2.37 (s, 3H), 2.23 (s, 3H), 1.66 (s, 6H)

ppm. ^{13}C NMR (100 MHz, CD$_2$Cl$_2$) δ: 173.2, 170.7, 160.5, 155.1, 150.8, 148.2, 144.2,

143.1, 139.7, 138.0, 134.9, 133.5, 133.4, 124.4, 124.1, 124.0, 115.9, 115.8, 113.4, 107.2,

107.1, 51.6, 50.6, 41.0, 33.2, 32.6, 25.9, 23.4, 20.4 ppm. HRMS (ESI): *m/z* 620.2141

[M+Na]$^+$ ([C$_{32}$H$_{31}$N$_5$O$_7$Na]$^+$ = 620.2116).

C.3.4 Synthesis of C.8

C.3 (Cürten, *et al.*, 2005; van Berkel, *et al.*, 2009) (100 mg, 0.46 mmol) and

propargyl alcohol (27 µL, 0.46 mmol) were dissolved in 2:1 THF/H$_2$O (6 mL) in a

scintillation vial. Copper sulfate pentahydrate (11.5 mg, 0.040 mmol), and sodium

ascorbate (36.5 mg, 0.184 mmol) were added and the reaction was warmed to 40 °C. The

reaction was stirred for 48 hours covered in foil. A small amount of yellow precipitate

formed during the course of the reaction. Reaction progress was monitored by TLC (10%

MeOH in DCM). Upon completion, the solvents were evaporated under reduced pressure

and the residue was purified by silica gel chromatography (5–10% MeOH in DCM) to

produce a yellow solid (79 mg; 63%). ^{1}H NMR (400 MHz, DMSO-d6) δ: 8.10 (s, 1H),

7.52 (d, *J* = 8.7 Hz, 1H), 6.58 (d, *J* = 8.6 Hz, 1H), 6.44 (s, 1H), 6.27 (bs, 2H), 5.80 (s,

2H), 5.30 (s, 1H), 5.23 (t, *J* = 5.9 Hz, 1H), 4.54 (d, *J* = 5.4 Hz, 2H) ppm. ^{13}C NMR (100

MHz, DMSO-d6) δ: 160.5, 155.8, 153.6, 151.0, 148.6, 125.7, 123.9, 111.4, 106.1, 105.8,

98.7, 55.1, 49.1 ppm. HRMS (ESI): *m/z* 567.723 [2M+Na]$^+$ ([C$_{26}$H$_{24}$N$_8$O$_6$Na]$^+$ =

567.1712).

C.3.5 Synthesis of C.9

C.5 (50 mg, 0.11 mmol) was added to a scintillation vial and was dissolved in 2:1

THF/H$_2$O (3 mL). Propargyl alcohol (6.4 μL, 0.11 mmol) was added followed by copper

sulfate pentahydrate (2.7 mg, 0.011 mmol) and sodium ascorbate (9.0 mg, 0.044 mmol).

The reaction was warmed to 40 °C and was stirred for 24 hours covered in foil. Reaction

progress was monitored by TLC (5% MeOH in DCM). Upon completion, the reaction

mixture was partitioned between EtOAc (20 mL) and H$_2$O (20 mL) with a small amount

of saturated brine added to disperse the emulsion that had formed. The organic phase was

collected. The aqueous phase was extracted with additional EtOAc (20 mL) and the

combined organic phases were washed with saturate brine (50 mL). The organic phase

was dried over sodium sulfate, filtered and the filtrate was evaporated under reduced

pressure. The crude product was purified by silica gel chromatography (5% MeOH in

DCM) to produce a white solid (42 mg; 75%). ^{1}H NMR (400 MHz, CDCl$_3$) δ: 7.76 (bs,

1H), 7.59 (s, 1H), 7.41–7.37 (m, 2H), 7.08 (dd, J = 8.8, 1.9 Hz, 1H), 6.75 (s, 1H), 6.64 (s,

1H), 5.85 (s, 1H), 5.63 (s, 2H), 4.82 (s, 2H), 2.53 (s, 2H), 2.41 (s, 3H), 2.38 (s, 3H), 2.24

(s, 3H), 1.70 (s, 6H) ppm. ^{13}C NMR (100 MHz, CDCl$_3$) δ: 171.5, 170.3, 160.3, 154.7,

150.3, 147.8, 142.6, 140.3, 139.3, 137.7, 133.4, 132.9, 124.0, 123.6, 122.3, 115.9, 113.1,

112.5, 107.2, 58.8, 51.3, 50.3, 40.7, 32.4, 25.7, 22.1, 20.3 ppm. HRMS (ESI): *m/z*

541.2064 [M+Na]$^+$ ([C$_{28}$H$_{30}$N$_4$O$_6$Na]$^+$ = 541.2058).

C.3.6 Spectroscopy Methods

Absorption measurements were made with a Cary model 50 spectrometer from Varian. Fluorometric measurements were with a QuantaMaster1 photon-counting spectrofluorometer from Photon Technology International, equipped with sample stirring. Stock solutions of **C.8**, **C.9**, and morpholinourea rhodamine (Lavis, *et al.*, 2006a) were made in DMSO and were diluted such that the final concentration of DMSO did not exceed 0.5% v/v for assays. Spectra of compounds were measured in PBS at a concentration of 156 nM.

Quantum yields of **C.8** and **C.9** were determined by obtaining their fluorescence emission spectra for dilute samples (A ≈ 0.05) in PBS. Aminomethyl coumarin (AMC), having a known quantum yield of 0.75 in methanol (Lavis and Raines, 2008) was diluted in methanol to match the absorbance of the unknown compound. The areas under the fluorescence emission spectra were calculated and compared for the unknown and AMC using the following equation: $\Phi_{sample} = \Phi_{standard}(\int F_{em, sample}/\int F_{em, standard})$

PLE (163 kDa) was from Sigma Chemical (St. Louis, MO; product number E2884) as a suspension in $(NH_4)_2SO_4$ (3.2 M), and was diluted to appropriate concentrations in PBS before use. Kinetic parameters were calculated with the programs Microsoft Excel 2008 and GraphPad Prism 4.

C.3.7 P19C RNase 1 Purification and Labeling

P19C RNase 1 was purified and labeled as described previously (Johnson, *et al.*, 2007) with the following modifications: A plasmid encoding P19C RNase 1 was obtained from R.J. Johnson. The labeling reactions were performed with a ten-fold excess of **C.7** or **C.1** in PBS containing 10% dimethyl formamide. Protein concentration was determined using a bicinchoninic assay. Degree of labeling was determined by unmasking a known amount of conjugate with excess PLE, and calculating the concentration by fluorescence spectroscopy compared to a standard curve of **C.8** or morpholinourea rhodamine. In addition, labeling was confirmed by matrix-assisted laser desorption ionization (MALDI) mass spectrometry (MS).

C.3.8 Mammalian Cell Culture

HeLa cells were from the American Type Culture Collection (Manassas, VA) and were grown in DMEM containing FBS (10% v/v), penicillin (100 units/mL) and streptomycin (100 µg/mL). Media and supplements were from Invitrogen (Carlsbad, CA). Cells were cultured at 37 °C in a humidified incubator containing CO_2(g) (5% v/v).

C.3.9 Microscopy

The internalization of **C.7**–P19C RNase 1 or **C.1**–P19C RNase 1 conjugates were monitored in live HeLa cells by confocal microscopy on a Becton Dickinson Pathway 855 laser scanning confocal microscope. Excitation was provided by two mercury arc lamps. Excitation light was passed through a 10-nm band pass for excitation centered at

380 nm, and emission light was passed through a 435 nm long-pass or a 24-nm band-pass filter centered at 470 nm. Excitation light was passed through a 10-nm band pass for excitation centered at 488 nm, and emission light was passed through a 30-nm band-pass centered at 520 nm. Excitation light was passed through a 20-nm band-pass for excitation centered at 635 nm and emission light was passed through a 75-nm band pass c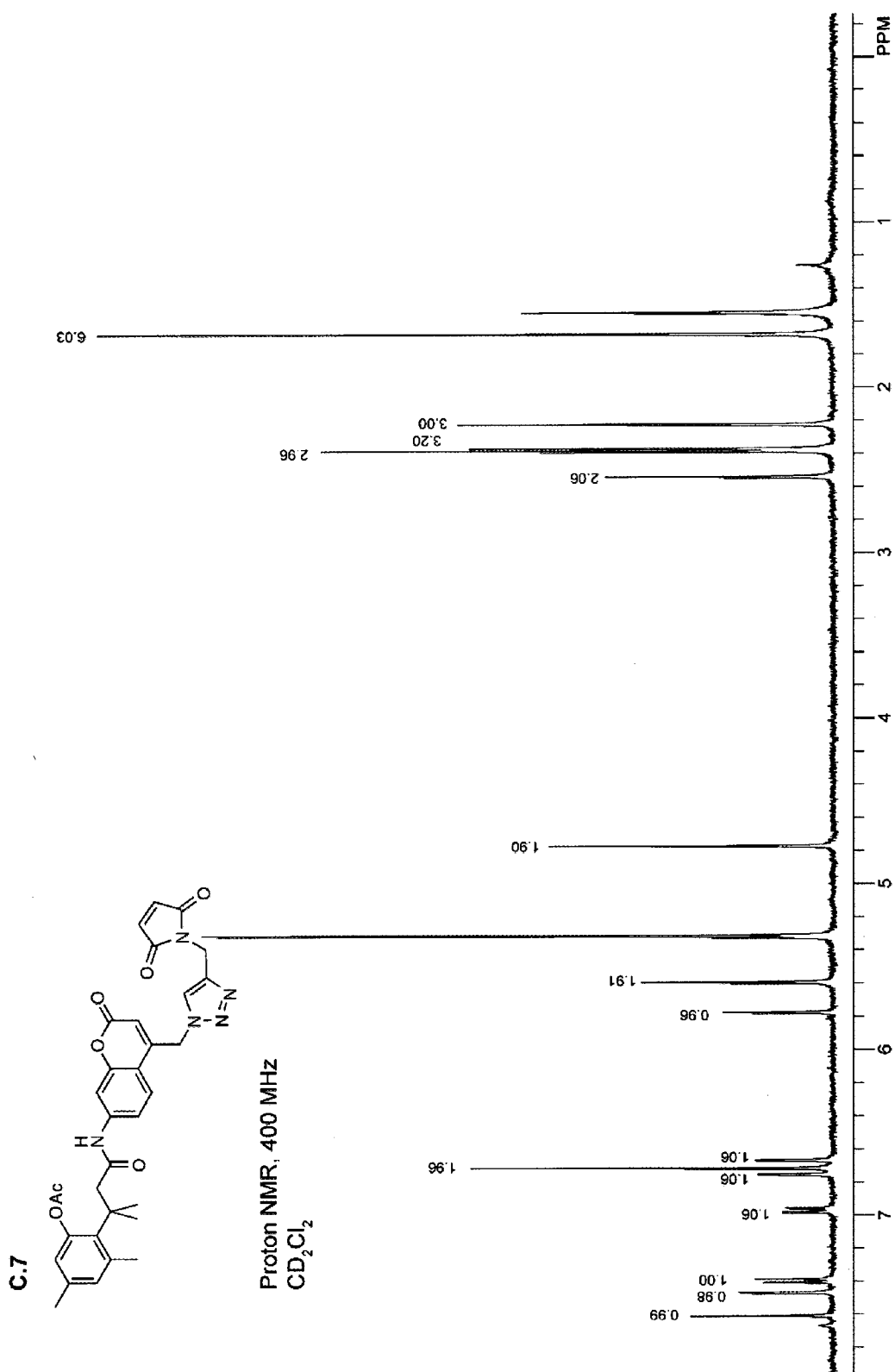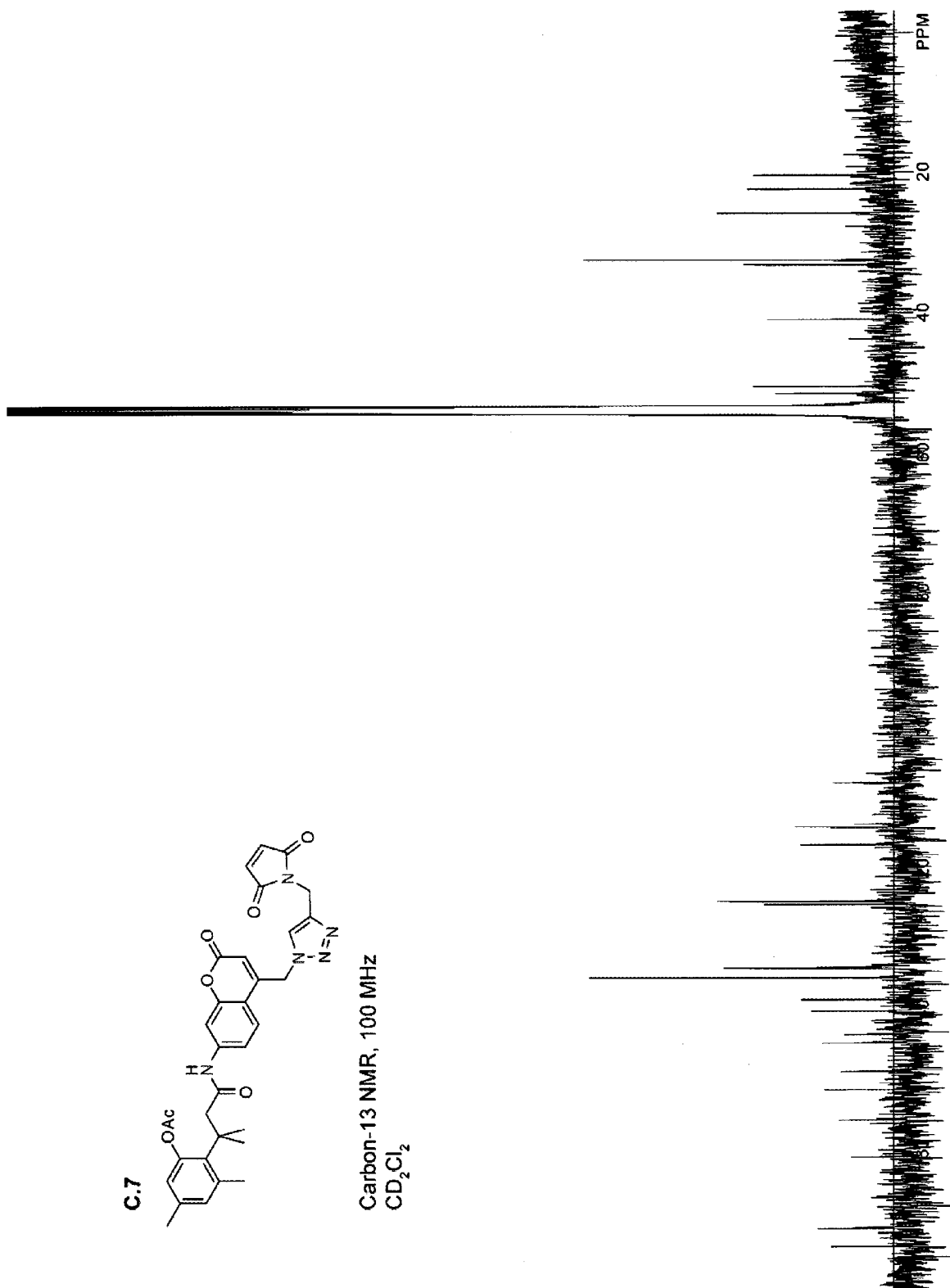entered at 700 nm. Alternatively, images were obtained by epifluorescence microscopy (Nikon SMZ1500). HeLa cells were plated on 8-well microscope slides at a density of 1×10^4 cells/well in 200 μL DMEM 24 hours prior to addition of conjugates. The **C.7**–P19C RNase 1 or **C.1**–P19C RNase 1 conjugate was added to the cells in fresh media at a concentration of 20 μM. Internalization was imaged after incubation at 37 °C for 3 hours. Nuclear counterstaining was performed for the last 5 minutes of incubation using DRAQ5 (Biostatus limited) at a concentration of 5 μM. Cells were washed with fresh media prior to imaging (3 × 100 μL).

C.5

Proton NMR, 400 MHz
CDCl$_3$

C.5

Carbon-13 NMR, 100 MHz
CDCl$_3$

C.7

Proton NMR, 400 MHz
CD$_2$Cl$_2$

PPM

6.03

3.00
3.20
2.96
2.06

1.90

1.91
0.96

1.96

1.06
1.06
1.06

1.00
0.98
0.99

C.7

Carbon-13 NMR, 100 MHz
CD$_2$Cl$_2$

PPM

C.8
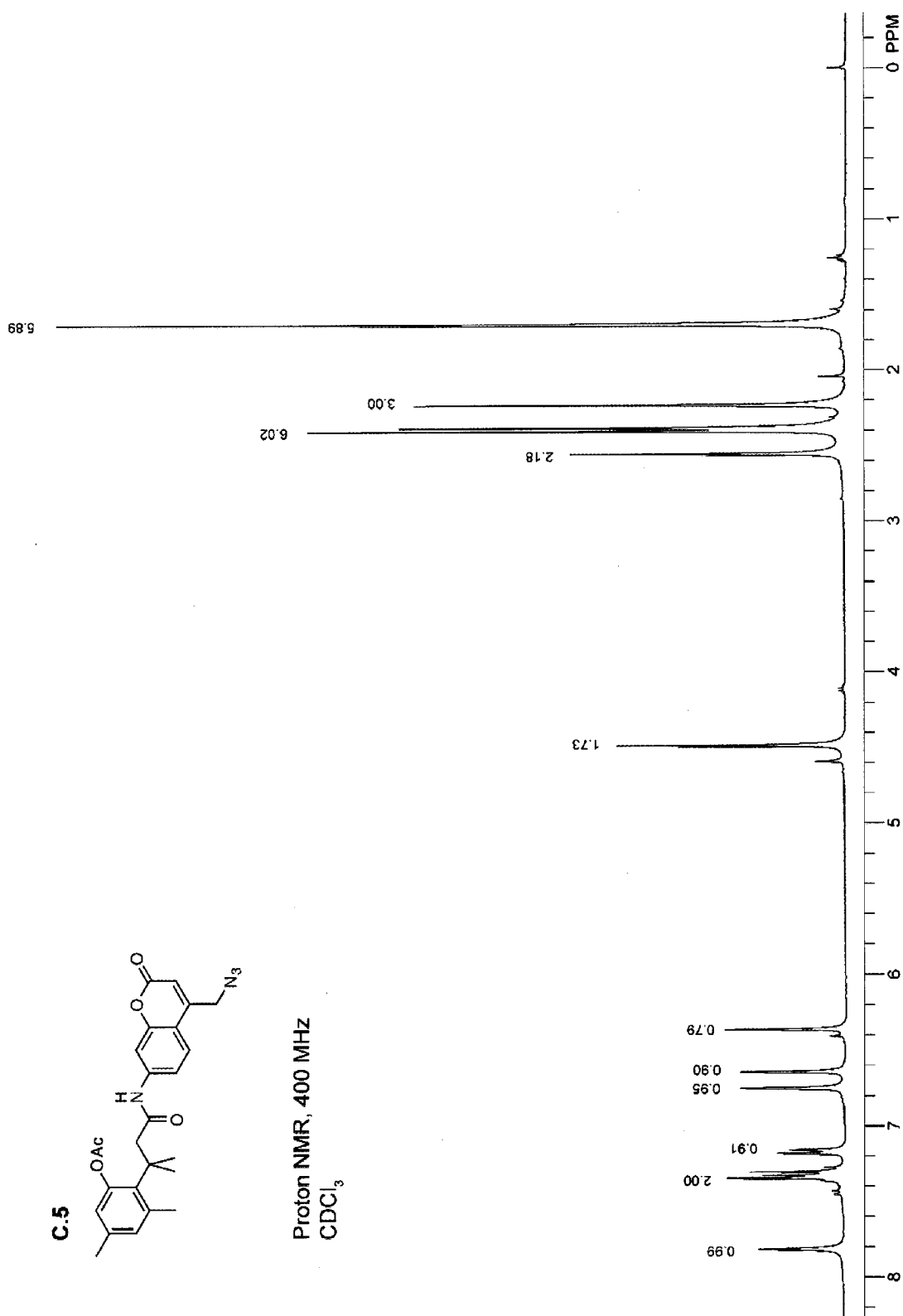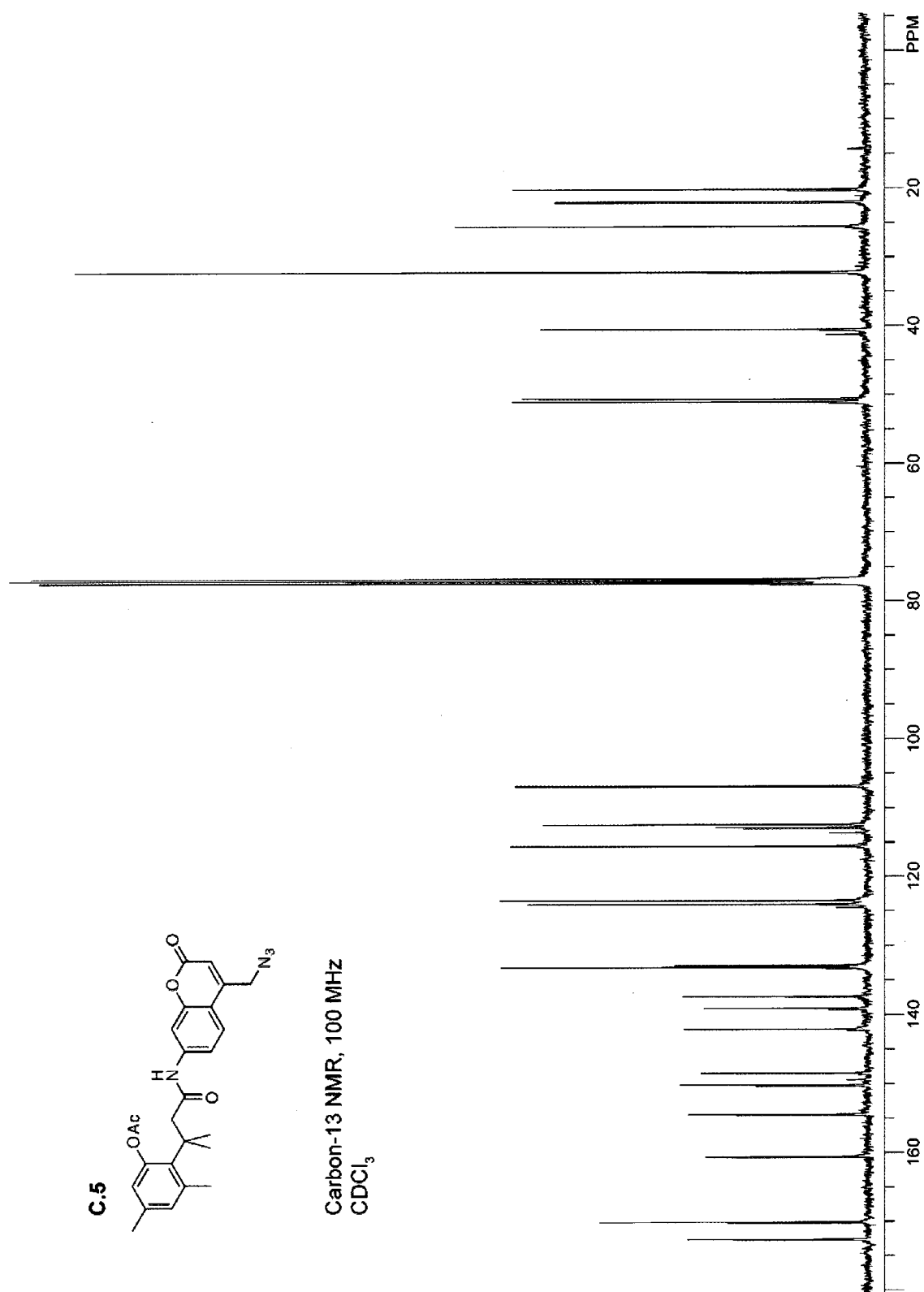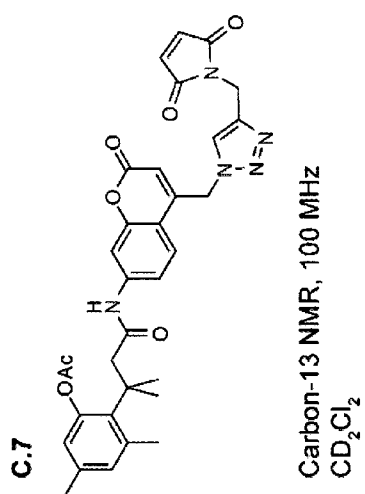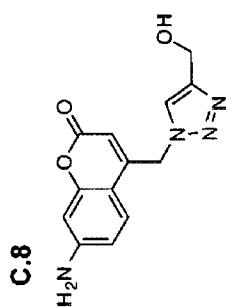
Proton NMR, 400 MHz
DMSO-d6

C.8
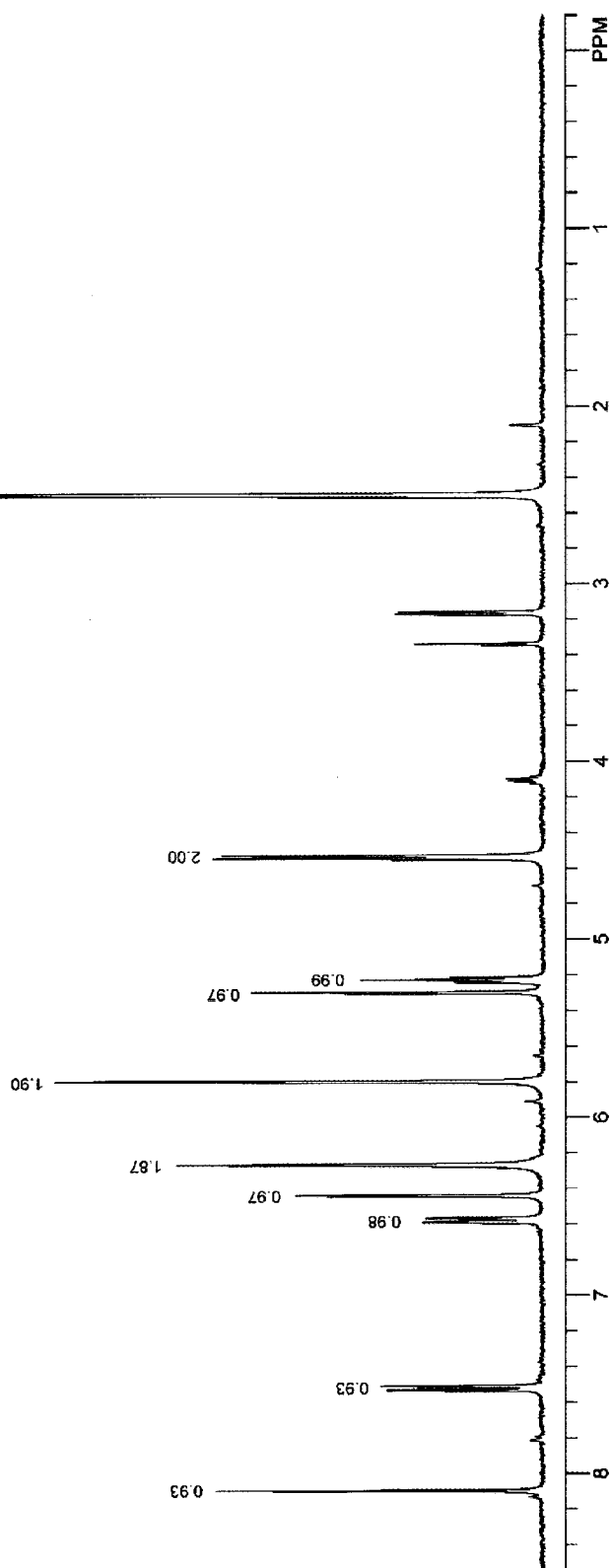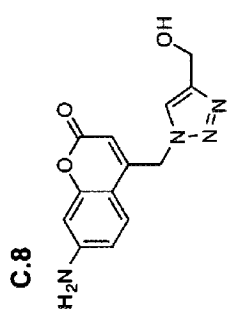
Carbon-13 NMR, 100 MHz
DMSO-d6

265

C.9

Proton NMR, 400 MHz
CDCl$_3$

C.9

Carbon-13 NMR, 100 MHz
CDCl$_3$
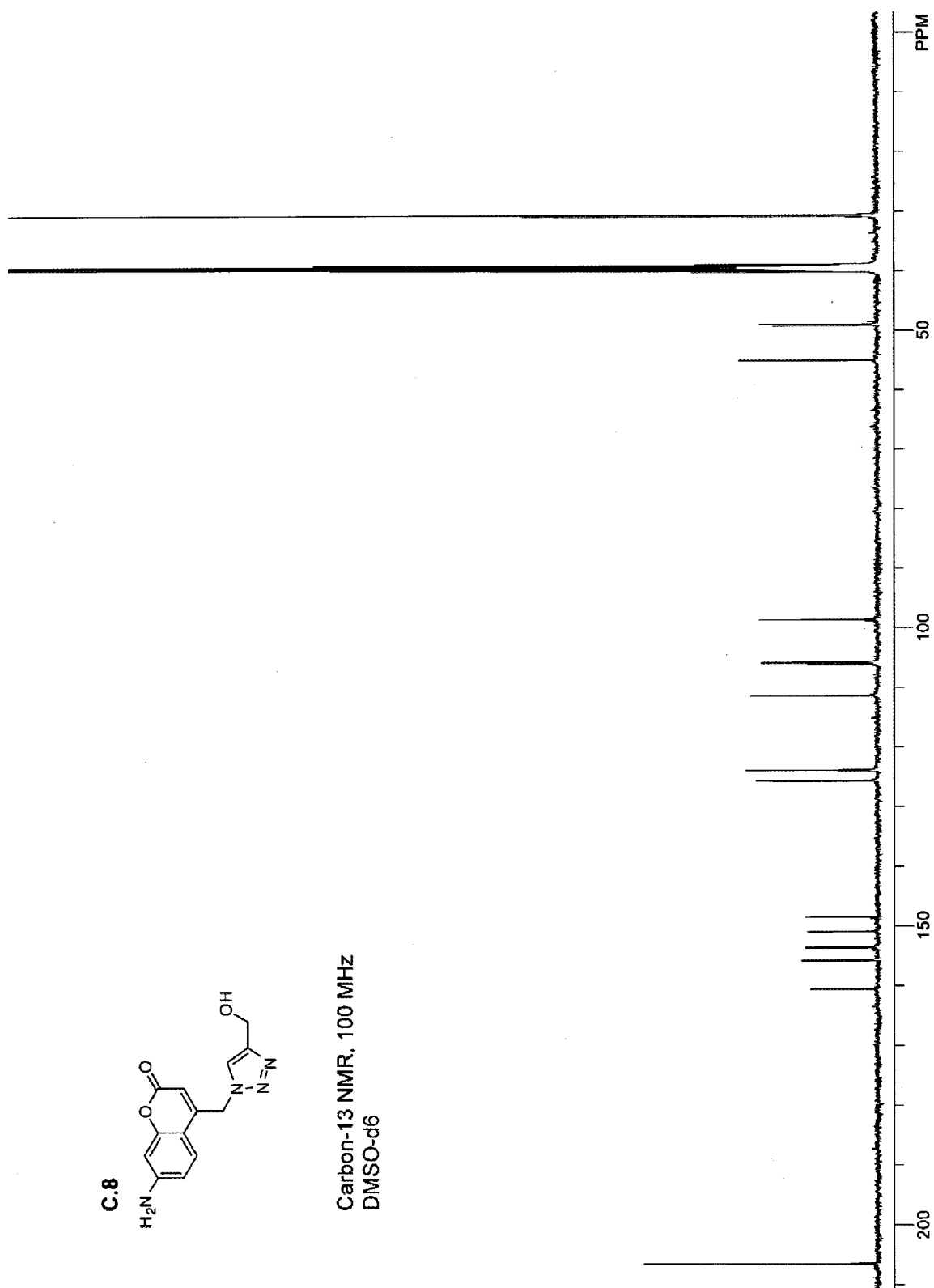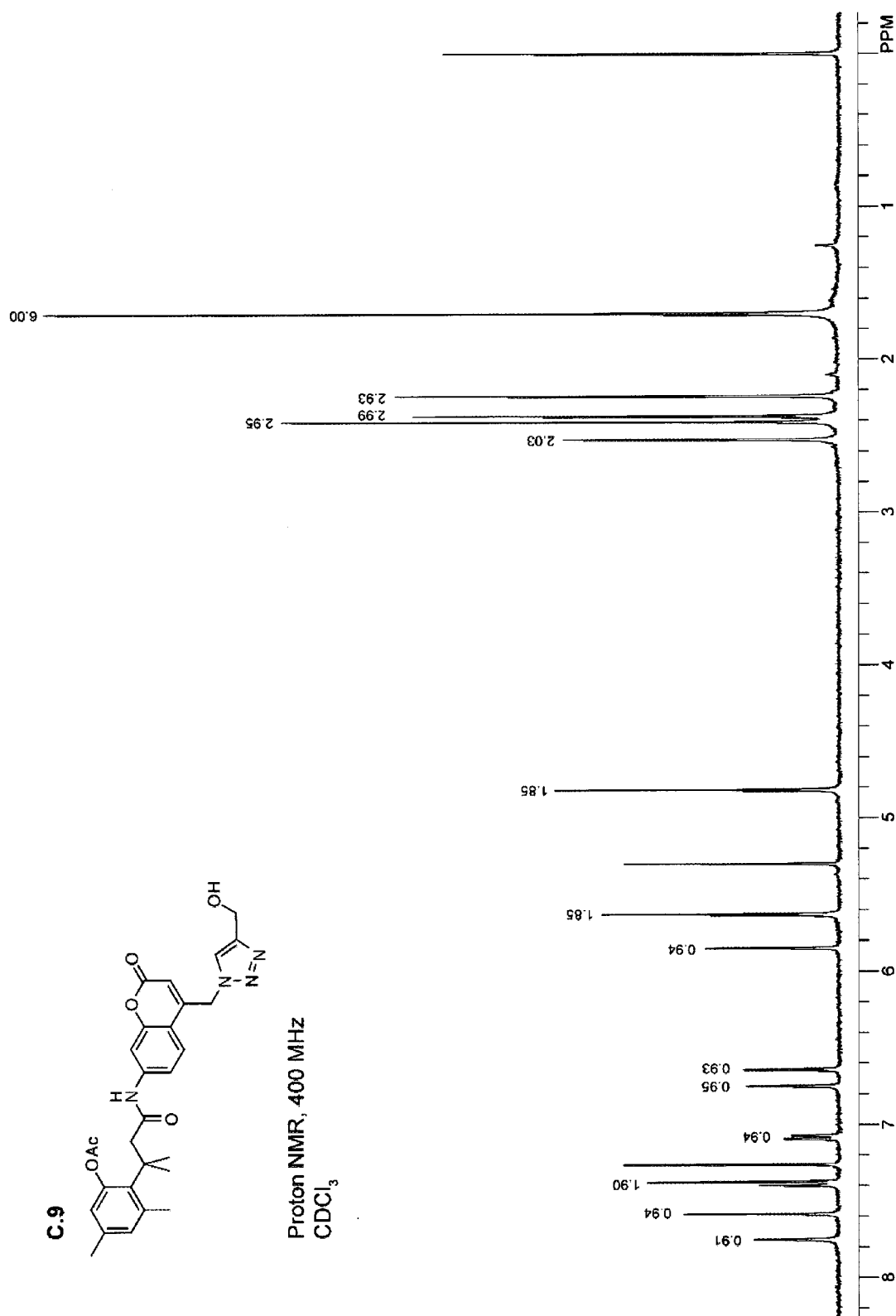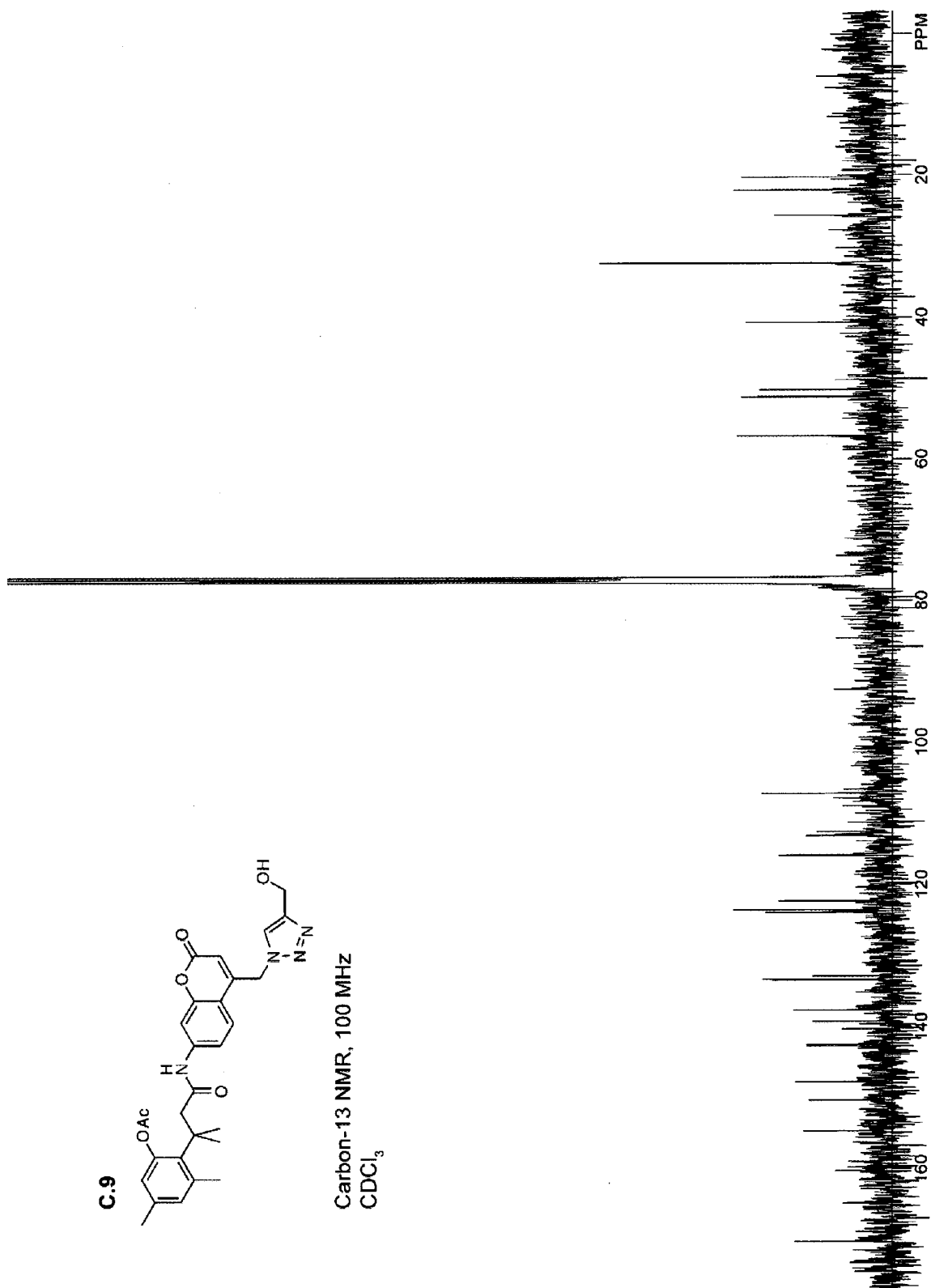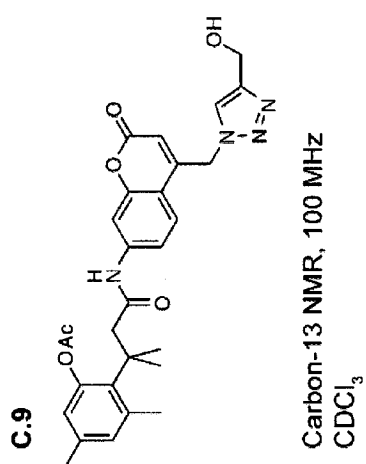
C.4   Conclusions

A blue-shifted profluorophore was synthesized that could be conjugated to ribonucleases. A fluorescence shift and increase in intensity occurred after cleavage by esterases. Unfortunately, despite moderate fluorescence intensity of the unmasked product, the auto-fluorescence in HeLa cells prevented observation of ribonuclease endocytosis.

Scheme C.1 Synthetic scheme for blue-shifted esterase substrates.
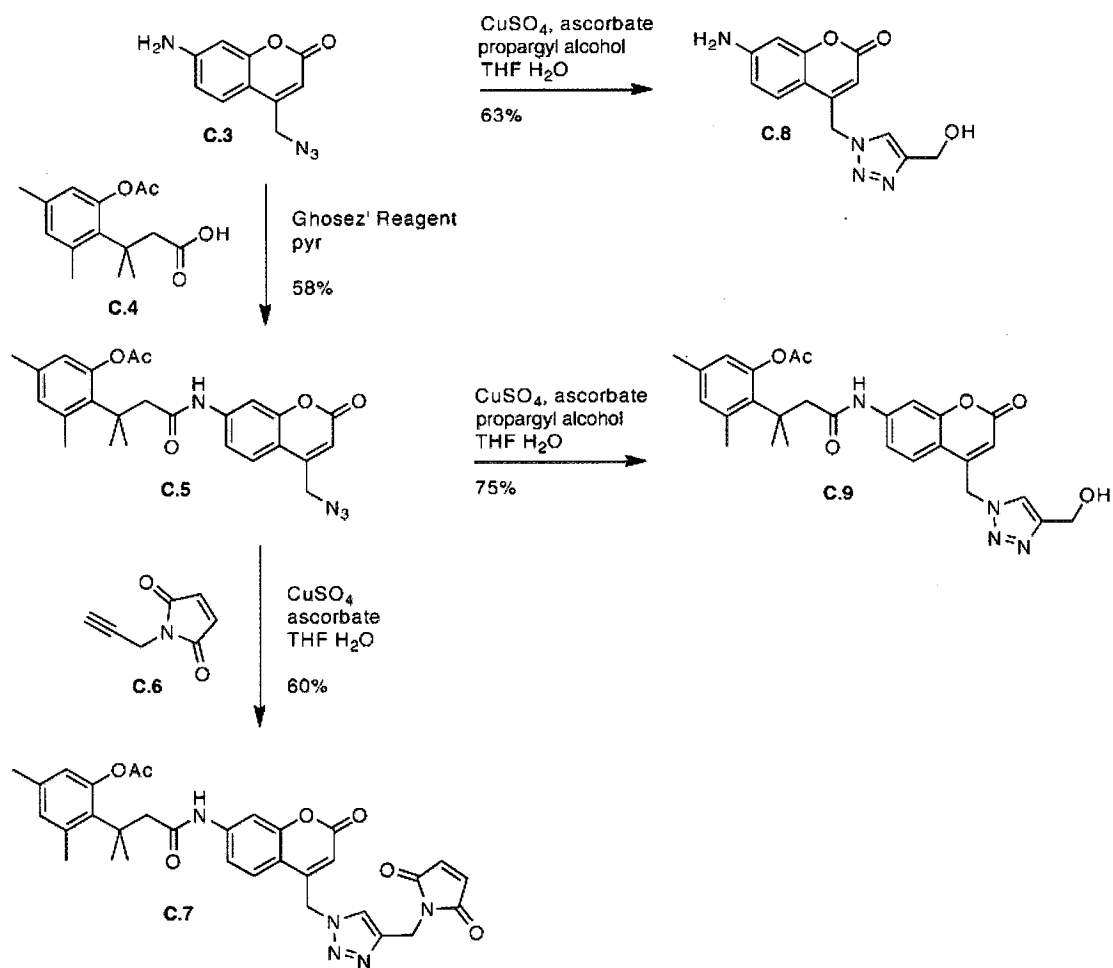
Figure C.1   Fluorogenic green and blue trimethyl lock esterase substrates.

C.1

C.2
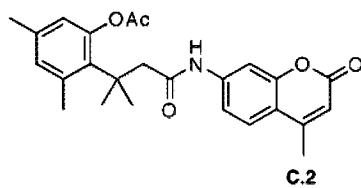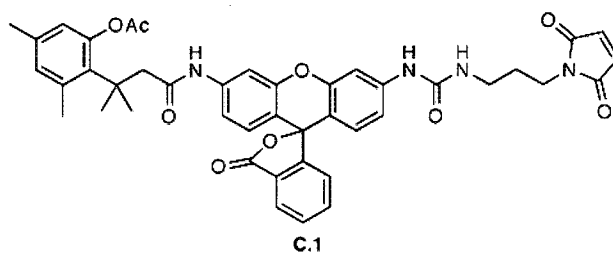
Figure C.2   Absorbance and fluorescence spectra. Fluorescence spectra were recorded

by excitation at the respective excitation maxima for each compound (156

nM in PBS). Absorbance spectra were normalized to the fluorescence

spectra by measuring fluorescence at the respective emission maxima for

each compound, and scanning the excitation wavelengths. Em, Emission

spectrum; Ex, Excitation spectrum; MURh, Morpholinourea rhodamine
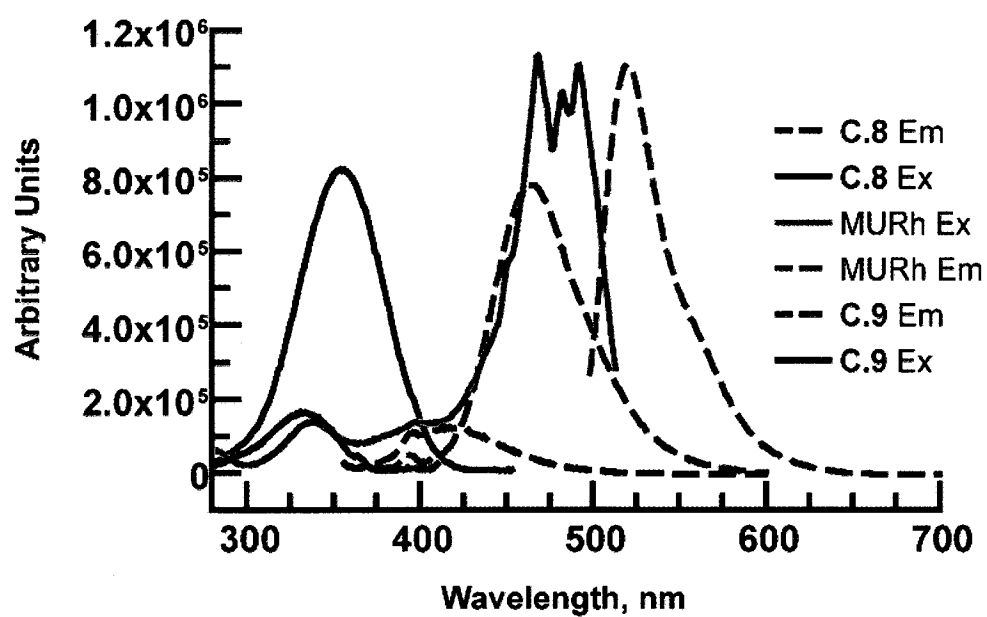
Figure C.3   Esterase-mediated hydrolysis of **C.9**. Michaelis–Menten plot of the

hydrolysis of **C.9** (0.41–26 µM) by PLE (5.5 nM) in PBS. Experiments

were performed in triplicate and uncertainties were expressed as standard

deviation. $K_M = 5.1 \pm 1.6$ µM; $k_{cat} = 0.75 \pm 0.14$ s^{-1}; $k_{cat}/K_M = (1.5 \pm 0.8) \times$

10^5 M^{-1}s^{-1}.
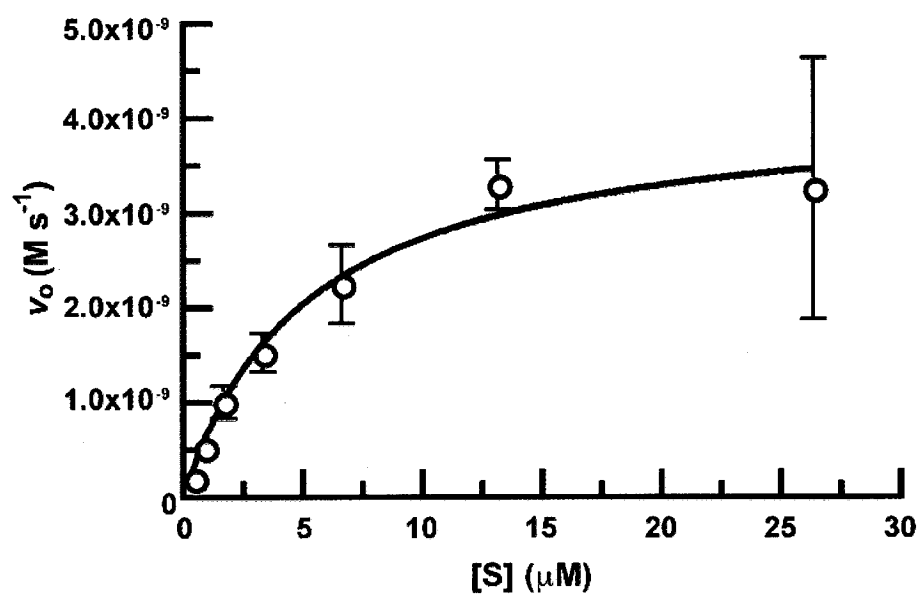
Figure C.4   Confocal and epifluorescence microscopy of ribonuclease conjugate

endocytosis. RNase 1 conjugated to **C.7** (A, D) or **C.1** (B, E) (20 μM) was

added to HeLa cells and incubated at 37 °C for 3 hours. The cells were

washed and then imaged by confocal (A-B) or epifluorescence microscopy

(C-E). (C) Unlabeled HeLa cells. Blue, **C.7**; Green, **C.1**; Red, DRAQ5

nuclear stain.

Unlabeled   20 μM RNase1 **C.7** Conjugate   20 μM RNase1 **C.1** Conjugate
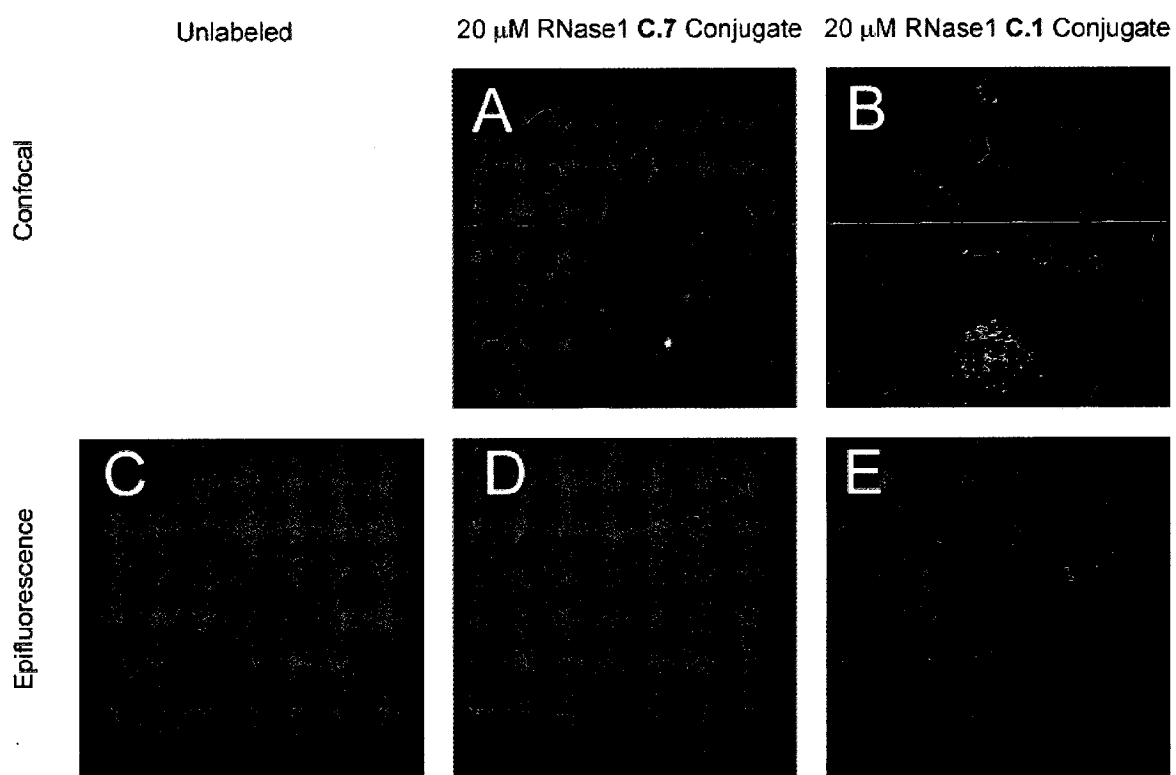
REFERENCES

Amsberry, K. L., Borchardt, R. T. (1990). The lactonization of 2'-hydroxyhydrocinnamic acid amides: A potential prodrug for amines. *J. Org. Chem.* **55**, 5867–5877.

Amsberry, K. L., Borchardt, R. T. (1991). Amine prodrugs which utilize hydroxy amide lactonization. I. A potential redox-sensitive amide prodrug. *Pharm. Res.* **8**, 323–330.

Amsberry, K. L., Gerstenberger, A. E., Borchardt, R. T. (1991). Amine prodrugs which utilize hydroxy amide lactonization. II. A potential esterase-sensitive amide prodrug. *Pharm. Res.* **8**, 455–461.

An, S., Kumar, R., Sheets, E. D., Benkovic, S. J. (2008). Reversible compartmentalization of de novo purine biosynthetic complexes in living cells. *Science* **320**, 103–106.

Anlezark, G. M., Melton, R. G., Sherwood, R. F., Coles, B., Friedlos, F., Knox, R. J. (1992). The bioactivation of 5-(aziridin-1-yl)-2,4-dinitrobenzamide (CB1954)—I. Purification and properties of a nitroreductase enzyme from *Escherichia coli*—A potential enzyme for antibody-directed enzyme prodrug therapy (ADEPT). *Biochem. Pharmacol.* **44**, 2289–2295.

Barker, D. L., Jencks, W. P. (1969). Pig liver esterase. Some kinetic properties. *Biochemistry* **8**, 3890–3897.

Baykov, A. A., Evtushenko, O. A., Avaeva, S. M. (1988). A malachite green procedure for orthophosphate determination and its use in alkaline phosphatase-based enzyme immunoassay. *Anal. Biochem.* **171**, 266–270.

Beija, M., Afonso, C. A. M., Martinho, J. M. G. (2009). Synthesis and applications of rhodamine derivatives as fluorescent probes. *Chem. Soc. Rev.* **38**, 2410–2433.

Borchardt, R. T., Cohen, L. A. (1972a). Stereopopulation control. II. Rate enhancement of intramolecular nucleophilic displacement. *J. Am. Chem. Soc.* **94**, 9166–9174.

Borchardt, R. T., Cohen, L. A. (1972b). Stereopopulation control. III. Facilitation of intramolecular conjugate addition of the carboxyl group. *J. Am. Chem. Soc.* **94**, 9175–9182.

Bridgewater, J. A., Springer, C. J., Knox, R. J., Minton, N. P., Michael, N. P., Collins, M. K. (1995). Expression of the bacterial nitroreductase enzyme in mammalian cells renders them selectively sensitive to killing by the prodrug CD1954. *Eur. J. Cancer* **31A**, 2362–2370.

Brookmeyer, R., Evans, D. A., Hebert, L., Langa, K. M., Heeringa, S. G., Plassman, B. L., Kukull, W. A. (2011). National estimates of the prevalence of Alzheimer's disease in the United States. *Alzheimer's & Dementia* **7**, 61–73.

Bruice, T. C., Pandit, U. K. (1960). The effect of geminal substitution ring size and rotamer distribution on the intramolecular nucleophilic catalysis of the hydrolysis of monophenyl esters of dibasic acids and the solvolysis of the intermediate anhydrides. *J. Am. Chem. Soc.* **82**, 5858–5865.

Brumback, A. C., Lieber, J. L., Angleson, J. K., Betz, W. J. (2004). Using FM1-43 to study neuropeptide granule dynamics and exocytosis. *Methods* **33**, 287–294.

Campbell, R. E. (2004). Realization of β-lactamase as a versatile fluorogenic reporter. *Trends Biotechnol.* **22**, 208–211.

Ceresole, M. Procedures for the preparation of dyes from the group of meta-amidophenol-phtaleins. D. R. Patent 44002, 1887.

Chandran, S. S., Dickson, K. A., Raines, R. T. (2005). Latent fluorophore based on the trimethyl lock. *J. Am. Chem. Soc.* **127**, 1652–1653.

Chang, L., Bertelsen, E. B., Wisén, S., Larsen, E. M., Zuiderweg, E. R., Gestwicki, J. E. (2008). High-throughput screen for small molecules that modulate the ATPase activity of the molecular chaperone DnaK. *Anal. Biochem.* **372**, 167–176.

Chao, T.-Y., Lavis, L. D., Raines, R. T. (2010). Cellular uptake of ribonuclease A relies on anionic glycans. *Biochemistry* **49**, 10666–10673.

Chao, T. Y., Raines, R. T. (2011). Mechanism of ribonuclease A endocytosis: Analogies to cell-penetrating peptides. *Biochemistry*, In press, doi: 10.1021/bi2009079.

Cheruvallath, Z. S., Cole, D. L., Ravikumar, V. T. (2003). A novel solid support for synthesis of oligonucleotide 3′-phosphorothioate monoesters. *Bioorg. Med. Chem. Lett.* **13**, 281–284.

Chinnapen, D. J.-F., Chinnapen, H., Saslowsky, D., Lencer, W. I. (2007). Rafting with cholera toxin: Endocytosis and trafficking from plasma membrane to ER. *FEMS Microbiol. Lett.* **266**, 129–137.

Cleland, W. W., Hengge, A. C. (2006). Enzymatic mechanisms of phosphate and sulfate transfer. *Chem. Rev.* **106**, 3252–3278.

Cochilla, A. J., Angleson, J. K., Betz, W. J. (1999). Monitoring secretory membrane with FM1-43 fluorescence. *Annu. Rev. Neurosci.* **22**, 1–10.

Coleman, J. E. (1992). Structure and mechanism of alkaline phosphatase. *Annu. Rev. Biophys. Biomol. Struct.* **21**, 441–483.

Conner, S. D., Schmid, S. L. (2003). Regulated portals of entry into the cell. *Nature* **422**, 37–44.

Cürten, B., Kullmann, P. H. M., Bier, M. E., Kandler, K., Schmidt, B. F. (2005). Synthesis, photophysical, photochemical and biological properties of caged GABA, 4-[[(2H-1-benzopyran-2-one-7-amino-4-methoxy)carbonyl] amino] butanoic acid. *Photochem. Photobiol.* **81**, 641–648.

Danaei, G., Friedman, A. B., Oza, S., Murray, C. J. L., Ezzati, M. (2009). 7. *Population Health Metrics* doi:10.1186/1478-7954-7-16.

Danforth, C., Nicholson, A. W., James, J. C., Loudon, G. M. (1976). Steric acceleration of lactonization reactions: An analysis of "stereopopulation control". *J. Am. Chem. Soc.* **98**, 4275–4281.

Denny, W. A. (2002). Nitroreductase-based GDEPT. *Curr. Pharm. Des.* **8**, 1349–1361.

Dillon, M. P., Haiying, C., Magg, H. (1996). Application of the "trimethyl lock" to ganciclovir, a pro-prodrug with increased oral bioavailability. *Bioorg. Med. Chem. Lett.* **6**, 1653–1656.

Dordunoo, S. K., Burt, H. M. (1996). Solubility and stability of taxol: effects of buffers and cyclodextrins. *Int. J. Pharm.* **133**, 191–201.

Ernster, L. (1967). DT diaphorase. *Methods Enzymol.* **10**, 309–317.

Farinas, E. T., Schwaneberg, U., Glieder, A., Arnold, F. H. (2001). Directed evolution of a cytochrome P450 monooxygenase for alkane oxidation. *Adv. Synth. Catal.* **343**, 601–606.

Fickling, M. M., Fischer, A., Mann, B. R., Packer, J., Vaughan, J. (1959). Hammett substituent constants for electron-withdrawing substituents: Dissociation of phenols, anilinium ions and dimethyl anilinium ions. *J. Am. Chem. Soc.* **81**, 4226–4230.

Fleming, C. D., Bencharit, S., Edwards, C. C., Hyatt, J. L., Tsurkan, L., Bai, F., Fraga, C., Morton, C. L., Howard-Williams, E. L., Potter, P. M., Redinbo, M. R. (2005). Structural insights into drug processing by human carboxylesterase 1: tamoxifen, mevastatin, and inhibition by benzil. *J. Mol. Biol.* **352**, 165–177.

Fu, Y., Buryanovskyy, L., Zhang, Z. (2005). Crystal structure of quinone reductase 2 in complex with cancer prodrug CB1954. *Biochem. Bioph. Res. Co.* **336**, 332–338.

Furstner, A., Weintritt, H. (1998). Total synthesis of roseophilin. *J. Am. Chem. Soc.* **120**, 2817–2825.

Gao, W., Xing, B., Tsien, R. Y., Rao, J. (2003). Novel fluorogenic substrates for imaging β-lactamase gene expression. *J. Am. Chem. Soc.* 11146–11147.

Gharat, L., Taneja, R., Weerapreeyakul, N., Rege, B., Plooi, J., Chikhale, P. J. (2001). Targeted drug delivery systems 6: Intracellular bioreductive activation, uptake and transport of an anticancer drug delivery system across intestinal Caco-2 cell monolayers. *Int. J. Pharm.* **219**, 1–10.

Greenwald, R. B., Choe, Y. H., Conover, C. D., Shum, K., Wu, D., Royzen, M. (2000). Drug delivery systems based on trimethyl lock lactonization: poly(ethylene glycol) prodrugs of amino-containing compounds. *J. Med. Chem.* **43**, 475–487.

Grohmann, M., Paulmann, N., Fleischhauer, S., Vowinckel, J., Priller, J., Walther, D. J. (2009). A mammalianized synthetic nitroreductase gene for high-level expression. *BMC Cancer* 9, Article ID 301. doi:10.1186/1471-2407-9-301.

Gruenberg, J., Maxfield, F. R. (1995). Membrane transport in the endocytic pathway. *Curr. Opin. Cell Biol.* **7**, 552–563.

Guo, X., Szoka, F. C. (2003). Chemical approaches to triggerable lipid vesicles for drug and gene delivery. *Acc. Chem. Res.* **36**, 335–341.

Gutte, B., Merrifield, R. B. (1971). The synthesis of ribonuclease A. *J. Biol. Chem.* **246**, 1922–1941.

Haigis, M. C., Raines, R. T. (2003). Secretory ribonucleases are internalized by a dynamin-independent endocytic pathway. *J. Cell Sci.* **116**, 313–324.

Hanahan, D., Weinberg, R. A. (2011). Hallmarks of cancer: The next generation. *Cell* **144**, 646–674.

Hao, M., Maxfield, F. R. (2000). Characterization of rapid membrane internalization and recycling. *J. Biol. Chem.* **275**, 15279–15286.

Hartley, B. S., Kilby, B. A. (1954). The reaction of *p*-nitrophenyl esters with chymotrypsin and insulin. *Biochem. J.* **56**, 288–297.

Haveaux, B., Dekoker, A., Rens, M., Sidani, A. R., Toye, J., Ghosez, L. (1979). α-Chloroenamines, reactive intermediates for synthesis: 1-Chloro-*N,N*,2-trimethylpropenylamine. *Org. Synth.* **59**, 26–34.

Hecht, M. H., Das, A., Go, A., Bradley, L. H., Wei, Y. (2004). De novo proteins from designed combinatorial libraries. *Protein. Sci.* **13**, 1711–1723.

Houlston, R. S. (2000). CYP1A1 polymorphisms and lung cancer risk: A meta-analysis. *Pharmacogenetics* **10**, 105–114.

Hu, L., Liu, B., Hacking, D. R. (2000). 5'-[2-(2-nitrophenyl)-2-methylpropionyl]-2'-deoxy-5-fluorouridine as a potential bioreductively activated prodrug of FUDR: Synthesis, stability and reductive activation. *Bioorg. Med. Chem. Lett.* **10**, 797–800.

Huang, S.-T., Lin, Y.-L. (2006). New latenet fluorophore for DT diaphorase. *Org. Lett.* **8**, 265–268.

Huang, S.-T., Peng, Y.-X., Wang, K.-L. (2008). Synthesis of a new long-wavelength latent fluorimetric indicator for analytes determination in the DT-diaphorase coupling dehydrogenase assay system. *Biosens. Bioelectron.* **23**, 1793–1798.

Huang, Z., Wang, Q., Ly, H. D., Gorvindarajan, A., Scheigetz, J., Zamboni, R., Desmarais, S., Ramachandran, C. (1999). 3,6-Fluorescein diphosphate: A sensitive fluorogenic and chromogenic substrate for protein tyrosine phosphatases*. *J. Biomol. Screen.* **4**, 327–334.

Hull, W. E., Halford, S. E., Gutfreund, H., Sykes, B. D. (1976). ^{31}P nuclear magnetic resonance study of alkaline phosphatase: The role of inorganic phosphate in limiting the enzyme turnover rate at alkaline pH. *Biochemistry* **15**, 1547–1561.

Itaya, K., Ui, M. (1966). A new micromethod for the colorimetric determination of inorganic phosphate. *Clin. Chim. Acta* **14**, 361–366.

Jiang, Y., Zhao, J., Hu, L. (2002). 2,2-Dimethyl-2-(*o*-nitrohphenyl)acetyl (DMNA) as an assisted cleavage protecting group for amines. *Tet. Lett.* **43**, 4589–4592.

Johnson, R. J., McCoy, J. G., Bingman, C. A., Phillips, G. N., Raines, R. T. (2007). Inhibition of the human pancreatic ribonuclease by the human ribonuclease inhibitor protein. *J. Mol. Biol.* **368**, 434–449.

Junge, W., Heymann, E. (1979). Characterization of the isoenzymes of pig-liver esterase. 2. Kinetic studies. *Eur. J. Biochem.* **95**, 519–525.

Karaman, R. (2009). Accelerations in the lactonization of trimethyl lock systems are due to proximity orientation and not to strain effects. *Res. Lett. Org. Chem.* 2009, Article ID 240253 doi:10.1155/2009/240253.

Knox, R. J., Boland, M. P., Friedlos, F., Coles, B., Southan, C., Roberts, J. J. (1988). The nitroreductase enzyme in Walker cells that activates 5-(aziridin-1-yl)-4-hydroxylamino-2-nitrobenzamide is a form of NAD(P)H dehydrogenase (quinone) (EC 1.6.99.2). *Biochem. Pharmacol.* **37**, 4671–4677.

Knox, R. J., Friedlos, F., Boland, M. P. (1993). The bioactivation of CB 1954 and its use as a prodrug in antibody-directed enzyme prodrug therapy (ADEPT). *Cancer Metastasis Rev.* **12**, 195–212.

Ko, S. B., Lee, Y. S., Lee, J. Y., Ham, W. H., Park, H. (1996). Synthesis and biological activity of C-3 pyridinylethene-substituted cephalosporins. *Arch. Pharm. Res.* **19**, 411–415.

Kok, J. W., Beest, M., Scherphof, G., Hoekstra, D. (1990). A non-exchangeable fluorescent phospholipid analog as a membrane traffic marker of the endocytic pathway. *Eur. J. Cell. Biol.* **53**, 173–184.

Lakadamyali, M., Rust, M. J., Zhuang, X. (2004). Endocytosis of influenze viruses. *Microbes Infect.* **6**, 929–936.

Lavis, L. D., Chao, T.-Y., Raines, R. T. (2006a). Fluorogenic label for biomolecular imaging. *ACS Chem. Biol.* **1**, 252–260.

Lavis, L. D., Chao, T.-Y., Raines, R. T. (2006b). Latent blue and red fluorophores based on the trimethyl lock. *ChemBioChem* **7**, 1151–1154.

Lavis, L. D., Raines, R. T. (2008). Bright ideas for chemical biology. *ACS Chem. Biol.* **3**, 142–155.

Lavis, L. D., Rutkoski, T. J., Raines, R. T. (2007). Tuning the pK_a of fluorescein to optimize binding assays. *Anal. Chem.* **79**, 6775–6782.

Lee, H. H., Palmer, B. D., Wilson, W. R., Denny, W. A. (1998). Synthesis and hypoxia-selective cytotoxicity of a 2-nitroimidazole mustard. *Bioorg. Med. Chem. Lett.* **8**, 1741–1744.

Leland, P. A., Raines, R. T. (2001). Cancer chemotherapy – ribonucleases to the rescue. *Chem. Biol.* **8**, 405–413.

Leroy, E., Bensel, N., Reymond, J.-L. (2003). A low background high-throughput screening (HTS) fluorescence assay for lipases and esterases using acyloxymethylethers of umbelliferone. *Bioorg. Med. Chem. Lett.* **13**, 2105–2108.

Levine, M. N., Lavis, L. D., Raines, R. T. (2008). Trimethyl lock: A stable chromogenic substrate for esterases. *Molecules* **13**, 204–211.

Levine, M. N., Raines, R. T. (2011). Sensitive fluorogenic substrate for alkaline phosphatase. *Anal. Biochem.* **418**, 247–252.

Leytus, S. P., Melhado, L. L., Mangel, W. F. (1983). Rhodamine-based compounds as fluorgenic substrates for serine proteinases. *Biochem. J.* **209**, 299–307.

Lorey, S., Faust, J., Mrestani-Klaus, C., Kähne, T., Ansorge, S., Neubert, K., Bühling, F. (2002). Transcellular proteolysis demonstrated by novel cell surface-associated substrates of dipeptidyl peptidase IV (CD26). *J. Biol. Chem.* **277**, 33170–33177.

Lowe, G., Yuthavong, Y. (1971). pH-Dependence and structure–activity relationships in the papain-catalysed hydrolysis of anilides. *Biochem. J.* **124**, 117–122.

Lyublinskaya, L. A., Belyaev, S. V., Strongin, A. Y., Matyash, L. F., Levin, E. D., Stepanov, V. M. (1974). A new chromogenic substrate for subtilisin. *Anal. Biochem.* **62**, 371–376.

Maeda, H., Sawa, T., Konno, T. (2001). Mechanism of tumor-targeted delivery of macromolecular drugs, including the EPR effect in solid tumor and clinical overview of the prototype polymeric drug SMANCS. *J. Control. Release* **74**, 47–61.

Maier, O., Oberle, V., Hoekstra, D. (2002). Fluorescent lipid probes: some properties and applications (a review). *Chem. Phys. Lipids* **116**, 3–18.

Makarov, A. A., Ilinskaya, O. N. (2003). Cytotoxic ribonucleases: Molecular weapons and their targets. *FEBS Lett.* **540**, 15–20.

Mangold, S. L., Carpenter, R. T., Kiessling, L. L. (2008). Synthesis of fluorogenic polymers for visualizing cellular internalization. *Org. Lett.* **10**, 2997–3000.

Mayor, S., Pagano, R. E. (2007). Pathways of clathrin-independent endocytosis. *Nature Rev. Mol. Cell Biol.* **8**, 603–612.

Mayor, S., Presley, J. F., Maxfield, F. R. (1993). Sorting of membrane components from endosomes and subsequent recycling to the cell surface occurs by a bulk flow process. *J. Cell Biol.* **121**, 1257–1269.

Menger, F. M., Ladika, M. (1987). Origin of rate accelerations in an enzyme model: The *p*-nitrophenyl ester syndrome. *J. Am. Chem. Soc.* **109**, 3145–3146.

Millán, J. L. (2006). Alkaline phosphatases: Structure, substrate specficitiy, and functional relatedness to other members of a large superfamily of enzymes. *Purinergic Signal.* **2**, 335–341.

Milstien, S., Cohen, L. A. (1970). Rate accelerations by stereopopulation control: Models for enzyme action. *Proc. Natl. Acad. Sci. U.S.A.* **67**, 1143–1147.

Milstien, S., Cohen, L. A. (1972). Stereopopulation control. I. Rate enhancement in the lactonizations of o-hydroxyhydrocinnamic acids. *J. Am. Chem. Soc.* **94**, 9158–9165.

Mosesson, Y., Mills, G. B., Yarden, Y. (2008). Derailed endocytosis: an emerging feature of cancer. *Nat. Rev. Cancer* **8**, 835–850.

Murphy, J. R. (2011). Mechanism of diphtheria toxin catalytic domain delivery to the eukaryotic cell cytosol and the cellular factors the directly participate in the process. *Toxins* **3**, 294–308.

Nam, N.-H., Kim, Y., You, Y.-J., Hong, D.-H., Kim, H.-M., Ahn, B.-Z. (2003). Water soluble prodrugs of the antitumor agent 3-[(3-amino-4-methoxy)phenyl]-2-(3,4,5-trimethoxyphenyl)cyclopent-2-ene-1-one. *Bioorg. Med. Chem.* **11**, 1021–1029.

Naughton, D. P. (2001). Drug targeting to hypoxic tissue using self-inactivating bioreductive delivery systems. *Adv. Drug Deliver. Rev.* **53**, 229–233.

Nicolaou, M. G., Wolfe, J. L., Schowen, R. L., Borchardt, R. T. (1996a). Facilitated intramolecular conjugate addition of amides of 3-(3',6'-dioxo-2'-4'-dimethyl-1'-4'-cyclohexadienyl)-3,3-dimethylpropionic acid. 2. Kinetics of degradation. *J. Org. Chem.* **61**, 6633–6638.

Nicolaou, M. G., Yuan, C., Borchardt, R. T. (1996b). Phosphate prodrugs for amines utilizing a fast intramolecular hydroxy amide lactonization. *J. Org. Chem.* **61**, 8636–8641.

Nielsen, P. E., Egholm, M., Berg, R. H., Buchardt, O. (1991). Sequence-selective recognition of DNA by strand displacement with a thymine-substituted polyamide. *Science* **6**, 1497–1500.

O'Brien, P. J., Herschlag, D. (2002). Alkaline phosphatase revisited: Hydrolysis of alkyl phosphates. *Biochemistry* **41**, 3207–3225.

O'Callaghan, C. H., Morris, A., Kirby, S. M., Shingler, A. H. (1972). Novel method for detection of β-lactamases by using a chromogenic cephalosporin substrate. *Antimicrob. Agents. Chemother.* **1**, 283–288.

Oldfield, C., Robinson, B. H., Freedman, R. B. (1990). Acid-base behaviour of 4-nitrophenol and 4-nitrophenyl-2-sulphonate in water-in-oil microemulsions stabilized by aerosol-OT. *J. Chem. Soc. Faraday Trans.* **86**, 833–841.

Ong, W., Yang, Y., Cruciano, A. C., McCarley, R. L. (2008). Redox-triggered contents release from liposomes. *J. Am. Chem. Soc.* **130**, 14739–14744.

Park, J. H., Agnello, C. F., Mathew, E. (1966). *S–N* transfer and dual acetylation in the *S*-acetylation and *N*-acetylation of 3-phosphoglyceraldehyde dehydrogenase by substrates. *J. Biol. Chem.* **241**, 769–771.

Park, J. H., Meriwether, B. P., Clodfelder, P., Cunningham, L. W. (1961). The hydrolysis of *p*-nitrophenyl acetate catalyzed by 3-phosphoglyceraldehyde dehydrogenase. *J. Biol. Chem.* **236**, 136–141.

Parkinson, G. N., Skelly, J. V., Neidle, S. (2000). Crystal structure of FMN-dependent nitroreductase from *Escherichia coli* B: A prodrug-activating enzyme. *J. Med. Chem.* **43**, 3624–3631.

Porstmann, B., Porstmann, T., Nugel, E., Evers, U. (1985). Which of the commonly used marker enzymes gives the best results in colorimetric and fluorimetric enzyme immunoassays: Horseradish peroxidase, alkaline phosphatase or β-galactosidase? *J. Immunol. Methods* **79**, 27–37.

Qureshi, S. A. (2007). β-lactamase: An ideal reporter system for monitoring gene expression in live eukaryotic cells. *Biotechniques* **42**, 91–96.

Raines, R. T. (1998). Ribonuclease A. *Chem. Rev.* **98**, 1045–1065.

Rea, R., Li, J., Dharia, A., Levitan, E. S., Sterling, P., Kramer, R. H. (2004). Streamlined synaptic vesicle cycle in cone photoreceptor terminals. *Neuron* **41**, 755–766.

Robinson, D., Willcox, P. (1969). 4-Methylumbelliferyl phosphate as a substrate for lysosomal acid phosphatase. *Biochim. Biophys. Acta.* **191**, 183–186.

Rowinsky, E. K., Casenave, L. A., Donehower, R. C. (1990). Taxol: A novel investigational antimicrotuble agent. *J. Natl. Cancer Inst.* **82**, 1247–1259.

Royer, D., Wong, Y.-S., Plé, S., Chiaroni, A., Diker, K., Lévy, J. (2008). Diastereodivergence and appendage diversity in the multicomponent synthesis of aryl-pyrrolo-tetrahydrocarbazoles. *Tetrahedron* **64**, 9607–9618.

Rutkoski, T. J., Kurten, E. L., Mitchell, J. C., Raines, R. T. (2005). Disruption of shape-complementarity markers to create cytotoxic variants of ribonuclease A. *J. Mol. Biol.* **354**, 41–54.

Schmidt, M., Baumann, H., Henke, E., Knoarzycka-Bessler, M., Bornscheuer, U. T. (2004). Directed evolution of lipases and esterases. *Methods Enzymol.* **388**, 199–207.

Schmidt, M., Bornscheuer, U. T. (2005). High-throughput assays for lipases and esterases. *Biomol. Eng.* **22**, 51–56.

Shan, D., Zheng, A., Ballard, C. E., Wang, W., Borchardt, R. T., Wang, B. (2000). A facilitated cyclic ether formation and its potential application in solid-phase peptide and organic synthesis. *Chem. Pharm. Bull.* **48**, 238–244.

Shigenaga, A., Tsuji, D., Nishioka, N., Tsuda, S., Itoh, K., Otaka, A. (2007). Synthesis of a stimulus-responsive processing device and its application to a nucleocytoplasmic shuttle peptide. *ChemBioChem* **8**, 1929–1931.

Shigenaga, A., Yamamoto, J., Hirakawa, H., Ogura, K., Maeda, N., Mirishita, K., Otaka, A. (2010a). Development of thiol-responsive amide bond cleavage device and its application for peptide nucleic acid-based DNA releasing system. *Tetrahedron Lett.* **51**, 2525–2528.

Shigenaga, A., Yamamoto, J., Hirakawa, H., Yamaguchi, K., Otaka, A. (2009). FRET-based assay of the processing reaction kinetics of stimulus-responsive peptides:

influence of amino acid sequence on reaction kinetics. *Tetrahedron* **65**, 2212–2216.

Shigenaga, A., Yamamoto, J., Nishioka, N., Otaka, A. (2010b). Enantioselective synthesis of stimulus-responsive amino acid via asymmetric α-amination of aldehyde. *Tetrahedron* **66**, 7367–7372.

Shigenaga, A., Yamamoto, J., Sumikawa, Y., Furuta, T., Otaka, A. (2010c). Development and photo-responsive peptide bond cleavage reaction of two-photon near-infrared excitation-responsive peptide. *Tet. Lett.* **51**, 2868–2871.

Sicart, R., Collin, M.-P., Reymond, J.-L. (2007). Fluorogenic substrates for lipases, esterases, and acylases using a TIM-mechanism for signal release. *Biotechnol. J.* **2**, 221–231.

Siegel, D. P., Epand, R. M. (1997). The mechanism of lamellar-to-inverted hexagonal phase transitions in phosphatidylethanolamine: Implications for membrane fusion mechanisms. *Biophys. J.* **73**, 3089–3111.

Sinkula, A. A., Yalkowsky, S. H. (1975). Rationale for design of biologically reversible drug derivatives: Prodrugs. *J. Pharm. Sci.* **64**, 181–210.

Snyder, S. L., Wilson, I. B. (1972). Phosphoramidic acids. A new class of nonspecific substrates for alkaline phosphatase from Escherichia coli. *Biochemistry* **11**, 1616–1623.

Steinman, R. M., Cohn, Z. A. (1972). The interaction of soluble horseradish peroxidase with mouse peritoneal macrophages in vitro. *J. Cell Biol.* **55**, 186–204.

Strasfeld, D. B., Ling, Y. L., Gupta, R., Raleigh, D. P., Zanni, M. T. (2009). Strategies for extracting structural information from 2D IR spectroscopy of amyloid: Application to islet amyloid polypeptide. *J. Phys. Chem. B* **113**, 15679–15691.

Sun, L., Martin, D. C., Kantrowitz, E. R. (1999). Rate-determining step of Escherichia coli alkaline phosphatase altered by the removal of a positive charge at the active center. *Biochemistry* **38**, 2842–2848.

Sykes, B. M., Hay, M. P., Bohinc-Herceg, D., Helsby, N. A., O'Connor, C. J., Denny, W. A. (2000). Leaving group effects in reductively triggered fragmentation of 4-nitrobenzyl carbamates. *J. Chem. Soc., Perk. T. 1* **2000**, 1601–1608.

Tang, P. C., Sun, L., McMahon, G., Blake, R. A. 3-(cyclohexanoheteroarylidenyl)-2-indolinone protein tyrosine kinase inhibitors. Patent US 6114371, September 5, 2000.

Testa, B., Mayer, J. M., *Hydrolysis in Drug and Prodrug Metabolism: Chemistry, Biochemistry and Enzymology*. Verlag Helvetica Chimica Acta: Zurich, Switzerland, 2003.

Thanassi, J. W., Cohen, L. A. (1969). The conservation of oxidative energy in phosphate-free systems. Formation of acyl anhydrides via the oxidation of hydroquinone monocarboxylic esters. *Biochim. Biophys. Acta* **172**, 389–398.

Thilo, L., Vogel, G. (1980). Kinetics of membrane internalization and recycling during pinocytosis in *Dictyostelium discoideum*. *Proc. Natl. Acad. Sci. U.S.A.* **77**, 1015–1019.

Thomsen, P., Roepstorff, K., Stahlhut, M., van Deurs, B. (2002). Caveolae are highly immobile plasma membrane microdomains, which are not involved in constitutive endocytic trafficking. *Mol. Biol. Cell* **13**, 238–250.

Turcotte, R. F., Lavis, L. D., Raines, R. T. (2009). Onconase cytotoxicity relies on the distribution of its positive charge. *FEBS J.* **276**, 4270–4281.

Ueda, Y., Mikkilineni, A. B., Knipe, J. O., Rose, W. C., Casazza, A. M., Vyas, D. M. (1993). Novel water soluble phosphatase prodrugs of Taxol possessing in vivo antitumor activity. *Bioorg. Med. Chem. Lett.* **3**, 1761–1766.

van Berkel, S. S., van der Lee, B., van Delft, F. L., Rutjes, F. P. J. T. (2009). A macrocyclic coumarin-containing tripeptide *via* CuAAC chemistry. *Chem. Commun.* **2009**, 4272–4274.

Vyas, D. M., Wong, H., Crosswell, A. R., Casazza, A. M., Knipe, J. O. (1993). Synthesis and antitumor evaluation of water soluble taxol phosphates. *Bioorg. Med. Chem. Lett.* **3**, 1357–1360.

Wang, B., Nicolaou, M. G., Liu, S., Borchardt, R. T. (1996). Structural analysis of a facile lactonization system facilitated by a "trimethyl lock". *Bioorg. Chem.* **24**, 39–49.

Wang, B. H., Gangwar, S., Pauletti, G. M., Siahaan, T. J., Borchardt, R. T. (1997). Synthesis of a novel esterase-sensitive cyclic prodrug system for peptides that utilizes a "trimethyl lock"-facilatated lactonization reaction. *J. Org. Chem.* **62**, 1363–1367.

Wani, M. C., Taylor, H. L., Wall, M. E. (1971). Plant antitumor agents. VI Isolation and structure of taxol, a novel antileukemic and antitumor agent from Taxus brevifolia. *J. Am. Chem. Soc.* **93**, 2325–2327.

Watkins, R. W., Lavis, L. D., Kung, V. M., Los, G. V., Raines, R. T. (2009). Fluorogenic affinity label for the facile, rapid imaging of proteins in live cells. *Org. Biomol. Chem.* **7**, 3969–3975.

Weerapreeyakul, N., Anorach, R., Khuansawad, T., Yenjai, C., Isaka, M. (2007). Synthesis of bioreductive esters from fungal compounds. *Chem. Pharm. Bull.* **55**, 930–935.

Wei, Y., Hecht, M. H. (2004). Enzyme-like proteins from an unselected library of designed amino acid sequences. *Protein Eng. Des. Sel.* **17**, 67–75.

Westermark, P., Andersson, A., Westermark, G. T. (2011). Islet amyloid polypeptide, islet amyloid and diabetes mellitus. *Physiol. Rev.* **91**, 795–826.

Winans, R. E., Wilcox, C. F. (1976). Comparison of stereopopulation control with conventional steric effects in lactonization of hydrocoumarinic acids. *J. Am. Chem. Soc.* **98**, 4281–4285.

Wolf, N. M., Morisseau, C., Jones, P. D., Hock, B., Hammock, B. D. (2006). Development of a high-throughput screen for soluble epoxide hydrolase inhibition. *Anal. Biochem.* **355**, 71–80.

Yatzeck, M. M., Lavis, L. D., Chao, T.-Y., Chandran, S. S., Raines, R. T. (2008). A highly sensitive fluorogenic probe for cytochrome P450 activity in live cells. *Bioorg. Med. Chem. Lett.* **18**, 5864–5866.

Zheng, A., Shan, D., Wang, B. (1999). A redox-sensitive resin linker for the solid phase synthesis of C-terminal modified peptides. *J. Org. Chem.* **64**, 156–161.

Zhou, W., Andrews, C., Liu, J., Shultz, J. W., Valley, M. P., Cali, J. J., Hawkins, E. M., Klaubert, D. H., Bulleit, R. F., Wood, K. V. (2008). Self-cleavable bioluminogenic luciferin phosphates as alkaline phosphatase reporters. *ChemBioChem* **9**, 714–718.